Synthesis and Characterization of Modified Polyadenosines for Applications as a pH-Responsive Nanodevice

Kieran Duke

A Thesis

in

The Department

of

Chemistry and Biochemistry

Presented in Partial Fulfillment of the Requirements

For the Degree of Master of Science (Chemistry) at

Concordia University

Montreal, Quebec, Canada

July 2021

CONCORDIA UNIVERSITY

SCHOOL OF GRADUATE STUDIES

This is to certify that the thesis prepared

By: Kieran Duke

Entitled: Synthesis and Characterization of Modified Polyadenosines for Applications as a pH-Responsive Nanodevice

And submitted in partial fulfillment of the requirements for the degree of

Master of Science (Chemistry)

Complies with the regulations of the University and meets the accepted standards with respect to originality and quality.

Signed by the final Examining Committee:

_____Chair

Dr. Ashlee Howarth

_____Examiner

Dr. Marek Majewski

_____Examiner

Dr. Steve Shih

_____Supervisor

Dr. Christopher J. Wilds

Approved by _____

Chair of Department or Graduate Program Director

_____2021 _____

Dr. Pascale Sicotte, Dean of Faculty

Abstract

Synthesis and Characterization of Modified Polyadenosines for Applications as a pH-Responsive Nanodevice

Kieran Duke

The need for structurally and functionally diverse nanomaterials is rapidly expanding with increasing applications in various fields including medicine and biotechnology. RNA has been gaining recognition as a nanomaterial due to its ability to engage in both Watson-Crick and non-canonical interactions as well as its capacity to adopt structural motifs distinct from those of DNA. One such structure, the poly(A) RNA duplex, first described by Rich *et al* in 1961, is parallel-stranded and stabilised by hydrogen bonds between the Hoogsteen edges of the adenine bases. Acidic conditions or ammonium (NH_4^+) promotes duplex formation. Poly(A) RNA lends itself for applications as a pH-responsive nanomaterial similar to other nucleic acid structures including the i-motif.

The aim of this thesis was to expand upon previous studies that investigated the influence of 2'-modifications on the poly(A) RNA duplex. Here, the effects of 2'-*O*-propargyl functionality, and additional Click chemistry derivatization employing copper(I)-catalyzed azide-alkyne cycloaddition was explored to assess relationships between structure and stability.

Incorporation of the 2'-*O*-propargyl functionality was found to be destabilizing towards duplex formation. Click chemistry derivatization was performed with small molecule azides

including 4-azidobutylamine and 1-(azidomethyl)pyrene. Duplexes that incorporated the amine functionality through the 1,4-triazole linkage were found to be destabilized, where as, pyrene modifications provided stabilization upon successive incorporations. Fluorescence analysis of pyrene-functionalized oligonucleotides provided insight into the localization of the pyrene group and potential flexibility differences between the ends of the duplex. These findings will guide the design of future duplex modifications to enhance its' application as a pH-responsive nanomaterial.

Acknowledgements

I would like to thank my supervisor, Dr. Christopher J. Wilds, for his constant mentorship over these past couple of years. The research was not always easy or straightforward, but you were always there with advice and guidance in those troubling times. I have developed both as a chemist and as a person because of you.

A special thanks to Dr. Anne Noronha, who not only synthesized all my oligonucleotides on the ABI 3400, but was also there for me throughout my degree.

To my committee members, Dr. Steve Shih and Dr. Marek Majewski, thank you for the constant advice, much needed criticism, and for helping to guide my research project towards its' ultimate completion.

Thank you to Dr. Heng Jiang and the newly retired Alain Tessier for help in running the ESI-MS analyses of my oligonucleotide samples.

Thank you to Dr. Constantin Yannopoulos for your help with the NMR analyses of my compounds.

Thank you to Vincent Lau for your help in setting up my variable temperature fluorescence analyses.

Thank you to the Majewski lab and William Leal for helping me with the Quantum yield analysis of my pyrene-functionalized poly(A) duplexes.

Lastly, a big thank you to all my current and past lab mates. Chris, William, Alex, Gab, Elizabeth, Azalea, and Sarah. You all helped contribute to my research in your own ways and I

could not have done it without you. All the time you spent welcoming me to the lab, teaching me various techniques, and putting up with me was worth it.

All the best to you all.

Dedication

This thesis is dedicated to my mom, dad, and brothers.

Love you all.

Table of Contents

List of Figures

List of Tables

List of Schemes

List of Abbreviations

ABI: Applied Biosystems

ACN: Acetonitrile

AMV-RT: Avian myeloblastosis virus reverse transcriptase

Anhyd.: Anhydrous

APS: Ammonium persulfate

ASO: Antisense oligonucleotide

CD: Circular dichroism

$CDCl_3$: Deuterated chloroform

CPG: Controlled pore glass

CuAAC: Copper(I)-catalyzed azide-alkyne cycloaddition reaction

DDTT: 3-[(Dimethylaminomethylene)amino]-3H-1,2,4-dithiazole-5-thione

DMF: Dimethyl formamide

DMT: Dimethoxytrityl

DNA: Deoxyribonucleic acid

EDTA: Ethylenediaminetetraacetic acid

ESI: Electrospray ionization

Et_2O: Diethyl ether

EtOAc: Ethyl acetate

FCC: Flash column chromatography

H_2O: Water

HCl: Hydrochloric acid

HPLC: High performance liquid chromatography

LC: Liquid chromatography

LNA: Locked nucleic acid

MeOH: Methanol

MOF: Metal-organic framework

MS: Mass spectrometry

Na_2HPO_4: Sodium phosphate dibasic

Na_2SO_4: Sodium sulfate

NaCl: Sodium chloride

NaN_3: Sodium azide

NaOAc: Sodium acetate

NaOH: Sodium hydroxide

ND: Not detected

NT: No transition observed

nt: Nucleotide

OD: Optical density

Oligo(s): Oligonucleotide(s)

ORN: Oligoribonucleic acid

PAGE: Polyacrylamide gel electrophoresis

PAH: Polycyclicaromatic hydrocarbon

Ph_3P: Triphenyl phosphine

PMDETA: N,N,N',N'',N''-pentamethyldiethylenetriamine

Poly(A): Polyadenylic acid

PS: Phosphorothioate

rA: Adenosine

RBF: Round-bottomed flask

RNA: Ribonucleic acid

RNAi: RNA interference

RNase H: Ribonuclease H

RP: Reverse phase

RT: Room temperature

rU: Uridine

SPS: Solid phase oligonucleotide synthesis

ssRNA: Single-stranded RNA

SVPDE: Snake venom phosphodiesterase

TBA: Thrombin binding aptamer

TBDMS: *Tert*-butyl dimethyl silyl

TBE: Tris, boric acid, EDTA buffer

TEMED: Tetramethylethylenediamine

TFO: Triplex-forming oligonucleotide

THF: Tetrahydrofuran

T_m: Melting temperature

TREAT-HF: Triethylamine trihydrofluoride

UV: Ultraviolet light

Chapter 1: Introduction

1.1 History and Structure of Nucleic Acids

The true beginnings of the field of nucleic acid chemistry date back to 1871, when Friedrich Miescher was the first person to isolate and characterize DNA from the nuclei of pus cells.[1,2] Referred to as 'nuclein' at the time, what Miescher actually discovered was a combination of DNA and many associated proteins.[1,2] These compounds were unique in that they contained a very high phosphorus content, which made them clearly distinct from proteins, carbohydrates, and lipids. Richard Altmann, a pupil of Miescher, was the first to purify nuclein from protein and is credited with coining the term 'nucleic acids' due to their acidic nature and cellular origin.[2,3] While initially hotly contested, it is now firmly established that DNA is responsible for the storage of our genetic information. This stored genetic information is transcribed into messenger RNA and then subsequently translated into proteins needed by our cells through a process known as the Central Dogma of Molecular Biology.

Today, it is known that DNA and RNA are long, acidic polymers of nucleotide subunits. They are composed of three main parts: (1) a pentofuranose sugar (2) a nitrogenous base and (3) a phosphate linkage (**Figure 1.1**).

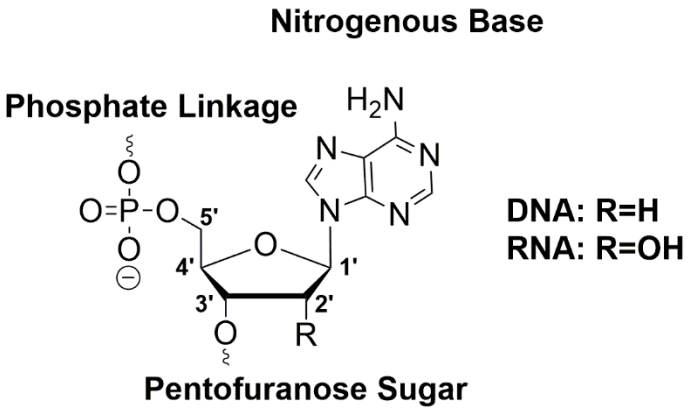

Figure 1.1: Structure of a Nucleotide Subunit.

These monomer subunits connect via a C3' to C5' phosphodiester linkage to form the backbone of long strands of nucleic acid. The identity of each individual monomer is bestowed by both the nucleobase, which is coupled to the sugar through a β-glycosidic linkage to the anomeric C1', and the group positioned at C2'. In DNA, there is a hydrogen at this C2' position (Deoxyribose); in RNA, a hydroxyl group (Ribose). There are three nucleobases which are commonly found in both DNA and RNA. These are Adenine (A), Guanine (G), and Cytosine (C). In DNA, there is an additional base, Thymine (T). Similarly, Uracil (U) is found in RNA. A nucleobase which is coupled to a pentofuranose sugar is referred to as a nucleoside, where as a nucleotide has an additional phosphate group at C5'. Nucleosides are named based on the attached nucleobase: adenosine (rA), guanosine (rG), cytidine (rC), and uridine (rU) for ribonucleosides and 2'-deoxyadenosine (dA), 2'-deoxyguanosine (dG), 2'-deoxycytidine (dC), and thymidine (dT) for 2'-deoxynucleosides.

The crystalline deoxyribonucleotides were first obtained by Klein and Thannhauser through the enzymatic digestion of DNA.[4] Alexander Todd followed this up by chemically synthesizing the DNA nucleotides, confirming their exact structures.[5,6] These nucleobases are categorized as either a purine or pyrimidine according to **Figure 1.2**.

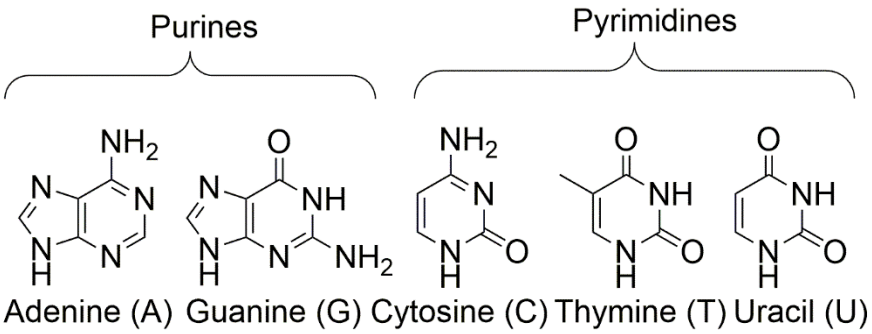

Figure 1.2: Structures of Purines and Pyrimidines.

The most important facet of these nucleobases is how they allow for the maintenance of genetic integrity due to their unique hydrogen bonding acceptor and donor patterns. Each nucleoside will form hydrogen bonding interactions with another in a purine-pyrimidine or pyrimidine-purine arrangement (A with T(U), G with C) as shown in **Figure 1.3**. These binding patterns were derived from experimental results obtained by Chargaff, who demonstrated that the proportions of these nucleobases were consistent across numerous biological sources.[7] The stabilization brought about by these favourable interactions are what allow single-stranded nucleic acids to hybridize and form higher ordered duplex structures in a predictable manner.

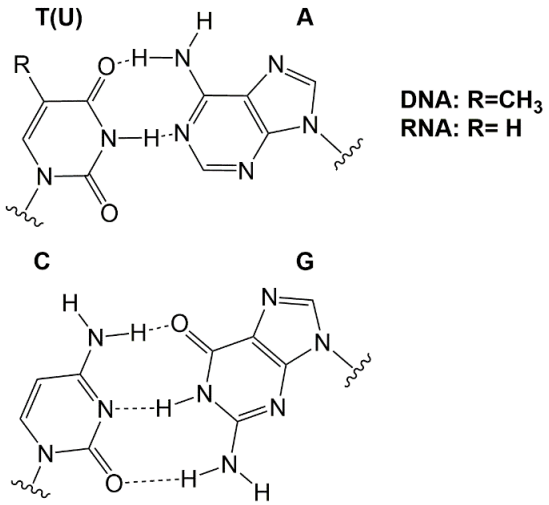

Figure 1.3: Watson and Crick Hydrogen Bonding Patterns of Nucleobases.

Modern nucleic acid chemistry began in 1953 when the structure of the DNA duplex was first proposed by James Watson and Francis Crick.[8] While many different structures had been previously proposed, including a number of triplex[9] and tetranucleotide structures,[10] Watson and Crick were the first to propose that DNA duplexes are formed from two antiparallel strands of DNA oriented in a right-handed helix and held together by hydrogen bonding interactions between the nucleobases. They based their model on the works of numerous other scientists including Furberg, who developed a similar model;[11] Astbury[12] and Wilkins,[13] who performed X-ray diffraction studies on DNA; and the unpublished works of Wilkins[14] and Franklin[15] whose diffraction studies were paramount in the eventual solving of the DNA helix.[16,17]

DNA helices can adopt several different forms due to the relative flexibility of the deoxyribose sugars. The pentofuranose sugars found in DNA and RNA adopt puckered conformations that minimize steric clashes and maximize favourable electronic interactions. While many different sugar pucker conformations are possible, including many twist (2 carbon displacement) and envelope (1 carbon displacement) puckers, the most commonly populated conformations are C3'-endo (North) and C2'-endo (South).[18] The term ‘endo’ refers to the position of the atom relative to C5' and the nucleobase. In a C2'-endo sugar pucker, the C2' atom is positioned on the same face of the sugar as both the nucleobase and C5', with the C3' atom being positioned on the opposite face (exo positioning). The energy barrier between the two conformations is low for DNA, where as, RNA tends to adopt the C3'-endo conformation due to steric clashes between the C2'-OH group and the nucleobase when adopting the C2'-endo conformation (**Figure 1.4**).[18] The low energy barrier for DNA results in a greater impact from

external sources such as low humidity and/or high salt, which will shift the conformation preference towards the C3'-endo (North) sugar pucker.[18]

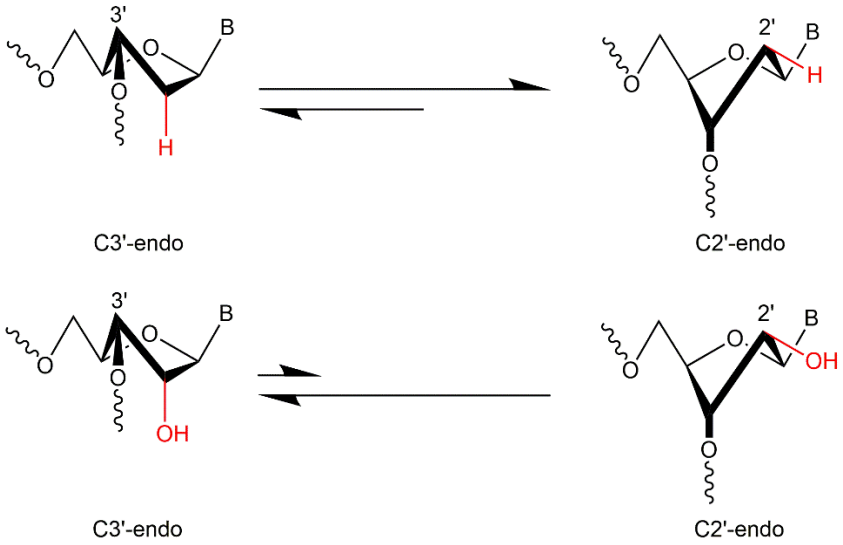

Figure 1.4: Pentofuranose Puckering in DNA and RNA.

This variable sugar puckering is what allows for the formation of numerous duplex structures in both DNA and RNA. DNA can adopt both A- and B-form helices (**Figure 1.5**). In the B-form helix the DNA nucleosides adopt a C2'-endo sugar pucker which represents an average conformation that is highly dependant on both environmental conditions and the specific sequence involved.[19] B-form helices are generally formed under hydrating conditions, and are favoured by mixed-base sequences.[19] The driving force for the formation of helices from ssDNA is the formation of favourable hydrogen bonds between complementary nucleobases (~ 2 kcal mol^{-1}); the sheltering of these hydrophobic nucleobases from the polar solvent, which leads to hydrophobic stacking; and solvation of the negatively charged phosphate backbones.[19] It is important to note that in the cell DNA rarely adopts a true duplex shape due to the packing necessary to fit all our genetic information into the nucleus. It is also worthwhile to point out that

nucleobases possess tautomeric forms (keto-enol, and amine-imine). However, at physiological pH nucleotides exist almost exclusively in the keto and amine forms.[18]

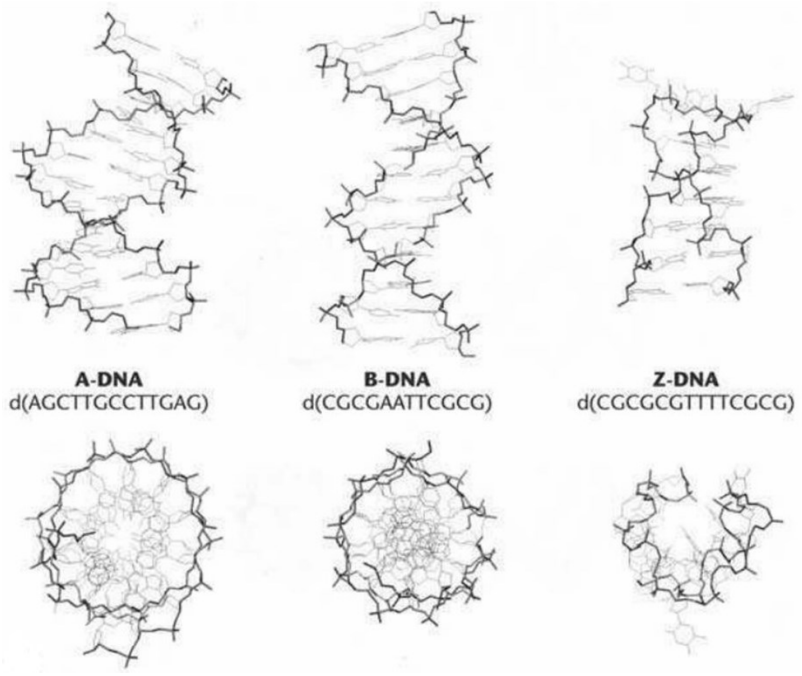

Figure 1.5: Structures of A, B, and Z-form DNA Determined by X-Ray Crystallography.[19] Reproduced with Permission by John Wiley and Sons.

B-DNA is the form originally described by Watson and Crick,[8] and is composed of two strands of DNA which run in an antiparallel fashion to form a right-handed duplex. This means that one strand runs in the 5' to 3' direction, where as, the other strand runs from 3' to 5'. There are roughly 10 bp per helical turn with a helical pitch, the distance for one complete turn of the helix, of 34 Å.[19] As a result, the nucleobases can adopt the optimal 3.4 Å Van der Waals separation distance. In the B-form duplex, the bases are positioned in the duplex core perpendicular to the helical axis as shown in **Figure 1.5**. As previously mentioned, a reduction in humidity or an increase in salt concentration can lead to a shift in the DNA sugar pucker towards the C3'-endo conformation.[18] This results in DNA adopting a right-handed, A-form duplex structure. Complementary RNA can also adopt this duplex form due to the C3'-endo sugar pucker being

more energetically favourable.[19] In contrast to the B-form duplex, the A-form duplex is more compressed with roughly 11 bp per helical turn and a helical rise of 28 Å.[19] The distance between successive base pairs is 2.56 Å which necessitates tilting of the base pairs by 20 ° to maintain the optimal 3.4 Å separation distance.[19] The A-form duplex has a slightly larger diameter (23 Å vs 20 Å) when compared to the B-form duplex, due to the bases not overlapping along the helical axis, as is the case for B-form DNA (**Figure 1.5**).

The hybridization of DNA (or RNA) leads to an asymmetrical hydrogen bonding motif that results in the formation of major and minor grooves (**Figure 1.6**). The major groove of B-DNA is wider than the minor groove, with both having similar depths.[19] Proteins that bind to DNA in a sequence-specific manner will tend to bind in the major groove due to the enhanced variability in the acceptor-donor patterns of the base pairs.[19] Proteins that bind in a more nonspecific manner tend to bind in the minor groove of the duplex, as will water molecules and ions which can help to stabilize the groove.[19–21] In A-form DNA, the major groove is deep and narrow, where as, the minor groove is shallow and wide.

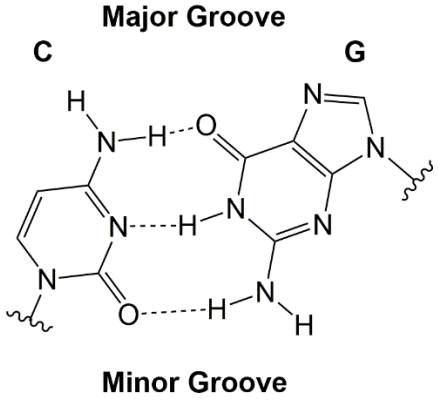

Figure 1.6: Location of the Major and Minor Grooves Relative to the Edges of the C:G Base Pair.

A demonstration of the polymorphism of DNA, the ability for DNA to take on many distinct forms, is shown with the discovery of Z-form duplex DNA (**Figure 1.5**). This duplex structure is left-handed, in contrast to both the A- and B-forms, requires the presence of Mg^{2+}, and only forms from regions of alternating C/G base pairs.[22] The repeating unit contains 12 bp per turn, with one base in a syn orientation and the other in an anti orientation (in contrast to A- and B-duplexes which have their bases positioned in an anti configuration).[19,23] In Z-form DNA there is a deep and narrow minor groove and an almost negligible major groove.[19] The term 'Z-DNA' comes from the irregular, zig-zagged nature of the DNA backbone. Research has shown that Z-form DNA may be stabilized by the binding of topoisomerases to the underlying dsDNA.[24]

Due to the additional hydroxyl group located at the C2'-position, RNA is capable of engaging in a variety of intramolecular interactions. While typically single-stranded, RNA can adopt a number of structures included loops, bulges, junctions (3WJ and 4WJ), duplexes from long range interactions, and pseudoknots.[18] These motifs all help to expand the library of structures that RNA can adopt both in vivo and in vitro.

1.2 Alternative Nucleic Acid Structures

In addition to the standard Watson and Crick hydrogen bonding, both DNA and RNA can adopt numerous non-canonical motifs which can lead to the formation of higher ordered structures such as triplexes, quadruplexes, and other duplex structures. Approximately 60 % of RNA engages in traditional Watson-Crick hydrogen bonding, with a large proportion of the remaining 40 % engaging in other kinds of edge-to-edge interactions with complementary base(s).[25] There are a total of three different nucleobase edges where hydrogen binding interactions can occur. These are

referred to as the Watson-Crick edge, the Hoogsteen (purines) or C-H (pyrimidines) edge, and the Sugar edge (**Figure 1.7**). Any edge from a nucleobase can potentially interact with any other edge on the complementary base. Moreover, these interactions can occur with either a cis (same direction) or trans (opposing directions) arrangement of the glycosidic bonds resulting in 12 different possible interaction 'families' (**Table 1.1**).[25] In DNA, these Hoogsteen edge interactions can also occur,[26,27] but interactions with the sugar edge are far less significant than with RNA due to the lack of the C2'-OH functionality.

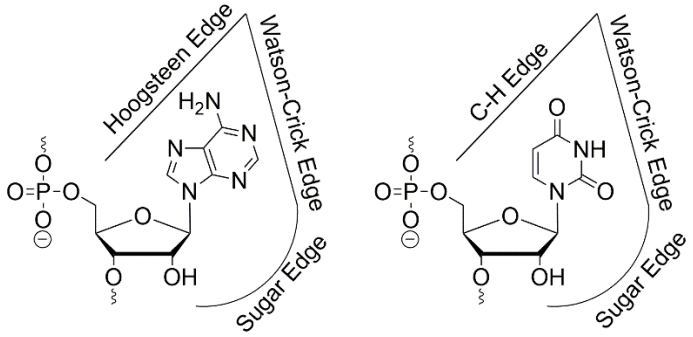

Figure 1.7: Interacting Edges of RNA.[25] Adapted with Permission from Cold Spring Harbor Laboratory Press.

No.	Glycosidic Bond Orientation	Interacting Edges	Strand Orientation
1	Cis	Watson-Crick/Watson-Crick	Antiparallel
2	Trans	Watson-Crick/Watson-Crick	Parallel
3	Cis	Watson-Crick/Hoogsteen	Parallel
4	Trans	Watson-Crick/Hoogsteen	Antiparallel
5	Cis	Watson-Crick/Sugar Edge	Antiparallel
6	Trans	Watson-Crick/Sugar Edge	Parallel
7	Cis	Hoogsteen/Hoogsteen	Antiparallel
8	Trans	Hoogsteen/Hoogsteen	Parallel
9	Cis	Hoogsteen/Sugar Edge	Parallel
10	Trans	Hoogsteen/Sugar Edge	Antiparallel
11	Cis	Sugar Edge/Sugar Edge	Antiparallel
12	Trans	Sugar Edge/Sugar Edge	Parallel

Table 1.1: The 12 Main Nucleic Acid Base Pair Families.[25] Adapted with Permission from Cold Spring Harbor Laboratory Press.

One non-canonical higher order structure which has been found to form is the i-motif. This motif forms from the stacking of intercalated hemiprotonated cytosine-neutral cytosine (C^+:C) base pairs under acidic conditions (**Figure 1.8**).[28,29] The structure was solved by NMR spectroscopy as a tetramer formed from d(TCCCCC),[30] it has since been shown to form in an intramolecular fashion from one single DNA strand derived from the telomere.[28]

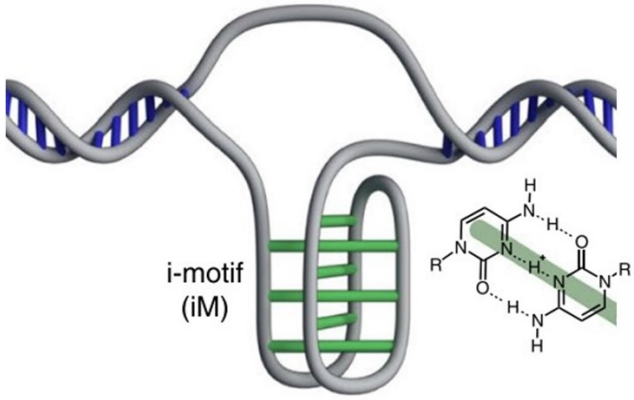

Figure 1.8: I-Motif Structure.[31] Adapted with Permission from Springer Nature.

For a long time, it has been speculated that i-motif formation may play a role in regulatory functions, but the requirement of acidic conditions for its formation led people to question its significance in biological systems.[32,33] Thankfully, studies have shown that i-motifs can forgo the low pH requirement for formation in the cases of molecular crowding[34] and transcription-induced negative superhelicity.[35] Recently, using antibody fragments which bind to these structures, i-motifs have been shown to form in vivo.[31] Beyond DNA, this structure has been observed for modified nucleosides such as L-DNA.[36] L-DNA is constructed from L-deoxyribose, the molecular mirror image of D-deoxyribose, which is normally found in nucleic acids in nature. The inverted chirality of this structure may be useful for the building of future DNA nanomaterials based on

this motif. The recent design of a DNA nanosensor for the monitoring of ligand-induced i-motif formation could allow for the identification of other routes for i-motif construction.[37]

In addition to the i-motif, other quadruplex structures such as the G-quadruplex, which are built around G-rich segments of DNA, are capable of being formed. Hydrogen bonding interactions between the Hoogsteen face of one base with the Watson-Crick face of another leads to the formation of cyclical G-quartets (**Figure 1.9**).[38] G-quadruplexes can form in either an intermolecular or intramolecular fashion with the strands in either a parallel or antiparallel orientation.[38]

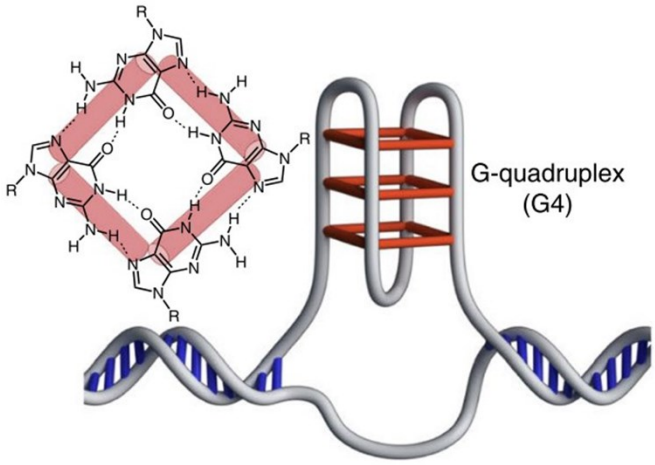

Figure 1.9: G-Quadruplex Structure.[31] Adapted with Permission by Springer Nature.

The inclusion of a monovalent cation such as sodium or potassium is required for their formation, where, the cation will position itself at the center of these G-quartets.[39] These structures are often more stable than dsDNA in vitro, with slower unfolding kinetics.[40] This would suggest that the formation of G-quadruplexes in vivo would severely hinder the metabolism of both RNA and DNA.[38] Stretches of DNA which can lead to the formation of these quadruplex structures are often found throughout the human genome including at the telomers, promoter sequences of genes/oncogenes,[41] and near DNA replication origins.[42] As a result, a lot of focus has been paid

on deciphering what roles this structure could have in cellular gene regulation and what ligands/small molecules could be used to potentially interfere with oncogene expression.[43] Recent work has shown that these structures are involved in telomere elongation and maintenance,[44,45] the initiation of DNA replication,[46] mRNA transcription,[47,48] and protein translation.[49]

Another major class of non-canonical nucleic acid structures are triplexes. These structures form from the association of a third ssDNA or RNA (TFO) with a preformed duplex. This third strand can associate with either the major or minor grooves, and does so in a way which does not disturb the underlying duplex.[50] Minor-groove triplexes are usually not stable in isolation but do form within large RNAs or from RNA-protein interactions.[50–53] Naturally-occurring triplexes are observed in the telomeres,[54,55] within mRNA pseudoknots,[56,57] in long non-coding RNAs (lncRNA),[58] ribosomal RNAs,[53] and many other locations.[50] Generally, the underlying duplex needs to have one strand which is purine-rich, with the other strand being pyrimidine-rich. In a pyrimidine triplex motif, a pyrimidine rich TFO will bind parallel to the purine strand of the duplex through Hoogsteen hydrogen bonding interactions (T:**A:T** and C^+:**G:C** triplexes (Bold denoted underlying duplex)) (**Figure 1.10**).[59] It is important to emphasize that pyrimidine triplexes containing cytosine are pH-dependant due to the protonation of cytosine being required (C^+:**G:C**).[59] In contrast, in a purine triplex motif, a purine-rich TFO will bind antiparallel to the purine strand of the duplex through reverse-Hoogsteen hydrogen bonding interactions (A:**A:T** and G:**G:C** triplexes) (**Figure 1.10**).[59] The presence of monovalent cations, especially potassium, will inhibit the formation of the purine motif triplexes because they will preferentially form four-stranded G-quadruplexes instead.[60]

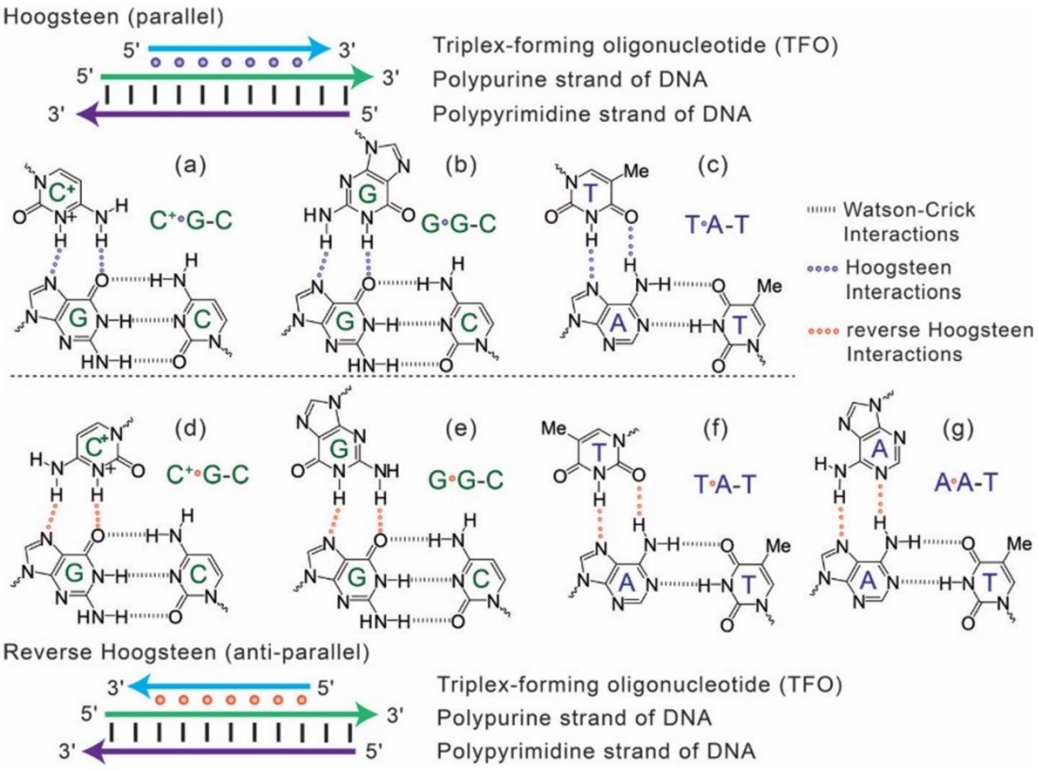

Figure 1.10: Binding Motifs of Nucleic Acid Triplexes.[61] Reproduced with Permission by John Wiley and Sons.

A variety of duplexes, triplexes, and quadruplexes can also be formed through the association of specific metal ions.[62] These metals, Ag, Hg, Fe, Zn, Cu, Ni, etc., can lead to the formation of structures which would normally be unstable or highly disfavoured.[62] Other motifs, such as DNA junctions, can also be constructed using metal catalysis.[63]

1.3 Applications of Nucleic Acids

Nucleic acids have found uses in a variety of fields including medicine, nanotechnology, structural biology, and modern computing.[64–67] While originally viewed as a store of our genetic information, the structures of DNA (and RNA) have both been harnessed in the modern age for

applications which would have seemed unfathomable 68 years ago when the DNA structure was originally reported by Watson and Crick. In today's age, just as much research is paid to harnessing nucleic acids for our own purposes as is paid to understanding how these molecules behave in nature.

Medicinal research is currently being performed around the globe on how nucleic acids can be used, both as a therapeutic drug treatment for a variety of diseases and conditions, and as a vehicle to allow for targeted drug delivery. With the recent declaration of a worldwide pandemic due to the COVID-19 virus, several mRNA vaccines have been approved (with many others still in clinical trials) that promote the production of antibodies to protect against this virus.[68–70] Besides antibody production, the other main pathways that incorporate nucleic acids are antisense therapies, RNAi, and CRISPR-Cas9 mediated gene editing.[71]

In antisense therapies, a therapeutic oligonucleotide is synthesized that is complementary to a target mRNA. This oligonucleotide, once administered, will then bind to the target mRNA in vivo leading to eventual knockdown of the target. Two different pathways exist depending on the design of the drug. In the RNase H recruitment route (**Figure 1.11 B**), the ASO contains regions of RNA (for strong binding to the target) and DNA (to allow for DNA/RNA hybrid duplex formation).[72] The presence of this DNA/RNA hybrid leads to the recruitment of RNase H, a nuclease, which will degrade the mRNA strand of double stranded DNA/RNA, leading to gene knockdown.[73] In the other route (**Figure 1.11 C**), the hybridization of the ASO with the target mRNA leads to a blocking of protein interactions, making it impossible for protein translation to occur.[74] Recruitment of RNase P is also possible with certain guide sequences (**Figure 1.11 D**).

A second nucleic acid-based therapy, RNAi, is a therapeutic approach which utilizes the cell's native machinery to downregulate gene expression (**Figure 1.11 A**). Within cells, small

interfering RNA (siRNA) can form short hairpin (shRNA) motifs which will be cleaved by the protein Dicer to give short fragments of double-stranded siRNA.[75] In contrast to this endogenous process, therapeutic siRNA does not require Dicer activity as it is usually introduced as a pre-formed, short, double-stranded fragment.[76] The siRNA is then loaded into the RISC protein complex, where the sense strand is removed followed by binding of the targeted mRNA.[75] Another protein, AGO2, then cleaves the target mRNA resulting in a knockdown of gene expression.

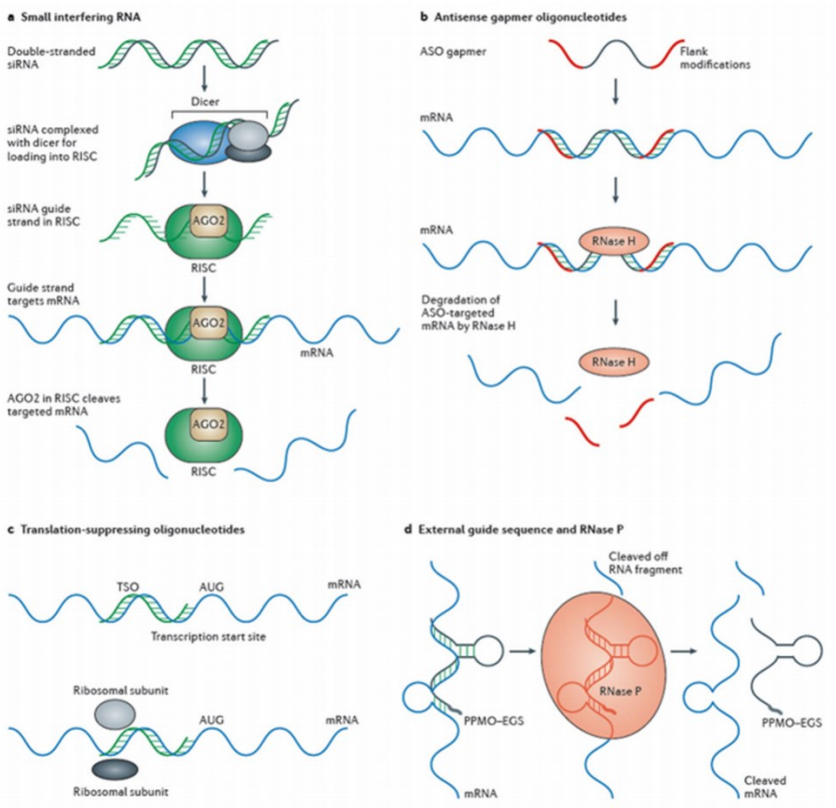

Figure 1.11: Nucleic Acid Therapeutic Mechanisms.[77] Reproduced with Permission by Springer Nature.

More recently, the gene editing process known as CRISPR-Cas9 (Clustered Regularly Interspaced Palindromic Repeats) has been investigated as a therapeutic approach. This approach is based on an adaptive immune system that was originally found in prokaryotes that stores

information from previous viral infections as a means of protecting against future infections.[78] Regions of DNA which contained short palindromic repeats were observed, with viral DNA in between.[78] The bacteria employ a series of Cas proteins (CRISPR-associated proteins) to deposit a piece of DNA from the viral vector within the host genome.[79,80] Referred to as CRISPR or CRISPR-Cas9 (for the technique using a specific Cas protein), this methodology has been extensively developed to the point where, by using custom guide RNA (gRNA), genes in bacteria,[81] humans,[82] or plants[83] can be reliably genetically modified by hijacking this process. The development of this process led to Emmanuelle Charpentier and Jennifer A. Doudna winning the 2020 Nobel Prize in Chemistry.[84,85]

In addition to being used as a therapeutic, nucleic acids have also found uses as carriers of drug molecules through either nucleic acid origami or spherical nucleic acids. The predictability of nucleic acid hybridization, and the high stability of DNA three-way and four-way junction motifs (3WJ and 4WJ)[86] has allowed for the synthesis of a vast array of nucleic acid architectures including cubes,[87] quadrilaterals,[88] truncated octahedrons,[89] and many others (**Figure 1.12**).[90]

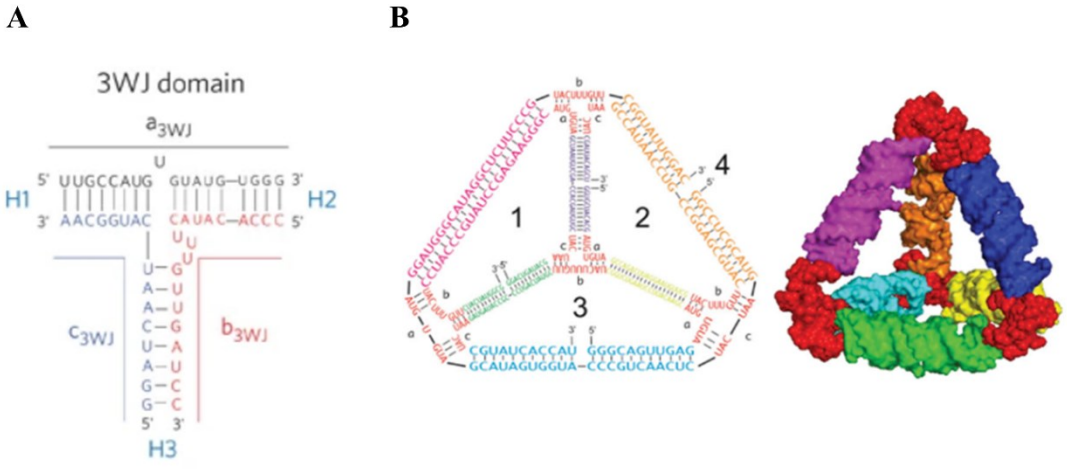

Figure 1.12: DNA Origami Structures. (**A**) DNA 3WJ motif.[86] (**B**) Self-assembled RNA Tetrahedron.[91] Reproduced with Permission by Springer Nature and John Wiley and Sons.

Due to the ease at which nucleic acids can be modified, these structures have been functionalized with a variety of aptamers and targeting ligands which can direct delivery of therapeutics to the desired location.[91,92] Furthermore, the inclusion of stimuli responsive linkages allows for the tailoring of drug release with changes in pH,[93] or light,[94] among others. DNA origami nanomaterials have been shown to be useful in slowing the growth of both Gram positive and Gram negative bacteria without having any detrimental effect on neighbouring mammalian cells, possibly demonstrating their future use as a means of overcoming antibiotic drug resistance.[92]

Nucleic acids can also be used to facilitate the delivery of drug molecules by encompassing the drug in a nucleic acid sphere. The covalent linking of an anticancer drug paclitaxel to DNA leads to the formation of a micellar nanostructure (**Figure 1.13**).[95] Normally, nucleic acids have a hard time passing through cellular membranes due to their negative charge, but these micellar structures can engage in scavenger receptor-mediated endocytosis which leads to cellular uptake in most cell types.[96,97] This paclitaxel-functionalized nucleic acid sphere was able to be taken up by SK-OV-3 cells (Human ovarian cancer cell line) followed by a reduction of an internal disulfide bond leading to release of the drug payload.[95] Other possible delivery mechanisms include using polymer-based delivery systems[98] or nanoparticles.[99]

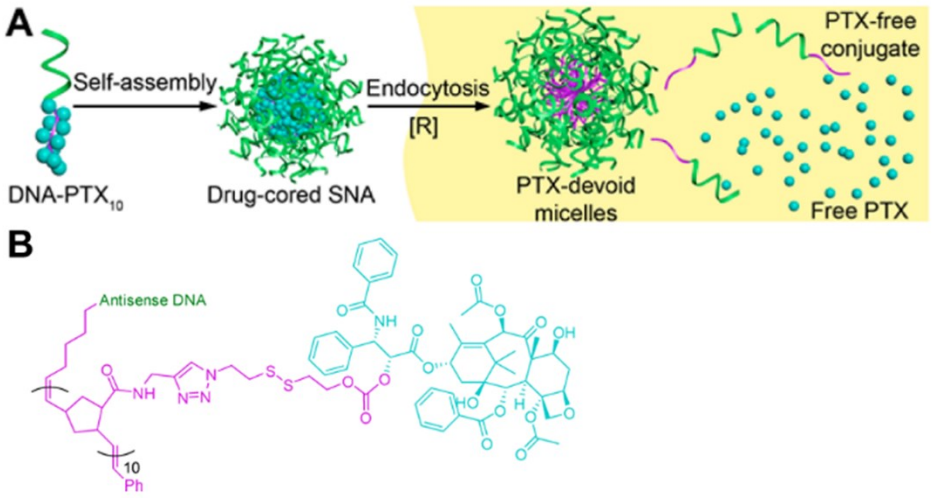

Figure 1.13: Spherical Nucleic Acids.[95] (**A**) Assembly of Micellar Structure and Bioreduction-Catalyzed Release of Drug Cargo. (**B**) Structure of the DNA/Drug Conjugate. Reproduced with Permission from *J. Am. Chem. Soc.* 2016, 138, 34, 10834–10837. Copyright 2021 American Chemical Society.

The last application, and the most relevant to this work, is the construction of stimuli-responsive nucleic acid switches. Much like the previously discussed Z-DNA and i-motifs, there are numerous nucleic acid structures which are responsive to changes in the environment. These changes can occur due to fluctuations in pH (i-motifs),[100] salt concentration (Z-DNA),[19] temperature,[101] or due to external influences such as light,[94,102] sound waves,[103] or metal ions/ligand binding.[104] Nucleic acids which are pH-responsive can potentially have applications for cancer treatment due to the more acidic nature of cancer cells in comparison to healthy human cells.[105,106] The Liu group were able to use the pH-responsiveness of i-motif formation to design a nucleic acid structure which could form a reversible DNA hydrogel network (**Figure 1.14 A**).[107] More recently, nucleic acid-functionalized MOFs were developed which were 'locked' with either a pH-responsive or metal-ion-responsive nucleic acid group (**Figure 1.14 B**).[108] A decrease in pH, or the addition of Mg^{2+}/Pb^{2+}, would then lead to an unlocking of these MOF nanoparticles and a corresponding release of the tethered anticancer drug.[108]

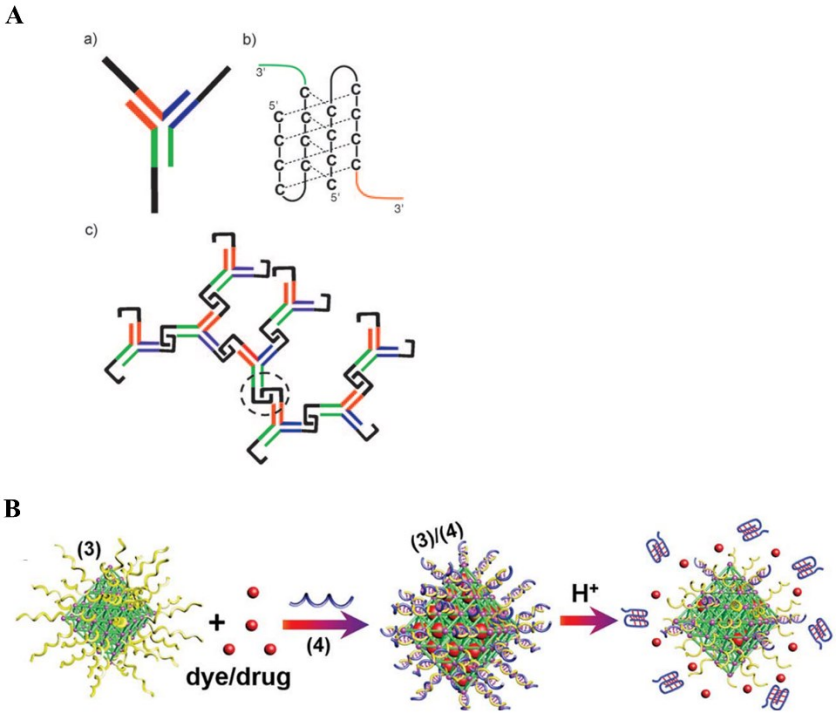

Figure 1.14: pH-Responsive Nucleic Acids. (**A**) i-motif Driven DNA Hydrogel.[107] (**B**) i-motif Driven Drug Release.[108] Reproduced with Permission by John Wiley and Sons and The Royal Society of Chemistry.

In all these applications (as a therapeutic, as a drug carrier, and as a stimuli-responsive switch) it is important to emphasize that native nucleic acids are generally not used. In all cases, the DNA or RNA is usually heavily chemically modified to improve target binding, and improve the resistance against nuclease digestion in vivo.[109,110]

1.4 Poly(A) RNA Duplex

In the late 1950's it was discovered that polyadenylic acid of a minimum of 29 rA units could lead to the formation of fibers under acidic conditions.[111] This was originally proposed to be a result of the overlap of rA regions to form an interrupted helix.[111,112] In 1961, Rich used X-ray

fiber diffraction analysis under these acidic conditions to solve the molecular structure.[113] It was proposed that a right-handed, parallel-stranded helix was being formed due to interactions with the Hoogsteen face of the nucleobases.[113] In this motif, the adenine-adenine base pairing is being stabilized by hydrogen bonding interactions between the N6 exocyclic amino group and the N7 internal nitrogen of the opposing nucleoside.[113] Furthermore, protonation of the N1 position under these acidic conditions leads to favourable interactions with the opposing phosphate backbone (**Figure 1.15 A**).[113]

In 2013, Gehring, Wilds and coworkers, were the first to successfully crystallize the poly(A) RNA duplex which diffracted to 1.0 Å resolution.[114] In contrast to the experiments performed by Rich, this crystal analysis was performed at neutral pH with help from the addition of a fragment of the poly(A) binding protein (PABP).[114] Their results were similar to those of Rich, namely, that the poly(A) duplex is right-handed, and the strands are oriented in a parallel fashion. Moreover, the binding between adenines was found to be N7-amino symmetric, where the N7 atom forms a hydrogen bond to the exocyclic amine on the opposing nucleobase.[114] They also observed an additional hydrogen bond between the phosphate backbone and the second proton from the exocyclic amine.[114] In total, four hydrogen bonding interactions are present, with 180 ° rotational symmetry (**Figure 1.15 B**).

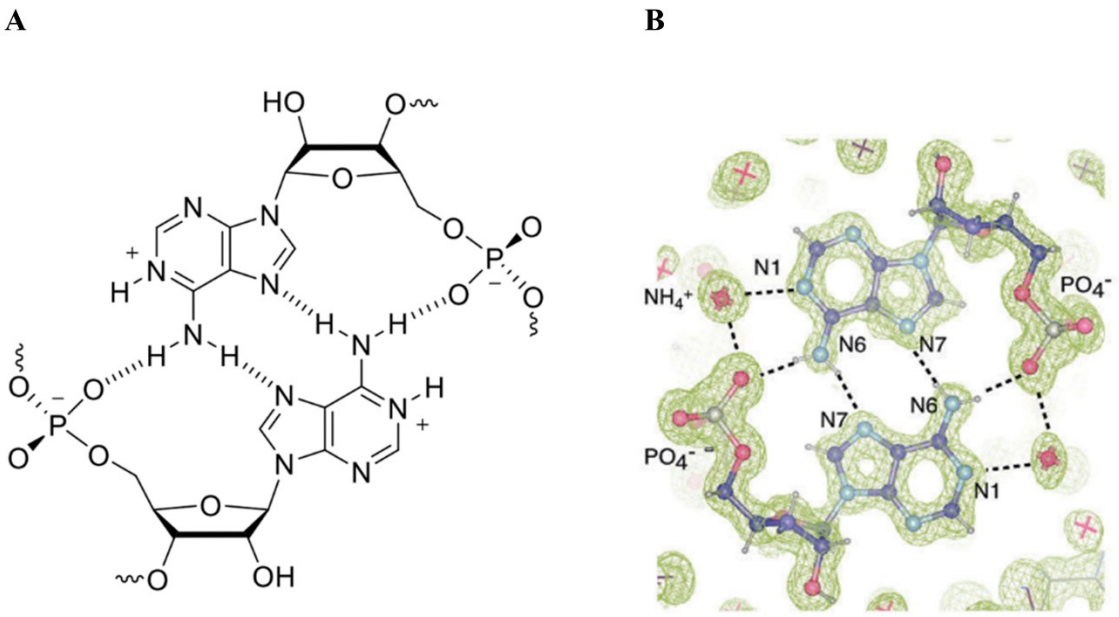

Figure 1.15: Poly(A) RNA Binding Motifs. (**A**) Under Acidic Conditions.[115] (**B**) At pH 7 with Added NH_4^+.[114] Reproduced with Permission by Oxford University Press and John Wiley and Sons.

Due to crystallization being performed at pH 7.2, protonation of N1 was not observed. Instead, an ammonium cation (NH_4^+) was positioned to interact with both the N1 position and a nonbridging backbone oxygen atom (**Figure 1.15 B**).[114] The structure formed by rA_{11} was a parallel stranded duplex of ten base pairs with a single nucleotide overhanging at each end, leading to a larger, continuous duplex (**Figure 1.16**).[114] The sugar puckers were confirmed to be C3'-endo (North), with trans glycosidic bonds, a pitch height of 30 Å for 8 bp, and a helical rise of 3.7 Å.[114] The helical rise would suggest that this structure is less compressed than either A- or B-form helices, however, the additional interaction between the N1 atom, ammonium cation, and the phosphate backbone leads to additional compacting of the structure[114] (the same occurs for the interaction between N1 and the backbone under acidic conditions). Crystallization of rA_7 at pH 3.5 in the presence of ammonium cations shows largely similar results to the structure solved at

neutral pH, albeit in more of a staggered zipper arrangement with alternating protonated and unprotonated N1 atoms.[116]

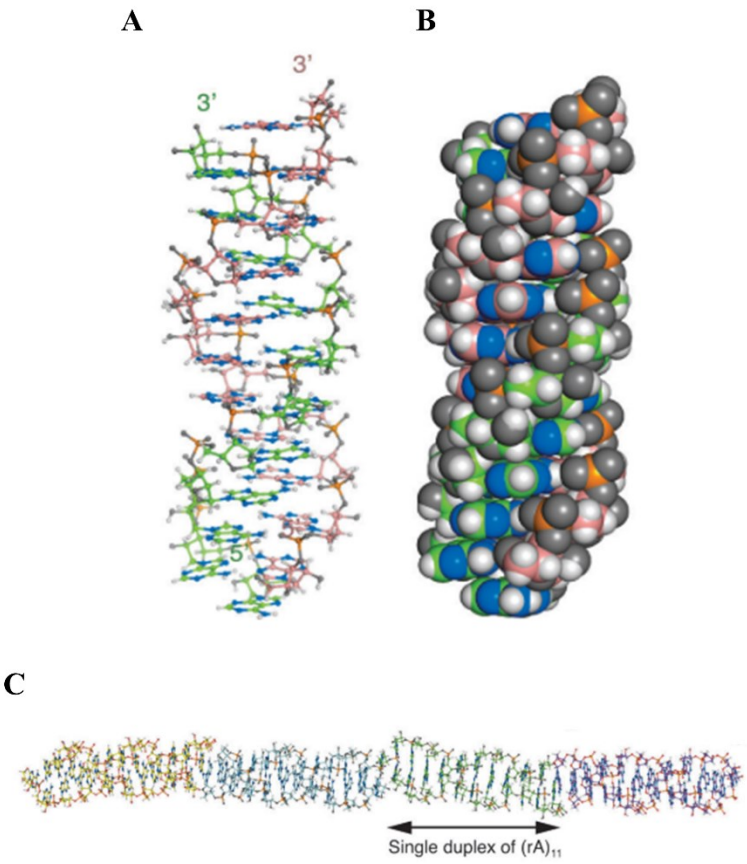

Figure 1.16: Crystal Structure of poly(A) RNA at pH 7.2 in the Presence of NH_4^+.[114] (**A**) Ball and Stick Model. (**B**) Space Filling Model. (**C**) Observed Continuous Duplex. Reproduced with Permission by John Wiley and Sons.

It has been proposed that these poly(A) RNA duplexes could be formed in vivo from the protein-mediated protonation of mRNA poly(A) tails, potentially as a means of inhibiting further polyadenylation, regulating the poly(A) binding protein, or to stabilise the mRNA.[117] Another hypothesis is that poly(A) RNA functions as a sensor for acid-catalyzed cellular stress.[118] Under acidic conditions, poly(A) duplex formation could lead to a clustering of mRNA, inhibiting their translation, until the cellular pH is restored.[118]

To further understand these structures, our group sought to study the influence of select chemical modifications to the C2'-position of the ribose sugar. 2'-deoxyribose (dA), 2'-*O*-methyl-ribose (mA), 2'-deoxy-2'-fluoro-ribose (rFA), arabinose (aA), and 2'-deoxy-2'-fluoro-arabinose (aFA) modifications were all explored[115] (**Figure 1.17**).

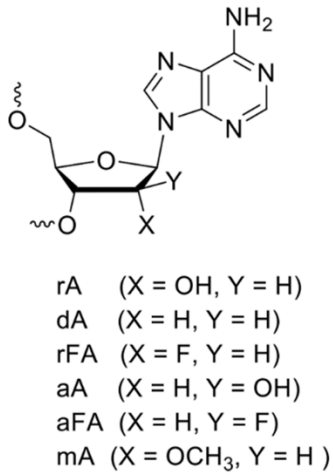

Figure 1.17: Previously-Explored poly(A) Modifications.[115] Reproduced with Permission by Oxford University Press.

Homopolymers of 2'-deoxyadenosine have been previously reported,[119,120] however, it was found that modification of the poly(A) RNA duplex with 2'-deoxyribose led to a decrease in thermal stability (~ -8 °C/mod for 9-mers and ~ -3 °C/mod for 16-mers).[115] Under these conditions, no duplex formation was observed for fully modified 2'-deoxyribose sequences.[115] Through NMR and X-ray crystal analysis, it was determined that the destabilization brought about by this modification was mainly due to its preference for the C2'-endo sugar pucker, leading to a possible loss in preorganization for duplex formation.[115]

The arabinose and 2'-deoxy-2'-fluoro-arabinose modifications were also found to be destabilizing, possibly due to their preference for other sugar puckers.[115] In contrast, the 2'-*O*-methyl-ribose and 2'-deoxy-2'-fluoro-ribose modifications, which favour the C3'-endo sugar

pucker normally found in poly(A) RNA, were found to be stabilizing at pH 4 and in the presence of ammonium cations.[115] The variety of effects brought about by these modifications emphasizes the need to further explore how chemical modifications can influence the poly(A) RNA duplex, possibly facilitating its use as a pH- or NH_4^+ responsive nanomaterial.

Recently, the Gleghorn group constructed a DNA nanoswitch based upon the poly(A) RNA duplex (**Figure 1.18**).[118] Their design allowed for the detection of hetero-duplex interactions while ignoring unwanted homo-duplexes, all while using concentrations far lower than needed for traditional analyses.[118] Using this design, they could differentiate between duplexes of different lengths and modifications.[118] They observed strong interactions for duplexes of poly(rA)/poly(LNA) and poly(rA)/poly(mA), where as, poly(LNA)/poly(LNA) showed no duplex formation.[118] This approach could allow for better discernment of duplex formation, especially hetero duplexes, in future studies.

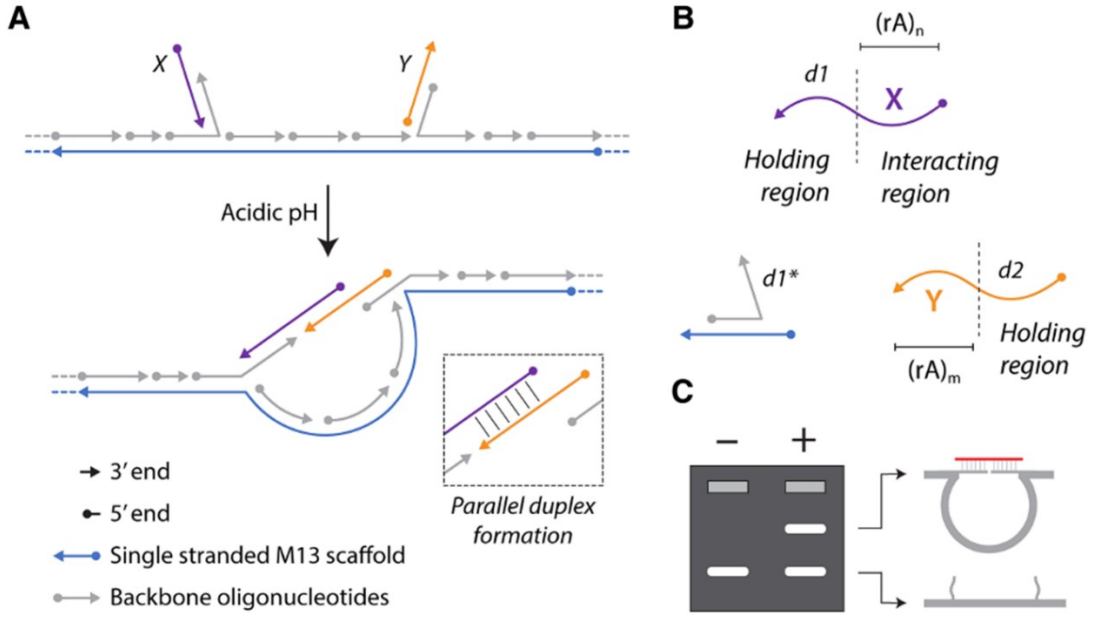

Figure 1.18: Poly(A) Duplex Nanoswitch.[118] (**A**) Loop Formation of Nanoswitch. (**B**) Chimeric Detector Oligonucleotides. (**C**) Detection of Duplex Formation Through Agarose Gel Electrophoresis. Reproduced with Permission by Cold Spring Harbor Laboratory Press.

1.5 Click Chemistry of Nucleic Acids

The field of chemistry contains numerous different reactions that have been used for a variety of applications. The problem with many of these reactions is that they can involve toxic by-products or reagents; they can have very limited applications; some require huge amounts of energy to reach completion; they can lead to complicated purification steps; and many are low yielding. In the eyes of Green Chemistry, many reactions, therefore, fall short of being ideal. In 2001, Barry Sharpless introduced a different way of thinking about reactions, bio(conjugation) reactions especially. He proposed that chemists take a page from nature, and focus on developing reactions that use small building blocks as a feedstock for producing larger molecules through carbon-heteroatom linkages.[121]

In his eyes, a reaction had to meet several stringent criteria to earn the status as a Click reaction. These were: that the reaction be modular, wide in scope, high yielding, produces only inoffensive by-products, easily purifiable products, and the reaction has to be stereoselective.[121] In addition, these reactions should have readily available starting materials, they should be performed in water if possible, and they should be thermodynamically driven.[121] Reactions which met his criteria included: (1) nucleophilic opening of rings (2) cycloaddition reactions and (3) protecting group reactions.[121]

Today, some of the most used Click reactions are the Huisgen 1,3-dipolar cycloadditions. These [3+2] cycloadditions comes in two varieties: the Cu(I)-catalyzed azide-alkyne cycloaddition (CuAAC),[122,123] and the strain-promoted azide alkyne cycloaddition (SPAAC),[124] although others also exist. Azide-alkyne cycloadditions can lead to either a 1,4- or 1,5-triazole product. Under

copper catalysis, only the 1,4-triazole product is formed, where as, with the strain-promoted scheme both isomers can be formed. Recently it was discovered that a ruthenium-catalyzed reaction can selectively lead to the 1,5-product.[125]

These Click reactions have been used extensively in the field of nucleic acid chemistry for the development of triazole backbones,[126,127] to conjugate a variety of small molecules or dyes to DNA/RNA,[128,129] to crosslink nucleic acids,[130,131] and for a host of other applications.[132] These reactions have also been developed with RNA.[133,134]

An approach for the real-time monitoring of Click chemistry DNA crosslinking was recently developed. This approach uses an α-hemolysin nanopore which can recognize the change in current induced by the formation of the forked DNA product (**Figure 1.19**).[135]

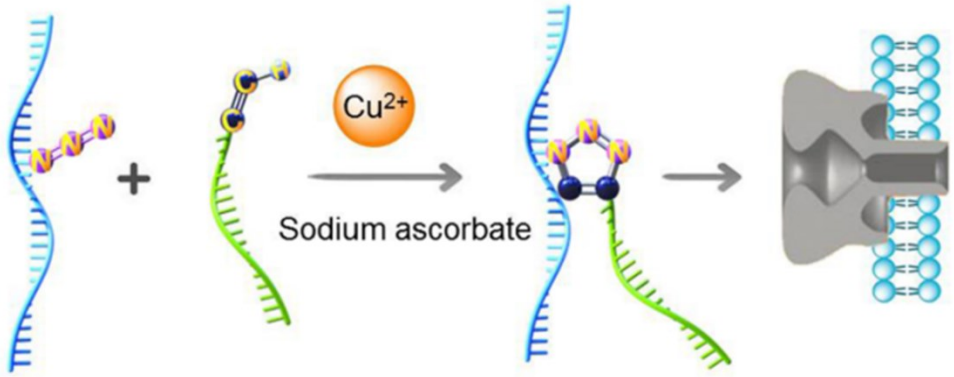

Figure 1.19: Nanopore-Based Real-Time Monitoring of DNA Crosslinking.[135] Reproduced with Permission from A*CS Sens.* 2019, 4, 5, 1323–1328. Copyright 2021 American Chemical Society.

Chapter 2: Purpose and Research Question

The tendency of poly(A) RNA to form a parallel-stranded duplex under acidic conditions or at pH 7 in the presence of ammonium cations has been well established.[113–115,118] Previous work in our lab has also shown the influence of select modifications to the C2'-position of the ribose sugar in these duplexes.[115]

In this work, we seek to expand the scope of chemical modifications by introducing a propargyl functionality at the C2'-*O*-position, thereby opening the door for facile post-synthetic derivatization of the poly(A) duplex through Click chemistry (**Scheme 2.1**). This will allow us to study the influence of both a cationic group, and a polyaromatic hydrocarbon modification on the structure and stability of the poly(A) duplex. The goal of this work was to evaluate what influence these modifications have on both the thermal stability and structure of the poly(A) RNA duplex.

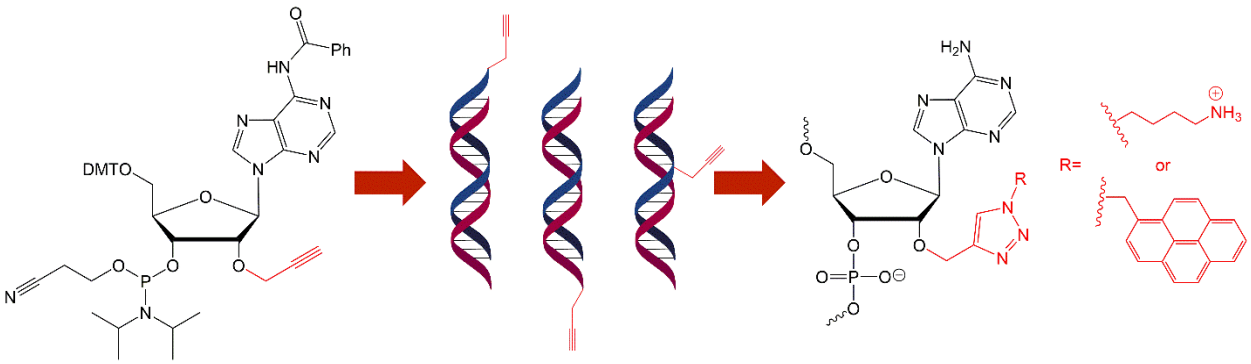

Scheme 2.1: Introduction of C2'-*O*-Propargyl Adenosine into poly(A) Oligonucleotides Followed by Post-Synthetic Click Chemistry Functionalization.

Oligonucleotides of both 11 nt and 16 nt in length were synthesized through SPS with propargyl modifications incorporated in increasing numbers (Chapter 3). Duplex stabilization was determined through UV thermal denaturation analysis with CD and native gel electrophoresis used

to establish if structural changes occurred because of the modification. Following this initial study, the oligonucleotides were coupled to chemically synthesized small molecules to produce the desired conjugates and trends between duplex structure and stability were examined (Chapters 4 and 5).

Finally, a preliminary study into the influence of backbone modifications, LNA and phosphorothioates, on this system were investigated (Chapter 6).

Chapter 3: Influence of C2'-*O*-Propargyl Modifications

3.1 Background on Propargyl-Modified Nucleic Acids

The modification of nucleic acid scaffolds with the propargyl functionality has enabled functionalization of these structures by Click chemistry through the copper(I)-catalyzed azide-alkyne cycloaddition reaction. This can allow for the coupling of a variety of small molecules,[133,136] proteins,[137] creating artificial triazole backbones,[138] or interstrand crosslinking of the DNA or RNA strands.[130,139]

The propargyl group can be incorporated at several different positions including the furanose sugar, or nucleobase with the exact site of incorporation leading to different effects. When incorporated onto the Hoogsteen or C-H edges of a nucleobase, the propargyl group will be positioned to interact at the major groove of a DNA or RNA duplex, which can allow for various studies including the interaction of groove-binding proteins. Modifications such as 7-ethynyl-8-aza-7-deazaadenosine (7-EAA), which contain an alkyne functionality like that of the propargyl group, have been shown to be only slightly destabilizing relative to native adenosine in a 12-mer duplex.[140] This modification, as well as the triazole products following Click chemistry, have also been shown to be well accommodated within A-form RNA duplexes and are capable of being read by reverse transcriptases.[141] The binding of proteins to the 5'-mRNA cap was explored by the Jemielity group. They observed that modification of the N1-position of guanosine with a propargyl group had no significant influence on the binding of either eIF4e (eukaryotic translation initiation factor) or DcpS (decapping scavenger).[142] Other modifications, such as N4-propargyl-deoxycytidine have demonstrated the flexibility of this group by showing the possibility of

conformational rotation to allow for the maintaining of standard Watson and Crick hydrogen bonding.[143]

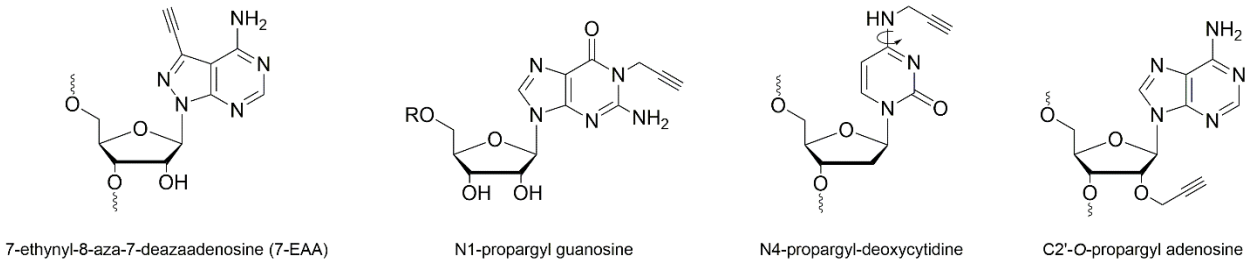

Figure 3.1: Propargylated Nucleic Acids. (R: Triphosphate Linkage to N7-methylguanosine).

Sugar-modified nucleic acids, such as, C2'-*O*-propargyl adenosine have been shown to stabilize RNA duplexes,[144,145] where as, the insertion of C2'-*O*-propargyl-5-methylisocytidine as a point mutation in DNA/DNA duplexes has been found to be destabilizing.[146] The degree of destabilization brought about by this C2'-modification in DNA duplexes depends on the orientation of the two nucleic acid strands. It can be either moderate (parallel stranded duplexes) or mildly destabilizing (antiparallel duplexes).[146] The positioning of propargyl functionality at this C2' position allows for coupling of small molecules or groove-binding proteins within the minor groove of a duplex.

In this work, the influence of C2'-*O*-propargyl inserts in both 11-mer and 16-mer duplexes under both the pH 4 and pH 7, 4.4 M NH_4Cl, conditions required for poly(A) duplex formation will be explored. These modifications were incorporated through SPS (**Figures A.1-A.2**) using commercially available propargylated phosphoramidites from ChemGenes (Wilmington, Massachusetts). Techniques including UV thermal denaturation analysis, CD spectroscopy, and native gel electrophoresis, will be employed as a way of determining what effect this modification has on the stability and structure of the poly(A) RNA duplex.

3.2 UV Thermal Denaturation (T_m) Analysis of C2'-*O*-Propargylated Duplexes at pH 4

To evaluate the influence that the incorporation of the C2'-*O*-propargyl group has on the thermal stability of poly(A) duplexes, the thermal denaturation of duplexes formed by 11- and 16-mers of poly(A) RNA was studied in buffer at pH 4. Moreover, the influence of single and sequential incorporations of the C2'-*O*-propargyl group was investigated (**Table 3.1**).

11-mer	16-mer
rA_{11}	rA_{16}
XrA_{10}	XrA_{15}
rA_5XrA_5	$rA_{10}XrA_5$
$rA_{10}X$	$rA_{15}X$
rA_4XXrA_5	rA_9XXrA_5
rA_4XXXrA_4	rA_8XXXrA_4
XrA_9X	

Table 3.1: Oligonucleotides Synthesized in This Study. (X: C2'-*O*-Propargyl Adenosine).

In **Figure 3.2**, a sigmoidal curve indicative of the transition between two states is observed for the UV thermal denaturation profiles for a series of duplexes formed by the 11-mers containing a single C2'-*O*-propargyl adenosine modification on each strand. With nucleic acids, the formation of an ordered, duplex structure is also associated with a hypochromic transition of the corresponding A_{260} absorbance reading.[147,148] This is caused by the stacking of nucleobases within the core of the duplex which leads to a decrease in the molar extinction coefficients due to the dipole-dipole interactions that occur between the bases.[18] When these duplexes are denatured upon heating, these interactions are broken and the extinction coefficients for the individual nucleobases increase leading to the observed increase in absorbance at 260 nm.

In **Figure 3.2**, all the duplexes formed by the 11-mers exhibit a typical sigmoidal curve upon denaturation of the duplexes into ssRNA. The modified duplexes, those that have been modified at either the 5', middle, or 3'-end, with the C2'-*O*-propargyl adenosine modification, all show transitions that are slightly left-shifted compared to the duplex formed by the rA_{11} control. This is an indication that this modification is destabilizing towards poly(A) duplex thermal stability.

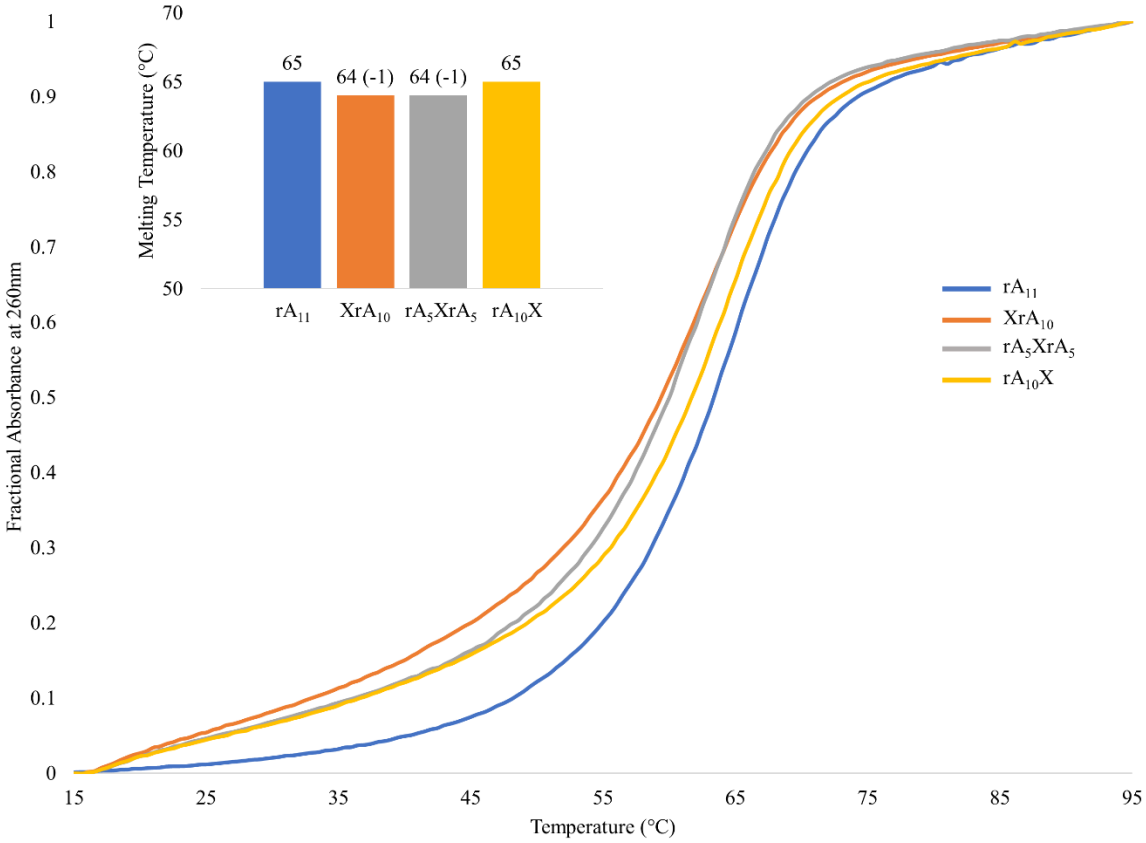

Figure 3.2: UV Thermal Denaturation Profiles of Duplexes Formed by C2'-*O*-Propargyl Modified 11-mers at pH 4. (Buffer: 40 mM Na_2HPO_4, 30 mM citric acid, pH 4). 3.7 µM single strand concentrations.

The inset of **Figure 3.2** shows this change in stability as a change in the T_m value. The incorporation of this modification at either the 5'-end, or in the middle, destabilizes the duplex by

-1 °C, where as, modification of the 3'-end elicits no change in the T_m value. Thus, the incorporation of a single propargyl modification has a negligible effect on stability of the duplex formed by the 11-mer at pH 4, regardless of the location of the modification.

The influence of the C2'-*O*-propargyl modification was also evaluated for the longer duplexes formed by the 16-mer at pH 4. As shown in **Figure 3.3**, the UV thermal denaturation curves all resemble the ideal sigmoidal transition which is normally seen for duplex denaturation. In this case, a slight destabilization of the curve for the duplex that was centrally modified is seen, where as, the others do not show any major changes with respect to the rA_{16} control. It is of note that these melting curves display transitions at much higher temperatures than was the case for the duplexes formed by the 11-mers. A longer duplex, with an increase in the number of base pairs, has a higher T_m value due to increased hydrogen bonding and base stacking interactions.[114] Incorporation of the propargyl modification in a central position of the duplex results in slight destabilization, similar to what was observed for the duplex formed by the 11-mer.

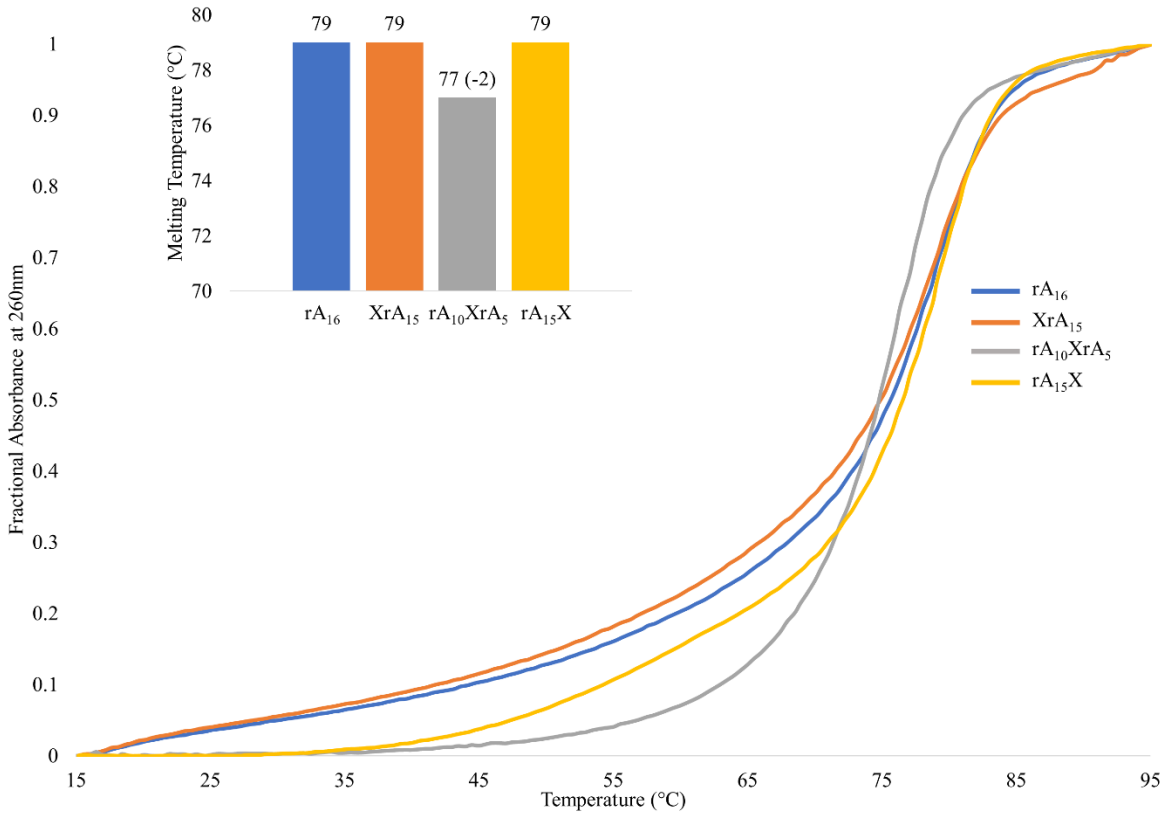

Figure 3.3: UV Thermal Denaturation Profiles of Duplexes Formed by C2'-*O*-Propargyl Modified 16-mers at pH 4. (Buffer: 40 mM Na_2HPO_4, 30 mM citric acid, pH 4). 2.6 µM single strand concentrations.

After having explored the influence of single incorporations on the T_m at pH 4, the study was expanded to evaluate the influence of multiple propargyl modifications at the center of these duplexes.

Figure 3.4 shows the UV thermal denaturation profile for duplexes formed by the 11-mers modified at both the 5' and 3'-ends, which exhibit similar thermal stability to that of the singly modified duplex. In contrast, when the duplex contains two consecutive modifications on each strand at a central position, a slight reduction in thermal stability is observed. This trend continues with the addition of a third propargyl group.

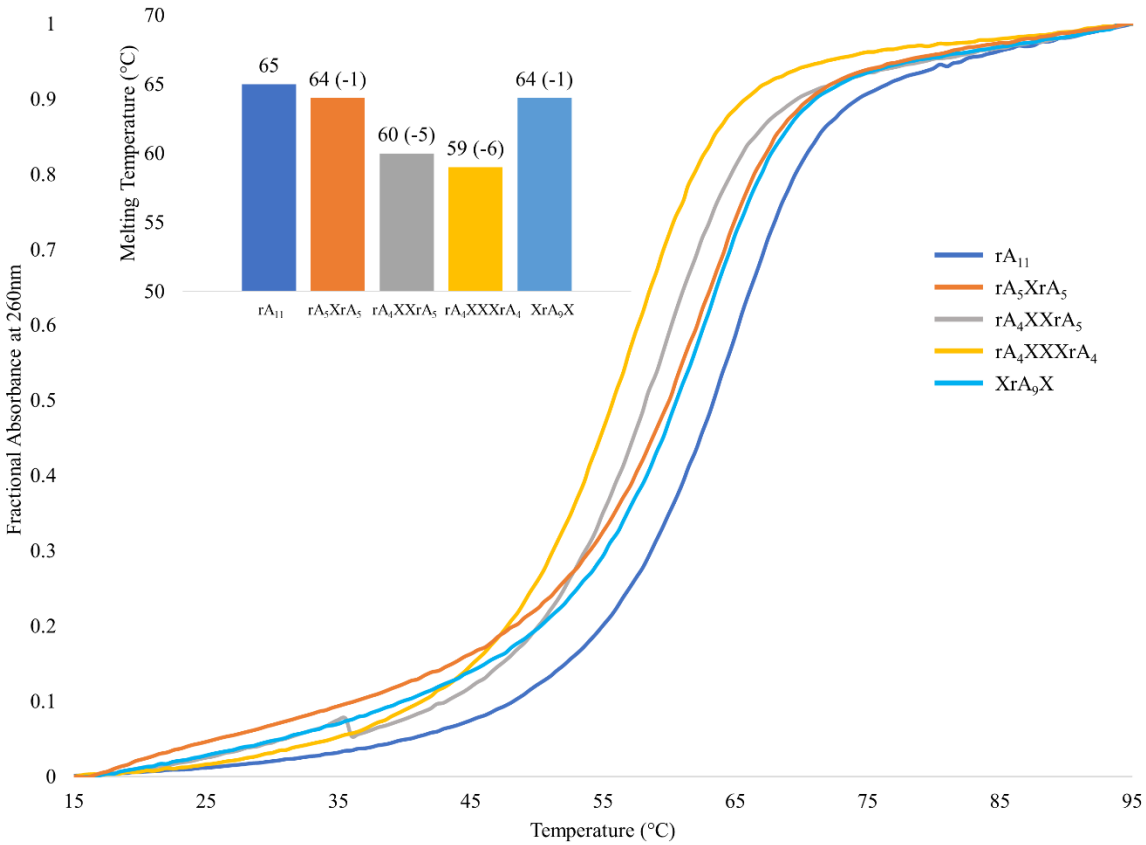

Figure 3.4: UV Thermal Denaturation Profiles of Duplexes Formed by 11-mer poly(A) Containing Successive C2'-*O*-Propargyl Groups at pH 4. (Buffer: 40 mM Na_2HPO_4, 30 mM citric acid, pH 4). 3.7 µM single strand concentrations.

The influence of successive incorporations for a duplex formed by a 16-mer was studied under the same conditions to evaluate the effect of duplex length on stability. In **Figure 3.5**, there is a shifting of the profiles towards lower temperatures, with more insertions leading to a lower T_m. The inset of **Figure 3.5** shows the influence of multiple incorporations on the T_m. This is consistent with the shorter duplexes, where a decrease in duplex stability is observed as more propargyl groups are inserted.

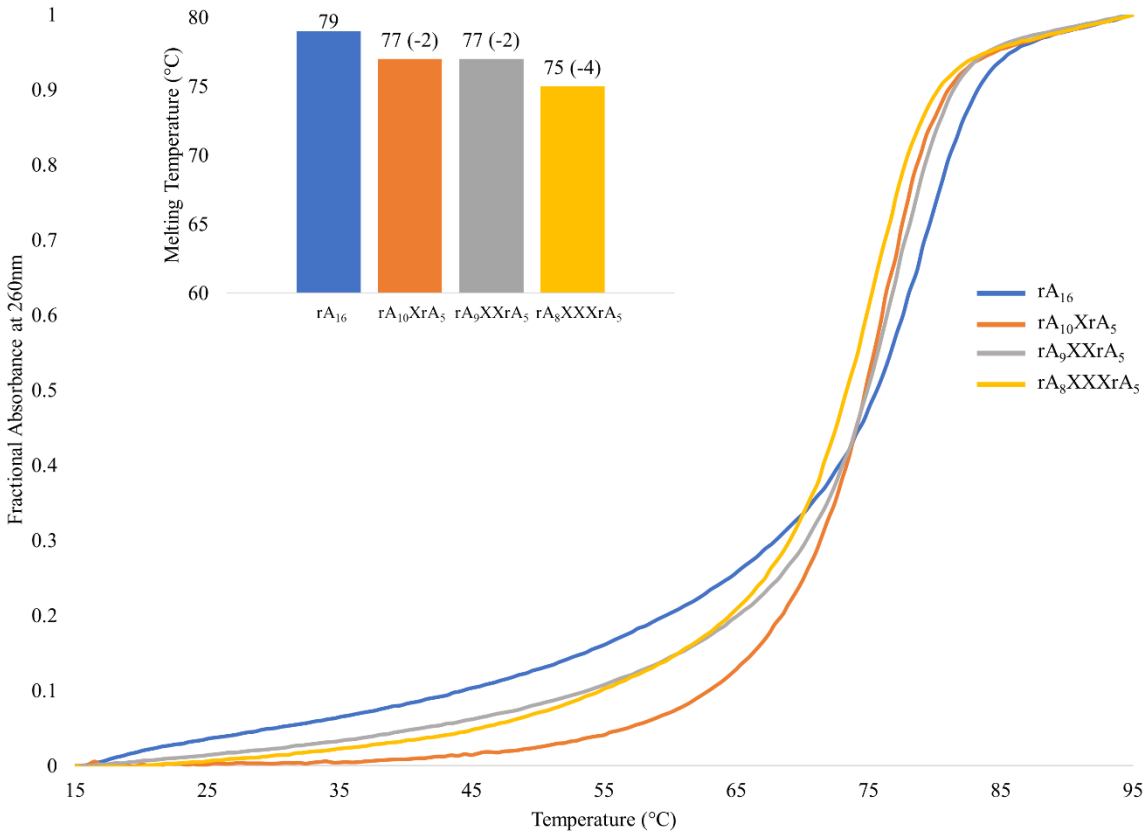

Figure 3.5: UV Thermal Denaturation Profiles of Duplexes Formed by 16-mer poly(A) Containing Successive C2'-*O*-Propargyl Modifications at pH 4. (Buffer: 40 mM Na_2HPO_4, 30 mM citric acid, pH 4). 2.6 μM single strand concentrations.

The reduction in thermal stability for the duplexes formed by the 16-mers is less than what was observed for the shorter, 11-mers. This also agrees with precedence, as generally, modifications will have a greater effect on the stability of shorter duplexes than on longer, more stable, ones. The measured T_m for the duplexes containing one and two central inserts is identical in this case. However, with three inserts the duplex stability decreases by 4 °C.

As discussed earlier, propargyl modifications have been previously reported to be stabilizing towards antiparallel RNA duplexes.[144] One possible explanation for this difference between poly(A) and the A-form RNA duplex could be due to differences in hydration surrounding the C2'-OH group. If these hydroxyl groups experience a higher degree of hydration in poly(A)

duplexes compared to A-form duplexes, then a modification of this position with an alkyl linker would have a larger impact on the surrounding hydration shell leading to a disruption of the favourable hydrogen bonds. Even using high resolution crystallography, determining the exact orientation and hydrogen bonding patterns of first shell water molecules can be difficult.[149]

There is also the possibility that the insertion of the alkyl group is causing steric disruptions within the structure of poly(A). This was not previously observed for the introduction of a methyl group at this same position.[115] In fact, crystal structures of RNA/DNA duplexes have shown that modifications of this length tend to face away from duplexes, where as, longer ones tend to associate more readily with the phosphate backbone or neighbouring nucleobases.[145]

3.3 CD Study of C2'-*O*-Propargylated Duplexes at pH 4

CD spectroscopy was used as a means of examining the structural ramifications of these modifications on the poly(A) duplex. This technique measures the differences in absorption of both left-handed and right-handed, circularly polarized light by chiral molecules, leading to the formation of elliptically polarized light.[150] In the case of nucleic acids, the light is absorbed by the purine and pyrimidine bases, to different degrees depending on the structure of the nucleic acid duplex (i.e. A-form vs B-form vs Z-form).[150] CD spectroscopy can be used to investigate the binding of ligands or proteins to nucleic acids, or to examine duplex folding/unfolding in response to external stimuli.[150] This technique requires relatively low concentrations of sample (in the range of μM) and is non-destructive. The downside of CD spectroscopy is that it provides qualitative structural information. In this work, all CD spectra are compared to the duplexes formed by the

rA_{11} and rA_{16} controls while working in the exact same buffer conditions, pH, concentrations, and at the same temperature.

The CD spectra of the duplexes formed by the 11-mers and 16-mers that have been modified with a single propargyl group in each strand can be seen in **Figures 3.6 A** and **B** respectively. These spectra were all recorded in the same pH 4, phosphate-citrate buffer, at 15 °C, using the same instrument. The pH 4 buffer alone shows no noticeable maxima or minima from 300-220 nm. The poly(A) duplexes, on the other hand, all display a major, negative, signal from approximately 250-235 nm and a major, positive signal from 295-250 nm. The longer duplexes formed by the 16-mers all display larger signals than those formed by the 11-mers due to enhanced absorption of the incoming light. Overall, no major differences in the overall shape of the curves with respect to the unmodified controls can be observed. This suggests that although the propargyl modification might be destabilizing based on T_m data, there is no impact on the overall structure of the poly(A) duplex under these pH 4 conditions.

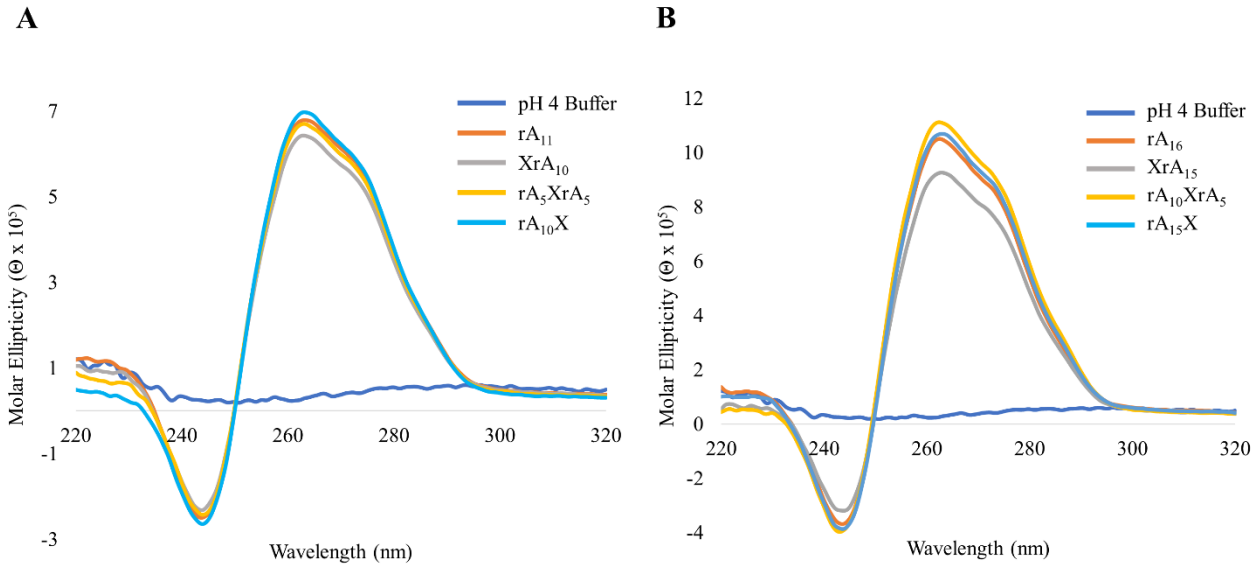

Figure 3.6: CD Spectra of C2'-*O*-Propargyl Modified Duplexes at pH 4. (**A**) 11-mers and (**B**) 16-mers. (Buffer: 40 mM Na_2HPO_4, 30 mM citric acid, pH 4). Strand concentrations were 3.7 µM for 11-mers and 2.6 µM for 16-mers. CD spectra recorded at 15 °C, 20 nm min^{-1}, 5 accumulations.

Figure 3.7 shows the CD spectra for the poly(A) duplexes which have been modified with numerous, successive, C2'-*O*-propargyl modifications at pH 4. Much like with the duplexes formed for the 11-mers and 16-mers containing a single modification, there is a prominent negative signal from 250-235 nm, with a positive signal from 295-250 nm. The overall shape of the curves all appear identical, indicating no major changes to the overall structure of the duplexes. The slight differences in signal intensity can be attributed to small differences in the concentrations, which would have no impact on the overall CD shape.

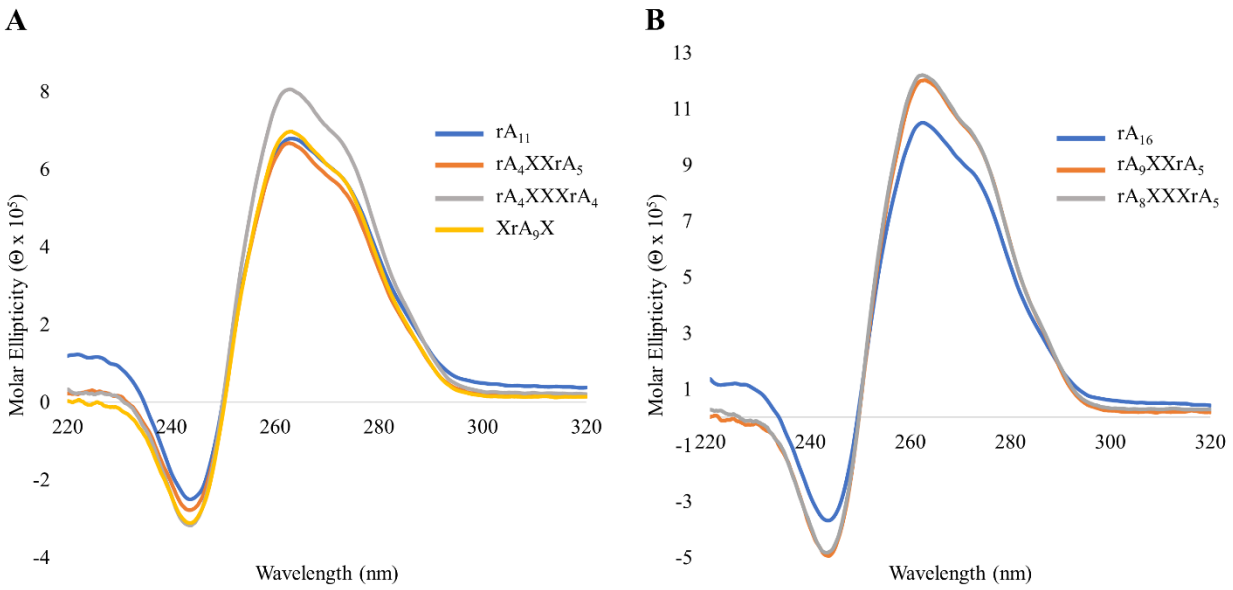

Figure 3.7: CD Spectra of Successive C2'-*O*-Propargylated Duplexes at pH 4. (**A**) 11-mers and (**B**) 16-mers. (Buffer: 40 mM Na_2HPO_4, 30 mM citric acid, pH 4). Strand concentrations were 3.7 µM for 11-mers and 2.6 µM for 16-mers. CD spectra recorded at 15 °C, 20 nm min^{-1}, 5 accumulations.

3.4 UV Thermal Denaturation (T_m) Analysis of C2'-*O*-Propargylated Duplexes at pH 7

The influence of these same modifications on poly(A) duplex formation under the pH 7, 4.4 M NH_4Cl conditions was investigated. In these studies, the longer duplexes formed by 16-mers, rather than 11-mers, were examined. The rationale for the investigation of the influence of the C2'-*O*-propargyl modification on duplex formation with longer poly(A) oligonucleotides is that it has been previously demonstrated that poly(rA) duplexes formed at pH 7 are less stable in contrast to pH 4.[115]

As shown in **Figure 3.8**, very little change in duplex stability was observed by UV thermal denaturation between the duplex formed by the rA_{16} control sequence and the modified oligonucleotides under the same, neutral pH, high salt conditions. This indicates that a single incorporation of the propargyl group in the 16-mers seems to have a very small effect on the longer duplexes under these conditions. Moreover, no change in stability is observed when the sequence is 5'-modified and when the modification is positioned at the center or 3'-end of the duplex the change is negligible.

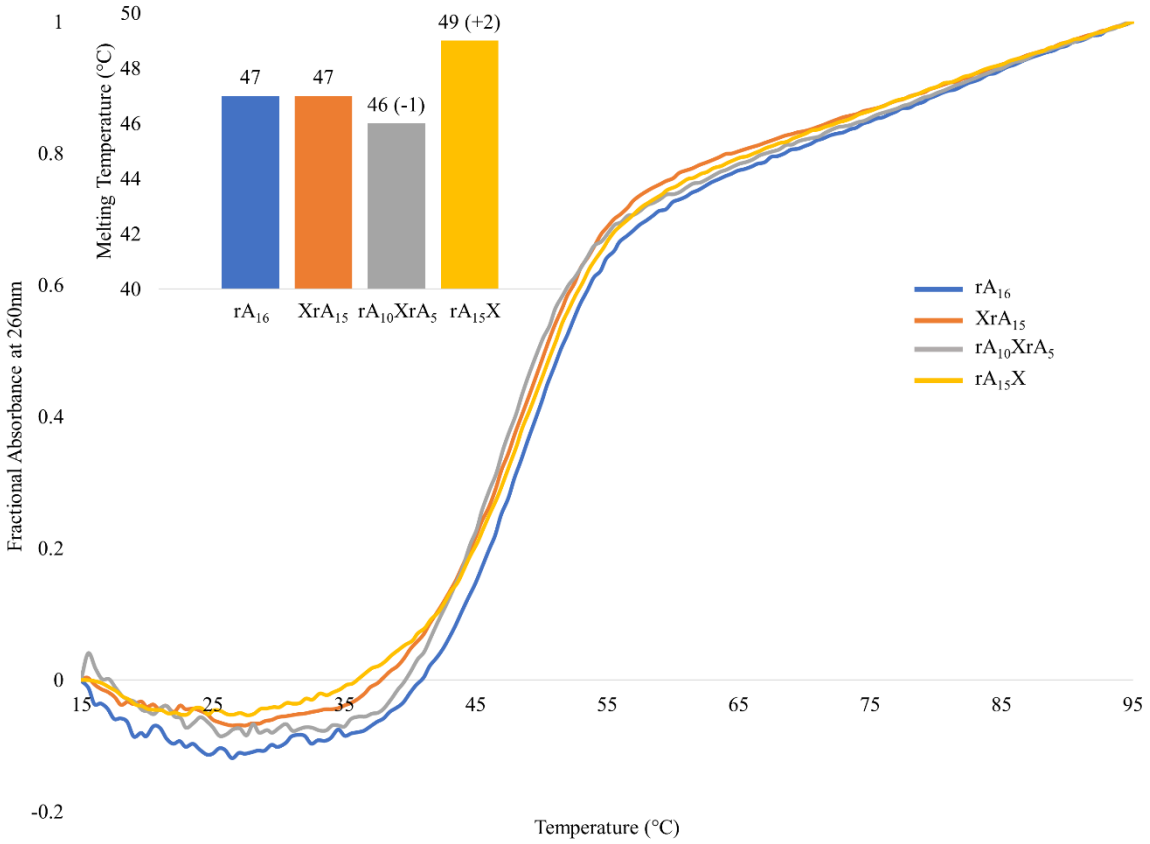

Figure 3.8: UV Thermal Denaturation Profiles of the Duplex Formed by the C2'-*O*-Propargyl Modified 16-mers at pH 7. (Buffer: 40 mM Na_2HPO_4, 30 mM citric acid, 4.4M NH_4Cl, pH 7). 2.6 µM single strand concentrations.

Figure 3.9 shows the influence of successive propargyl modifications on the stability of duplexes formed by the 16-mers under these neutral pH, high ammonium salt, conditions. It is observed that upon each additional incorporation of this modification into the duplex, the thermal stability of the duplex is reduced. The duplexes formed at pH 7 and 4.4 M NH_4Cl are destabilized by the propargyl modification in a similar manner to duplexes formed at pH 4.

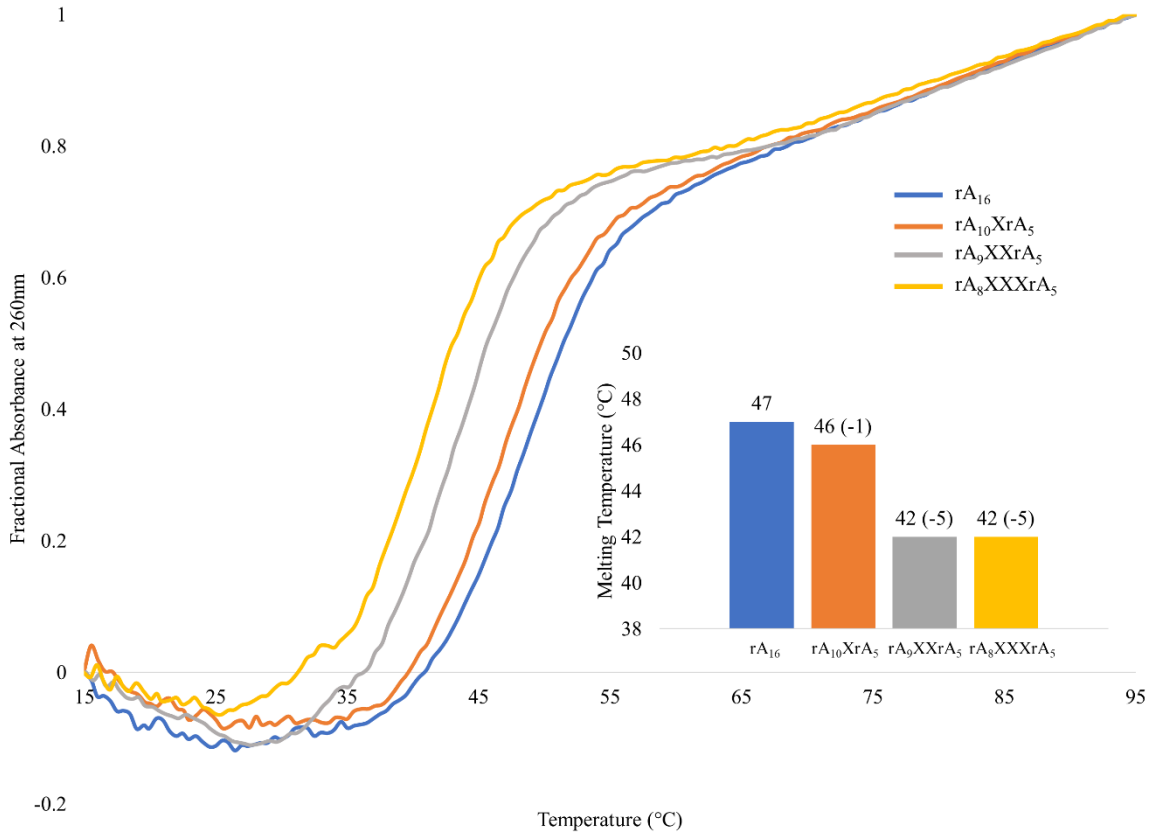

Figure 3.9: UV Thermal Denaturation Profiles of Duplexes Formed by Successive C2'-*O*-Propargylated 16-mers at pH 7. (Buffer: 40 mM Na_2HPO_4, 30 mM citric acid, 4.4M NH_4Cl, pH 7). 2.6 µM single strand concentrations.

Even though **Figure 3.9** seems to demonstrate a shift towards lower temperatures with each additional incorporation, the determined T_m values for duplexes formed by the doubly and triply-modified sequences are identical. This can be attributed to the general uncertainty that is associated with each measurement. Regardless, an overall destabilizing trend is seen with the increasing number of modifications and observed destabilization. An interesting point of note is that the destabilization observed at pH 7 is similar in magnitude to the destabilization seen at pH 4, suggesting a pH-independent mechanism.

3.5 CD Study of C2'-*O*-Propargylated Duplexes at pH 7

CD spectroscopy was also employed to examine the structure of the duplexes formed at neutral pH. As seen in **Figures 3.10 A** and **B**, there are no noticeable perturbations to the duplex structure when either a single or multiple propargyl modifications are incorporated. These modifications seem to be well accommodated within the duplex structure.

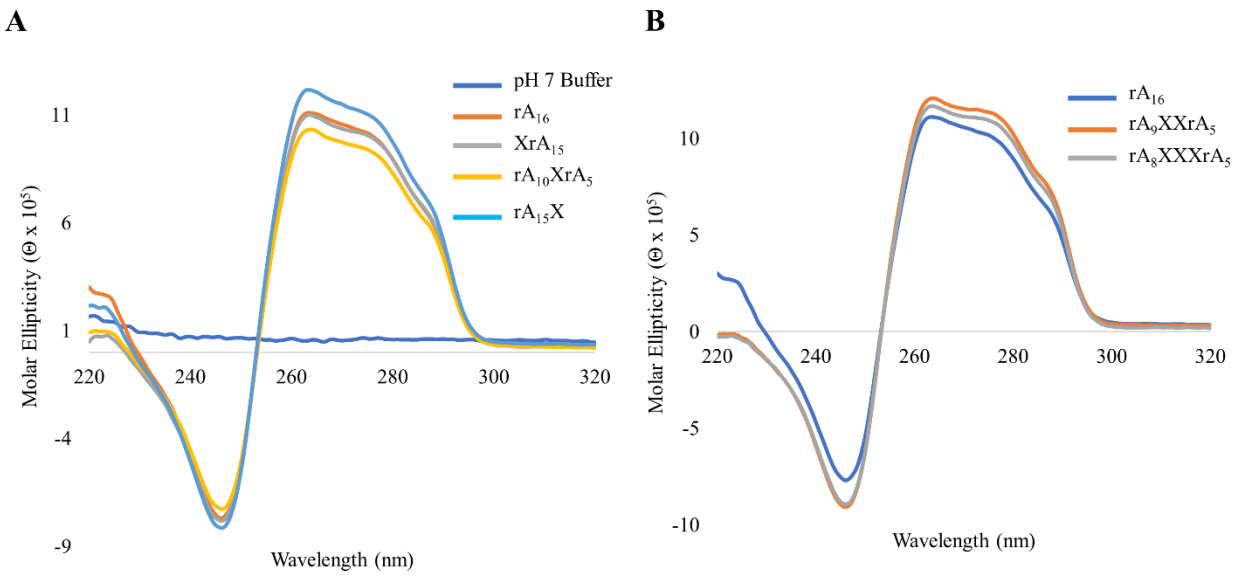

Figure 3.10: CD Spectra of C2'-*O*-Propargyl Modified Duplexes at pH 7. (**A**) Single and (**B**) multiple incorporations. (Buffer: 40 mM Na_2HPO_4, 30 mM citric acid, 4.4 M NH_4Cl, pH 7). Strand concentrations were 2.6 µM. CD spectra recorded at 15 °C, 20 nm min^{-1}, 5 accumulations.

3.6 Native PAGE Analysis of Propargyl-Modified Duplexes

Lastly, to confirm duplex formation for the modified poly(A) native PAGE was employed. This technique allows for visualization of duplex formation due to the slower migration of larger (duplex) versus smaller (single stranded) species in the acrylamide gel. The acrylamide solutions are made without the inclusion of a denaturing agent, which is added for applications such as

purification of crude oligonucleotides. 20 % acrylamide/bisacrylamide (19:1) solutions using the pH 4 and pH 7 phosphate-citrate buffers were polymerized, and oligonucleotide samples loaded in a 40 % sucrose solution (diluted with the corresponding phosphate-citrate buffer) to allow for poly(A) duplex formation. Samples were heated to 95 ℃ and slowly cooled to room temperature to ensure duplex formation.

For the native PAGE at pH 4, as shown in **Figure 3.11 A**, the rA_{11} sequence, and the modified poly(A) sequences, all run the same distance in the gel. In contrast, rU_{11}, which is a single stranded control that should not form higher ordered structures under these buffer conditions runs much further down the gel. These results correlate that these modified sequences adopt a structure that is similar in shape and size to the duplex formed by rA_{11} as observed previously.[114,115]

The same trends are observed with the longer duplexes, as shown in **Figure 3.11 B** with faster migration of the rU_{16} control relative to the retained migrations of the rA_{16} and modified 16-mer poly(A) sequences.

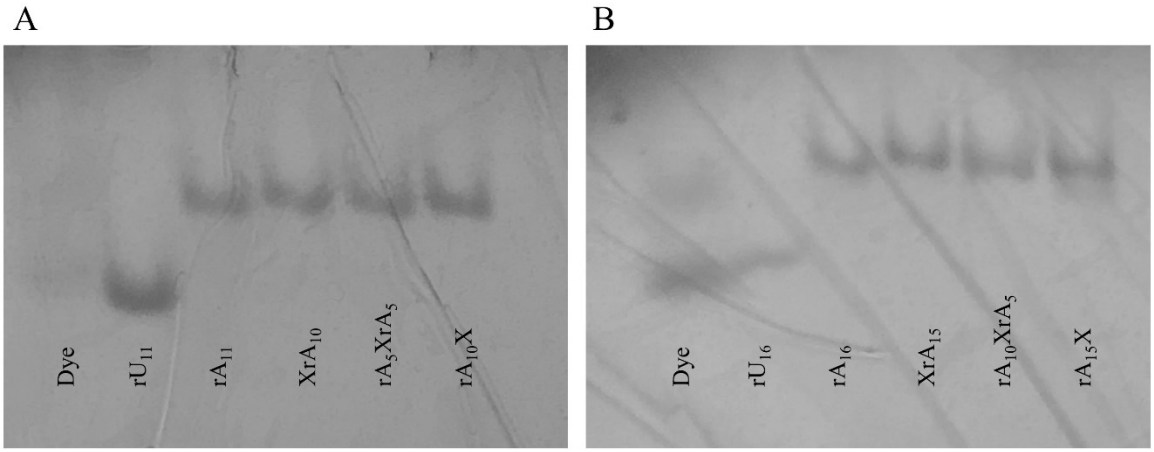

Figure 3.11: 20 % Acrylamide/Bisacrylamide (19:1) Native PAGE of C2'-*O*-Propargyl Modified poly(A) Duplexes at pH 4. (**A**) 11-mers and (**B**) 16-mers. (Buffer: 40 mM Na_2HPO_4, 30 mM citric acid, 1.1 mM EDTA, pH 4). The gels were run at 100 V for 5 h and visualized under short-wave UV shadowing. 0.1 OD of each oligo loaded in 10 μL of 40 % sucrose, pH 4 loading buffer.

In contrast to the above results, in **Figure 3.12** similar migration patterns for rU_{16}, rA_{16}, and the modified 16-mer sequences are observed when the gel was run at pH 7 in the absence of high ammonium salt content, previously established as necessary for duplex formation under these conditions.[114] The stark contrast in migration observed between **Figure 3.11 B** and **Figure 3.12** reaffirms the notion that a higher ordered, duplex structure has been successfully formed under the pH 4 buffer conditions.

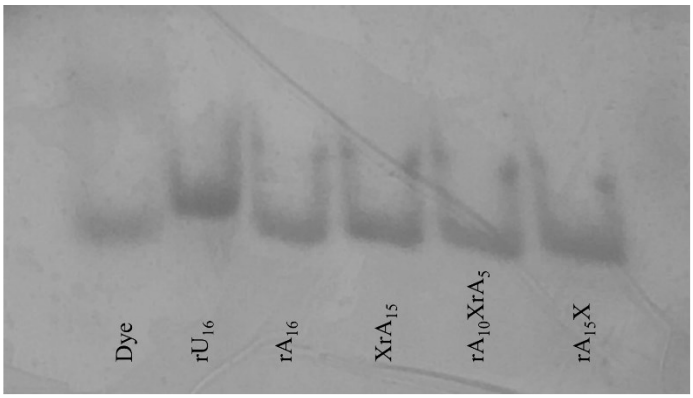

Figure 3.12: 20 % Acrylamide/Bisacrylamide (19:1) Native PAGE of C2'-*O*-Propargyl Modified 16-mer poly(A) Duplexes at pH 7. (Buffer: 40 mM Na_2HPO_4, 30 mM citric acid, 1.1 mM EDTA, pH 7). The gels were run at 100 V for 5 h and visualized under short-wave UV shadowing. 0.1 OD of each oligo loaded in 10 μL of 40 % sucrose, pH 7 loading buffer.

3.7 Summary of Propargyl Modifications

In summary, it was observed that duplex formation with poly(A) 11-mers or 16-mers containing a single modification of C2'-*O*-propargyl adenosine leads to negligible effects on thermal stability and global structure as assessed by UV thermal denaturation and CD spectroscopy at pH 4. The same is true for the longer duplexes under pH 7 conditions. When these duplexes are modified with increasing numbers of this propargyl modification, a decrease in duplex thermal

stability under all explored experimental conditions was observed. Through a series of native PAGE experiments, the modified duplexes formed complexes with reduced mobility relative to a rU control, similar to the poly(A) controls at pH 4. Finally, the CD spectra of duplexes containing these modifications exhibited minimal differences relative to the controls suggesting that they have a minimal effect on overall structure of the poly(A) duplexes and are well accommodated.

Chapter 4: Synthesis and Evaluation of a Modified poly(A) Duplex Containing a C2'-*O*-Alkylamine Substituent

4.1 Modification of Nucleic Acids with Cationic Groups

The modification of oligonucleotides with cationic groups leads to what are referred to as zwitterionic nucleic acids,[151] a term coined by two different research groups. Hashimoto looked at the tethering of aminohexyl groups onto the nucleobase at the C5 position of dT (**Figure 4.1 A** and **B**).[152,153] They found that the incorporation of these zwitterionic nucleosides leads to enhanced DNA/DNA duplex thermal stability, relative to duplexes bearing alkyl modifications of the same length, and severely reduces the thermal denaturation sensitivity of these duplexes to the ionic strength of the solution.[152,153] In a slightly different approach, the group of Noe looked at the incorporation of aminohexyl groups to the C2'-*O*-position of the sugar residue (**Figure 4.1 C**).[154,155]

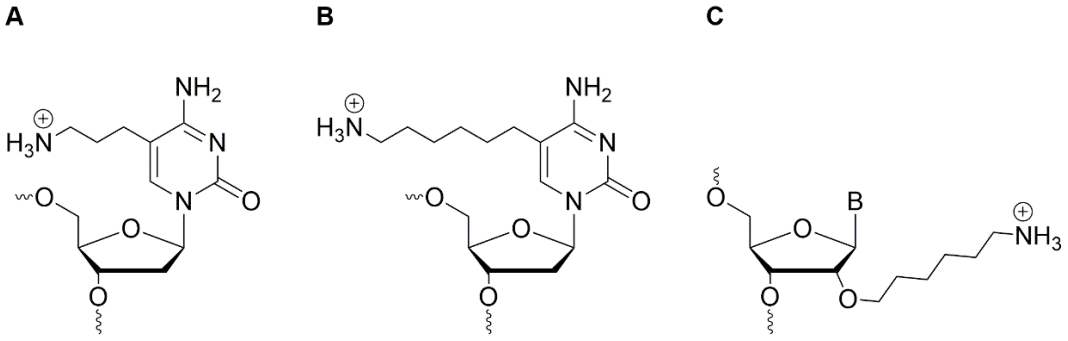

Figure 4.1: C5-Modified Zwitterionic Oligonucleotides.

More recently, various zwitterionic nucleic acids have been synthesized and shown to have a high resistence towards nuclease degradation.[156–159] Crystal structure analyses have shown that a critical metal ion is displaced by these positively-charged C2'-*O*-groups, resulting in the observed nuclease resistance.[160] The nuclease resistance provided by these cationic groups makes them ideal for use with Gapmer-designed ASO's.[72] An early report by Griffey showed that ASO's incorporating a C2'-*O*-aminopropyl group had a 5-10 fold greater effect at reducing C-*raf* mRNA than commonly-used phosphorothioate modifications.[157] Moreover, Nawale demonstrated that 4'-guanidinium modifications positioned at the 3'-overhangs of siRNA can lead to enhanced guide strand recruitment within the RISC complex.[161]

A common issue in modern nucleic acid therapies is that nucleic acids are not readily internalized by cells due to their polyanionic charge. Many strategies involve the modification of these nucleic acid-based drugs to allow for better targeting or internalization into the desired cells. Other approaches involve the use of lipid nanoparticles,[162] polymers,[163] or nucleic acid origami[91] to allow for drug internalization. The incorporation of cationic charges into nucleic acid-based drugs reduces the net negative charge of nucleic acids and can help to allow for their transport across cell membranes.[156,158]

In this work, we sought to functionalize the C2'-*O*-position of poly(A) RNA duplexes with a butylamine group to promote duplex stabilization through favourable backbone interactions. We investigated a facile methodology to introduce the alkyl amine functionality at the C2'-*O*-position through use of C2'-*O*-propargyl modified oligonucleotides and bifunctional alkanes containing an azide group for Click-coupling. Influences on duplex stability and structure were examined under both conditions for poly(A) duplex formation.

4.2 Synthesis of 4-azidobutylamine

The synthesis of 4-azidobutylamine was achieved through a two-step reaction pathway, as shown in **Scheme 4.1**, from commercially available 1,4-dibromobutane starting material (Chapter 8.19). Nucleophilic substitution of both bromine groups is achieved with excess sodium azide to give the disubstituted compound (**1**). Reduction of one azide functionality with triphenylphosphine gives the bifunctional alkane product (**2**). The successful conversion of functional groups into an azide and amine was confirmed using FT-IR (**Figures A.27** and **A.28**). NMR (**Figures A.19-A.22**) and MS (**Figure A.31**) were also employed to confirm product identity. No major side products were observed during these reactions. The product is somewhat volatile so care must be taken to avoid loss through evaporation.

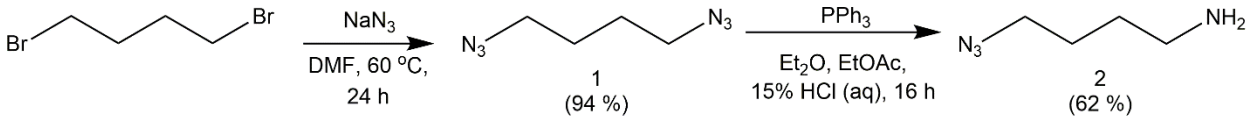

Scheme 4.1: Synthesis of 4-azidobutylamine (**2**).

4.3 Coupling of poly(A) to 4-azidobutylamine Through CuAAC

4-Azidobutylamine was coupled to single-stranded poly(A) oligonucleotides through use of the Click reaction as shown in **Scheme 4.2**. This copper-catalyzed, 1,3-dipolar cycloaddition reaction was first described by Sharpless and Meldal in 2002,[122,123] and leads to disubstituted 1,4-triazoles. To accomplish the Click reaction with the propargylated poly(A) oligonucleotides, the reaction conditions based off those developed by Das were employed[133] (Chapter 8.20).

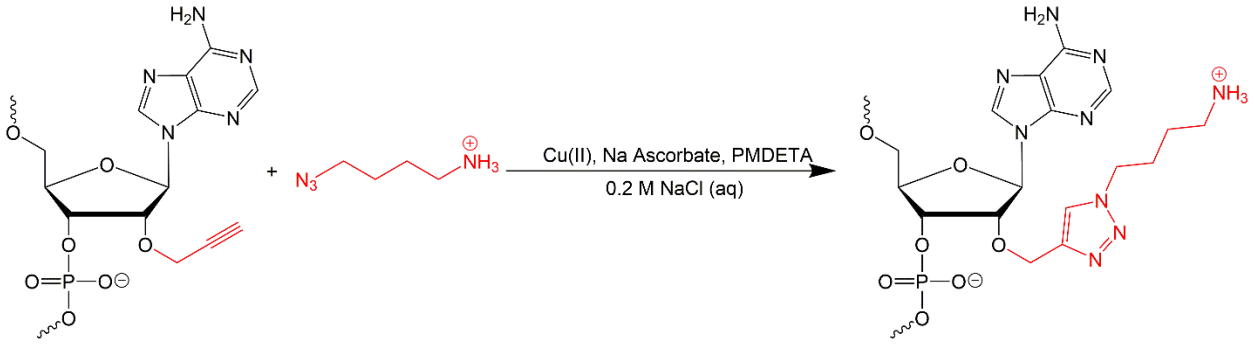

Scheme 4.2: Coupling of poly(A) to 4-azidobutylamine Through CuAAC.

C2'-*O*-propargyl modified poly(A) oligonucleotides prepared in Chapter 3 were covalently coupled to 4-azidobutylamine by introducing Cu(II) acetate. Sodium ascorbate was also added to allow for the reduction of Cu(II) to Cu(I), the catalytic form of the metal. A ligand, PMDETA, was added to stabilize the Cu(I) ions and increase the rate of the reaction. An alternative strategy, using ACN in a pseudo-ligandless approach was also explored and found to be just as effective as the PMDETA approach (Data not shown). This approach had been previously demonstrated by Das.[134] Utmost care must be paid during these reactions as the tendency for RNA to degrade is much higher than that of DNA during similar Click reactions.[133]

Oligonucleotide conjugates were purified through denaturing PAGE (**Figures A.5-A.7**). Products were seen to migrate slower than unmodified poly(A) due to a reduction in the net charge of the oligonucleotides as a result of the introduction of the cationic amine group. To confirm successful coupling of 4-azidobutylamine to the propargyl-modified oligos, mass spectrometry was employed (**Table A.2**).

4.4 UV Thermal Denaturation (T_m) Analysis of Butylamine-Modified poly(A) Duplexes at pH 4

The influence of the butylamine substituent at the C2'-*O*-position of adenosine of an 11-mer poly(A) on the formation and stability of duplexes formed at pH 4 was assessed by UV thermal denaturation. The denaturation curves for duplexes formed by the 11-mers containing a single modification at the 5'- or 3'-end, as well as, at the center are shown in **Figure 4.2**.

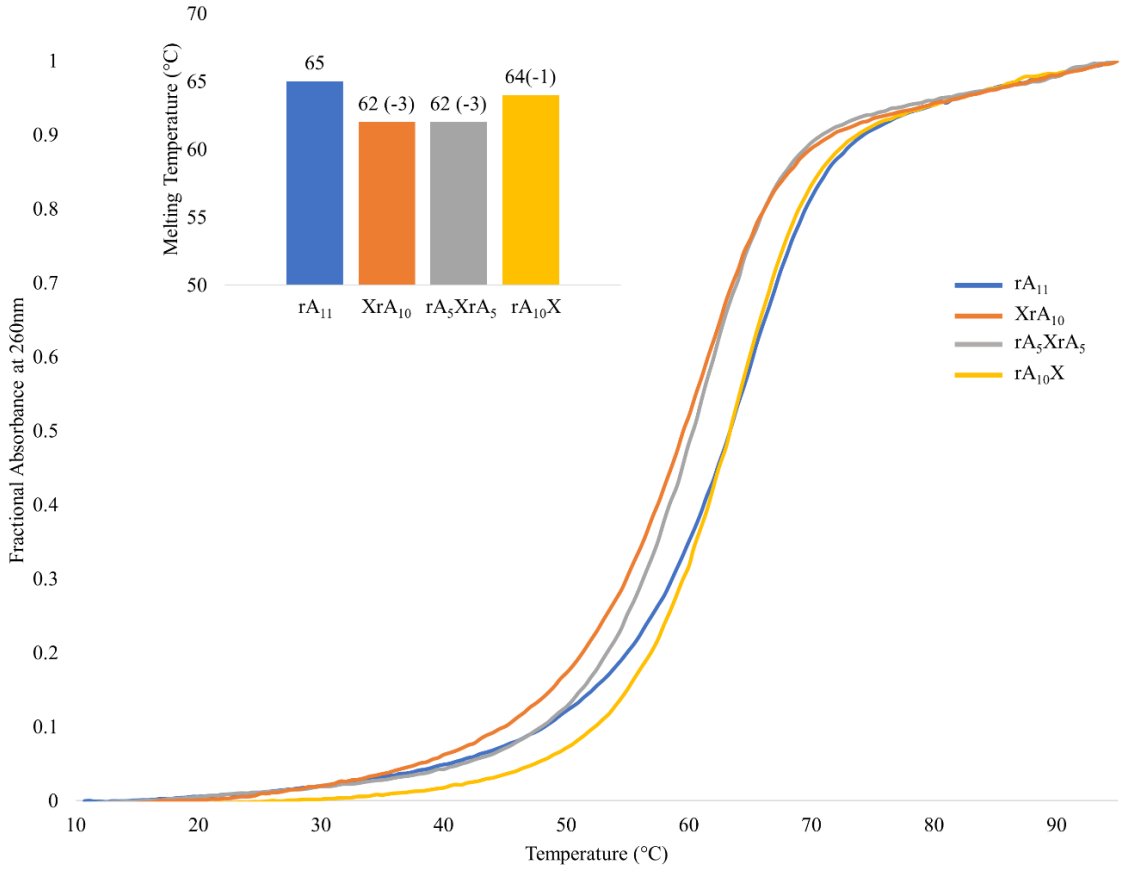

Figure 4.2: UV Thermal Denaturation Profiles of Duplexes Formed by Butylamine-Modified 11-mers at pH 4. (Buffer: 40 mM Na_2HPO_4, 30 mM citric acid, pH 4). 3.7 µM single strand concentrations.

The presence of the butylamine modification at the 5'-end and central position of the 11-mer destabilizes the duplex by 3 °C, where as, a negligible effect on duplex stability is observed when the duplex is modified at the 3'-end, possibly due to reduced steric effects at this position.

Looking at the 16-mer series (**Figure 4.3**), the reduction in duplex stability with these single modifications was minimal relative to the rA_{16} control. When compared to the rA_{11} series, the data demonstrates that the destabilizing effect of these single modifications is reduced for longer duplexes.

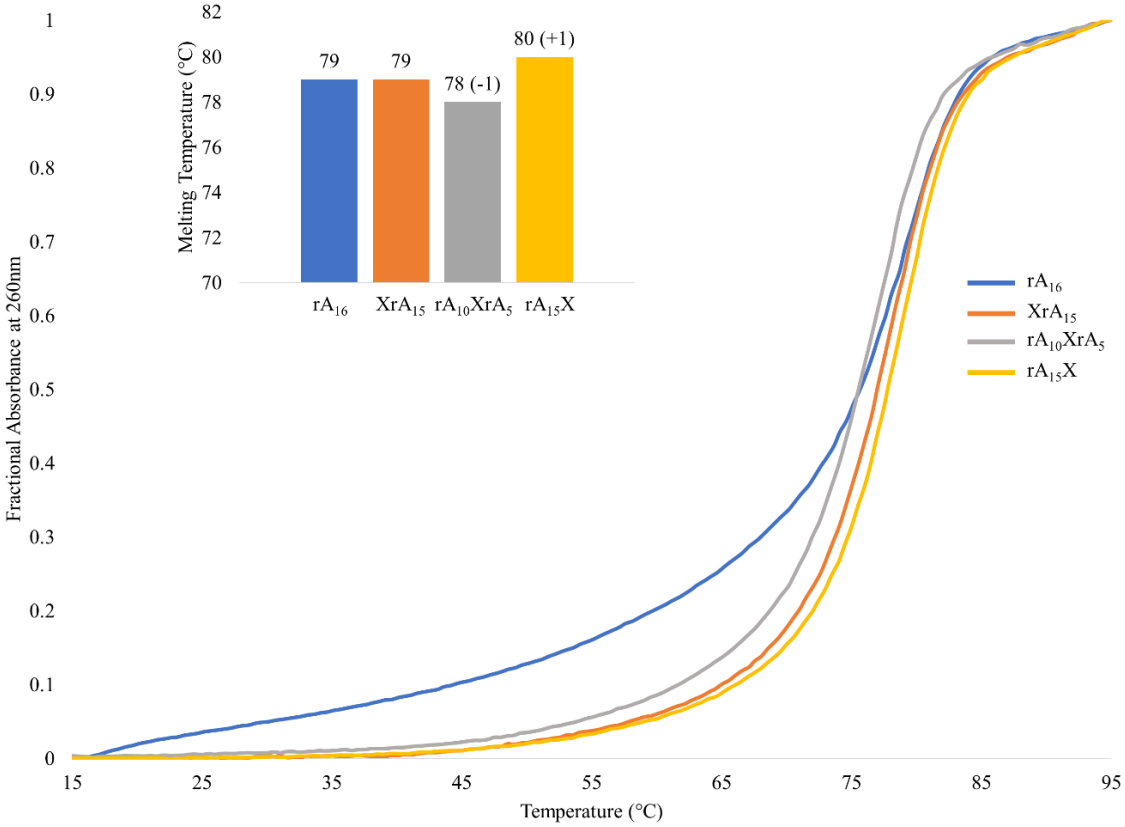

Figure 4.3: UV Thermal Denaturation Profiles of Duplexes Formed by the Butylamine-Modified 16-mers at pH 4. (Buffer: 40 mM Na_2HPO_4, 30 mM citric acid, pH 4). 2.6 µM single strand concentrations.

After having looked at the effect of a single incorporation of this cationic group, the study was expanded to include the poly(A) oligonucleotides containing multiple Click-coupled cationic groups at the center of these duplexes. In **Figure 4.4**, the UV thermal denaturation curves of duplexes formed by 11-mers containing additional incorporations is shown, demonstrating increasing destabilization with the exception being when the duplex is modified at both ends. In this case, the stability is comparable to that observed for the duplex formed by rA_5XrA_5. This observed destabilization is additive in nature, as shown by the inset of **Figure 4.4**, suggesting that potentially unfavourable interactions between neighbouring butylamine groups seems to be minimized and/or completely absent in this scenario. This observed destabilization is more significant than what was observed with the propargyl modifications. This suggests that some combination of the increased linker length, introduced cationic group, or the presence of the newly formed triazole ring is resulting in the increased destabilization. Increased linker length and the formation of the triazole ring could both lead to increased steric interactions with neighbouring nucleobases; introduction of the cationic group in increasing numbers could result in charge-charge repulsion if they are positioned too close in proximity.

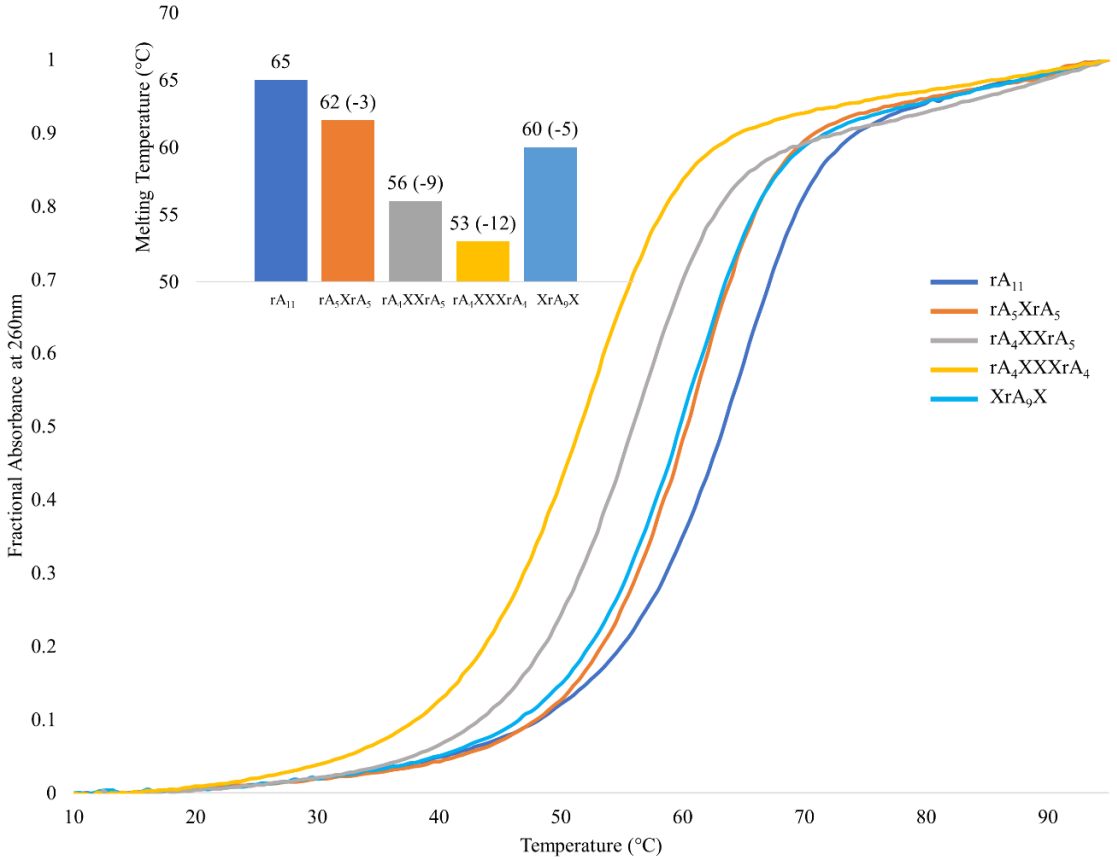

Figure 4.4: UV Thermal Denaturation Profiles of Duplexes Formed by 11-mer poly(A) Containing Successive Butylamine Modifications at pH 4. (Buffer: 40 mM Na_2HPO_4, 30 mM citric acid, pH 4). 3.7 µM single strand concentrations.

For the 16-mer series, a very similar trend is observed in **Figure 4.5** below. With each additional butylamine modification, which was incorporated through the 1,4-triazole ring to the C2'-*O*-position, a corresponding drop in duplex stability at pH 4 is observed. This observed destabilization is, again, additive, and is more significant than the destabilization which was originally observed when looking at propargyl group modifications. The increased size of the group relative to the propargyl modification could be responsible for the observed increase in destabilization.

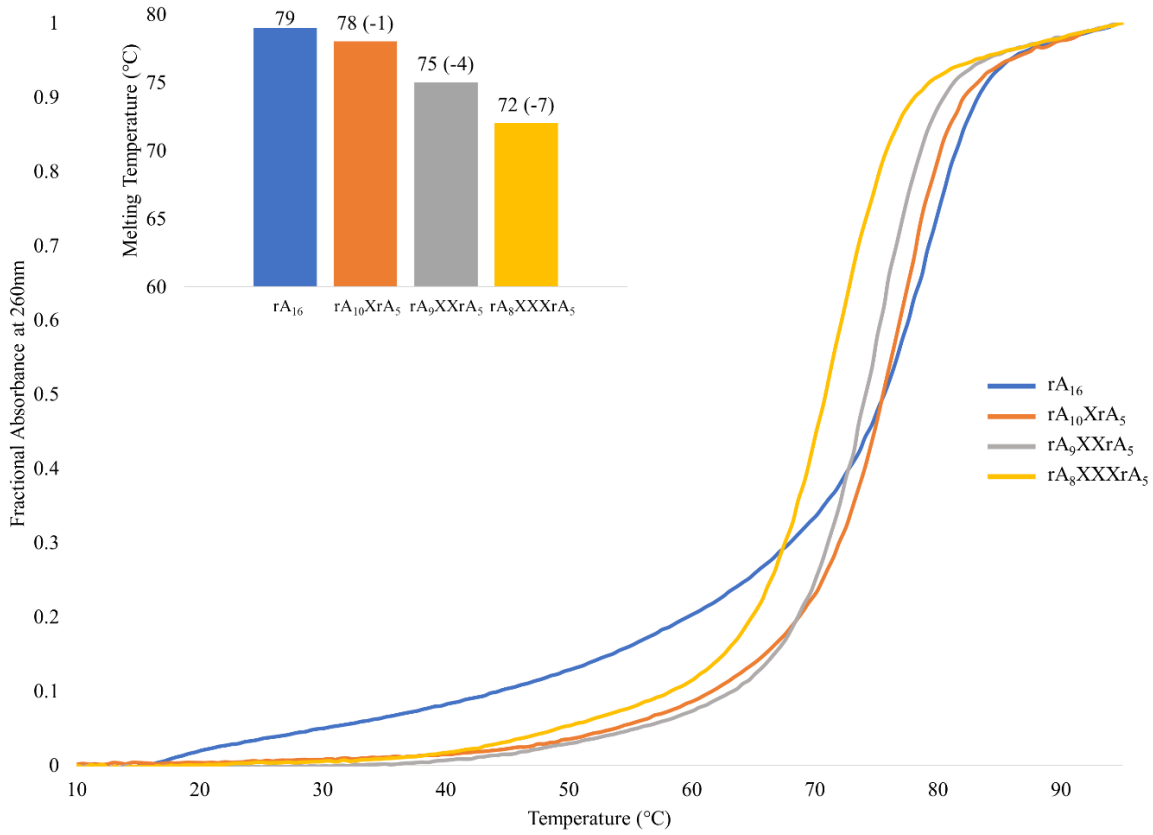

Figure 4.5: UV Thermal Denaturation Profiles of Duplexes Formed by 16-mer poly(A) Containing Successive Butylamine Modifications at pH 4. (Buffer: 40 mM Na_2HPO_4, 30 mM citric acid, pH 4). 2.6 µM single strand concentrations.

4.5 Thermal Reversibility of Butylamine-Modified Duplex Unfolding at pH 4

After having established the destabilizing effect brought about by this butylamine modification, the effect it may have on the ability for the poly(A) duplex to reform following the thermally driven dissociation of the duplex was examined. For the poly(A) duplex to be suitable for use as a pH-responsive nanostructure, it is necessary that following dissociation, due to either a change in temperature, pH, or ammonium concentration, that the duplex can revert to its initial state.

Below, in **Figure 4.6 A**, the melting traces for duplexes formed by 11-mer poly(A) that have been singly modified with the butylamine group at pH 4 are shown. In all cases, there is a shift of the transition to a lower temperature for the sigmoidal curves when cooling the samples from 95 to 4 ℃. This shift, hysteresis, suggests that the kinetics of duplex refolding are slightly slower than those of duplex melting under these conditions (pH 4 buffer, 0.5 ℃/min temperature change).[148] The magnitudes of these shifts, 4, 3, and 2 ℃, for the 5', central, and 3'-end modifications respectively, are small and are in line with what has been observed for an unmodified poly(A) duplex under identical conditions (**Figure A.33**).

The 16-mer series show similar results with a small hysteresis of the melting curve being seen in all cases (**Figure 4.6 B**). While the rate of folding is slightly slower than the rate of dissociation under these conditions, the absorbance reading at 260 nm returns to its initial value, suggesting that duplex refolding does occur (Data not shown).

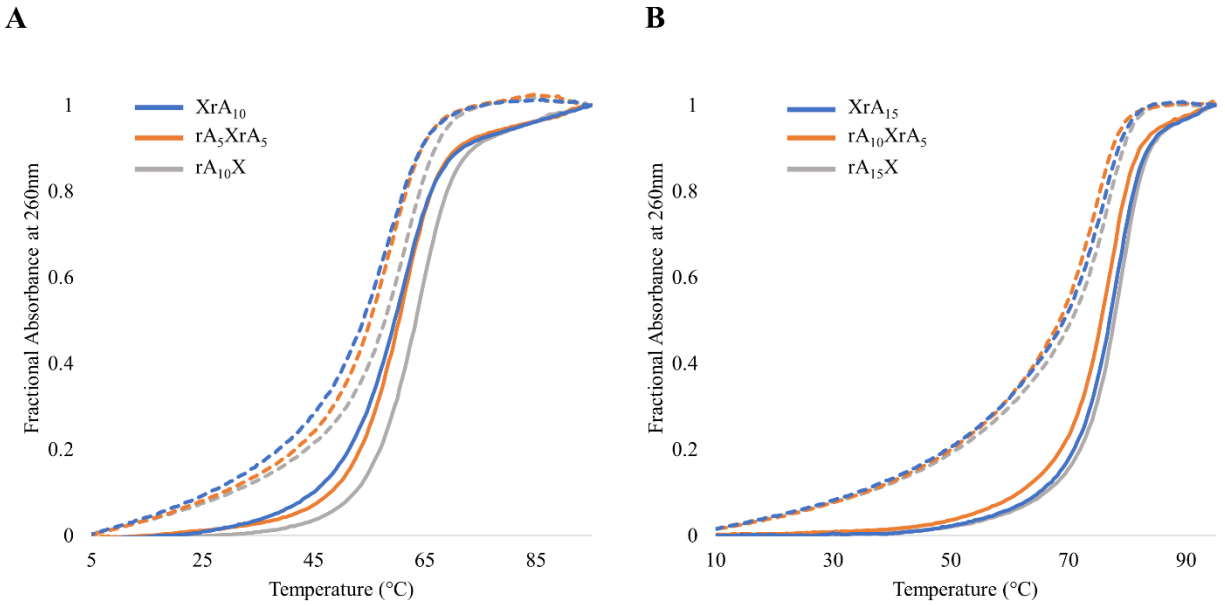

Figure 4.6: Thermal Reversibility Profiles at 260 nm of Butylamine-Modified poly(A) Duplexes at pH 4. (**A**) 11-mers and (**B**) 16-mers. (Buffer: 40 mM Na_2HPO_4, 30 mM citric acid, pH 4). Single strand concentrations were 3.7 µM for 11-mers and 2.6 µM for 16-mers. (Solid: Heating, Dashed: Cooling).

4.6 CD Analysis of Butylamine-Modified poly(A) Duplexes at pH 4

The pH 4 CD spectra of poly(A) duplexes coupled to a single butylamine group per strand are shown in **Figure 4.7**. A larger signal for the longer, 16-mer, series of duplexes is observed from 220-320 nm, with a slightly smaller signal for the duplex formed by XrA_{15}. This slightly smaller signal is due to a small concentration difference which would have had no effect on any of the stability studies that were performed. The overall shape of the spectra are similar to the rA_{11} and rA_{16} controls, indicating that these modifications have not led to any major structural changes of the duplex.

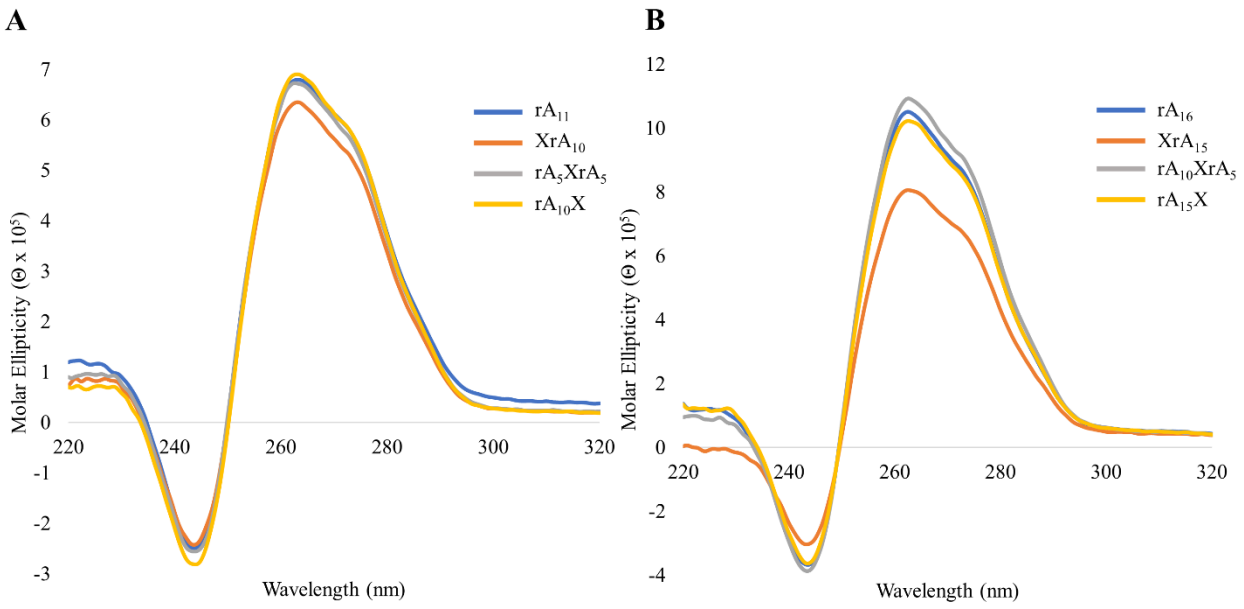

Figure 4.7: CD Spectra of poly(A) Duplexes Containing a Single Butylamine Modification at pH 4. (**A**) 11-mers and (**B**) 16-mers. (Buffer: 40 mM Na_2HPO_4, 30 mM citric acid, pH 4). Single strand concentrations were 3.7 µM for 11-mers and 2.6 µM for 16-mers. CD spectra recorded at 15 °C, 20 nm min^{-1}, 5 accumulations.

For the duplexes which were functionalized with multiple butylamine groups a similar trend is seen (**Figure 4.8**). No major changes to the shape of the curves can be seen, suggesting

that this modification is well tolerated by the parallel-stranded duplex. The previously observed thermal destabilization does not seem to correlate with a change in duplex structure.

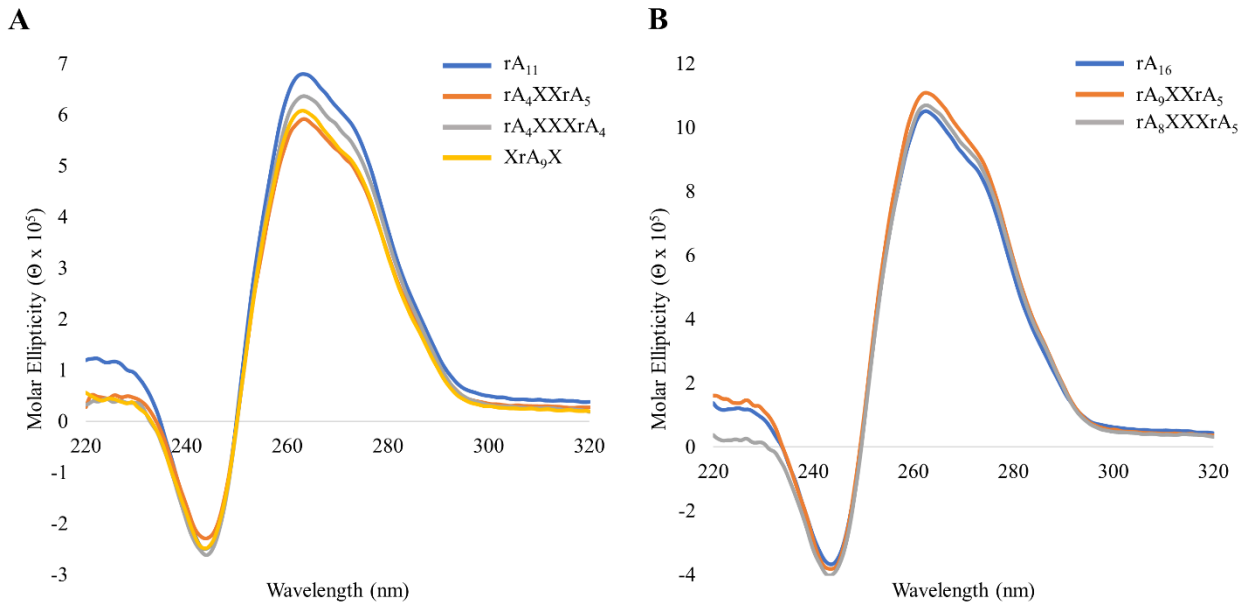

Figure 4.8: CD Spectra of poly(A) Duplexes Containing Multiple Butylamine Modifications at pH 4. (**A**) 11-mers and (**B**) 16-mers. (Buffer: 40 mM Na_2HPO_4, 30 mM citric acid, pH 4). Strand concentrations were 3.7 µM for 11-mers and 2.6 µM for 16-mers. CD spectra recorded at 15 °C, 20 nm min^{-1}, 5 accumulations.

4.7 UV Thermal Denaturation (T_m) Analysis of Butylamine-Modified poly(A) Duplexes at pH 7

The stability of duplex formation by 16-mer poly(A) sequences that incorporated the Click-coupled butylamine group at pH 7, with 4.4 M NH_4Cl, was assessed by UV thermal denaturation (**Figure 4.9**). At pH 4, these same duplexes were found to be negligibly impacted by the butylamine modification (**Figure 4.3**). In contrast, here, at neutral pH with high ammonium salt content, a significant destabilization (-5 °C) that occurs when the duplex is modified at a central

position is seen. In contrast, when the duplex is modified at either the 5'- or 3'-end minimal deviations from the control are observed.

Seeing as how this destabilization was not observed at pH 4, it is possible that this destabilization is a consequence of either the change in pH or the ammonium salt content. In water, the pKa for n-butylamine is 10.59,[164] and it is reasonable to assume that the butylamine linked to the C2'-*O*-position of the modified nucleobase would be similar. Thus, this primary amine would be protonated under both the pH 4 and pH 7 conditions explored in this study. Consequently, pH is unlikely to be a cause for this observed destabilization. The presence of high ammonium salt, however, would be expected to cause charge neutralization of both the phosphate backbone and the introduced cationic amine. This is turn, could result in the reduction, or possible elimination, of favourable electrostatic interactions between the backbone and amine group. Without these favourable interactions, this C2'-modification would be expected to be highly destabilizing due to steric clashes with the neighbouring nucleobases.

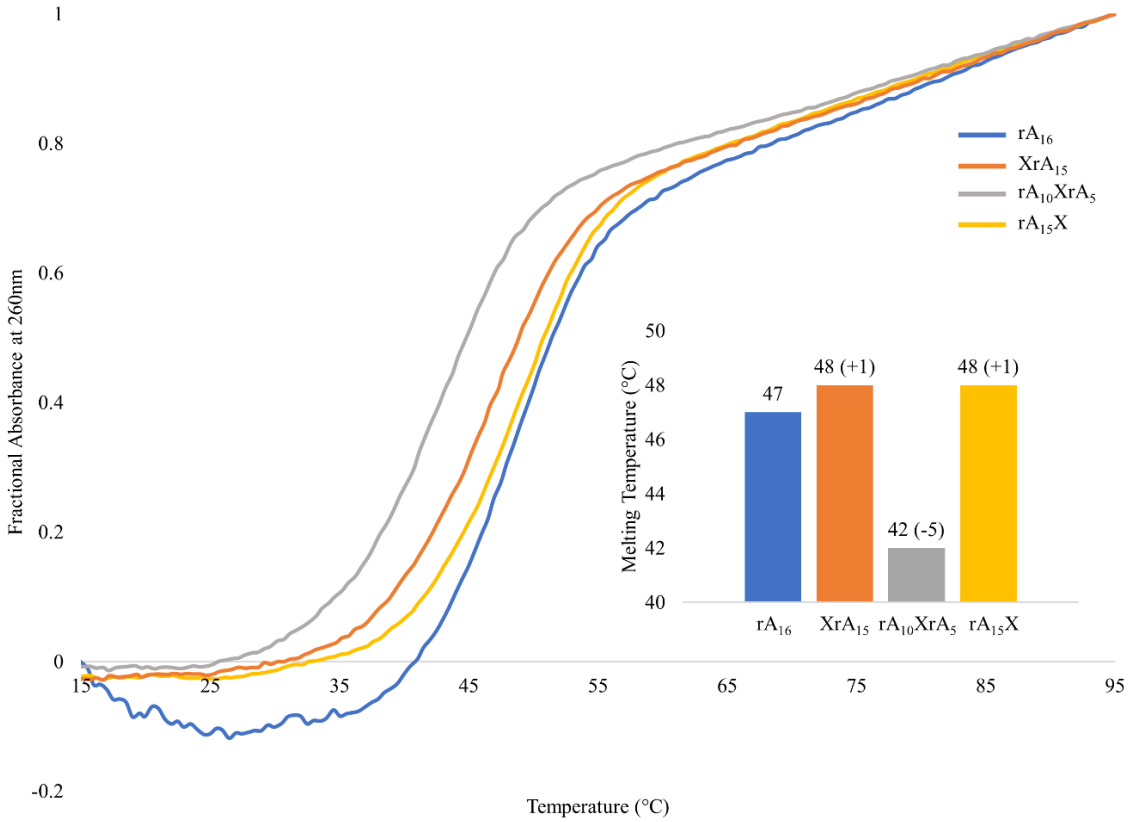

Figure 4.9: UV Thermal Denaturation Profiles of Duplexes Formed by Butylamine-Modified 16-mer poly(A) at pH 7. (Buffer: 40 mM Na_2HPO_4, 30 mM citric acid, 4.4 M NH_4Cl, pH 7). 2.6 µM single strand concentrations.

For the 16-mers containing numerous butylamine modifications, a decreased stability was observed for the duplexes with each added modification (**Figure 4.10**). However, in comparison to the studies at pH 4, a similar destabilization per additional modification on duplex stability was not observed. In this series, the introduction of the first modification is more destabilizing with less of an effect observed with additional modifications. While this may be due to the general error associated with these measurements, it is also possible that the primary modification leads to some sort of fundamental change in the duplex which allows for subsequent modifications to become more tolerated. The high concentration of ammonium cations in this system would be expected to compete with potential interactions mediated by the butylamine group. It is therefore reasonable

to hypothesize that with increasing numbers of butylamine modifications, favourable interactions between this group and the phosphate backbone would become more significant.

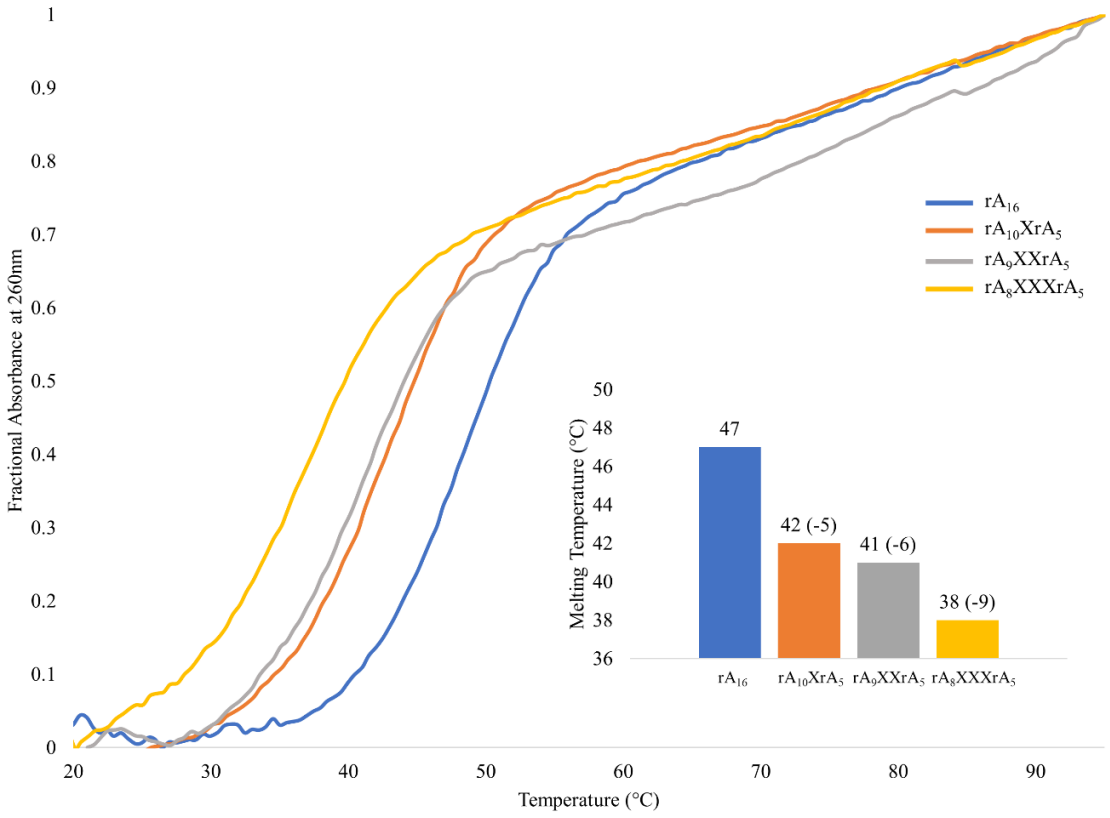

Figure 4.10: UV Thermal Denaturation Profiles of Duplexes Formed by 16-mer poly(A) Containing Multiple Butylamine Modifications at pH 7. (Buffer: 40 mM Na_2HPO_4, 30 mM citric acid, 4.4 M NH_4Cl, pH 7). 2.6 µM single strand concentrations.

4.8 Thermal Reversibility of Butylamine-Modified Duplex Unfolding at pH 7

In **Figure 4.11 A** it is observed that modified rA_{16} containing a single butylamine modification per strand can anneal at pH 7 with a small hysteresis relative to the denaturation curves, comparable to the unmodified (**Figure A.34**). This indicates that the destabilization

observed when the duplex is centrally modified under these conditions does not impact the kinetics of duplex annealing.

Similarly, as seen in **Figure 4.11 B** where multiple incorporations of the butylamine group are present at pH 7 only a minor difference is observed in the temperature of the transition between the association and dissociation curves. This lends itself towards future use as a responsive nucleic acid based nanodevice under these conditions.

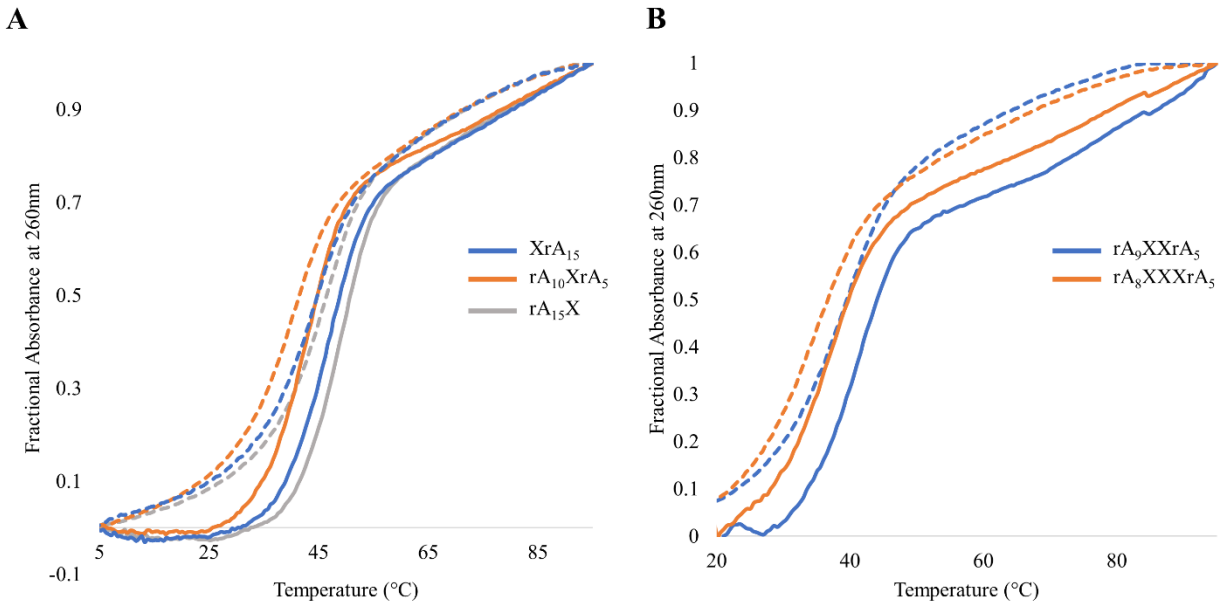

Figure 4.11: Thermal Reversibility Profiles at 260 nm of Duplexes Formed by Butylamine-Modified 16-mer poly(A) at pH 7. (**A**) Single and (**B**) Multiple modifications. (Buffer: 40 mM Na_2HPO_4, 30 mM citric acid, 4.4 M NH_4Cl, pH 7). 2.6 µM single strand concentrations. (Solid: Heating, Dashed: Cooling).

4.9 CD Analysis of Butylamine-Modified poly(A) Duplexes at pH 7

CD analysis of these duplexes formed by 16-mers at pH 7 and 4.4 M NH_4Cl show no major changes from the spectra for the control duplexes (**Figure 4.12**). Notably, duplexes formed with a

central butylamine modification give identical traces to those with multiple modifications, suggesting that the primary modification does not lead to a structural change that allows for subsequent modifications to be more tolerated by the duplex.

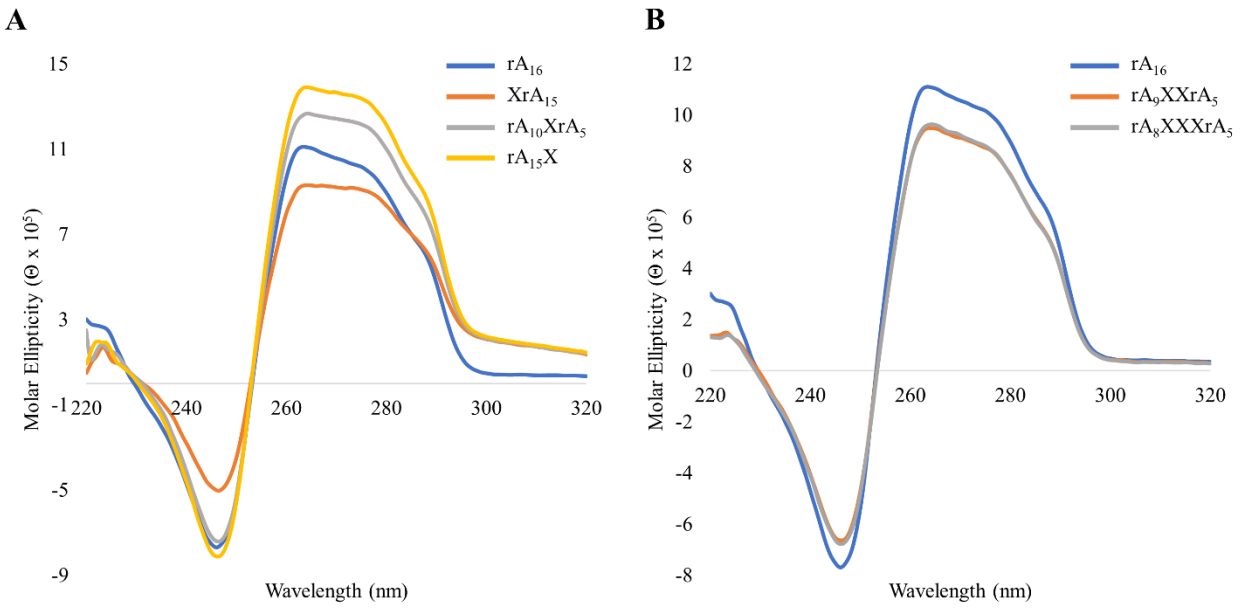

Figure 4.12: CD Spectra of Butylamine-Modified poly(A) Duplexes at pH 7. (**A**) Single and (**B**) Multiple incorporations. (Buffer: 40 mM Na_2HPO_4, 30 mM citric acid, 4.4 M NH_4Cl, pH 7). Strand concentrations were 2.6 µM. CD spectra recorded at 15 °C, 20 nm min^{-1}, 5 accumulations.

4.10 Native PAGE Analysis of Butylamine-Modified poly(A) Duplexes

After having studied the influence of this modification under various conditions using thermal denaturation and CD analysis, validation of duplex formation was performed by native PAGE analysis. This technique is useful to detect formation of higher ordered structures such as duplexes, triplexes, quadruplexes, or nucleic acid aggregates.[165] Native PAGE was performed at pH 4 to allow for proper annealing of the poly(A) duplex. A 12.5 % native PAGE gel was prepared that contained both single-stranded and duplex controls in addition to the poly(A) samples. As

shown in **Figure 4.13**, at pH 4 a higher retention of the rA_{16} (lane 3) is observed relative to the rU_{16} (lane 2). The significant difference in the mobility is an indication that poly(A) duplex formation has occurred. Moreover, a higher retention is observed for the butylamine-modified sequences (lanes 4-5) in comparison to the rA_{16} (lane 3). This higher retention exhibited by butylamine-modified oligonucleotides can be attributed to the introduction of cationic moieties within the duplex structure.

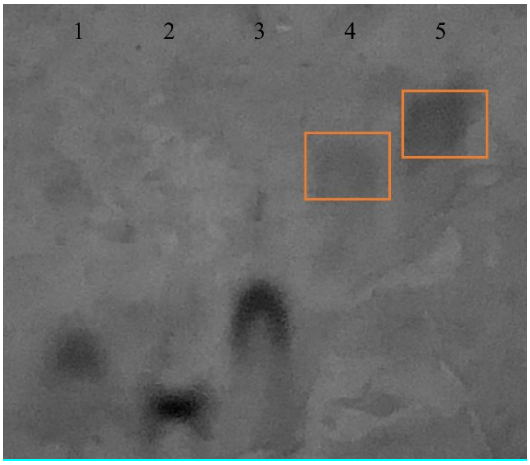

Figure 4.13: 12.5 % Acrylamide/Bisacrylamide (19:1) Native PAGE of Butylamine-Modified poly(A) Duplexes. (Buffer: 40 mM Na_2HPO_4, 30 mM citric acid, 1.1 mM EDTA, pH 4). Run at 100 V for 5 h and visualized under short-wave UV shadowing. 0.1 OD of each oligo loaded in 10 µL of 40 % sucrose, pH 4 loading buffer. (Lane 1: Dye; lane 2: rU_{16}; lane 3: rA_{16}; lane 4: rA_9XXrA_5; lane 5: rA_8XXXrA_5).

It has been well established that there is a linear correlation between nucleic acid length and migration distance in denaturing or native gels.[165] This is due to a constant charge to size ratio that is maintained in nucleic acids of different lengths. By introducing cationic amino groups, the net negative charge of the duplexes is reduced, therefore causing them to be less affected by the electrical current that permeates the length of the gel.

This higher retention was also observed when these oligonucleotides were purified through denaturing PAGE following the Click reaction (**Figures A.5-A.7**). Thus, it can be stated that there is no evidence for any major structural changes based on these native gel results.

4.11 Influence of Butylamine Modifications on a Hybrid (rA/dT) Duplex

The influence of this butylamine modification was investigated on a series of antiparallel duplexes to compare with the results observed for the parallel stranded poly(A) duplex. These hybrid duplexes were prepared by combining equal concentrations of modified single-stranded rA_{11} and dT_{11} in a phosphate-citrate buffer at pH 7.4.

The UV thermal denaturation curve for the duplex is shown in **Figure 4.14**. These duplexes are far less stable than those formed by 11-mer poly(A) at pH 4. There is a very small initial baseline for these sigmoidal transitions, however, a melting temperature of 20 ℃ can be derived for the rA_{11} control sequence. Destabilization occurs when the duplex is centrally modified, with a negligible effect being seen when the ends are modified. These results are slightly less destabilizing that what was observed for the duplexes formed by 11-mer poly(A) at pH 4. The compressed structure of the poly(A) duplex[114] may explain why modifications seem to have a higher influence on poly(A) in comparison to antiparallel duplexes.

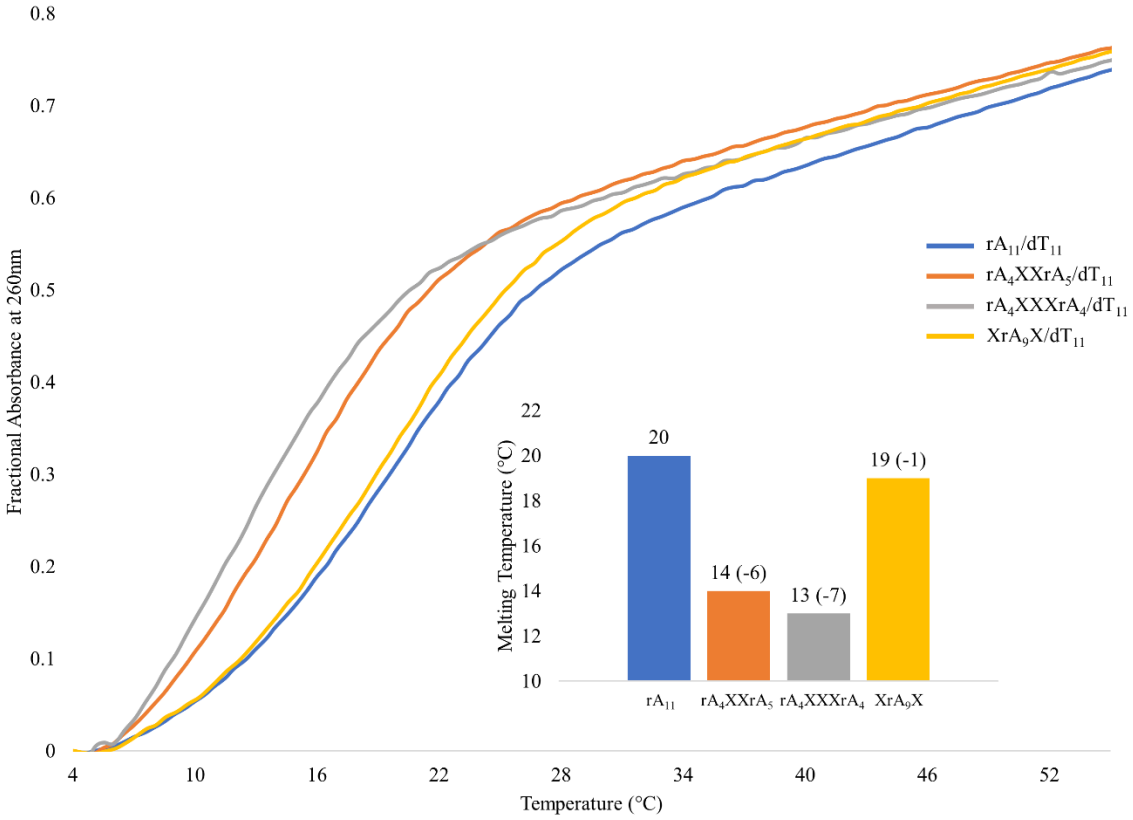

Figure 4.14: UV Thermal Denaturation Profiles of Duplexes Formed by an 11-mer rA Containing Multiple Butylamine Modifications and an 11-mer dT at pH 7.4. (Buffer: 40 mM Na_2HPO_4, 30 mM citric acid, pH 7.4). 1.85 µM single strand concentrations.

The CD spectra of these duplexes were acquired between 320-200 nm to allow for differentiation between possible A- and B-form duplexes. As shown in **Figure 4.15** these modified hybrid duplexes formed by 11-mer rA and dT have positive maxima around 270 nm and negative minima centered around 245 nm. Hybrid duplexes of rA/dT are capable of forming both A-form and B-form duplexes depending on the experimental conditions and modifications incorporated.[166] In this case, the spectra resemble a B-form helical structure, as shown by the lack of CD signal around 210 nm. The similarity of the CD spectra suggests that the introduction of butylamine modifications does not seem to have any major impact on the structure of the hybrid duplex under these conditions.

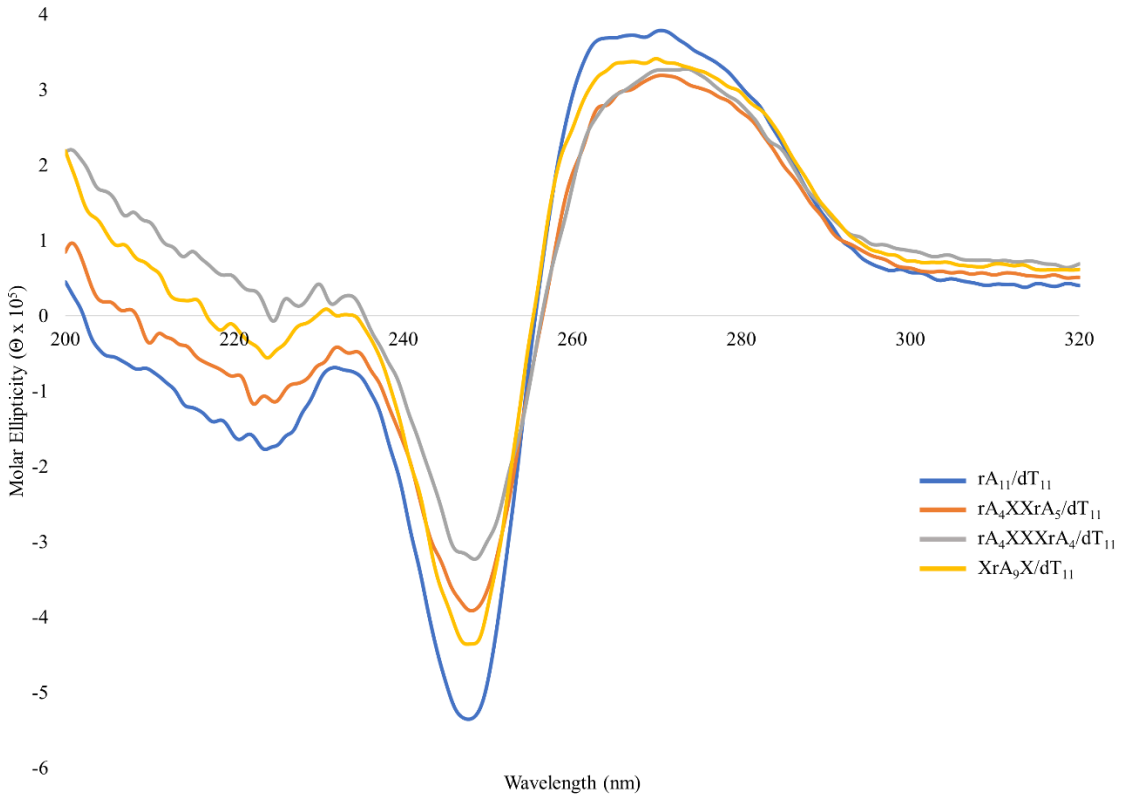

Figure 4.15: CD Spectra of Duplexes Formed by an 11-mer rA Containing Multiple Butylamine Modifications and an 11-mer dT at pH 7.4. (Buffer: 40 mM Na_2HPO_4, 30 mM citric acid, pH 7.4). Strand concentrations were 1.85 µM. CD spectra recorded at 15 °C, 20 nm min^{-1}, 5 accumulations.

4.12 Summary of Butylamine Modifications

In summary, modification of the poly(A) duplex with a butylamine group, through a 1,4-triazole linkage at the C2'-*O*-position, leads to destabilization of this parallel-stranded duplex. The introduction of cationic groups have been previously seen to provide stabilization through favourable backbone interactions.[151,158,167] For the poly(A) duplex, this destabilization was found to be additive with each additional modification introduced. No structural changes resulted from duplex modification. It was also seen through UV thermal denaturation analysis that the introduction of butylamine at a central duplex position is more destabilizing under the pH 7, 4.4

M NH_4Cl conditions than at pH 4. This is thought to be due to the elimination of favourable electrostatic interactions between the cationic amine group and the negatively charged phosphate backbone under these conditions. This butylamine modification, while destabilizing, is still thought to have less of an influence on the diminishment of duplex stability than alkyl modifications of the same length due to favourable backbone interactions.

Chapter 5: Influence of Pyrene via 1,4-Triazole Linker at C2'

5.1 Pyrene-Modified Oligonucleotides

The modification of nucleic acids with fluorescent tags is commonly performed to allow for their visualization;[168] for use in automated nucleic acid sequencing;[169,170] for DNA fingerprinting;[171] and for the construction of DNA microarrays,[172] among many others. One of the more commonly studied fluorophores in recent years is pyrene.[173] This PAH has been extensively studied and found to have a myriad of uses in nucleic acid chemistry including structure stabilization,[174,175] mismatch detection,[176] and target specific fluorescence.[174,177]

The fluorescence emission of pyrene depends on the group's microenvironment.[178,179] For B-form DNA, the group will intercalate between neighbouring nucleobases which leads to a corresponding drop in fluorescence intensity.[174,180] Due to the more compressed structure of A-form RNA duplexes, pyrene tends to be positioned into the grooves, leading to a much higher fluorescence signal than in DNA.[174,180] The intercalation of pyrene between neighboring stacked nucleobases has also been shown to depend on neighbouring nucleobase identity[181] and linker rigidity, whereas a more rigid linker can promote intercalation.[182] Pyrene is also capable of forming excited state dimers (excimers), which has recently been used to detect proper RNA target binding in multicellular organisms.[183] Along similar lines, Tang recently constructed a triple-helix molecular switch which can allow for the detection of Argonaute 2 through use of the pyrene excimer signal.[184] They claim this same methodology could be employed for the detection of endogenous Ago2 in cancer cells.[184]

The stabilization of a thrombin binding aptamer (TBA) G-quadruplex by pyrene-modified uridine nucleotides was also recently achieved.[185] The authors found this TBA analogue to be more resistant towards nuclease degradation under human serum conditions than the unmodified aptamer.[185] New two-component probes for miRNA detection have also been designed which incorporate clusters of pyrene-modified adenosine residues.[186] These probes form what are termed three-way junction (3WJ) structures in the presence of the RNA target, which can then be detected by a change in the fluorescence pattern.[186]

In this work, we sought to study the influence of coupling a pyrene group to the C2'-*O*-position of the poly(A) duplex through a 1,4-triazole linkage using Click chemistry. We speculated that poly(A) duplex stabilization could be achieved through either (1) pyrene intercalation or (2) π-stacking interactions between adjacent pyrene modifications in the groove of the duplex.

5.2 Synthesis of 1-(azidomethyl)pyrene

The synthesis of 1-(azidomethyl)pyrene was achieved through a two-step pathway as shown below in **Scheme 5.1** from commercially available 1-pyrenemethanol starting material (Chapter 8.19). The nucleophilic substitution of the hydroxyl group was achieved with excess PBr_3 in THF to give 1-(bromomethyl)pyrene (**3**). This reaction was initially attempted with toluene as the solvent, but the reaction yield was low, and purification was difficult. Using THF as the solvent, purification via vacuum filtration was possible as (**3**) precipitated out of solution in the form of a white solid. The product was used as is, with minor impurities, for the subsequent synthesis step. A second nucleophilic substitution was performed, where the bromo functionality of (**3**) was converted into an azide using excess sodium azide in DMF. Following extraction and washing

steps, (**4**) was purified through FCC by isolating the fluorescent band that appears under short-wave UV irradiation of the column. The successful conversion of the functional group into an azide was confirmed using FT-IR (**Figures A.29** and **A.30**). NMR (**Figures A.23-A.26**) and MS (**Figure A.32**) were also employed to confirm product identity.

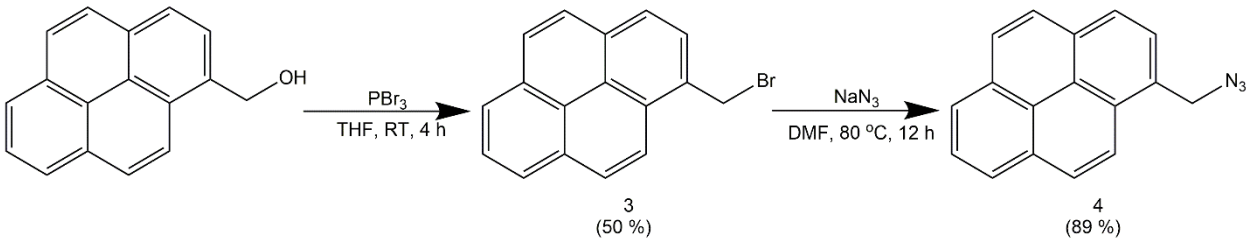

Scheme 5.1: Synthesis of 1-(azidomethyl)pyrene (**4**).

5.3 Coupling of poly(A) to 1-(azidomethyl)pyrene Through CuAAC

1-(Azidomethyl)pyrene was coupled to poly(A) oligonucleotides containing the C2'-*O*-propargyl modification in solution (**Scheme 5.2**) according to the same procedure as described in Chapter 4.3 with minor modifications. Due to the inherent insolubility of the pyrene compounds in water, solutions of 1-(azidomethyl)pyrene in DMSO were prepared. Prior to degassing, 2 eq. of this pyrene solution were added for every C2'-*O*-propargyl modification contained within the poly(A) oligonucleotide to be coupled. Click reactions were stopped by removal of the Cu(I) through desalting (**Chapter 8.20**). PAGE was then employed to purify the reaction products. It was observed that the poly(A)-pyrene conjugates migrated more slowly through the polyacrylamide gel than the unmodified poly(A) oligonucleotides (**Figures A.8-A.17**). Very little starting material was observed on the polyacrylamide gels, suggesting these reactions were near quantitative. Mass spectrometry was employed to confirm the identity of the products (**Table A.3**).

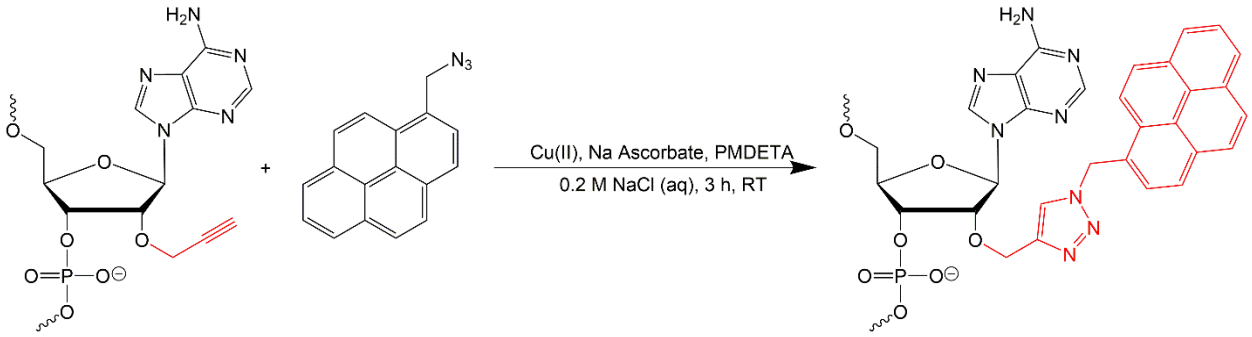

Scheme 5.2: Coupling of poly(A) to 1-(azidomethyl)pyrene Through CuAAC.

5.4 UV Thermal Denaturation (T_m) Analysis of Pyrene-Modified poly(A) Duplexes at pH 4

The influence of pyrene incorporation at the C2'-*O*-position through a 1,4-triazole linker on poly(A) duplex stability was examined by UV thermal denaturation. This included both the 11-mer and 16-mer series with either a single incorporation of the modifications or multiple, centrally positioned modifications (**Table 3.1**).

As observed in **Figure 5.1**, the incorporation of pyrene at the 5'- and 3'-ends of an 11-mer poly(A) under acidic conditions has a small influence on the melting temperature of the resulting duplexes. Interestingly, when pyrene is positioned at the center of the duplex, a significant destabilization (-28 °C) was observed. This large decrease in stability suggests that the pyrene group is not intercalating into the core of the duplex structure, as can happen with pyrene-functionalized DNA, which is generally associated with a stabilization.[174] In this case, the data suggests that pyrene is being positioned into the groove of the duplex where unfavourable steric clashes are disrupting the ability for the poly(A) duplex to hybridize properly. This perceived disruption is less significant when the pyrene groups are positioned at the ends of the duplex.

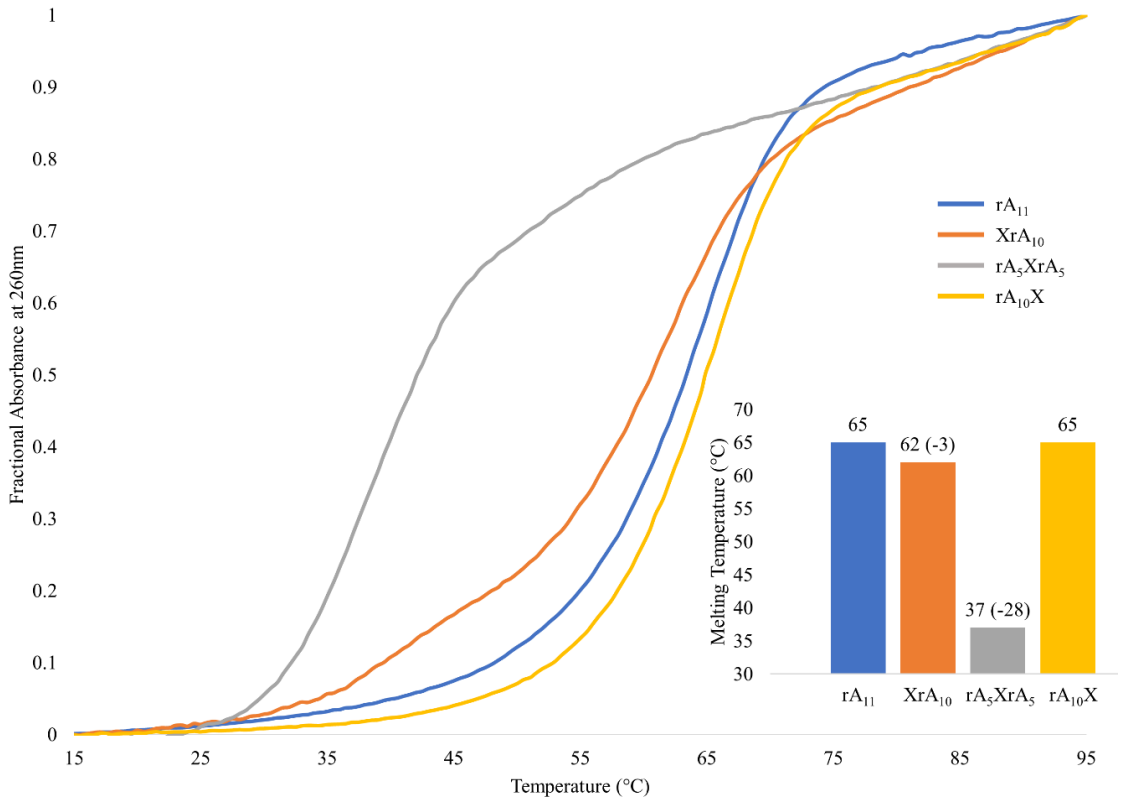

Figure 5.1: UV Thermal Denaturation Profiles of Duplexes Formed by Pyrene-Modified 11-mers at pH 4. (Buffer: 40 mM Na_2HPO_4, 30 mM citric acid, pH 4). 3.7 µM single strand concentrations.

For the longer, 16-mer series a similar trend is observed, where, modification with pyrene at an internal position leads to a major reduction in duplex stability (**Figure 5.2**). The effect is less pronounced than with the shorter, 11-mer series. Destabilization was also observed when monitoring the melting curves at 350 nm (**Figures A.36** and **A.37**), which is a characteristic pyrene absorption peak.

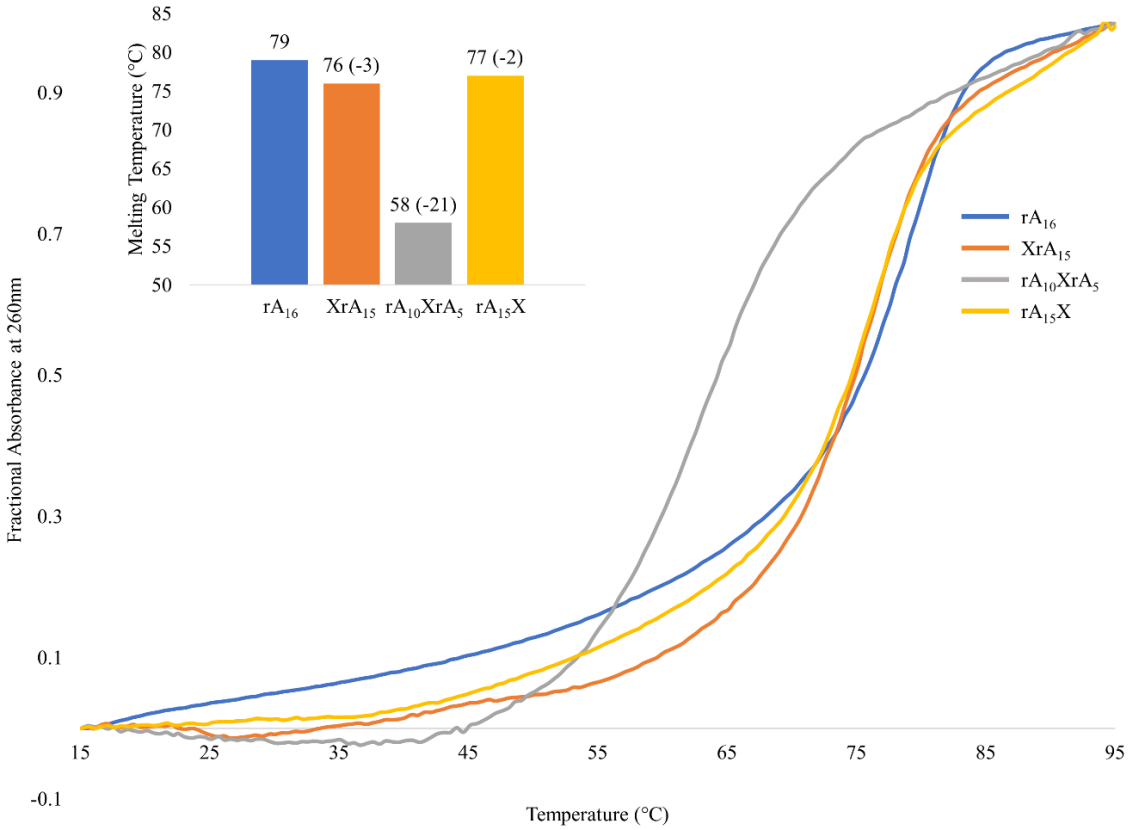

Figure 5.2: UV Thermal Denaturation Profiles of Duplexes Formed by Pyrene-Modified 16-mers at pH 4. (Buffer: 40 mM Na_2HPO_4, 30 mM citric acid, pH 4). 2.6 μM single strand concentrations.

Reassuringly, when additional pyrene modifications are incorporated at this central position, a corresponding increase in duplex stability (**Figure 5.3**) is observed. It was hypothesized that the incorporation of multiple pyrene groups to the duplex exterior could lead to stabilization through π-π stacking interactions. Here, an additive correlation between the number of pyrene groups incorporated and the resulting melting temperature of the duplex is seen. It is important to note that if pyrene stacking is occurring that there are, in fact, two distinct stacking networks (one per oligonucleotide strand) due to both strands being modified.

An interesting observation from this data is that duplexes modified at both ends show a highly stabilized species being formed (cyan curve). Previous crystal structures of the poly(A)

duplex at both acidic pH and neutral pH have shown the presence of a large, intermolecular duplex that forms from overhanging nucleosides.[114–116] The incorporation of pyrene at both ends of the duplex may lead to a stabilization of this structure. To our knowledge, this structure has not yet been shown to form in solution and this may represent the first experimental data showing its formation. Another possibility is that incorporation of pyrene at both ends of the duplex allows for the formation of a circular RNA motif that is held together by π-π stacking interactions at the point of closure.

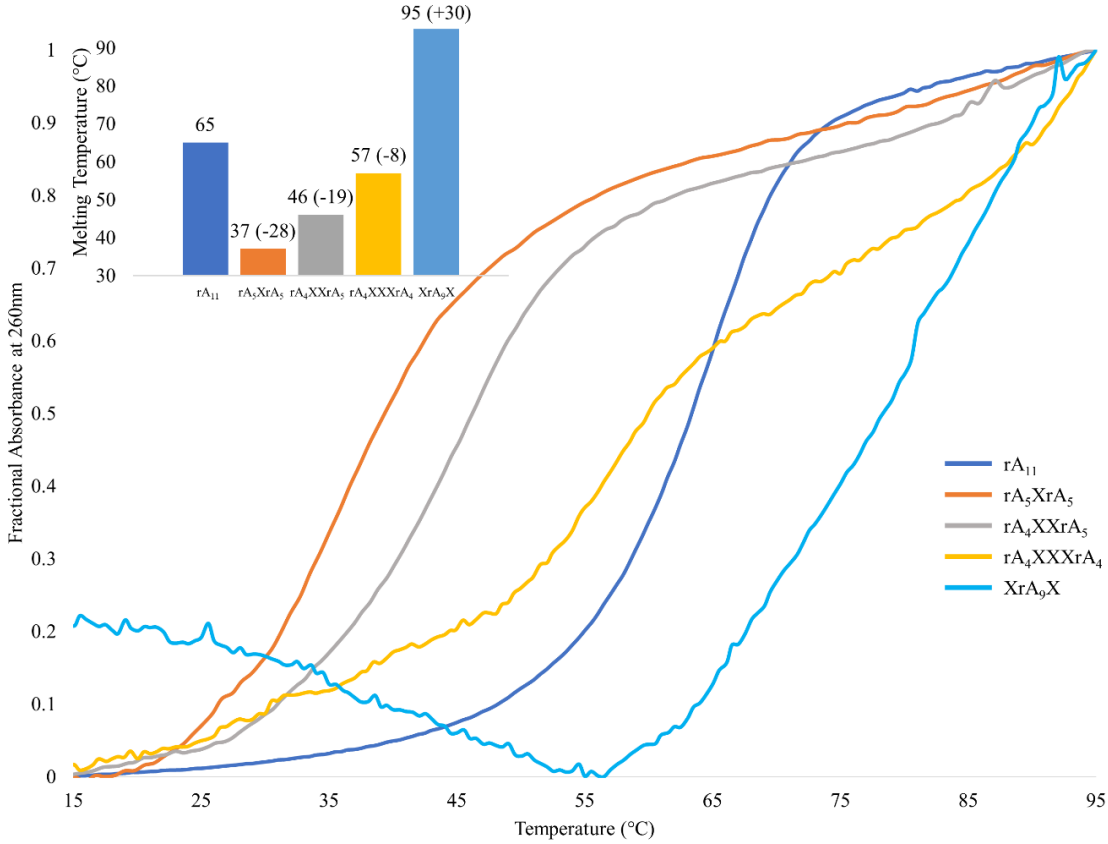

Figure 5.3: UV Thermal Denaturation Profiles of Duplexes Formed by poly(A) 11-mers Containing Successive Pyrene Modifications at pH 4. (Buffer: 40 mM Na_2HPO_4, 30 mM citric acid, pH 4). 3.7 μM single strand concentrations.

The longer oligonucleotide duplexes show similar trends as the 11-mer series, although to a lesser extent. In **Figure 5.4**, additional pyrene incorporations lead to a small stabilization of the

duplex (+5 °C). This is shown for both duplexes formed by doubly and triply substituted 16-mer poly(A). In this case, the derived melting temperatures are shown to plateau. This may be due to this stabilization being less significant in longer duplexes. It would still be expected that upon further modification, the T_m would continue to increase, but to smaller degree than with shorter duplexes.

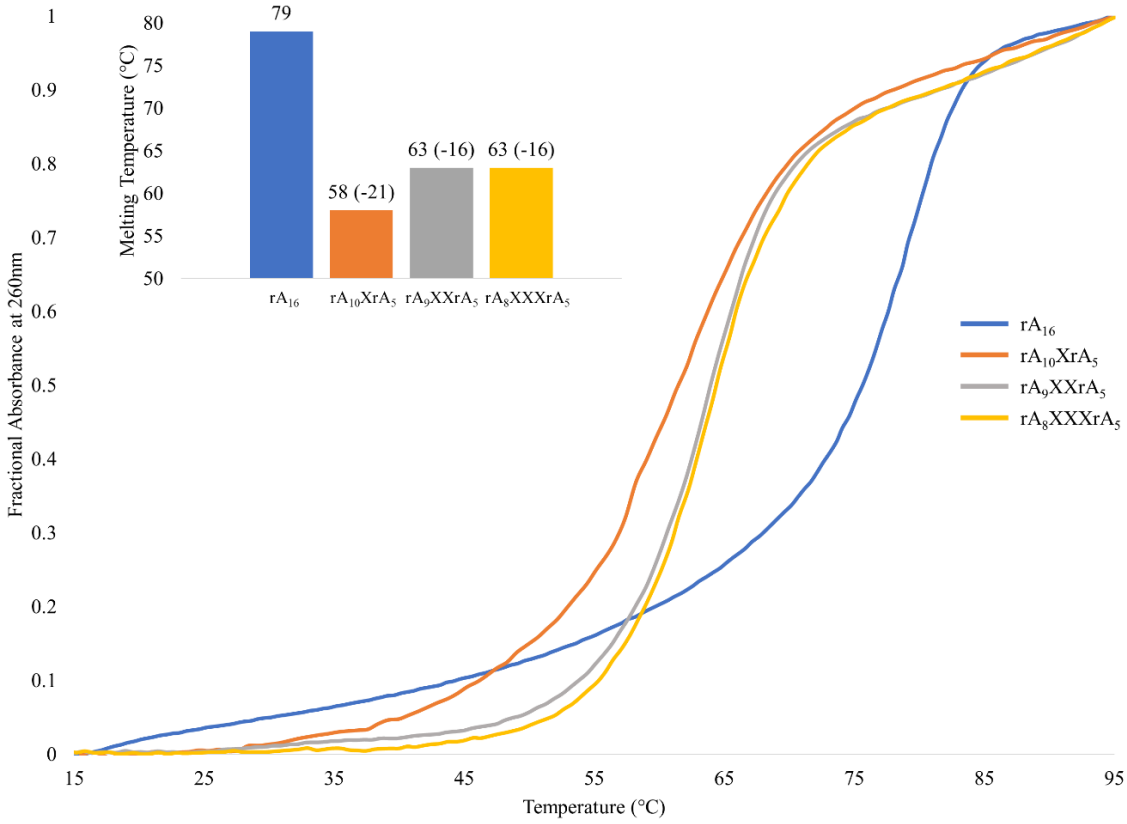

Figure 5.4: UV Thermal Denaturation Profiles of Duplexes Formed by poly(A) 16-mers Containing Successive Pyrene Modifications at pH 4. (Buffer: 40 mM Na_2HPO_4, 30 mM citric acid, pH 4). 2.6 µM single strand concentrations.

5.5 Thermal Reversibility of Pyrene-Modified Duplex Unfolding at pH 4

With the large changes in poly(A) duplex stability seen through T_m analysis, it is important to establish whether these pyrene modifications also lead to a change in the ability of these duplexes to anneal. In **Figure 5.5 A** the effect of pyrene incorporation on the refolding of the duplex formed by the 11-mers at pH 4 is shown. Regardless of the position of modification, there is a noticeable hysteresis of the annealing curve in comparison to the melting curve. The change was more significant with a central duplex modification (-10 °C) than with terminal modifications (-2 and -5 °C). This suggests that the destabilization of central pyrene modification also inhibits the rate of proper duplex annealing.

The presence of this modification on the duplex formed by the longer, 16-mer series, also leads to a hysteresis of the curves (**Figure 5.5 B**). The T_m values only differ by 2-4 °C, a difference comparable to that seen for the rA_{16} control, indicating that pyrene inclusion has no major effect on the annealing to form the longer duplexes.

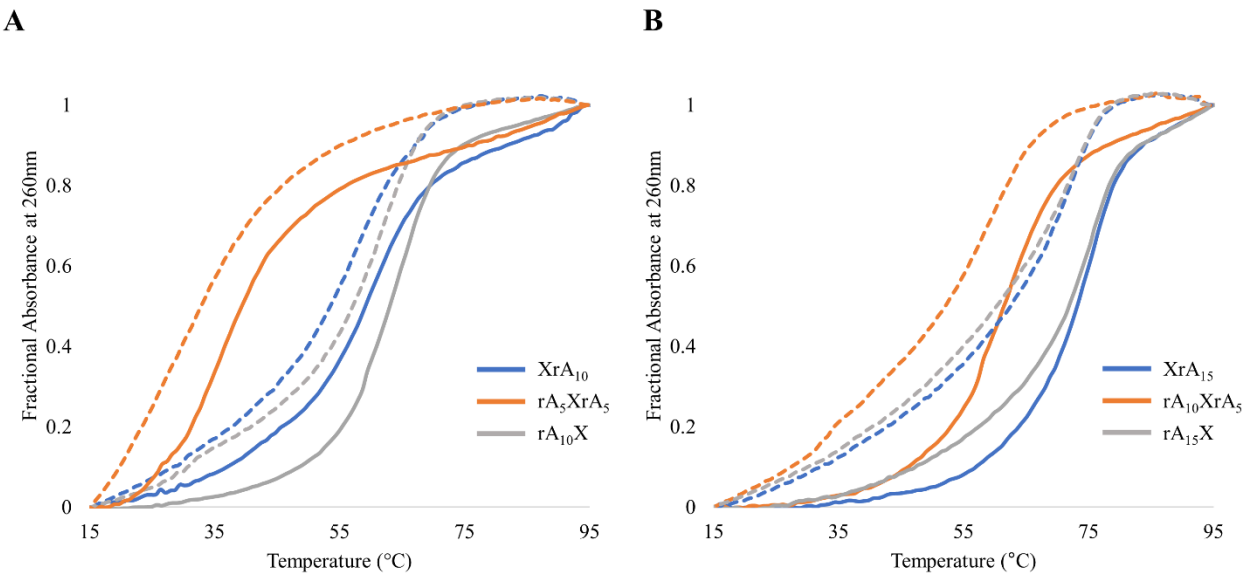

Figure 5.5: Thermal Reversibility Profiles at 260 nm of Pyrene-Modified poly(A) Duplexes at pH 4. (**A**) 11-mers and (**B**) 16-mers. (Buffer: 40 mM Na_2HPO_4, 30 mM citric acid, pH 4). Single strand concentrations were 3.7 μM for 11-mers and 2.6 μM for 16-mers. (Solid: Heating, Dashed: Cooling).

5.6 CD Analysis of Pyrene-Modified poly(A) Duplexes at pH 4

Structural changes to the poly(A) duplex because of pyrene modifications were examined using CD spectroscopy. **Figure 5.6** shows the CD traces of these duplexes at pH 4. The molar ellipticity maxima and minima for these pyrene-modified duplexes are less pronounced than for the respective control sequences, which may be attributed to pyrene absorption at 260 nm. As a result of this absorption, concentrations used of pyrene-containing oligonucleotides are slightly less than desired due to contributions from both the oligonucleotide and pyrene moieties towards this value.[187] Numerous reports have been published on pyrene-containing oligonucleotides where no mention is paid to correcting for this effect. Similarly, orders of magnitude difference in poly(A) concentrations would be needed to begin to see any significant changes to the stability of these duplexes.[188] Apart from differences in magnitude, the curves seen in **Figure 5.6** have very similar

shapes to the control sequences, indicating that pyrene modification does not lead to significant changes to the poly(A) duplex structure. There is a very slight shift in the crossover point for those duplexes which are modified at the 5'-end, but this may just be an aberration caused by the concentration differences.

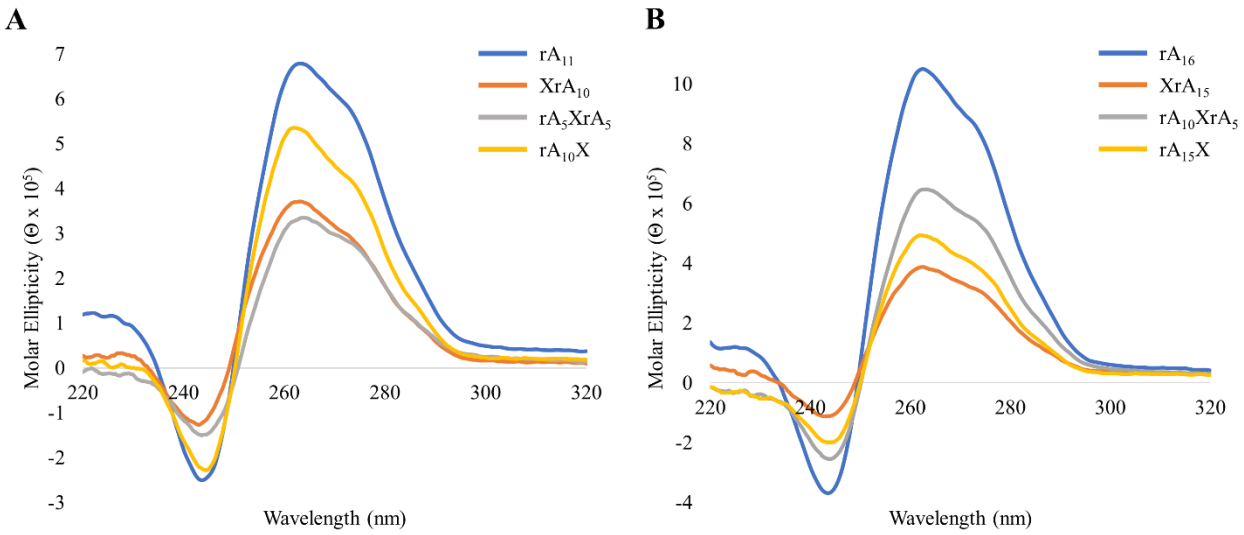

Figure 5.6: CD Spectra of poly(A) Duplexes Containing a Single Pyrene Modification per Strand at pH 4. (**A**) 11-mers and (**B**) 16-mers. (Buffer: 40 mM Na_2HPO_4, 30 mM citric acid, pH 4). Single strand concentrations were 3.7 µM for 11-mers and 2.6 µM for 16-mers. CD spectra recorded at 15 °C, 20 nm min^{-1}, 5 accumulations.

Poly(A) duplexes modified with multiple pyrene groups on each strand show similar decreases in the expected maxima and minima (**Figure 5.7**). They do all, however, adhere to the general shape of the control sequence spectra, suggesting no major changes to the duplex structure at pH 4. Of special note, is that the duplex formed by XrA_9X shows the lowest signals at the maxima and minima out of all the duplexes. This is not expected to be due to a concentration difference, as both XrA_9X and rA_4XXrA_5 contain the same number of pyrene modifications and were found to have similar A_{260} readings at 95 °C (Data not shown). This suggests that there are

differences in the global stacking structure of this duplex in comparison to those modified at a central position or with just a single modification.

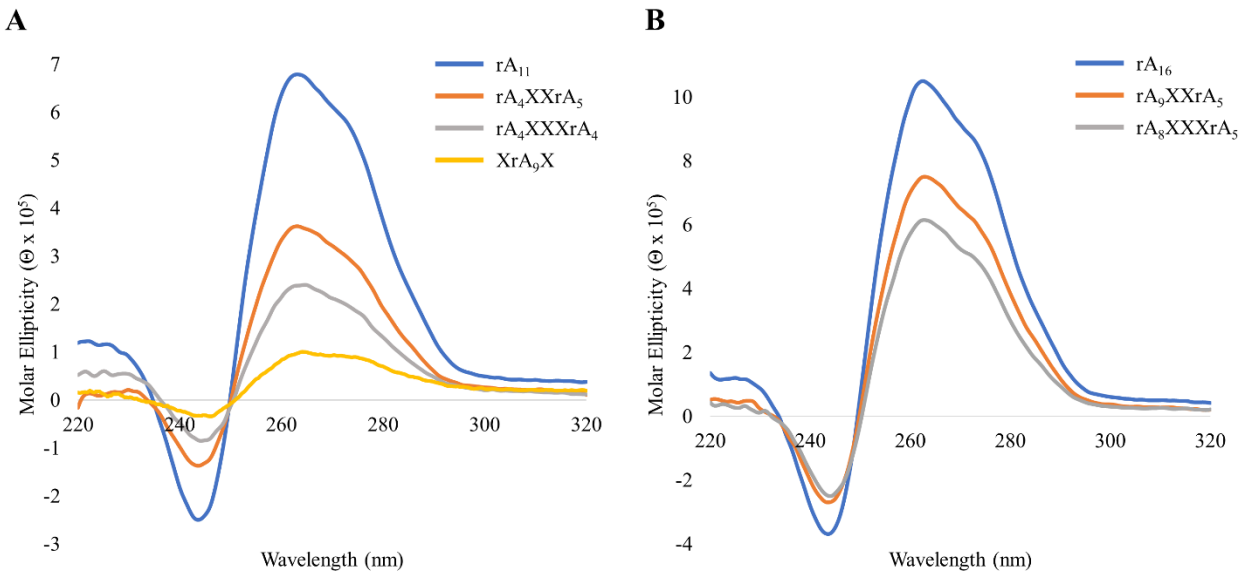

Figure 5.7: CD Spectra of poly(A) Duplexes Containing Multiple Pyrene Modifications per Strand at pH 4. (**A**) 11-mers and (**B**) 16-mers. (Buffer: 40 mM Na_2HPO_4, 30 mM citric acid, pH 4). Single strand concentrations were 3.7 µM for 11-mers and 2.6 µM for 16-mers. CD spectra recorded at 15 °C, 20 nm min^{-1}, 5 accumulations.

5.7 UV Absorption of Pyrene-Modified poly(A) Duplexes at pH 4

Characteristic pyrene absorption peaks in the range of 300-400 nm allow for exploration of the microenvironment surrounding the group and deduce possible conformations and interactions that pyrene may be involved in. **Figure 5.8 A** shows the UV spectra of poly(A) duplexes formed by singly-modified 11-mers and 16-mers at pH 4. In both **Figure 5.8 A** and **B**, two distinct absorbance maxima centered around 334.5 and 350.5 nm are seen. In addition, a small shoulder is visible around 321 nm. These absorption spectra are slightly redshifted (+8 nm from those seen for 2'-*O*-(1-pyrenylmethyl)uridine),[177] but are in line with values reported earlier for the

same modification.[174] Generally, intercalation of pyrene into the double helix is associated with a shift of the absorption spectrum to higher wavelengths due to the π-stacking interactions with adjacent nucleobases.[189] While still possible, the destabilization observed during previous melting analyses would suggest that intercalation is not occurring in this case. Another possibility would be inter- or intra-strand interactions between pyrene groups as this would also be expected to lead to an observed redshift. Unfortunately, as seen in **Table 5.1**, the magnitude of these observed shifts does not seem to change with increasing numbers of pyrene modifications. This leads us to postulate that the pyrene groups may be engaging in weak interactions with the aromatic 1,2,3-triazole linkers.

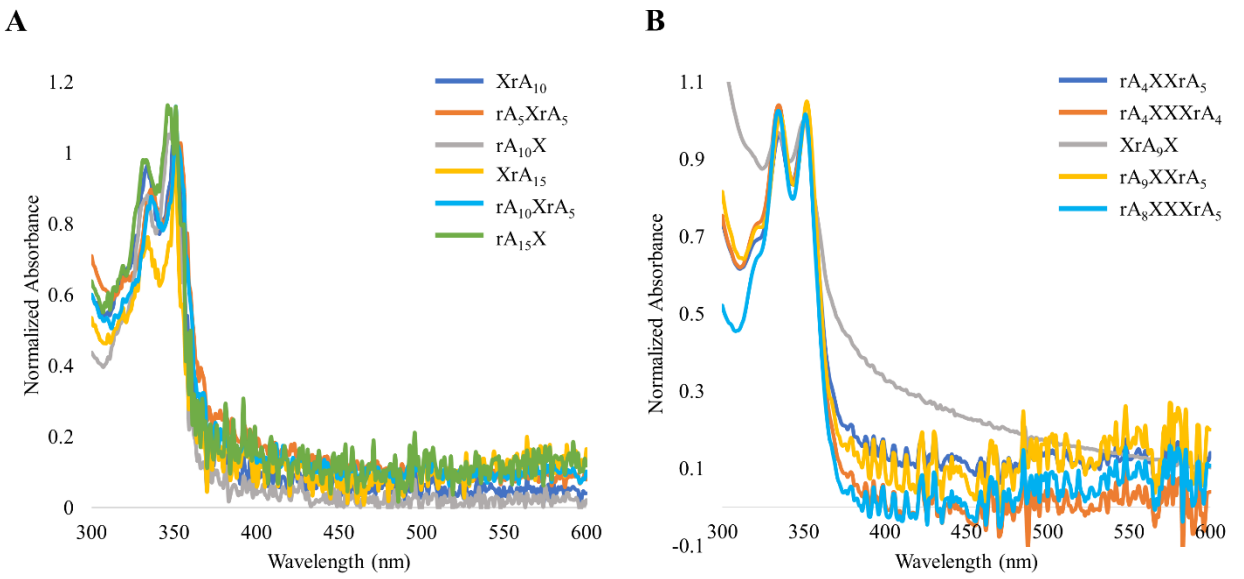

Figure 5.8: UV Spectra of Pyrene-Modified poly(A) Duplexes at pH 4. (**A**) Single and (**B**) Multiple modifications in 11-mers and 16-mers. (Buffer: 40 mM Na_2HPO_4, 30 mM citric acid, pH 4). Single strand concentrations were 3.7 μM for 11-mers and 2.6 μM for 16-mers. UV spectra recorded at RT, 400 nm min^{-1}. Spectra corrected for absorbance differences at 350 nm.

Sequence	Absorbance Maxima 1 (nm)	Absorbance Maxima 2 (nm)
XrA_{10}	334	351
rA_5XrA_5	336	351
$rA_{10}X$	334	349
XrA_{15}	334	350
$rA_{10}XrA_5$	336	351
$rA_{15}X$	333	351
rA_4XXrA_5	335	351
rA_4XXXrA_4	335	351
XrA_9X	335	350
rA_9XXrA_5	336	352
rA_8XXXrA_5	334	351

Table 5.1: UV Absorption of Pyrene-Modified Duplexes at pH 4.

When temperature is varied, the UV absorption pattern of these pyrene-functionalized poly(A) duplexes exhibits redshifting of the absorbance maxima. As shown in **Figure 5.9 A**, upon heating the poly(A) duplex formed by $rA_{10}X$ there is a corresponding blueshift in the absorption maxima by ~ 3 nm. Subsequently, when this same sample is then cooled back down to 10 °C, the maxima undergo a bathochromic shift back to their initial position (**Figure 5.9 B**). Duplexes modified at the 5' or center, as well as duplexes with multiple central modifications all showed identical shifting patterns, indicating that the observed interaction occurs irrespective of modification location or number of groups incorporated (Data not shown). The magnitude of this shift is slightly larger (4-5 nm) when the duplex is modified in the middle, compared to when it is modified at either end (2-3 nm).

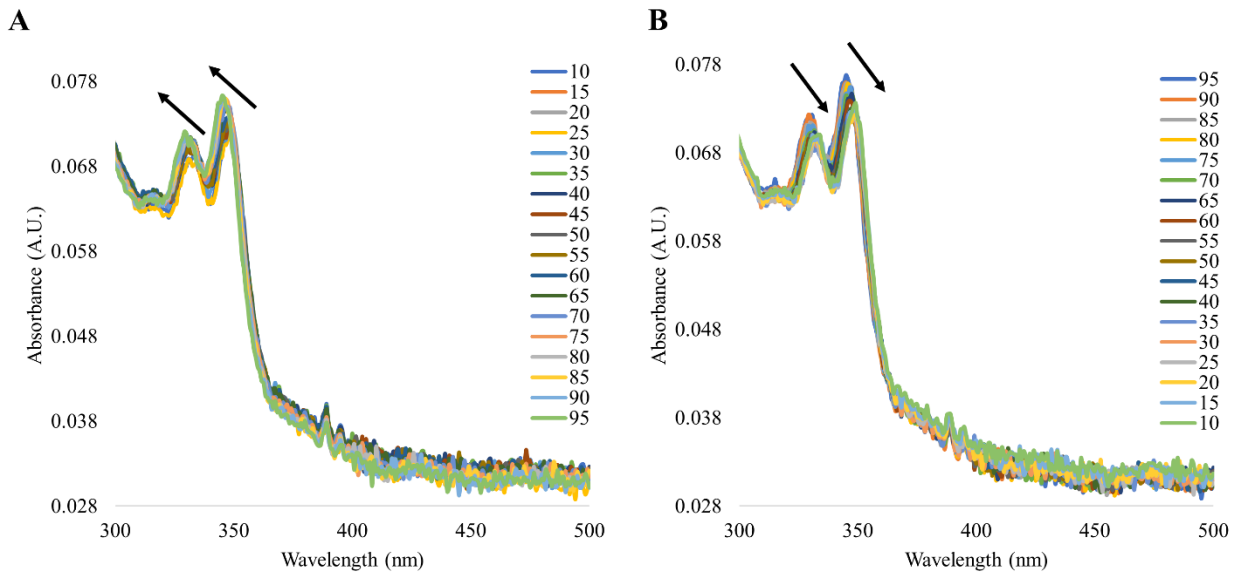

Figure 5.9: Effect of Temperature on UV Absorption of a Pyrene-Modified poly(A) Duplex Formed from $rA_{10}X$ at pH 4. (**A**) Heating and (**B**) Cooling. (Buffer: 40 mM Na_2HPO_4, 30 mM citric acid, pH 4). Single strand concentrations were 3.7 μM. 400 nm min^{-1}, 2.5 °C min^{-1}.

5.8 Fluorescence Analysis of Pyrene-Modified poly(A) Duplexes at pH 4

Pyrene-functionalized oligonucleotides are often employed as fluorescent probes for targeted binding and higher-ordered structure formation.[174,177,180,182,187,190,191] The fluorescence emission spectrum of pyrene is highly dependant on the environment and, as such, events such as intercalation and electronic coupling have a drastic effect on the observed fluorescence. There are numerous characteristic fluorescence peaks, named bands I-V, which appear at ~ 375, 379, 385, 395, and 410 nm respectively.[191] However, normally only bands I and III are seen due to a broadening of the signals.[192] Furthermore, Band I is usually higher in intensity when pyrene is positioned in a polar environment, where as, Band III is usually significantly higher when the group is positioned in a hydrophobic environment.[178,193]

The fluorescence spectra for poly(A) duplexes that are modified with a single pyrene group at pH 4 are shown in **Figure 5.10**. All spectra show emission maxima at ~ 380 and 400 nm, with small shoulders around 420 nm. For the 5'-modified duplexes there is an additional, broad, band centered at 482 nm. It is assumed that the two maxima at 380 and 400 nm are Bands I and III, respectively which originate from the emission of pyrene monomers. In comparison to the previously reported fluorescence band positions, these experimental results are redshifted like what was observed for the absorbance spectra, reaffirming the possibility of interactions between the pyrene and other groups. The intensity ratios of Band III to Band I, as shown in **Table 5.2**, are all equal to approximately 1 or less. This suggests that the pyrene groups are positioned in a more polar environment such as the grooves of the poly(A) duplex.

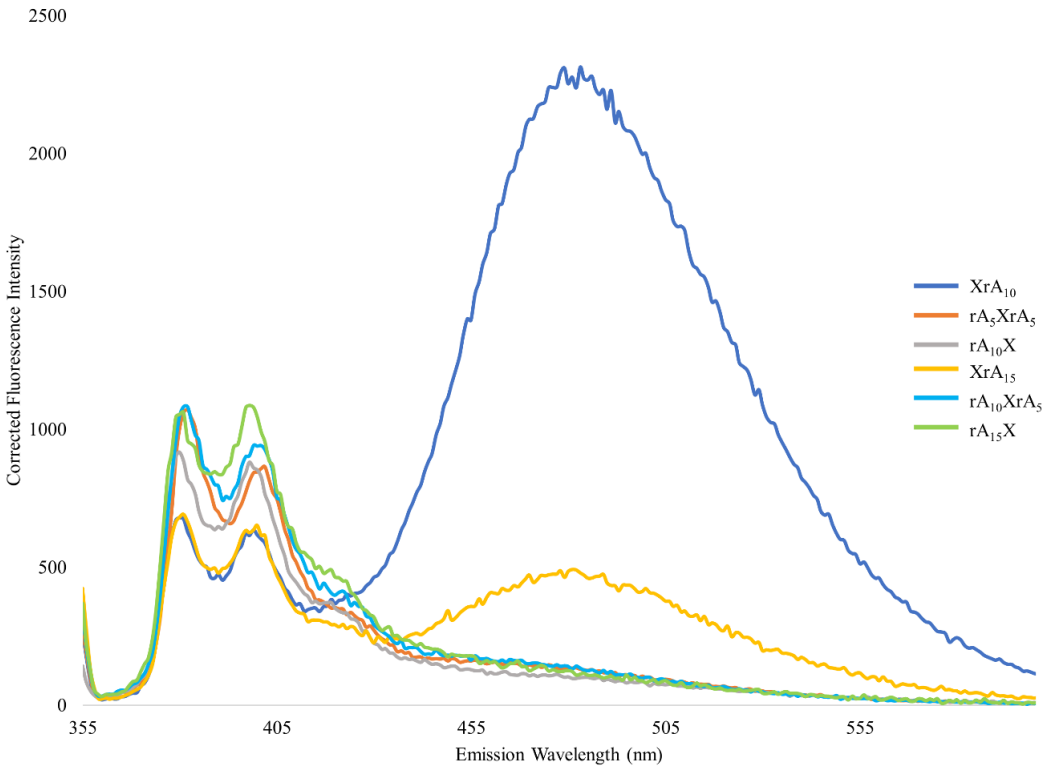

Figure 5.10: Fluorescence Emission of Pyrene-Functionalized poly(A) Duplexes with a Single Incorporation per Strand at pH 4. Excitation at 350 nm. (Buffer: 40 mM Na_2HPO_4, 30 mM citric acid, pH 4). Single strand concentrations were 3.7 µM for 11-mers and 2.6 µM for 16-mers. Fluorescence intensity corrected for absorbance differences at 350 nm.

The broad bands that appear at ~ 482 nm have experienced a large (82 nm) redshift relative to the monomer emission signals. Fluorescence bands at this position have been previously attributed to the formation of pyrene excited state dimers (excimers).[174,191] These dimers occur when a pyrene in an electronically excited state interacts with a ground state pyrene.[194] Efficient excimer formation suggests that the pyrene groups have adopted a coplanar orientation and are within 3.4 Å.[173]

The formation of excimers through 5'-pyrene modification but not with 3'-pyrene modification leads to two possible conclusions. Either the pyrene groups located at the 5'-end of the duplex are in closer proximity than those at the 3'-end or the poly(A) duplex is more flexible at that end, allowing for the pyrene groups to adopt the coplanar orientation required for efficient excimer formation. **Table A.5** shows the intra-strand and inter-strand distances between adjacent O2' atoms for a poly(A) duplex crystallized at pH 7 (PDB 4JRD).[114] In **Table A.5**, the distance between O2' atoms on adjacent strands is shown to be almost identical at both ends of the duplex (~ 12.3 Å). The similarity between the ends of the duplex, and the relatively large distance observed, suggests that excimer formation here must be due to a sheering event or just a heightened flexibility of the poly(A) duplex at the 5'-end, which would allow opposing pyrene groups to come close enough in proximity to adopt the needed conformation. Previous work by Dioubankova et al. looked at the influence of pyrene incorporated through an ara-carbamate linkage at the C2'-position of uridine.[195] They saw excimer formation when their DNA duplexes were modified at the 5'-end with pyrenes on opposing strands. When these strands were extended, to position the pyrene groups in a more central position, this observed excimer signal was lost.[195] They attributed the formation of this excimer interaction to near-terminal duplex distortion.[195]

The introduction of increasing numbers of pyrene modifications into these poly(A) duplexes leads to excimer formation in all cases (**Figure 5.11**). The signals emitted from pyrene monomers are drastically reduced and instead, broad signals centered around 479 nm are observed. The intensity of this band increases accordingly with the number of pyrene groups that are incorporated. For the duplex formed by XrA_9X, a signal far lower than rA_4XXrA_5 is seen, which agrees with the previous experiment that only showed excimer formation at the 5'-end of the duplex. Quantum yield analysis of these pyrene-modified duplexes shows an increase in the yield for duplexes containing increased numbers of modified nucleobases (**Table 5.2**). It is also observed that the quantum efficiency of the 5'-modified duplexes is higher for the shorter duplexes. In contrast, the longer duplexes bearing multiple, central, pyrene modifications show a higher efficiency than the shorter duplexes.

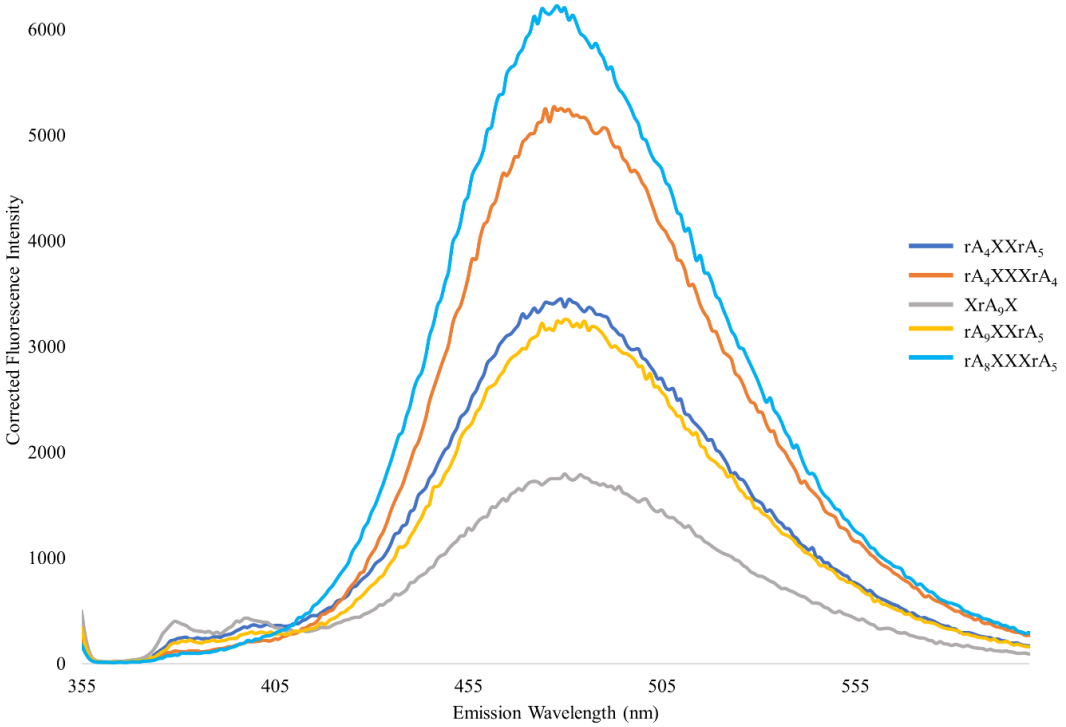

Figure 5.11: Fluorescence Emission of Pyrene-Functionalized poly(A) Duplexes with Multiple Incorporations per Strand at pH 4. Excitation at 350 nm. (Buffer: 40 mM Na_2HPO_4, 30 mM citric acid, pH 4). Single strand concentrations were 3.7 µM for 11-mers and 2.6 µM for 16-mers. Fluorescence intensity corrected for absorbance differences at 350 nm.

Sequence	Band 1 (nm)	Band 3 (nm)	Excimer Band (nm)	I_{III}/I_I	Quantum Yield (%)
XrA_{10}	380	397	483	0.905	15.41
rA_5XrA_5	382	402	-	0.812	-
$rA_{10}X$	380	398	-	0.960	-
XrA_{15}	381	400	481	0.918	1.56
$rA_{10}XrA_5$	381	399	-	0.865	-
$rA_{15}X$	381	398	-	1.03	-
rA_4XXrA_5	382	403	479	1.05*	45.29
rA_4XXXrA_4	383	402	478	1.05*	62.26
XrA_9X	379	398	480	1.05*	4.42
rA_9XXrA_5	383	399	480	1.04*	55.17
rA_8XXXrA_5	381	398	478	1.04*	>100

Table 5.2: Fluorescence Analysis of Pyrene-Modified poly(A). *Estimated Values.

To further explore the possibility of intercalation of the pyrene group into the poly(A) duplex core, a series of temperature-dependant fluorescence experiments were performed. **Figure 5.12** shows the temperature-dependant fluorescence of rA_5XrA_5 at 380 nm. If pyrene is intercalating into the duplex of poly(A), a drastic increase in the monomer fluorescence upon denaturing of the duplex would be expected. This is due to the alleviation of fluorescence quenching by the neighbouring nucleobases.[181] **Figure 5.12** shows a decrease in fluorescence emission at 380 nm upon an increase in temperature above the melting temperature of the duplex. This corroborates earlier results which suggested that pyrene was, in fact, not intercalated. The decrease in emission can be explained by the increased flexibility of the ssRNA, which will lead to enhanced quenching of the pyrene compared to when it is positioned in the duplex groove.

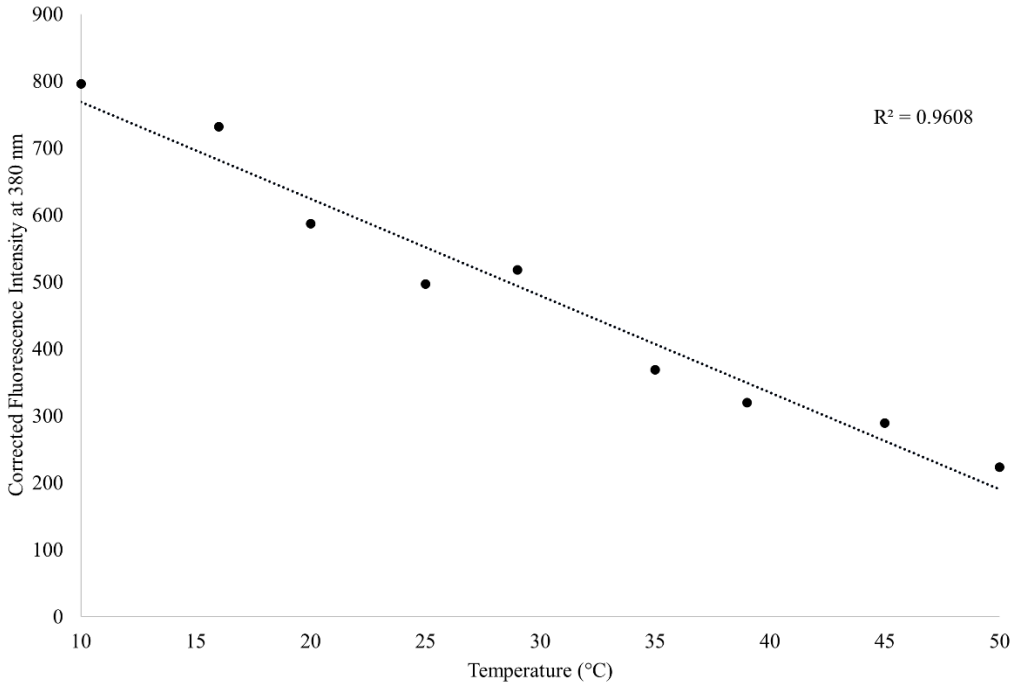

Figure 5.12: Fluorescence Emission of the Pyrene-Functionalized poly(A) Duplex Formed by rA_5XrA_5 at pH 4. Excitation at 350 nm. (Buffer: 40 mM Na_2HPO_4, 30 mM citric acid, pH 4). Single strand concentrations were 3.7 μM. Fluorescence intensity corrected for absorbance differences at 350 nm.

Similar results are observed for the duplex formed by the doubly modified 11-mer as shown in **Figure 5.13**, where a drastic decrease in the excimer emission at 480 nm is observed. Interestingly, the midpoint for this transition occurs at approximately 33 ℃, lower than the UV thermal denaturation temperature of this duplex (46 ℃). A decrease in the emission at 380 nm is also observed. Photobleaching was found to be a non-factor for these experiments (**Figure A.35**).

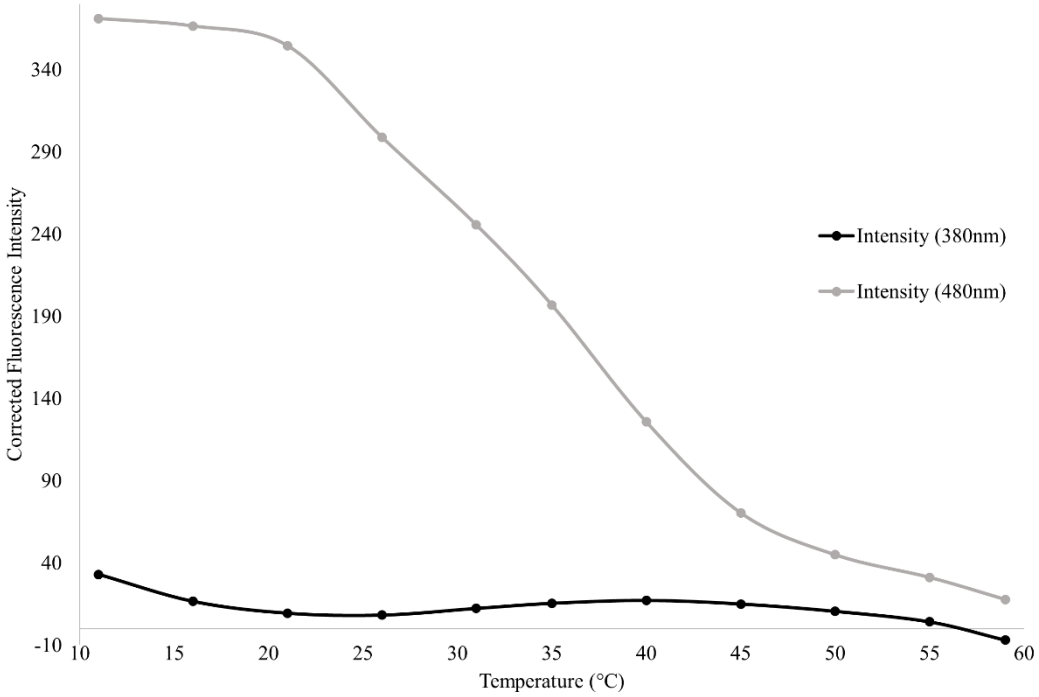

Figure 5.13: Fluorescence Emission of the Pyrene-Functionalized poly(A) Duplex Formed by rA_5XXrA_4 at pH 4. Excitation at 350 nm. (Buffer: 40 mM Na_2HPO_4, 30 mM citric acid, pH 4). Single strand concentrations were 3.7 μM. Fluorescence intensity corrected for absorbance differences at 350 nm.

5.9 Native PAGE Analysis at pH 4

Native PAGE analysis of the pyrene-modified poly(A) duplexes shows a higher retention of the bands relative to the double-stranded poly(A) duplex controls (**Figure 5.14**). This increased

retention can be attributed to the large size of the pyrene group rather than any higher order structures. In contrast, no major band was observed for XrA_9X. This oligonucleotide, which was previously hypothesized to be forming a staggered duplex like structure, was incapable of permeating into the gel over multiple experimental attempts, which supports the theory of a potential multimerized structure being formed.

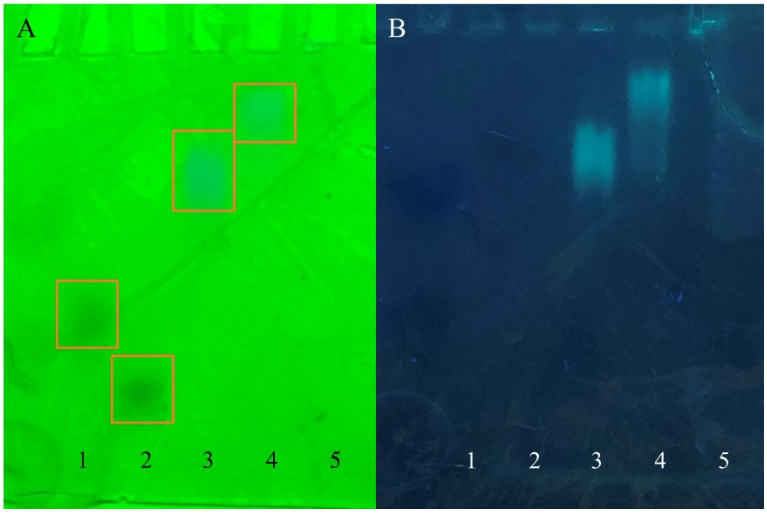

Figure 5.14: 12.5 % Acrylamide/Bisacrylamide (19:1) Native PAGE of Pyrene-Modified poly(A) Duplexes. (**A**) Short-wave UV shadowing and (**B**) Long-wave UV shadowing. (Buffer: 40 mM Na_2HPO_4, 30 mM citric acid, 1.1 mM EDTA, pH 4). Run at 100 V for 5 h. 0.1 OD of each oligo loaded in 10 µL of 40 % sucrose, pH 4 loading buffer. (Lane 1: rA_{11}; lane 2: rU_{11}; lane 3: rA_4XXrA_5; lane 4: rA_4XXXrA_4; lane 5: XrA_9X).

5.10 UV Thermal Denaturation (T_m) Analysis of Pyrene-Modified poly(A) Duplexes at pH 7

UV thermal denaturation analysis of poly(A) duplexes at pH 7 demonstrated, similar to trends observed at pH 4, the large effect that the incorporation of a pyrene has on duplex stability. **Figure 5.15** shows that the incorporation of this modification on either end of the duplex leads to

negligible results, where as, modification at a central position leads to a large destabilization of the duplex. This large destabilization, coupled with the fact that poly(A) duplexes at pH 7 are less stable, is demonstrated by the lack of a sigmoidal transition for the denaturation curve.

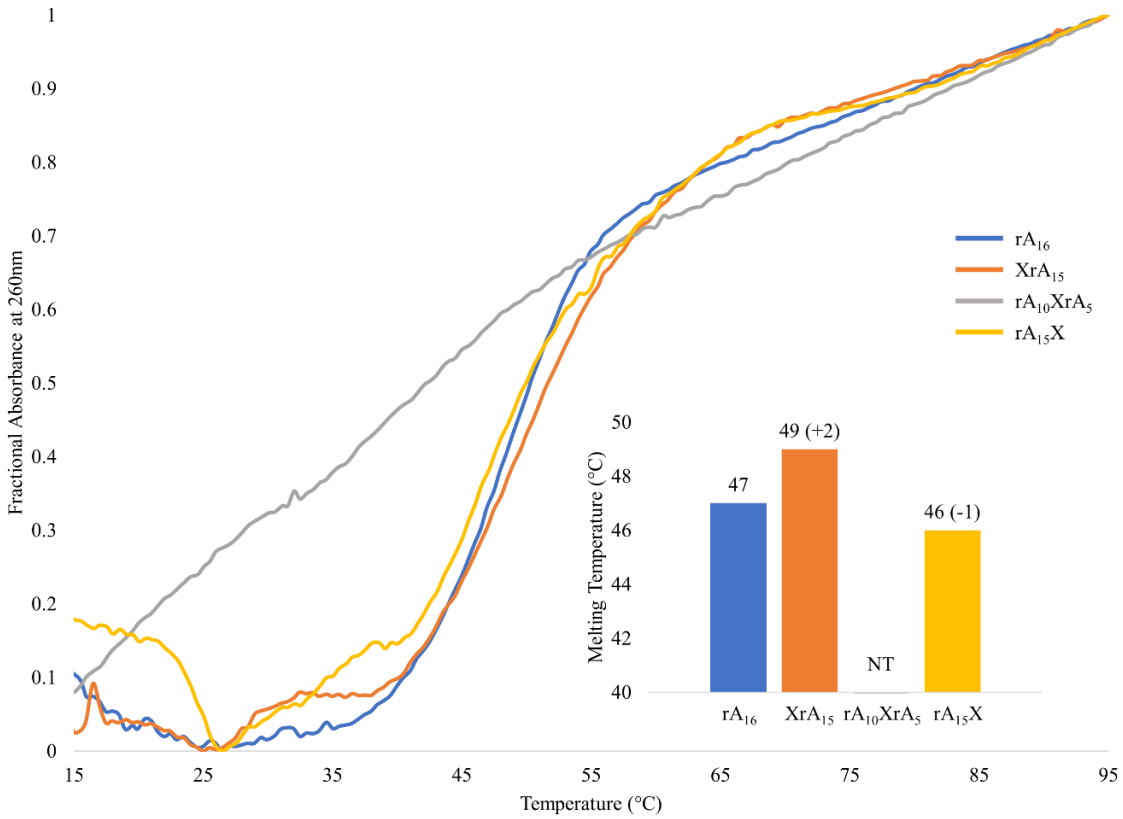

Figure 5.15: UV Thermal Denaturation Profiles of Duplexes Formed by 16-mer poly(A) Containing a Single Pyrene Modification at pH 7. (Buffer: 40 mM Na_2HPO_4, 30 mM citric acid, 4.4 M NH_4Cl, pH 7). 2.6 µM single strand concentrations. NT: No transition observed.

The incorporation of multiple pyrene groups at this central position leads to more stable duplexes, albeit, none with the characteristic sigmoidal transition that is indicative of a two-state transition. The incorporation of two pyrene groups leads to a multi-phasic transition with an upper transition at 59 °C as shown in **Figure 5.16**. This suggests that more than a single structure may have formed. Incorporation of an additional pyrene modification leads to a highly stabilized species with no observable upper plateau. It is important to note that the increasing pyrene content

of these oligonucleotides is also expected to lead to a decrease in oligonucleotide solubility in this high salt buffer system. One possible explanation for the abnormal melting behaviour of both rA_9XXrA_5 and rA_8XXXrA_5 is that decreased solubility at low temperatures leads to a precipitation of the oligonucleotides and the formation of nucleic acid aggregates. Upon heating, the oligonucleotide solubility would increase accordingly, and duplex melting would occur, but strange transitions may be observed due to the initial agglomeration.

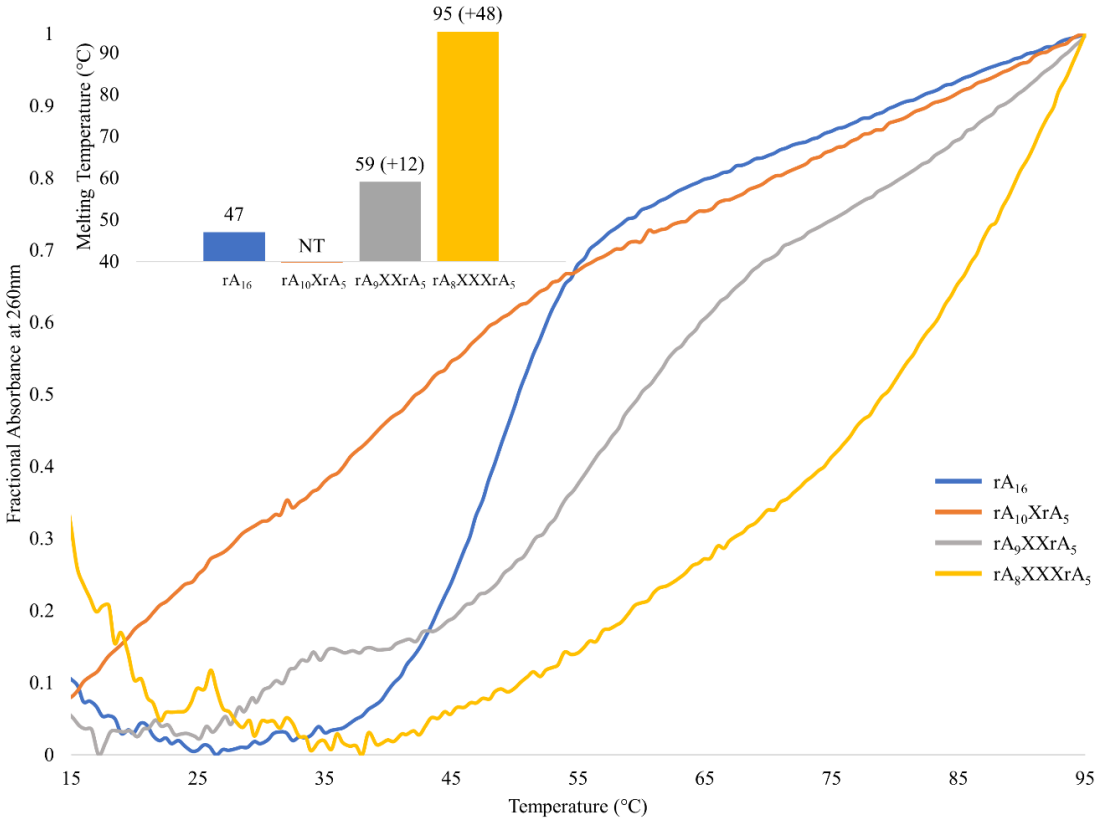

Figure 5.16: UV Thermal Denaturation Profiles of Duplexes Formed by 16-mer poly(A) Containing Multiple Pyrene Modifications at pH 7. (Buffer: 40 mM Na_2HPO_4, 30 mM citric acid, 4.4 M NH_4Cl, pH 7). 2.6 µM single strand concentrations. NT: No transition observed.

5.11 Thermal Reversibility of Pyrene-Modified Duplex Unfolding at pH 7

The dissociation and annealing curves of the pyrene-modified poly(A) duplexes containing a single modification at pH 7 are shown in (**Figure 5.17 A**). Duplexes that are modified at the termini show a sigmoidal transition upon heating and cooling (~ 2 ℃ hysteresis), where the absorbance returns to what was initially recorded before heating. However, for the centrally modified poly(A) no sigmoidal transition is observed for either heating or cooling.

No duplex formation is seen for duplexes incorporating multiple pyrene groups (**Figure 5.17 B**). The lack of a clear sigmoidal transition for either the doubly or triply modified 16-mer poly(A) oligonucleotides suggests that no stable duplexes are being formed under these conditions; or that their formation is far slower than the initial melting. The significant hysteresis that is observed between the melting and annealing curves demonstrates the large effect that these pyrene groups have on the ability for these nucleic acids to adopt any form of higher ordered structure.

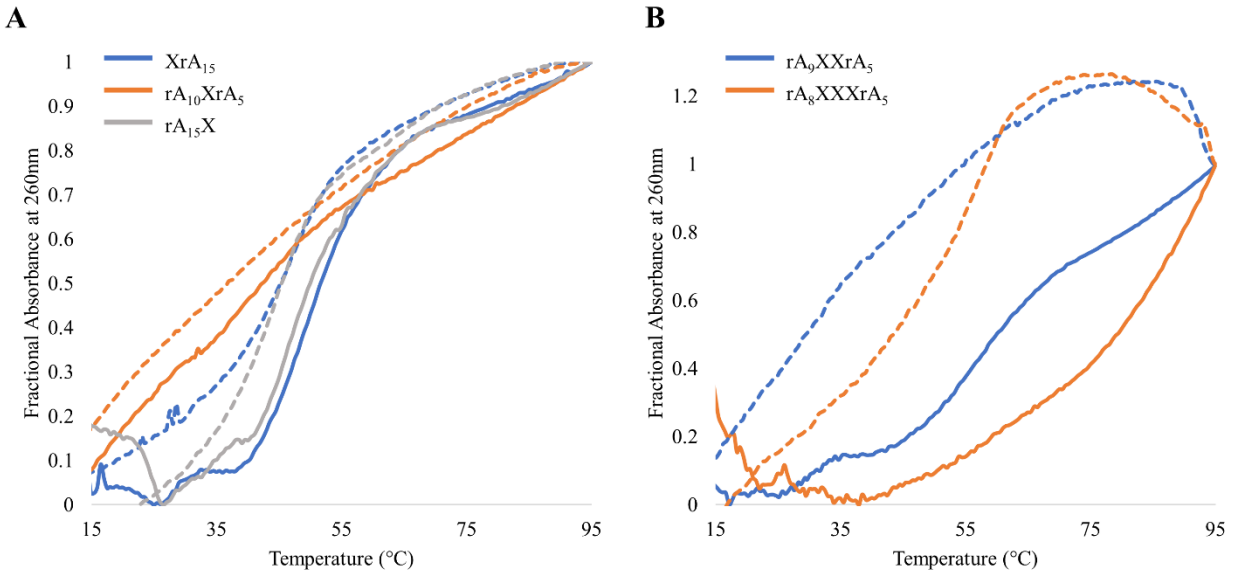

Figure 5.17: Thermal Reversibility Profiles of poly(A) Duplexes Formed by 16-mer poly(A) at pH 7. (**A**) Single and (**B**) Multiple pyrene incorporations. (Buffer: 40 mM Na_2HPO_4, 30 mM citric acid, 4.4 M NH_4Cl, pH 7). 2.6 µM single strand concentrations. (Solid: Heating, Dashed: Cooling).

5.12 CD Analysis of Pyrene-Modified poly(A) Duplexes at pH 7

The CD spectra of the pyrene-modified poly(A) duplexes formed at pH 7 show a reduced ellipticity relative to the rA_{16} control under the same conditions (**Figure 5.18 A**), similar to what was previously observed for the pyrene-modified duplexes at pH 4. The crossover point and negative cotton peak is slightly shifted for the centrally-modified duplex. This may suggest a slight perturbation of the duplex structure due to the inclusion of pyrene at this position, which results in the observed duplex destabilization. No shifts in the crossover point were observed for the same duplexes at pH 4.

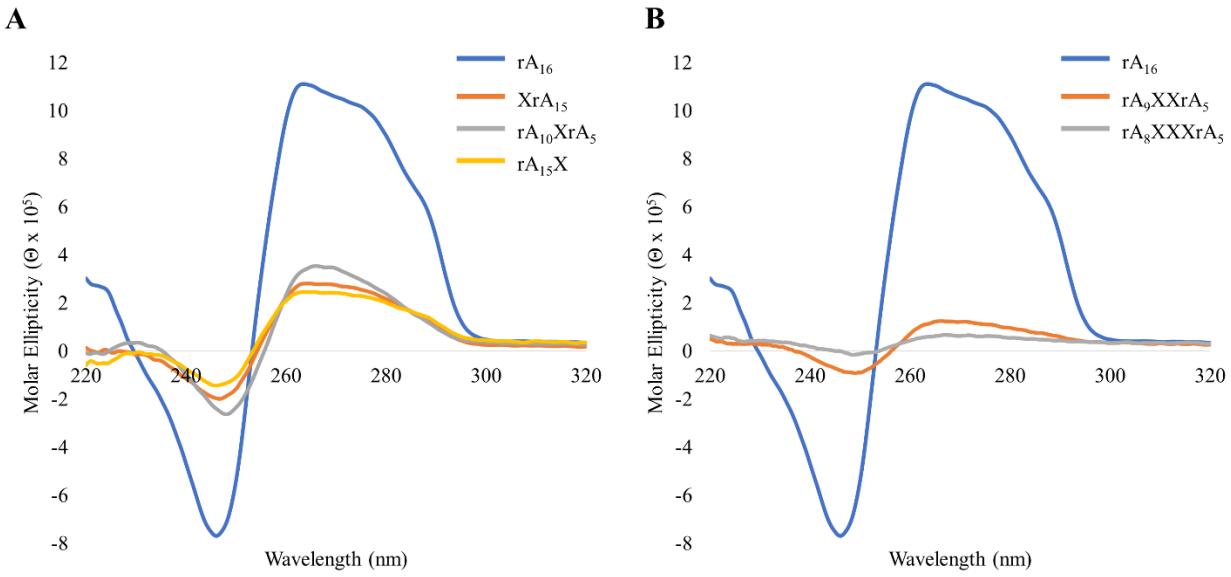

Figure 5.18: CD Spectra of poly(A) Duplexes Containing Pyrene Modification(s) at pH 7. (**A**) Single and (**B**) Multiple incorporations. (Buffer: 40 mM Na_2HPO_4, 30 mM citric acid, 4.4 M NH_4Cl, pH 7). 2.6 µM single strand concentrations. CD spectra recorded at 15 °C, 20 nm min^{-1}, 5 accumulations.

Poly(A) duplexes with multiple pyrene modifications show a severely reduced ellipticity under these pH 7 conditions (**Figure 5.18 B**); even more so than the duplexes that were modified

with only a single pyrene group. A shift in both the positive and negative cotton peaks towards longer wavelengths can also be observed for both sequences. This reduced ellipticity correlates with the previous UV thermal denaturation results that showed no clear signs of stable duplexes being formed. At these low temperatures, solubility issues may be leading to a precipitation of any duplex structures, contributing to the reduced signal intensity.

5.13 UV Analysis of Pyrene-Modified poly(A) Duplexes at pH 7

UV spectra of these poly(A) duplexes shows the characteristic pyrene absorption maxima in the region from 310-360 nm (**Figure 5.19**). For all sequences, absorbance maxima were observed at approximately 335 and 350 nm. The lack of any shifting in these absorption peaks indicates that there are no additional interactions with pyrene in addition to those already seen at pH 4.

The UV analysis of oligonucleotides containing multiple pyrenes was difficult as baseline issues were always present (**Figure 5.19 B**). This is possibly due to the presence of a high salt content, in addition to solubility issues. The triply modified sequence, rA_8XXXrA_5, had visible maxima at the expected region, but these were not resolved enough to characterize.

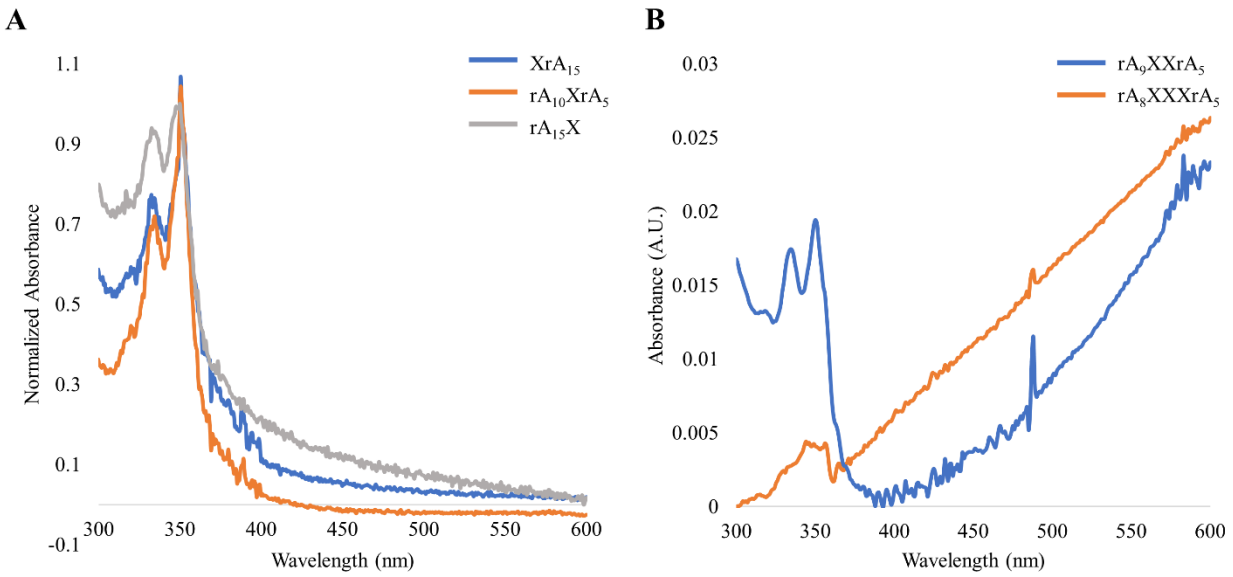

Figure 5.19: UV Spectra of Pyrene-Modified poly(A) Duplexes at pH 7. (**A**) Single and (**B**) Multiple pyrene incorporations. (Buffer: 40 mM Na_2HPO_4, 30 mM citric acid, 4.4 M NH_4Cl, pH 7). 2.6 µM single strand concentrations. UV spectra recorded at RT, 400 nm min^{-1}. Spectra corrected for absorbance differences at 350 nm.

Sequence	Absorbance Maxima 1 (nm)	Absorbance Maxima 2 (nm)
XrA_{15}	334	351
$rA_{10}XrA_5$	335	351
$rA_{15}X$	333	350
rA_9XXrA_5	334	350
rA_8XXXrA_5	ND	ND

Table 5.3: UV Absorption of Pyrene-Modified Duplexes at pH 7. ND: Not determined.

5.14 Fluorescence Analysis of Pyrene-Modified poly(A) Duplexes at pH 7

Fluorescence analysis of poly(A) oligonucleotides with a single pyrene incorporation on each strand at pH 7 show mainly monomer emission peaks at approximately 380 and 400 nm (**Figure 5.20 A**). Oligonucleotides that are modified at either the 5' or 3'-ends also show a very

small band around 480 nm which is indicative of excimer formation. Excimer formation for the 3'-modified duplex was not observed at pH 4. Moreover, the excimer seen here for the 5'-modified species is far less significant than the one seen for the same duplex at pH 4. Structural differences between the poly(A) duplex at pH 4 and pH 7 could possibly attribute to this effect, as could quenching of the excimer signal. It has been reported that the addition of salt can affect the aggregation of pyrene, which will have an effect on fluorescence quenching.[196]

The incorporation of additional pyrene groups leads to a reduction in the monomer emission signals and an increase in the excimer signal (**Figure 5.20 B**). This excimer signal increases with increasing numbers of pyrene groups as expected. The ratio of Band 3 to Band 1 is small for all species, indicating that there is no intercalation of pyrene (**Table 5.4**).

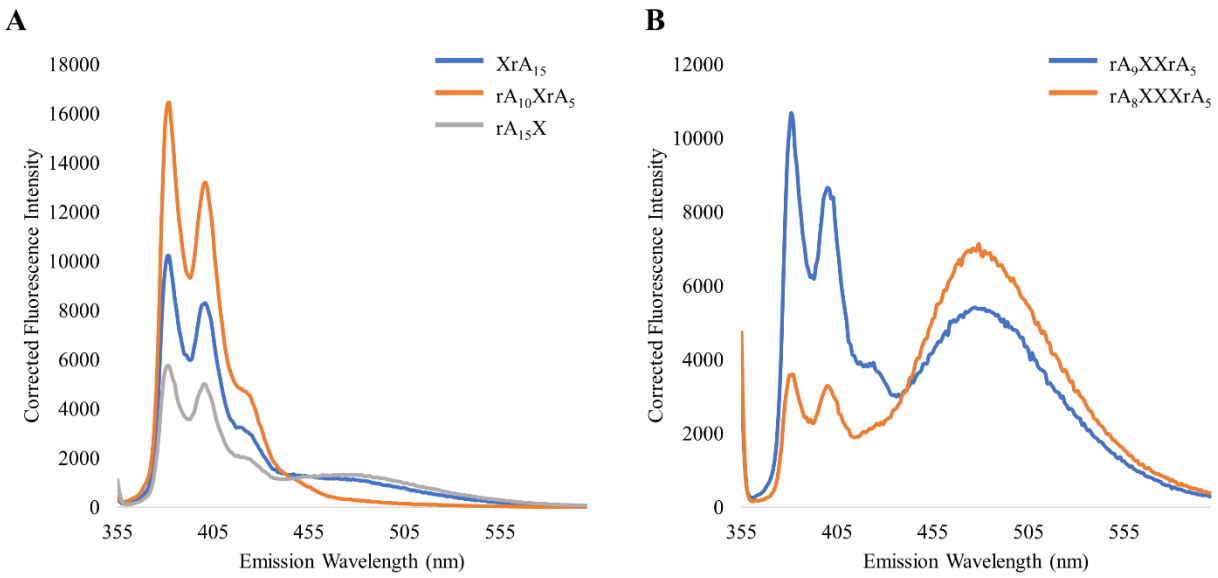

Figure 5.20: Fluorescence Emission of Pyrene-Modified poly(A) Duplexes at pH 7. (**A**) Single and (**B**) Multiple pyrene incorporations. Excitation at 350 nm. (Buffer: 40 mM Na_2HPO_4, 30 mM citric acid, 4.4 M NH_4Cl, pH 7). 2.6 µM single strand concentrations. Fluorescence intensity corrected for absorbance differences at 350 nm.

Sequence	Band 1 (nm)	Band 3 (nm)	Excimer Band (nm)	I_{III}/I_I
XrA_{15}	382	401	470	0.814
$rA_{10}XrA_5$	382	401	-	0.803
$rA_{15}X$	381	401	473	0.873
rA_9XXrA_5	381	400	477	0.811
rA_8XXXrA_5	382	400	479	0.916

Table 5.4: Fluorescence Analysis of Pyrene-Modified poly(A) at pH 7.

5.15 Influence of Pyrene Modifications on a Hybrid rA/dT Duplex

Finally, the influence of pyrene modification on a rA/dT hybrid duplex was explored to allow for comparison between the modification of parallel and antiparallel duplexes. **Figure 5.21** shows the influence of this modification on the stability of the hybrid duplex. Like what was previously observed when exploring butylamine modifications, these curves show a very limited initial plateau. The melting point of the control rA_{11}/dT_{11} duplex is 20 °C under these pH 7.4 conditions. The incorporation of multiple pyrene groups results in a stabilizing effect on the hybrid duplex. Interestingly, the duplex which incorporates two pyrene modifications was found to be more stable than the same duplex with three. The most stable duplex in the series investigated incorporated pyrene at the 5'- and 3'-ends of the duplex. One explanation could be that this hybrid duplex is adopting a structure which allows for pyrene intercalation, which was not observed for the poly(A) duplex. Modification at the ends of the duplex could allow for pyrene to base stack with the neighbouring nucleobases. In contrast, when pyrene modifications are incorporated successively, in the middle of the duplex, there may be less space available for the interactions. With more pyrene incorporations, this space may be further reduced, which would explain the higher stability of rA_4XXrA_5 when compared to rA_4XXXrA_4. The neighbour-exclusion principle

suggests that the intercalation of small molecules into DNA or RNA duplexes can only occur every 2-3 bp due to the resulting extension of the helix and a very large negative cooperativity of the binding process.[197,198]

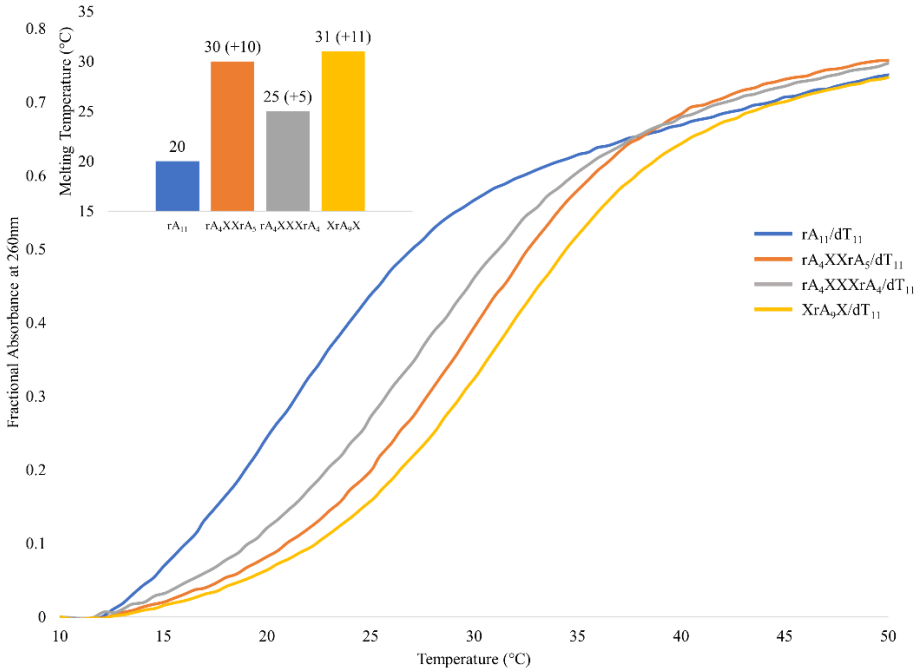

Figure 5.21: UV Thermal Denaturation Profiles of Duplexes Formed by an 11-mer rA Containing Multiple Pyrene Modifications and an 11-mer dT at pH 7.4. (Buffer: 40 mM Na_2HPO_4, 30 mM citric acid, pH 7.4). 1.85 µM single strand concentrations.

The CD analysis of these duplexes shows that they all adopt a structure like that of the control sequence (**Figure 5.22**). These spectra all show major, positive signals from 300-255 nm, followed by a large negative signal from 255-235 nm. It used to be thought that hybrid duplexes always adopted an A-form like structure.[166] However, many reports have shown this to not always be the case.[199–201] rA/dT duplexes, specifically, can form either an A-form or B-form duplex depending on the level of hydration.[201] Zimmerman found the B-form duplex of rA/dT to be heteronomous, meaning the individual strands adopt different sugar puckers (C3'-endo for rA, C2'-

endo for dT).[201] In these buffer conditions, these rA/dT hybrid duplexes also adopted a more B-like structure.[202]

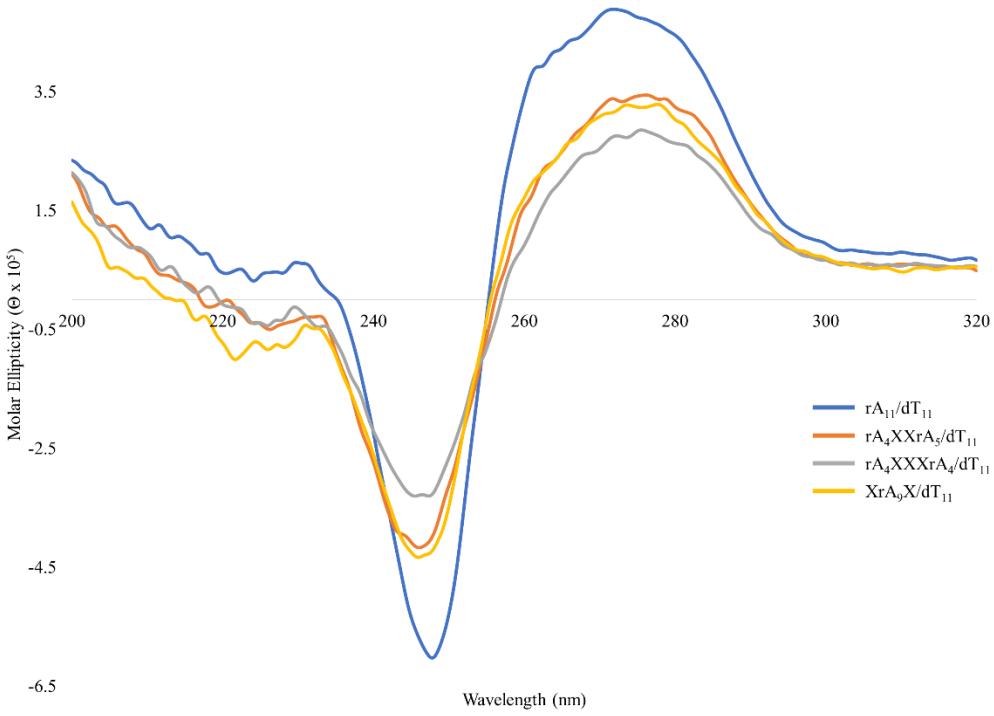

Figure 5.22: CD Spectra of Duplexes Formed by an 11-mer rA Containing Multiple Pyrene Modifications and an 11-mer dT at pH 7.4. (Buffer: 40 mM Na_2HPO_4, 30 mM citric acid, pH 7.4). 1.85 μM single strand concentrations. CD spectra recorded at 15 °C, 20 nm min^{-1}, 5 accumulations.

The UV absorption pattern for these duplexes is identical to those seen for the modified poly(A) duplexes. Characteristic pyrene absorption maxima are observed at ~ 334 and 350 nm (**Figure 5.23**). Moreover, identical shifting patterns in the absorption spectrum (ΔA: ~ 4 nm) upon heating and cooling the duplex are observed (Data not shown). This suggests that the previously seen ground state interactions (**Chapter 5.7**) are also present here, indicating that they may originate from interactions with the nearby 1,2,3-triazole ring.

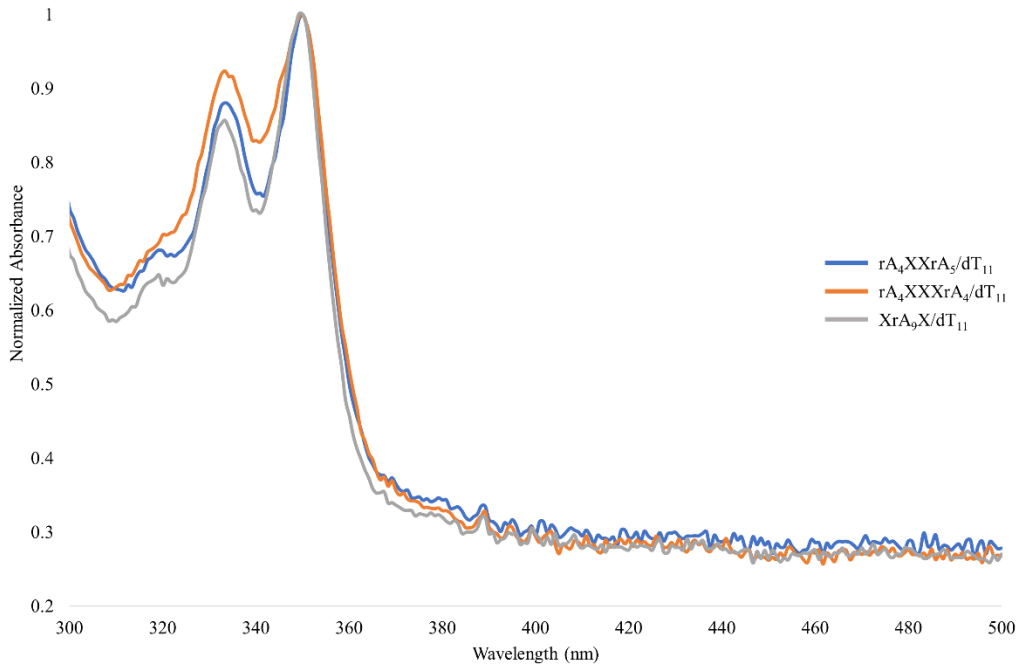

Figure 5.23: UV Spectra of Duplexes Formed by an 11-mer rA Containing Multiple Pyrene Modifications and an 11-mer dT at pH 7.4. (Buffer: 40 mM Na_2HPO_4, 30 mM citric acid, pH 7.4). 1.85 µM single strand concentrations. UV spectra recorded at RT, 400 nm min^{-1}. Spectra corrected for absorbance differences at 350 nm.

Sequence	Absorbance Maxima 1 (nm)	Absorbance Maxima 2 (nm)
rA_4XXrA_5	334	350
rA_4XXXrA_4	333	350
XrA_9X	334	349

Table 5.5: UV Absorption of Pyrene-Modified rA/dT Hybrid Duplexes at pH 7.4.

Fluorescence shows no shift in the emission spectra of these duplexes (**Figure 5.24**). In all cases a prominent emission signal from the pyrene monomers (360-410 nm) is observed. Clear excimer signals (~ 470 nm) are also seen for the centrally modified duplexes, with an increase in pyrene modifications leading to a larger signal as expected. A very small excimer signal for the duplex modified at the termini is also present. While no shift is seen for the monomer emission signals, there is a significant (~ 10 nm) shift in the excimer emission band relative to what was

seen with the poly(A) duplexes (**Figure 5.11**). This leads us to believe that the pyrene-pyrene dimers are not forming as strong of an interaction here as they were in poly(A) duplexes. This is most likely due to the duplex adopting a more B-like structure, which may be positioning these groups slightly farther away from each other or in a more unfavourable conformation. Even with the adoption of a more B-like structure, fluorescence results suggest that no intercalation of the pyrene is occurring. In this case, intercalation was expected, and this may be an indication that the linker being used to couple the pyrene to the nucleobase may be responsible for keeping the pyrene positioned outside the duplex. Quantum yield results demonstrate in a concentration independent manner that the intensity of the excimer band is dependent on the number of pyrene modifications (**Table 5.6**).

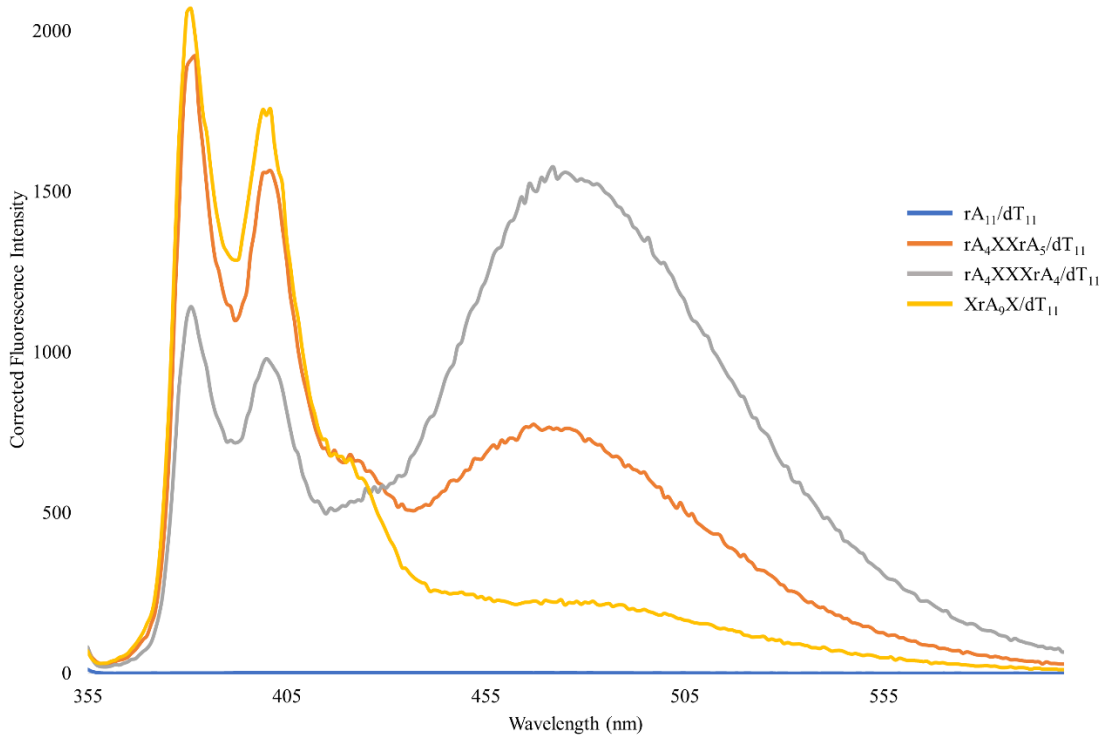

Figure 5.24: Fluorescence Emission of Duplexes Formed by an 11-mer rA Containing Multiple Pyrene Modifications and an 11-mer dT at pH 7.4. Excitation at 350 nm. (Buffer: 40 mM Na_2HPO_4, 30 mM citric acid, pH 7.4). 1.85 µM single strand concentrations. Fluorescence intensity corrected for absorbance differences at 350 nm.

Sequence	Band 1 (nm)	Band 3 (nm)	Excimer Band (nm)	I_{III}/I_I	Quantum Yield (%)
rA_4XXrA_5	382	401	467	0.815	31.77
rA_4XXXrA_4	381	400	472	0.858	88.69
XrA_9X	381	401	470	0.848	15.39

Table 5.6: Fluorescence Analysis of Pyrene-Modified Hybrid Duplexes at pH 7.4.

5.16 Summary of Pyrene Modifications

In summary, it was seen that the introduction of pyrene through a 1,4-triazole linker at the C2'- position of poly(A) has major effects on both duplex stability and solubility. At pH 4, it was shown through duplex melting analysis that the introduction of pyrene at a central position has a very destabilizing effect on the duplex. This destabilization is not observed when the duplex is modified at a terminal position. With the incorporation of additional pyrene modifications at neighbouring sugar residues, an increase in duplex stability due to favourable pyrene-pyrene interactions is seen. These interactions were observed through fluorescence analysis which showed a reduction in pyrene monomers and a stark increase in the number of dimers with additional pyrene modifications. At pH 7, duplex formation was seen to be severely hindered, especially when the duplex was modified in the middle, due to solubility issues caused by the introduction of pyrene under these high salt conditions. Overall, no evidence for pyrene intercalation was seen suggesting that pyrene is being positioned inside the grooves of the duplex.

Chapter 6: Influence of poly(A) Duplex Backbone Modifications

6.1 Backbone-Modified Nucleic Acids

Chemical modification of nucleic acids has long been recognized as a means to modulate their properties.[75,109,110,203,204] Modifications to the backbone of nucleic acids can be at the phosphate linkage or pentofuranose sugar. Examples of phosphate linkage modifications include phosphorothioates,[205–207] dithioates,[207] phosphoroselenoates,[208,209] and boranophosphates[210] which have been shown to influence both the hybridization behaviours and nuclease resistance of nucleic acids. The incorporation of phosphorothioates (**Figure 6.1**) into nucleic acid backbones has been shown to confer resistance towards nuclease digestion.[211] The pioneering work done by Eckstein showed that phosphorothioate dinucleotides were highly stabilized against SVPDE and spleen phosphodiesterase in contrast to the standard phosphodiester linkage.[211] While destabilizing to duplex stability,[212] phosphorothioates have been shown to improve the lifetime of nucleic acids *in vivo*, thereby improving their ability to activate RNase H. Due to the introduction of a chiral center, SPS of phosphorothioate oligonucleotides leads to a diastereomeric mixture of products (R_p/S_p).[206] Work has shown that the R_p diastereomer is better at activating RNase H,[213] where as, the S_p diastereomer is more resistant to 3'-exonucleases.[214] Recently approved antisense oligonucleotides such as, Nusinersen® (Spinraza), Mipomersen® (Kynamro), Fomivirsen® (Vitravene), and Inotersen® (Tegsedi), have used this modification as a means of protecting ASO's from digestion so they can perform their therapeutic role.[215–217] In fact, eight of the currently thirteen approved oligonucleotide drugs feature this modification.[204] Oligonucleotides with modified backbone linkages have been employed for other applications such as rolling circle amplification, where, a

DNA polymerase from the *Bacillus subtilis* bacteriophage Φ 29 can be used to continuously replicate genes contained within an enclosed DNA circle, often as a means of producing scaffolds for nanotechnology or for developing biomolecular targets.[218] This process requires the preparation of a circular DNA template, which can be challenging to prepare from the linear DNA construct due to the formation of various secondary structures and procedures to close the circular DNA template.[219,220] Artificial backbone linkages such as triazoles,[126,132] phosphoramidates,[221–223] or amides[224,225] are relatively easy to form and have been used in rolling circle amplification to allow for the circularization of DNA in aqueous media, thereby overcoming the challenges associated with using enzymes or forming natural phosphodiester linkages and moreover do not hinder the processing of the circular DNA template by polymerases.[138]

LNA is an example of a sugar modified oligonucleotide that contains a methylene bridge that links the C4' and O2' atoms of the ribose sugar (**Figure 6.1**). First reported by Wengel and Obika in 1998, LNA is locked into the C3'-endo (North) sugar pucker conformation, which leads to enhanced binding to both DNA and RNA targets.[226,227] Hybrid duplexes formed with either DNA or RNA are stabilized with LNA, due to the preorganization by the LNA to form A-form duplexes,[228] and the steering of complementary nucleotides of the DNA strand towards the C3'-endo conformation.[229,230] Numerous therapeutic oligonucleotides are currently in development that incorporate these LNA modifications including Miravirsen, MRG-106, and ISTH0036.[216,217]

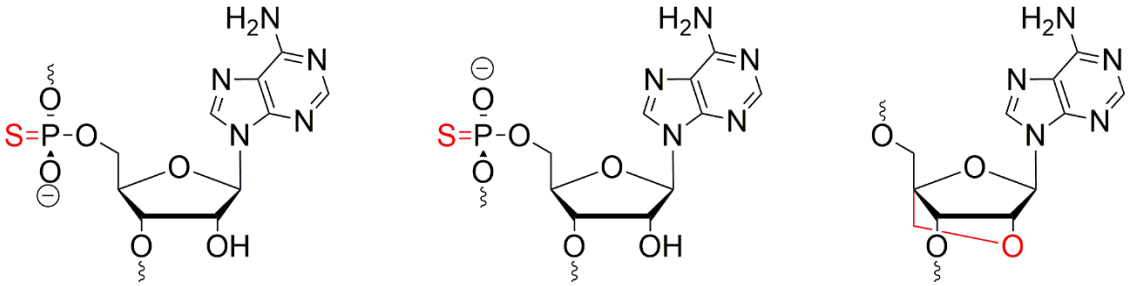

Figure 6.1: Backbone Modifications in This Study. (Red: Denotes modified positions).

6.2 Incorporation of LNA Modifications

The influence of an LNA modification on the stability and structure of the poly(A) duplex was explored with incorporation of a single LNA residue in 11- and 16-mers in the middle or at the 3'-end of the oligonucleotide (**Figure A.3**).

Solid-phase synthesis of these oligonucleotides followed slight modifications to the standard protocols (Chapter 8.2): The LNA phosphoramidite concentration was 0.1 M with a coupling time of 450 s. The oxidation step following LNA addition was set to 60 s, where, three rounds of oxidation were performed followed by a detritylation of 100 s as recommended by the manufacturer (Glen Research).

6.2.1 UV Thermal Denaturation (T_m) Analysis of LNA-Modified Duplexes at pH 4

For an 11-mer poly(A), the incorporation of an LNA modification at either the 3'-end or at the central position of this duplex resulted in no significant change to the melting curve relative to the control sequence (**Figure 6.2**). Overall, the T_m values of these modified duplexes are 1-2 °C

lower relative to the control. Likewise for the 16-mer series, no significant change in the sigmoidal transitions (**Figure 6.3**) was observed which suggests a negligible effect on duplex stability for the poly(A) duplex due to these LNA incorporations. These preliminary findings suggest that the incorporation of LNA modifications, which have been observed to form more thermally stable duplexes with single stranded targets due to the locked C3'-endo conformation, are well tolerated within the poly(A) duplex. Recent work, however, has shown the stabilization of poly(A)/poly(LNA) duplexes, where as, poly(LNA)/poly(LNA) duplex formation was not observed,[118] suggesting that opposing LNA modifications are unfavourable in this motif. Given the greater nuclease stability of LNA over RNA, these modifications are still valuable for potential *in vivo* applications.

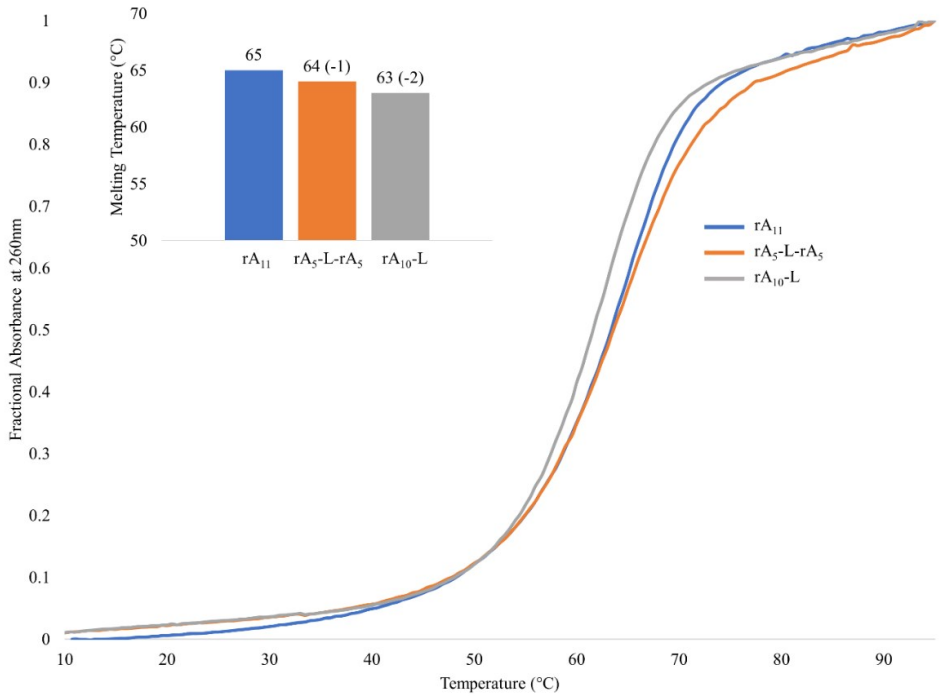

Figure 6.2: UV Thermal Denaturation Profiles of poly(A) Duplexes Formed by LNA-Modified 11-mers at pH 4. (Buffer: 40 mM Na_2HPO_4, 30 mM citric acid, pH 4). 3.7 µM single strand concentrations. L: LNA modification.

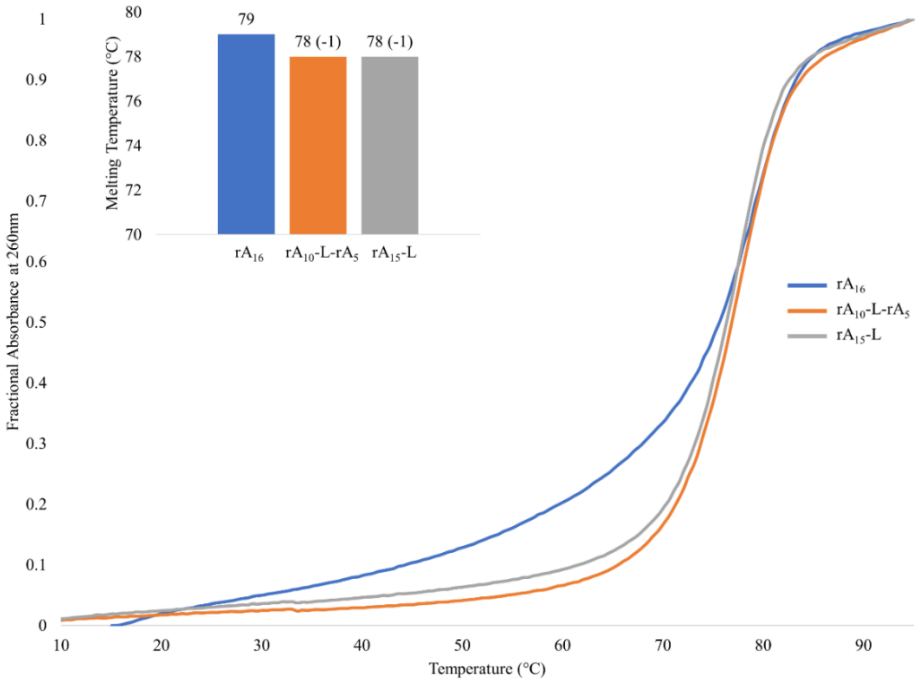

Figure 6.3: UV Thermal Denaturation Profiles of poly(A) Duplexes Formed by LNA-Modified 16-mers at pH 4. (Buffer: 40 mM Na_2HPO_4, 30 mM citric acid, pH 4). 2.6 µM single strand concentrations. L: LNA modification.

6.2.2 Thermal Reversibility of LNA-Modified Duplex Unfolding at pH 4

Heating and cooling UV absorption profiles at 260 nm were acquired for the LNA-modified poly(A) sequences at a rate of 0.5 °C/min to evaluate the unfolding of these duplexes in comparison to their folding at this data acquisition rate. The sigmoidal curves for the 11-mers at pH 4 both showed a slight shift to the left towards lower temperatures by 2 °C (**Figure 6.4 A**) when modified in the middle of the duplex (rA_5-L-rA_5) or at the 3'-end with LNA (rA_{10}-L). This suggests that there is a slight hysteresis occurring in this system. The inclusion of a single LNA unit, while not destabilizing to the duplex itself, does seem to have a slight impact on the rate at which the duplex is able to fold at pH 4. However, these results are in line with those observed for control rA_{11} duplexes studies under identical conditions (**Figure A.33**).

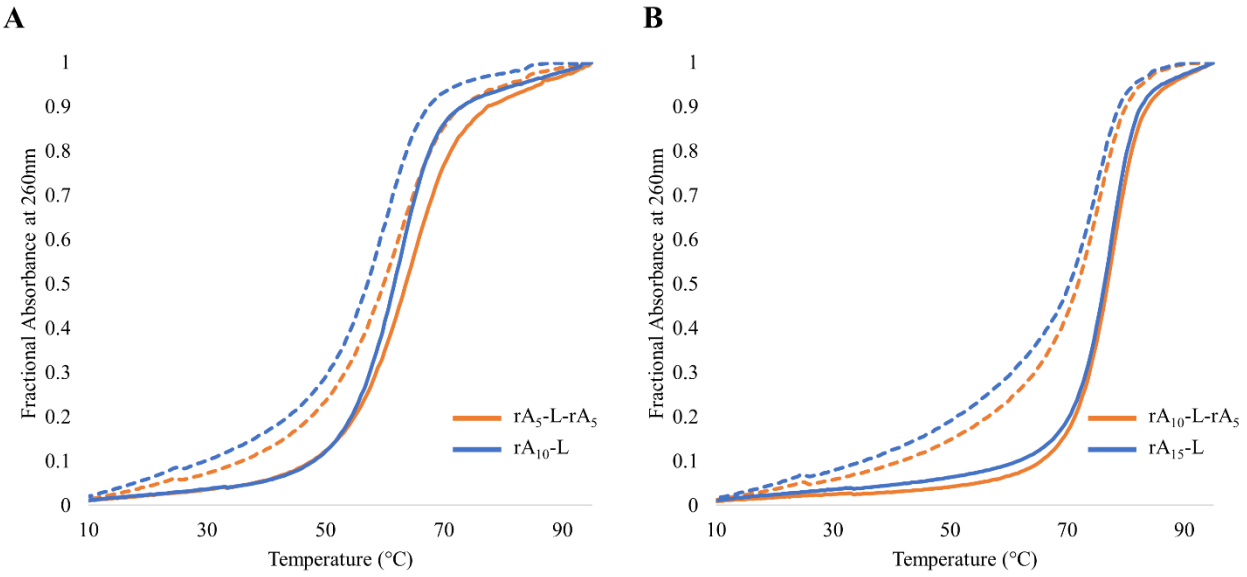

Figure 6.4: Thermal Reversibility Profiles at 260 nm of LNA-Modified poly(A) Duplexes at pH 4. (**A**) 11-mers and (**B**) 16-mers. (Buffer: 40 mM Na_2HPO_4, 30 mM citric acid, pH 4). Single strand concentrations were 3.7 µM for 11-mers and 2.6 µM for 16-mers. (Solid: Heating, Dashed: Cooling).

Similarly for the 16-mer series, both sequences (rA_{10}-L-rA_5 and rA_{15}-L) showed a small, 2 °C reduction in the annealing temperature of the duplex relative to the melting temperature (**Figure 6.4 B**), analogous to the unmodified poly(A) duplex (**Figure A.33**).

6.2.3 CD Analysis of LNA-Modified Duplexes at pH 4

LNA-modified poly(A) duplexes were studied using CD spectroscopy to evaluate if any structural changes may have resulted from the introduction of LNA monomers within the duplex. The duplexes formed by 11-mers containing the LNA residue showed positive peaks at 260 and 275 nm, with a negative band at 245 nm and a slightly higher ellipticity within the 290-320 nm region relative to the native poly(A) 11-mer (**Figure 6.5 A**). The 16-mer series showed identical maxima and minima to the control (**Figure 6.5 B**), with a slightly higher ellipticity within the 290-

320 nm region. Overall, no major structural perturbations were seen for the LNA-modified poly(A) duplexes relative to their unmodified counterparts.

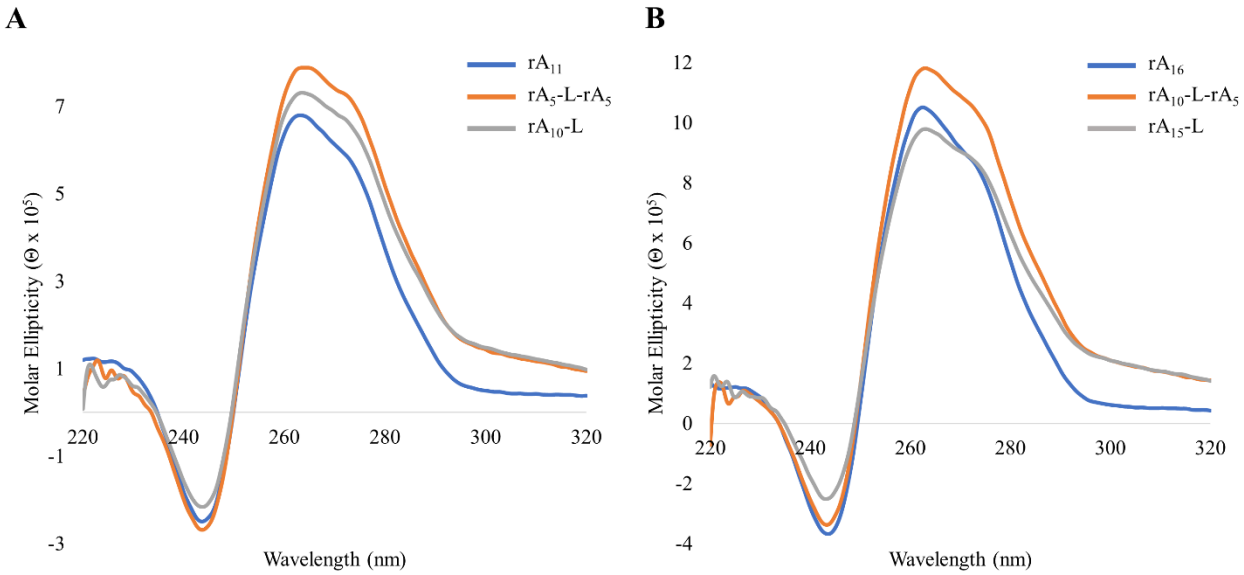

Figure 6.5: CD Spectra of LNA-Modified poly(A) Duplexes at pH 4. (**A**) 11-mers and (**B**) 16-mers. (Buffer: 40 mM Na_2HPO_4, 30 mM citric acid, pH 4). Single strand concentrations were 3.7 µM for 11-mers and 2.6 µM for 16-mers. CD spectra recorded at 15 °C, 20 nm min^{-1}, 5 accumulations.

6.2.4 UV Thermal Denaturation (T_m) Analysis of LNA-Modified Duplexes at pH 7

These LNA-modified duplexes were then studied at pH 7 and 4.4 M NH_4Cl, the conditions that also lead to poly(A) duplex formation. The UV thermal analysis of 16-mer, LNA-modified, duplexes at pH 7 shows a minor effect on the melting temperature (**Figure 6.6**) with slight destabilization of the centrally modified (-1 °C) and stabilization of the 3'-modified (+2 °C) duplexes.

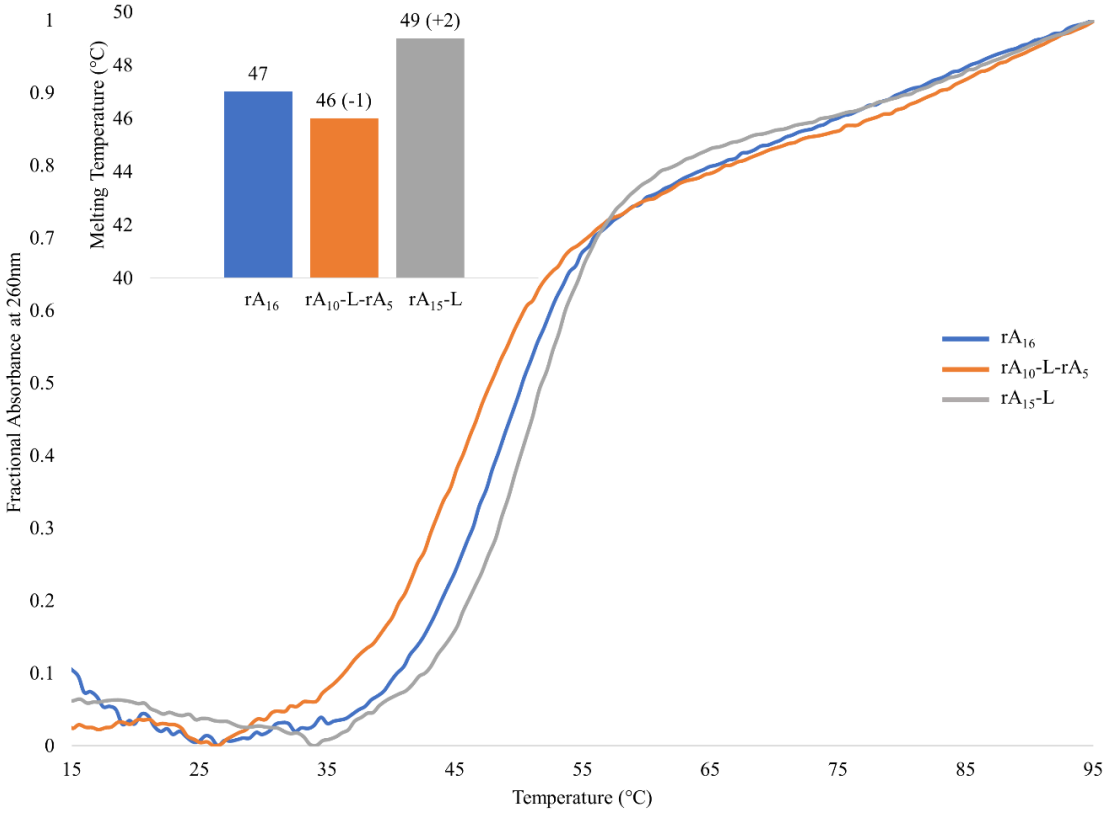

Figure 6.6: UV Thermal Denaturation Profiles of Duplexes Formed by LNA-Modified 16-mers at pH 7. (Buffer: 40 mM Na_2HPO_4, 30 mM citric acid, 4.4 M NH_4Cl, pH 7). 2.6 µM single strand concentrations.

6.2.5 Thermal Reversibility of LNA-Modified Duplex Unfolding at pH 7

The denaturation and association of these duplexes under the neutral pH and high ammonium salt conditions was examined and found to be nearly identical to what was observed under acidic conditions (pH 4). The annealing of the 16-mer to form the duplex displayed a small hysteresis (-4 °C) relative to the denaturation for both the centrally modified and 3'-modified duplexes (**Figure 6.7**). While slightly more significant than the hysteresis observed at pH 4, this small change in the melting temperature suggests that, overall, the LNA modification is well

accommodated in the poly(A) duplex and does not severely impact the rate at which the duplex forms under either condition.

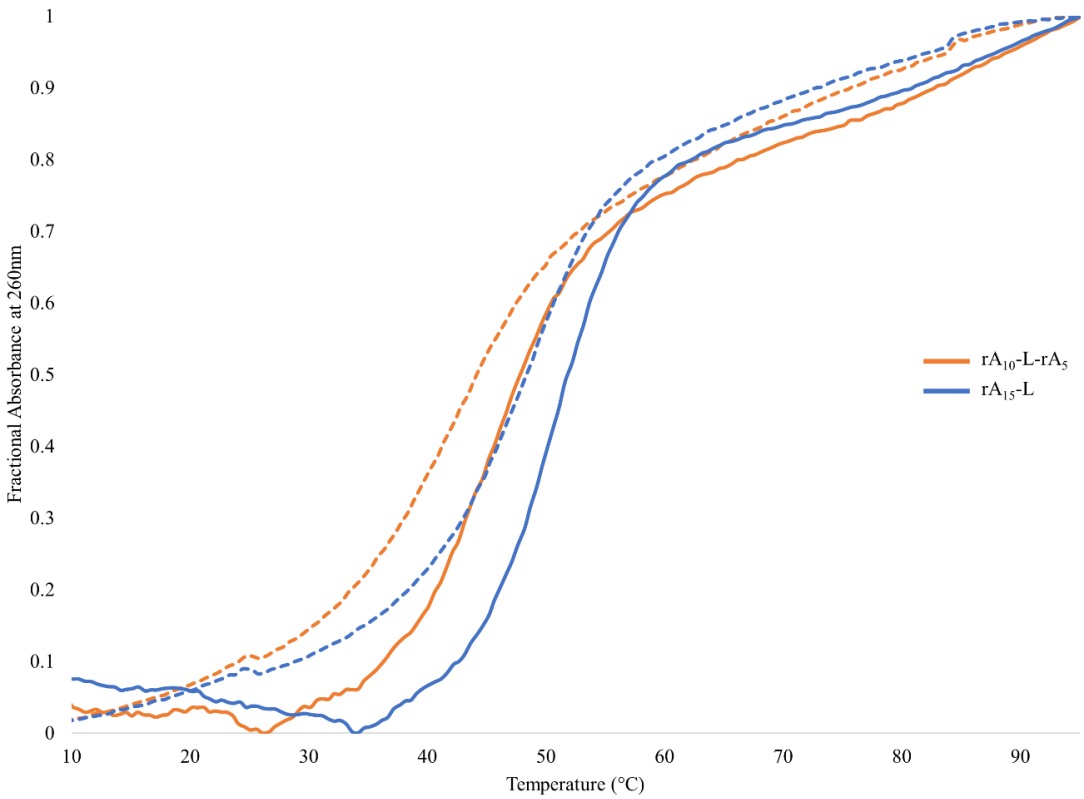

Figure 6.7: Thermal Reversibility Profiles at 260 nm of Duplexes Formed by LNA-Modified 16-mers at pH 7. (Buffer: 40 mM Na_2HPO_4, 30 mM citric acid, 4.4 M NH_4Cl, pH 7). 2.6 µM single strand concentrations. (Solid: Heating, Dashed: Cooling).

6.2.6 CD Analysis of LNA-Modified Duplexes at pH 7

CD analysis of the LNA-modified duplexes shows similar trends as the rA_{16} control (**Figure 6.8**). Maxima were observed in the region from 260-290 nm and a minimum was observed at 245 nm for all sequences. Minor differences can be seen, such as increased ellipticity in the 290-320 nm region, but the overall shapes of the curves are identical indicating that no major structural changes have occurred because of this modification.

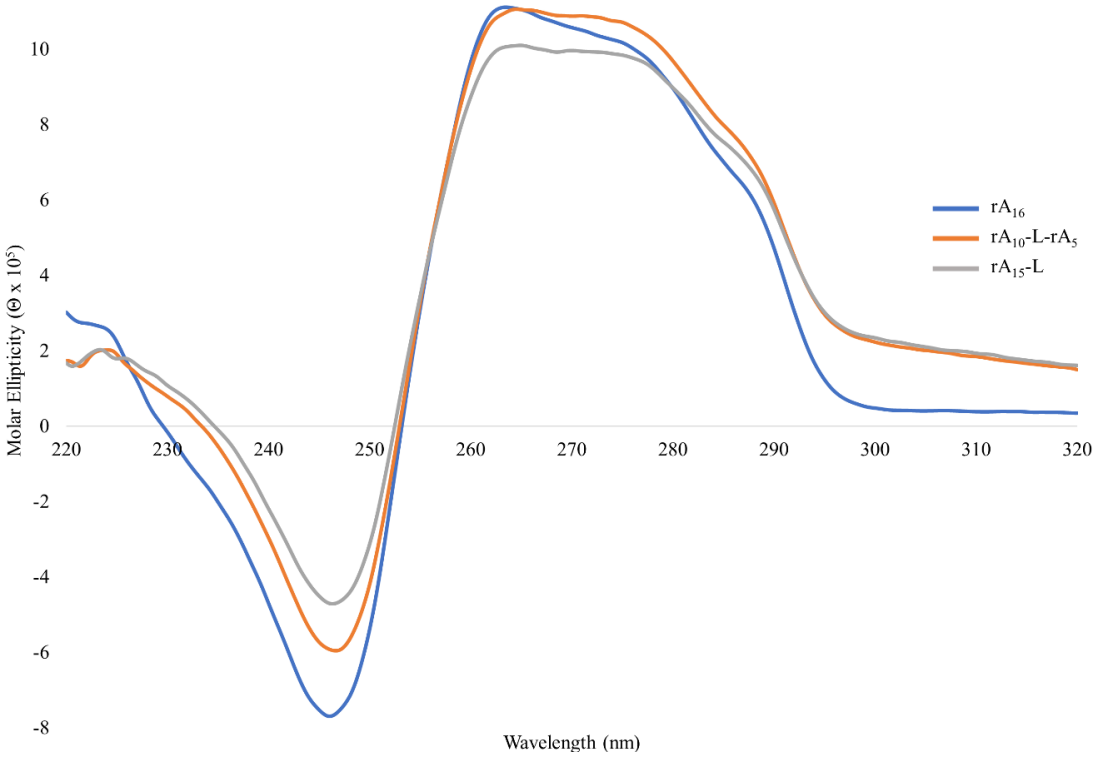

Figure 6.8: CD Spectra of Duplexes Formed by LNA-Modified 16-mers at pH 7. (Buffer: 40 mM Na_2HPO_4, 30 mM citric acid, 4.4 M NH_4Cl, pH 7). Single strand concentrations were 2.6 µM. CD spectra recorded at 15 °C, 20 nm min^{-1}, 5 accumulations.

6.3 Incorporation of Phosphorothioate Modifications

The influence on duplex stability of replacing the phosphodiester with a phosphorothioate linkages within the poly(A) backbone was explored. Specifically, an 11-mer poly(A) was prepared containing a 5'-internal phosphorothioate linkage by solid-phase synthesis (**Figure A.4**) according to a slightly modified procedure (Chapter 8.2) where, following the addition of the final rA monomer to the growing oligonucleotide, sulfurization with DDTT was performed. Sulfurization of the backbone was confirmed by MS analysis (**Table A.4**). The introduction of the phosphorothioate linkage generates a new stereocenter at the phosphorus atom, and a pair of resulting diastereomers. Separation of the diastereomers was performed using RP-HPLC (Chapter

8.8, **Figure A.18**) based on the procedure developed by Pallan.[207] The Rp-diastereomer was thought to elute first followed by the Sp-diastereomer, however, structural analysis was not performed to confirm this.

6.3.1 UV Thermal Denaturation (T_m) Analysis of a Phosphorothioate-Modified 11-mer poly(A) Duplex

The UV thermal denaturation profile of the 11-mer poly(A) sequence functionalized with a 5'-end phosphorothioate linkage reveals that this modification is destabilizing compared to the all phosphodiester (unmodified) duplex by 3 °C (**Figure 6.9**). The duplexes formed with the individual R_P and S_P diastereomers, are also destabilizing with a 4 °C reduction of the melting temperature.

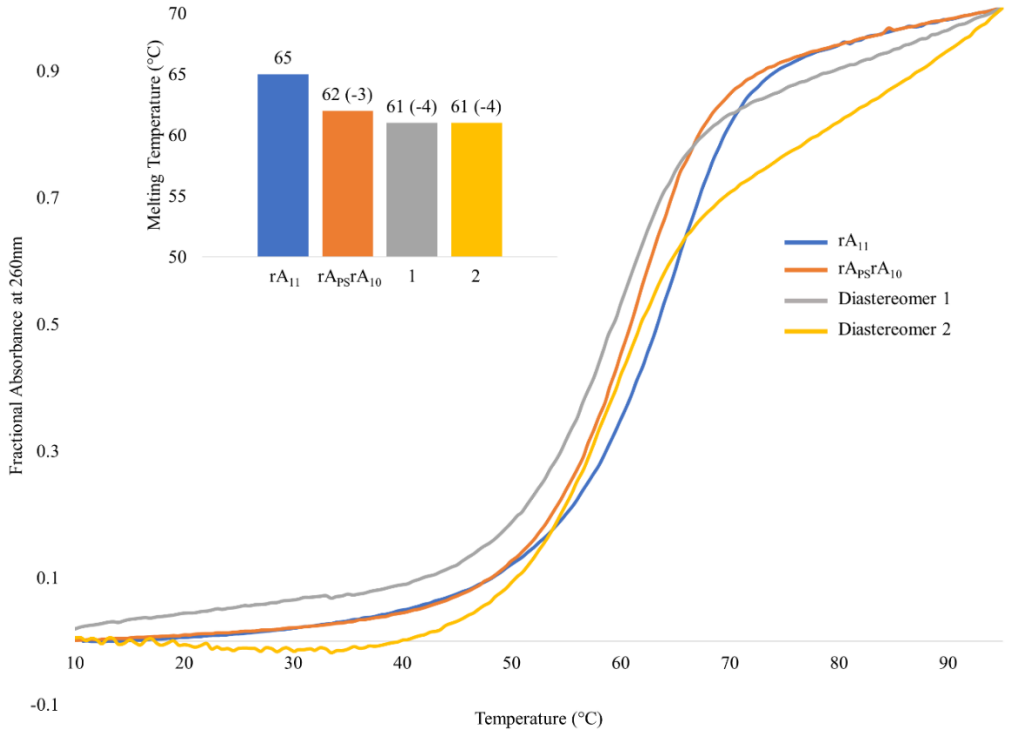

Figure 6.9: UV Thermal Denaturation Profiles of Duplexes Formed by Phosphorothioate-Modified 11-mer poly(A) at pH 4. (Buffer: 40 mM Na_2HPO_4, 30 mM citric acid, pH 4). 3.7 µM

single strand concentrations for control and diastereomeric mixture. Single strand concentrations for isolated diastereomers were 1.48 μM.

The similar destabilization observed by the diastereomers suggests that the poly(A) duplex can equally accommodate both within the backbone. There seems to be no preference for either, suggesting that the hydrogen bonding interaction formed between the nonbridging atom (sulfur or oxygen) and the protonated N1 atom seems to be equal in strength regardless of the atom at that position. Generally, hydrogen bonds to sulfur are weaker than the corresponding bonds to oxygen as they arise due to charge-dipole instead of charge-charge interactions.[231] It has been reported that all S_P-PS-ORN, and oligonucleotides containing a diastereomeric mixture, lead to duplex destabilization, where as, oligonucleotides containing all R_P-PS-ORN have been shown to be slightly stabilizing.[232] Recently, Østergaard *et al* expanded upon this by showing that the substitution of individual backbone linkages within an all R_P-gapmer sequence with S_P phosphorothioates led to reduced DNA/RNA hybrid stability.[233] They also showed the reverse to be true as well, where, the inclusion of R_P linkages within an all S_P backbone led to enhanced hybridization between ASO's and the mRNA target.[233] In this work, an equal destabilization for both diastereomer-pure duplexes is observed, suggesting that their presence within the backbone of poly(A) behaves slightly differently than in standard anti-parallel stranded A-form duplexes.

6.3.2 Thermal Reversibility of Phosphorothioate-Modified Duplex Unfolding at pH 4

The denaturation and annealing curves of the phosphorothioate-modified poly(A) duplex at pH 4 is shown in **Figure 6.10**. A reduction of 3 °C for the annealing curve was observed for the

poly(A) duplex containing the phosphorothioate backbone modification, which is comparable with the all-phosphodiester backbone poly(A) duplex (**Figure A.33**).

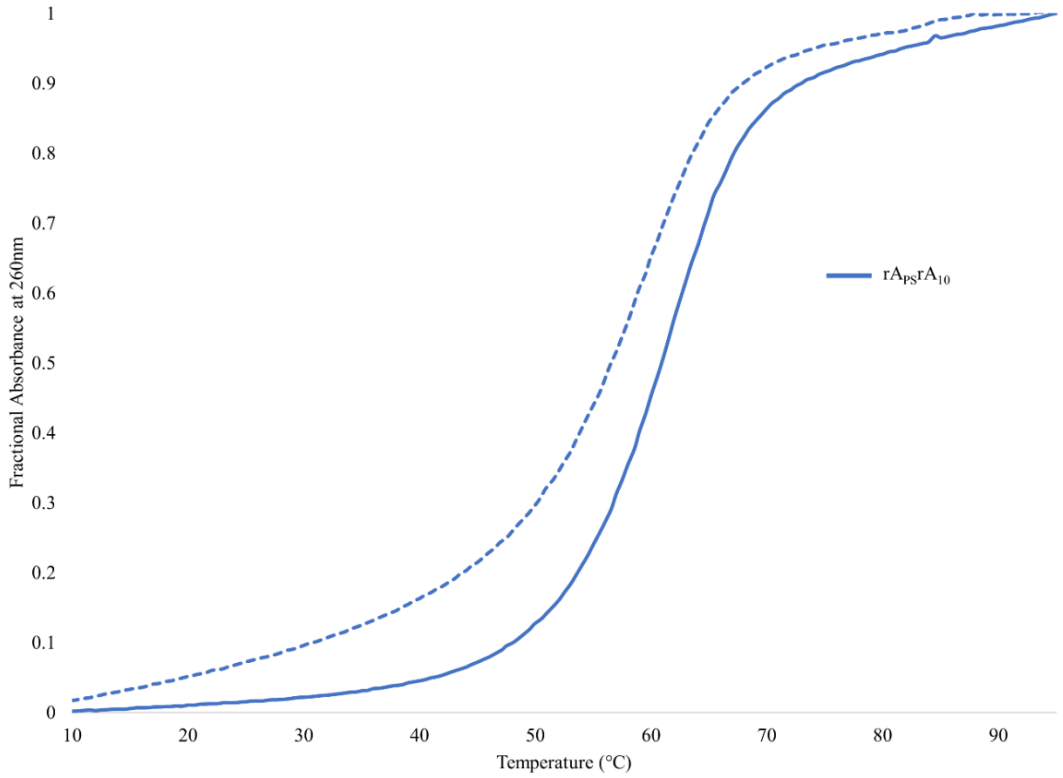

Figure 6.10: Thermal Reversibility Profile at 260 nm of the Duplex Formed by Phosphorothioate-Modified poly(A) 11-mers at pH 4. (Buffer: 40 mM Na_2HPO_4, 30 mM citric acid, pH 4). 3.7 µM single strand concentrations. (Solid: Heating, Dashed: Cooling).

6.3.3 CD Study of Phosphorothioate-Functionalized poly(A) at pH 4

The CD spectra of the poly(A) duplex containing the phosphorothioate linkage at pH 4 shows no significant deviation, with only a slightly lower molar ellipticity in the region from 220-235 nm, from the signature for the all-phosphodiester poly(A) duplex. (**Figure 6.11**).

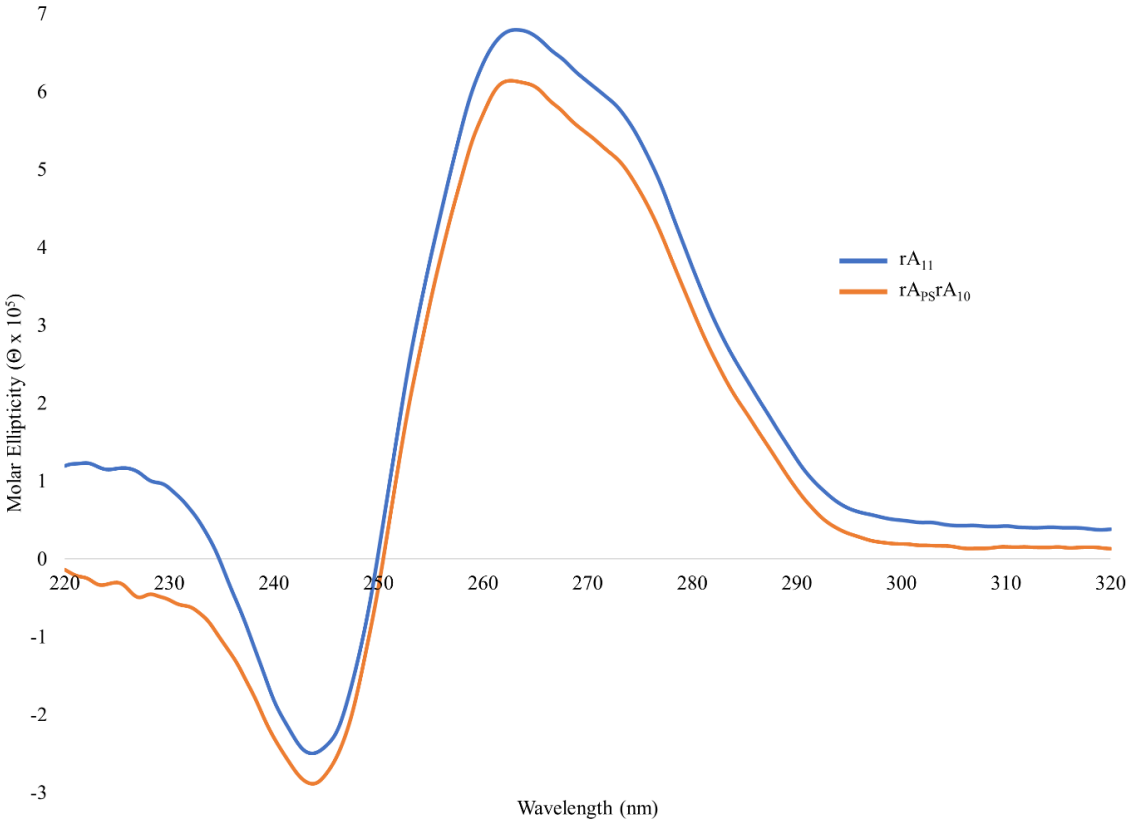

Figure 6.11: CD Spectra of the Duplex Formed by Phosphorothioate-Modified poly(A) 11-mers at pH 4. (Buffer: 40 mM Na_2HPO_4, 30 mM citric acid, pH 4). Single strand concentrations were 3.7 μM. CD spectra recorded at 15 °C, 20 nm min^{-1}, 5 accumulations.

6.4 Summary of Backbone Modifications

In summary, the incorporation of backbone modifications such as LNA and phosphorothioates into the poly(A) RNA duplex were explored. LNA was seen to have a negligible effect on the thermal stability of duplexes formed by both 11-mer and 16-mers at pH 4, with the longer of the two duplexes formed under neutral pH, high ammonium salt conditions, also being seen to be minimally affected by the incorporation of a single LNA monomer. CD spectroscopy did not show any major perturbations to the duplex structure for any of the duplexes formed at pH 4 or 7. The inclusion of a single phosphorothioate modification was found to be destabilizing

towards the thermal stability of the poly(A) duplex. Individually isolated diastereomers had a similar influence on duplex stability suggesting that the poly(A) duplex can form regardless as to whether a sulfur or oxygen atom is involved in hydrogen bonding interactions with the protonated N1 atom of the opposing nucleobase. Future work is needed to explore the influence of additional incorporations of these backbone modifications and whether LNA analogs such as 2'-amino-LNA,[234] which can allow for further functionalization of the sugar, can be used to further tune the properties of the poly(A) duplex. Other backbone modifications such as phosphoroselenoates and boranophosphates have also been reported and could possibly have differing effects on duplex structure and stability.

Chapter 7: Conclusions

7.1 Summary

In this work, we sought to examine the influence of modifications to the C2'-position of the ribose sugar in poly(A) RNA duplexes. C2'-*O*-propargyl modifications were incorporated through SPS and then subsequently derivatized with small molecules through Cu-catalyzed Click chemistry. We determined that the propargyl modification was destabilizing at both pH 4 and neutral pH with 4.4 M NH_4^+. In both cases, a relationship was seen between the number of modifications and the decrease in duplex stability. No major structural changes were seen through CD or native gel electrophoresis. Poly(A) duplexes modified with butylamine through a 1,4-triazole linkage were also seen to be destabilizing in a similar fashion. This destabilization was found to be more significant at neutral pH with high ammonium salt concentrations than at pH 4. This is thought to be due to an elimination of favourable backbone interactions that are present at pH 4. Modification of the duplex with 1-methylpyrene through a 1,4-triazole linkage was found to be very destabilizing when the modification was at a central position. Modification of duplexes at the termini showed negligible results. By incorporating numerous, adjacent, modifications we were able to observe an increase in stability associated with pyrene-pyrene stacking interactions in the grooves of the duplex. This was confirmed by fluorescence analysis which showed a reduction in pyrene monomers with a corresponding increase in dimer formation. At pH 7, modification with pyrene at a central position was highly destabilizing. Solubility issues associated with the incorporation of pyrene under these high salt conditions was thought to be responsible for the low signals seen through CD, fluorescence, and UV analysis. Lastly, modification of the

poly(A) backbone was seen to have a variety of effects. LNA was seen to be negligible, where as, destabilization was observed with the inclusion of phosphorothioate linkages.

7.2 Future Work

There are numerous directions where this project can be taken in the future. With the amine-functionalized poly(A) duplexes, it would be interesting to explore what effect spacing out the modifications would have. The observed destabilization of the butylamine-modified poly(A) could possibly be attributed to unfavourable interactions between neighbouring alkyl amine groups.[235] By spacing out these modifications such that they appear every two or three nucleosides this contribution towards destabilization may be alleviated.

With the pyrene-modified duplexes, we observed a significant stabilization brought about by the introduction of neighbouring groups. This is thought to be due to favourable stacking interactions between the pyrenes within the grooves of the duplex. To further expand upon these results, a homopolymer of pyrene-modified poly(A) should be synthesized and studied through both NMR spectroscopy and crystal structure analysis. This could allow for determination of the positioning of the pyrene groups, the conformation of their stacking arrangement, and any distortions to the duplex structure which were not observed through CD spectroscopy. Furthermore, some sort of higher order structure was seen to be formed when poly(A) oligonucleotides were modified at both the 5'- and 3'-ends with this pyrene modification. It was thought that this could be a stabilization of the continuous duplex which was previously observed through crystal structure analysis.[114] Duplexes of different sizes should be constructed to see if this motif appears consistently across the range. If so, native gel analysis could be performed, this time

at a higher voltage while under cooling, to attempt to visualize these structures. NMR spectroscopy may also lend further information as to the identity of this structural motif.

In this study of backbone-modified poly(A) duplexes, it was observed that LNA had a negligible effect on duplex thermal stability. Previous work by the Gleghorn group reported the formation of stable poly(A)/poly(LNA) duplexes, where as, poly(LNA)/poly(LNA) duplexes did not form.[118] This suggests that the lack of a proton at C2', or the enhanced rigidity of the LNA,[118] impedes duplex formation. They also observed that poly(LNA) TFO's are incapable of forming triplexes with underlying DNA duplexes.[118] It would be interesting, therefore, to examine the influence of alternating rA, LNA nucleosides in a longer poly(A) duplex. The rigid structure and lack of C2'-OH may be less significant if placed between more flexible rA nucleosides which can successfully interact with the backbone.

In addition to the studied phosphorothioates, the influence of other modified nucleic acid backbones such as phosphoroselenoates and boranophosphates can be examined for their influence on poly(A) duplex formation (**Figure 7.1**).

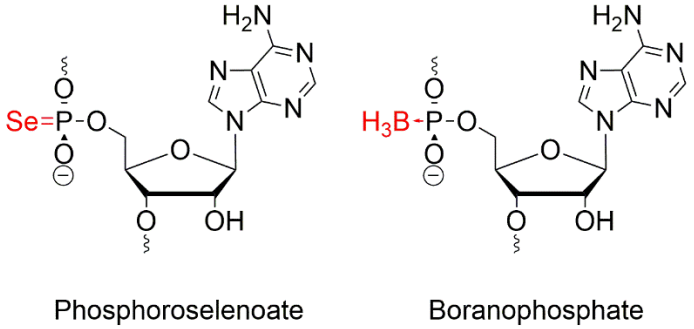

Phosphoroselenoate Boranophosphate

Figure 7.1: Possible Phosphate-Modified Linkages to Explore.

Both groups are less electronegative than oxygen, potentially strengthening the interaction between the protonated N1 and the nucleic acid backbone of the poly(A) duplex. Phosphoroselenoates have one of the nonbridging oxygen atoms replaced by a selenium atom. In contrast to other heavy atoms such as bromine, selenium is easily incorporated during SPS by substituting the use of a saturated solution of potassium selenocyanide for I_2 in THF/pyridine/H_2O at the oxidation step of the cycle.[209] These modifications have been shown to enhance nuclease resistance and facilitate crystal structure determination.[209,236]

Boranophosphates have a nonbridging oxygen atom replaced by a borane (BH_3) group. This group is more hydrophobic than oxygen, while remaining isoelectronic, possibly facilitating enhanced cellular membrane penetration.[206,237] This modification has shown enhanced stability under both acidic and basic conditions, as well as against SVPDE and CSPDE digestion.[206,237] Modification of siRNA shows an increase in activity relative to the unmodified phosphodiester-linked siRNA.[238] The exception being when sequences are modified with multiple modifications at the center of the strands.[238] When compared to phosphorothioate-modified siRNA, BP-siRNA was found to be more active.[238] A recent report outlined the stereocontrolled synthesis of boranophosphate DNA through use of an oxazaphospholidine approach.[210] It was shown that the individual diastereomers exhibit different RNase H activity, and propensities for duplex formation.[210]

We can also look at changing the linkage between the attached small molecule and the C2'-position of the ribose sugar. Instead of using copper-catalyzed Click chemistry to give a 1,4-triazole linkage, we could explore the use of ruthenium as a catalyst which would lead to 1,5 triazole linkages.[125,127] The presence of a 1,5-triazole, instead of a 1,4-triazole, would position the attached small molecules closer to both the ribose sugar and the nucleobase, potentially facilitating

the intercalation of pyrene into the duplex or a strengthening of the interactions between the cationic amine and the negatively charged phosphate backbone. Post synthetic coupling of small molecules could also be achieved using Sonogashira coupling.[239–242] However, this approach could be limited by the base-sensitivity of RNA. The lengths of the various linkers can also be varied to explore the relationship between linker length and stabilization.

In the introduction of this thesis, reference was made to the work of the Liu group and their development of a pH-responsive DNA hydrogel.[107] Through a change in environmental pH, cytosine-rich regions of their designed DNA structures would form i-motif-based crosslinks.[107] This hydrogel was shown to be fast and responsive for both the encapsulation and release of gold nanoparticle drug analogues.[107] Poly(A) RNA could be explored for the same application with the added benefit of being responsive to both pH and NH_4^+. This would require the synthesis of three distinct RNA oligonucleotides through SPS. Each oligo would have regions designed for hybridization with the other oligonucleotides, followed by a terminal poly(A) sequence (**Figure 7.2**).

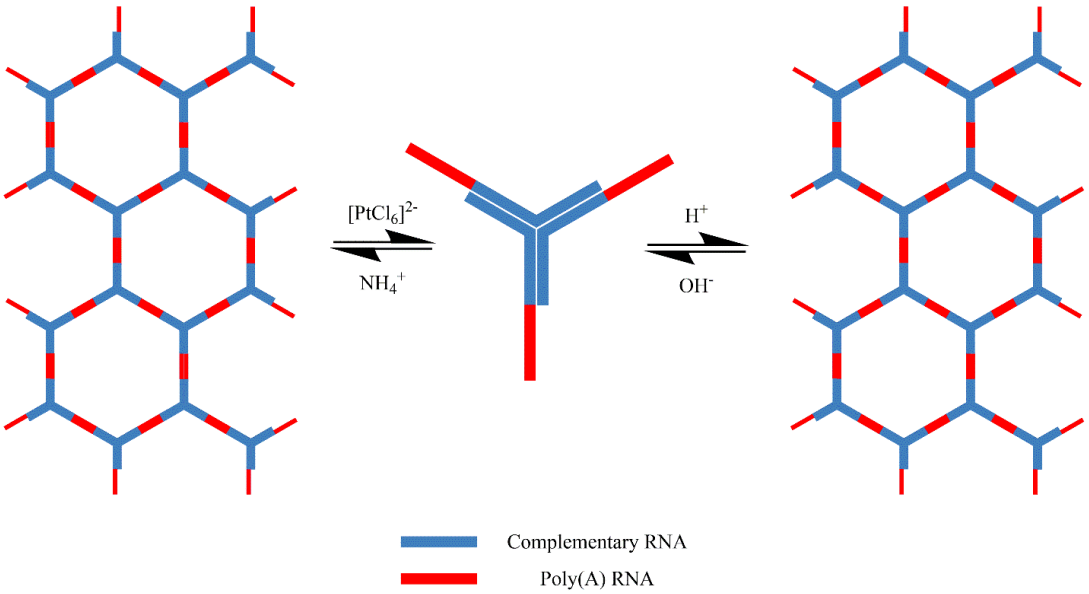

Figure 7.2: Proposed pH- and NH_4^+-Responsive poly(A) RNA Hydrogel.

It would be important for the complementary binding segments to lack C-rich regions to minimize any possible unwanted i-motif formation. When combined in an appropriate buffer system, the Y-shaped structures would form similar to the previous work by Liu.[107] A drop in pH would lead to poly(A) duplex formation and the establishment of the RNA network (**Figure 7.2**). A corresponding increase in pH would cause this network to dissociate back into individual Y-shaped motifs. A second approach could be taken where poly(A) duplex formation could be catalyzed by the introduction of ammonium cations. To break down the network we would need to remove the cations. One possible means of doing so would be to introduce a platinum salt such as sodium hexachloroplatinate(IV) which would precipitate the ammonium ions,[243] thereby allowing for the release of any entrapped compounds.

Chapter 8: Materials and Methods

8.1 Materials

The nucleosides 5'-*O*-dimethoxytrityl-3'-*O*-[(2-cyanoethyl)-(N,N-diisopropyl)]-2'-*O*-TBDMS-N6-benzoyl adenosine, 5'-*O*-dimethoxytrityl-3'-*O*-[(2-cyanoethyl)-(N,N-diisopropyl)]-N6-benzoyl-(2'-*O*, 4'-C methylene)-adenosine, and 5'-*O*-dimethoxytrityl-3'-*O*-[(2-cyanoethyl)-(N,N-diisopropyl)]-2'-deoxythymidine were purchased from Glen Research (Sterling, Virginia). 5'-*O*-dimethoxytrityl-3'-*O*-[(2-cyanoethyl)-(N,N-diisopropyl)]-2'-*O*-propargyl-N6-benzoyl-adenosine was purchased from the ChemGenes Corporation (Wilmington, Massachusetts). 1,4-dibromobutane and 1-pyrenemethanol were purchased from the Aldrich Chemical Company (Milwaukee, Wisconsin) and all other chemicals and solvents were purchased from the Aldrich Chemical Company (Milwaukee, Wisconsin). All reagents for solid-phase oligonucleotide synthesis were purchased from Glen Research (Sterling, Virginia). Both functionalized and universal CPG solid supports were purchased from either ChemGenes Corporation (Wilmington, Massachusetts) or Glen Research (Sterling, Virginia).

8.2 Solid-Phase Synthesis of Oligonucleotides

The solid-phase synthesis of the oligonucleotides was performed using an ABI 3400 DNA synthesizer with minor deviations from the manufacturer's recommended procedure. Oligonucleotides functionalized at the 3'-end required the use of universal CPG (1400 Å, 31 μmol g^{-1}), where as, all other sequences were synthesized using CPG (500 Å, 83 μmol g^{-1}) that was pre-

functionalized with protected adenosine. Oligonucleotides were generally synthesized on a 3 μM scale. The phosphoramidites were prepared as 0.15 M solutions in anhydrous ACN. Detritylation was performed with 3 % TCA in DCM over 45 s. Couplings required 0.25 M 5-ethyl-1H-tetrazole in anhydrous ACN over a period of 450 s. Capping was done with acetic anhydride in pyridine/THF and 16 % 1-methylimidazole in THF over a total of 27 s, including reagent delivery. Oxidation was then performed using 0.02 M I_2 in THF/pyridine/H_2O over a total period of 32 s. All solvents used were HPLC grade.

Modified nucleosides required deviations from the standard procedures. C2'-*O*-propargyl adenosine phosphoramidites required a coupling time of 900 s instead of the standard 450 s as per the manufacturer's recommendation (ChemGenes). The concentration of LNA phosphoramidites was 0.1 M, coupling was performed over 450 s, and the oxidation was performed over 3 × 60 s rounds. Detritylation of LNA was done over 100 s as per the manufacturer's recommendations (Glen Research). Phosphorothioate-modified linkages required sulfurization with DDTT (150 s) following addition of the final rA monomer. DDTT (0.1 M) was prepared in anhydrous pyridine/THF (40:60 (v/v)) as per the supplier's recommendations (Glen Research). This sulfurization step was followed by a capping step.

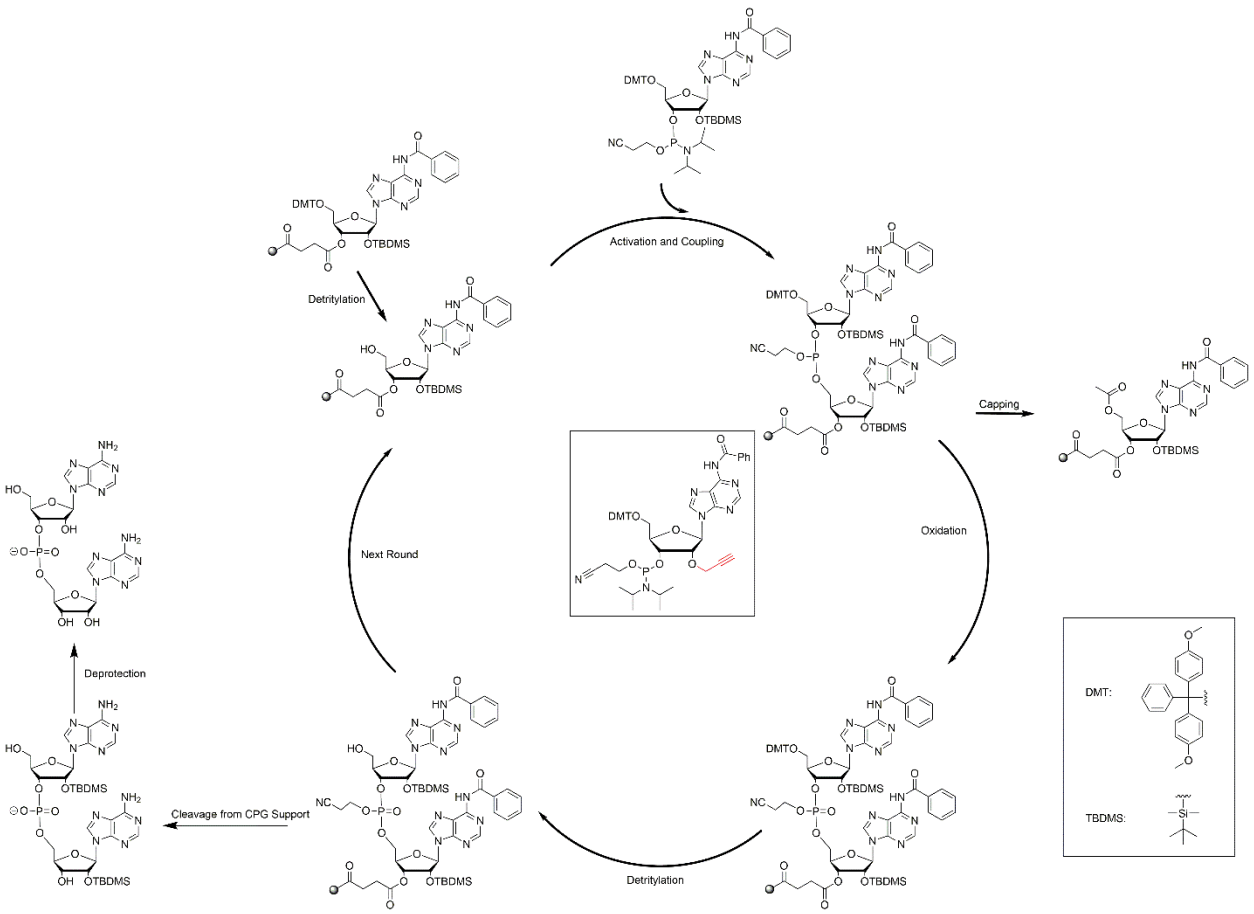

Scheme 8.1: Solid-Phase Oligonucleotide Synthesis Cycle.

8.3 Deprotection of Oligonucleotides

Deprotection of oligonucleotides began with removal of the CPG-bound crude oligonucleotides from the SPS columns. This CPG was transferred to individual, sterilized, 2 mL screw-cap vials. 1 mL of 3:1 (ammonium hydroxide/ethanol) was added to allow for cleavage of the oligonucleotides from the solid support as well as to remove the 2-cyanoethyl and benzoyl protecting groups. These vials were vortexed, centrifuged, then placed in a 55 °C water bath for a minimum of 4 h to allow for the deprotections to be completed. Following deprotection, the vials were cooled for 5 min in a freezer before being vortexed again. The supernatant containing the

now-deprotected oligonucleotides was transferred to a new 2 mL screw cap vials, with the CPG solid support being thoroughly washed with 2 × 300 μL of 50 % (ACN/H_2O). These washings were pooled with the supernatant and the vials were dried down overnight on the speed-vac. To the crude, dried, RNA oligonucleotides, 200 μL TREAT-HF was added to allow for removal of the 2'-*O*-TBDMS protecting groups. These vials were heated at 65 ℃ for a minimum of 2 h before being placed in the freezer to cool for 5 min. 400 μL of dry methanol was added to precipitate the RNA. The vials were, again, vortexed and centrifuged to pellet the RNA. Carefully, the TREAT-HF solution was removed without disturbing the pellet. The pellet was then washed with 2 × 400 μL of dry MeOH before being dried on the speed-vac.

8.4 Quantification of Oligonucleotides

To a vial of dried, crude, oligonucleotide, 1 mL of 0.1 M sodium acetate was added to dissolve the poly(A) oligonucleotides. This solution was vortexed followed by the removal of 5 μL of crude RNA stock, to which, was added 995 μL of autoclaved, HPLC grade H_2O in a 1 mL Eppendorf tube. The Varian Cary 300 Bio UV-Visible Spectrophotometer was used for quantification of oligonucleotide samples. The spectrophotometer was blanked with 1 mL 18 MΩ H_2O before the oligonucleotide sample was analyzed at 260 nm in a quartz cuvette. Total oligonucleotide concentration was back calculated based on the absorbance reading for the 5 μL sample. Using the Beer-Lambert law ($A=\varepsilon \times c \times l$), oligonucleotide concentrations were determined from total absorbance values of the oligonucleotide stock solutions. Extinction coefficients were calculated using the nearest neighbour approximation.[244]

8.5 Analytical Gel Analysis

Analytical gel analysis was performed on 0.1-0.15 OD of the crude oligonucleotide samples. 20 % denaturing PAGE solution (19:1, acrylamide/bisacrylamide) in 1X TBE buffer was made. 5 mL of PAGE solution was polymerized with 12.5 µL of 20 % APS and 6.25 µL of TEMED between two standard glass plates (7 cm × 10 cm). Samples were loaded in 10 µL of formamide and run at 200 V until desired separation is achieved (~ 1.5 h). A dye solution containing bromophenol blue and xylene cyanol was used as markers due to their similar mobility to oligonucleotides (8 and 28 nt respectively). Gels were visualized by either short or long-wave UV shadowing.

8.6 Preparatory Gel Purification

Preparatory gel purification was performed on approximately 16 OD of the crude oligonucleotide samples. These samples were loaded in 25 µL of formamide onto gels that were polymerized with 40 mL of 20 % denaturing PAGE solution (19:1, acrylamide/bisacrylamide), 200 µL APS, and 100 µL TEMED between two standard glass plates (20 × 20 cm). Samples were run at 400 V until the desired separation was achieved (~ 3 h). Bands were excised and placed into 15 mL Falcon™ tubes. The oligonucleotides were extracted with 8 mL of 0.1 M NaOAc with gentle rocking on a table shaker overnight.

8.7 Desalting of Oligonucleotides

Following purification, oligonucleotides were desalted using C-18 SEP PAK cartridges. The cartridges were prepared by running 10 mL of 100 % ACN, then 10 mL of 50 % ACN/H_2O, followed by a final wash with 10 mL of 0.1 M NaOAc. Solutions containing purified oligonucleotides were then passed through the cartridge resulting in their retention by the C-18 stationary phase. Salts were removed by passing 4 × 10 mL of HPLC H_2O through the cartridge followed by elution of the oligonucleotides with 4.5 mL of MeOH/H_2O/ACN (2:1:1). The purity of all the oligonucleotides was assessed to be above 90 % through analytical gel electrophoresis.

8.8 RP-HPLC Purification

RP-HPLC purification of phosphorothioate-modified oligonucleotides was performed with a Waters 2487 Dual λ Absorbance Detector instrument with a Waters C18 (5 μm, 4.6 × 150 mm) column. A gradient of running buffer A with increasing concentrations of buffer B (0 to 45 % over 30 mins); Buffer A (1X): 0.05 M sodium phosphate buffer (pH 5.8), 2 % (v/v) ACN. Buffer B: 10 % (v/v) 10X Buffer A, 48 % (v/v) HPLC ACN. 500 μL samples were injected (0.1 OD for analytical runs, 0.5 OD for preparatory runs) and the eluent from the column containing the desired oligonucleotide product was collected in 15 mL Falcon™ tubes for desalting.

8.9 Thermal Denaturation Analysis

UV thermal denaturation *(T_m)* analysis of oligonucleotides was done on a Varian Cary 300 Bio UV-Visible Spectrophotometer equipped with a temperature controller. RNA samples of 0.5 OD were dissolved in 1 mL of phosphate-citrate buffer of appropriate pH. These samples were heated to 95 ℃ for 5 min in a sand bath and then slowly cooled to RT on the benchtop. Samples were then placed in a 4 ℃ fridge overnight. Before analysis, samples were degassed for 2 min on a speed-vac to remove dissolved gases that may interfere with data collection. Samples were added to 1 mL quartz cuvettes and capped to ensure no loss of solvent due to evaporation. Samples were heated from 4 ℃ to 95 ℃ at a rate of 0.5 ℃/min. Data was collected at 260 nm (unless stated otherwise) at every interval of 0.5 ℃. T_m data collection that was done by heating (denaturation) and then cooling (annealing) in a single run had the same rate of temperature change and data collection. T_m values were determined at the point of maximal slope for the sigmoidal transition according to the method of Puglisi and Tinoco.[147]

8.10 Circular Dichroism Analysis

CD analysis of oligonucleotides was done on a Jasco J-815 CD Spectropolarimeter with Julabo F25 temperature controller. RNA samples of 0.5 OD were dissolved in phosphate-citrate buffer of desired pH. These samples were heated to 95 ℃ for 5 min and slowly cooled to RT to ensure proper formation of duplex structures. These samples were analyzed in a 1 mL quartz cuvette using the spectropolarimeter. Data was collected from 320-200 nm, at 15 ℃, with a ramp rate of 20 nm/min. The scans were the average of 5 accumulations and were done with the molar

ellipticity (difference between absorption of right-handed and left-handed circularly polarized light) plotted as a function of wavelength. Oligonucleotide extinction coefficients were calculated based on the nearest neighbour approximation and modifications were assumed to have a negligible effect on these values.

8.11 Native Gel Electrophoresis

Running buffers for native gel electrophoresis consisted of 40 mM Na_2HPO_4, 30 mM citric acid, 1.1 mM EDTA, and were adjusted to desired pH with HCl or NaOH. 20 % Native PAGE solution was made from 50 % of a 40 % (19:1, acrylamide/bisacrylamide) PAGE stock solution and 50 % of native buffer of desired pH. Gels were polymerized using 4.5 mL of 20 % native PAGE solution of desired pH, 12.5 µL APS, and 6.25 µL TEMED between two standard glass plates (7 × 10 cm). Gels were pre-run at 100 V for 20 min. Samples loaded in 40 % sucrose loading buffer (40 % (w/v) sucrose in 1 mL native buffer of desired pH). Samples run at 100 V until desired separation was achieved (~ 5 h), then visualized by either short-wave or long-wave UV shadowing.

8.12 Fluorescence Analysis

Fluorescence analysis of oligonucleotides was performed on a Varian Cary Eclipse Fluorescence Spectrophotometer. Samples of 0.5 OD were dissolved in the phosphate-citrate buffer of the appropriate pH, heated to 95 °C for 5 min, then cooled overnight in a 4 °C fridge. In a 1 ml, quartz, fluorescence, cuvette, samples were excited at 350 nm and emission signals were

generally obtained from 355-500 nm at RT. Data was corrected for the absorbance differences at 350 nm.

8.13 Variable Temperature Fluorescence Analysis

Variable temperature fluorescence experiments were performed on a Shimadzu RF-5301PC Spectrofluorophotometer with a VWR Model 1162 temperature controller. RNA samples were dissolved in the appropriate buffer, heated to 95 ℃ for 5 min, then cooled overnight in a 4 ℃ fridge and added to a 5 mL quartz fluorescence cuvette. The temperature was increased at a rate of 0.5 ℃/min (identical to the UV thermal denaturation experiments). Scans were acquired every 5 ℃ by excitation at 350 nm following by recording the emission intensity at either 380 (pyrene monomer emission) or 480 nm (pyrene excimer emission).

8.14 UV-Vis Analysis

UV scans of the pyrene-containing oligonucleotides were performed using a Varian Cary 300 Bio UV-Visible Spectrophotometer to characterize pyrene absorption. 0.5 OD of RNA samples were dissolved a phosphate-citrate buffer of the appropriate pH. These samples were heated to 95 ℃ then slowly cooled overnight in the 4 ℃ fridge. Before acquiring the spectra, the instrument was blanked with 18 MΩ H_2O before adding the sample to the 1 mL quartz cuvette. These samples were scanned from 600-300 nm at RT and a scanning rate of 400 nm/min. Data was corrected at 350 nm to correct for any slight concentrations differences between the samples.

8.15 Variable Temperature UV-Vis Analysis

Variable temperature UV-Vis analysis was performed on pyrene-containing oligonucleotides using the Varian Cary 300 Bio UV-Visible Spectrophotometer equipped with a temperature controller. Samples were dissolved in the appropriate phosphate-citrate buffer and heated to 95 °C then slowly cooled overnight in the 4 °C fridge. Samples were then added to a 1 mL quartz cuvette and scanned from 500-300 nm. The temperature ramp was set to 2.5 °C/min and samples were scanned every 5 °C between 10 and 95 °C.

8.16 LC-ESI-Orbitrap MS Analysis

ESI-MS analysis of oligonucleotide samples was performed at the Concordia University Centre for Biological Applications of Mass Spectrometry (CBAMS) on an Agilent Technologies 1100 LC system coupled to a Thermo Fisher Scientific LTQ Orbitrap Velos MS equipped with a heated ESI source run on negative mode. The LC setup used a Spursil C18-EP column (50 × 2.1 mm, 3 μm particle diameter, Dikma Technologies) and oligonucleotides were eluted using a 20 min gradient at an initial flow rate of 250 μL min^{-1} (Mobile Phase A: 10 mM ammonium acetate and 1 mM ammonium fluoride (aq) solution, Mobile Phase B: ACN). 2 % B was run and held for 3 min. This was linearly increased to 50 % B by the 8 min mark, and then increased again to 90 % B by the 10 min mark. 90 % B was held until the 12 min mark. The buffer system was reduced to 2 % B to recondition the column at a flow rate of 400 μL min^{-1} for 6 min, and then the flow was reduced to 250 μL min^{-1} for the final 2 min. Dried samples (0.1 OD) were reconstituted in 50 μL

of mobile phase A. Injection volume was 10 μL. The divert valve was switched to the detector after 4 min. MS spectra (*m/z* 300-2000) were acquired in the Orbitrap at a resolution of 60,000. Uncharged monoisotopic mass of oligonucleotides was calculated using Thermo Freestyle™ software (v1.7 SP1).

8.17 LC-ESI-QTOF MS Analysis

ESI-QTOF-MS analysis was performed on oligonucleotide samples at the Concordia University Centre for Biological Applications of Mass Spectrometry (CBAMS) on an Agilent Technologies HP 1200 LC coupled to a Waters Micromass Q-TOF Ultima API MS. Samples were ionized using ESI before being analyzed. Detection was run in full scan, negative ion detection mode.

8.18 Quantum Yield Analysis

Quantum yield analysis was performed on a Horiba PTI QuantaMaster 8075 spectrofluorometer. Samples were heated to 95 °C then slowly cooled overnight in a 4 °C fridge. Instrument was calibrated with appropriate buffers. 5 nm slit width, 1 nm step rate, and 1 s integration time.

8.19 Synthesis of Azide-Bearing Small Molecules

(1) 1,4-diazidobutane

To a dried RBF, 5.0 g (23.2 mmol, 1 eq.) of 1,4-dibromobutane was added. This was dissolved in 10 mL of DMF at RT and 4.5 g (69.5 mmol, 3 eq.) of sodium azide was then slowly added. The solution was heated to 80 ℃ for 20 h under constant stirring. The solution was then cooled to RT, 10 mL of H_2O was added, followed by extraction with Et_2O (4 × 7 mL). The organic layer was washed with H_2O (3 × 5 mL). The product was dried with Na_2SO_4 (anhyd.) and then concentrated to give 2.6 g (21.9 mmol, 94 %) of a clear oil (**1**). ^{1}H NMR (500 MHz, $CDCl_3$, ppm): δ 3.30 (t, J=9.3 Hz, 4H, N_3CH_2), 1.66 (m, 4H, $CH_2\underline{CH_2}\underline{CH_2}CH_2$). ^{13}C (125.7 MHz, $CDCl_3$, ppm): δ 50.93, 26.17. ATR-FTIR (cm^{-1}): 2940, 2870, 2080, 1250. The ^{1}H and ^{13}C chemical shifts of the product were in agreement with those reported in the literature for this compound.[245,246]

(2) 4-azidobutylamine

To a RBF, 1.3 g (9.28 mmol, 1 eq.) (**1**) was added and dissolved in 4 mL Et_2O, 4 mL EtOAc, 3 mL 10 % HCl (aq), and 3 mL H_2O. 2.2 g (8.35 mmol, 0.9 eq.) of Ph_3P was added slowly on ice over 1 h. The solution was left to react overnight with stirring. The reaction mixture was transferred to a separatory funnel and the RBF was rinsed with 10 % HCl(aq) (3 × 3 mL). The organic layers were discarded, and the aqueous layer was washed with DCM (2 × 5 mL). The aqueous layer was then basified to pH 13 with 2 M NaOH. The final product was extracted with DCM (3 × 4 mL), dried over Na_2SO_4 (anhyd.), then concentrated in vacuo to give 0.657 g (5.76 mmol, 62 %) of a yellowish oil (**2**). ^{1}H NMR (500 MHz, $CDCl_3$, ppm): δ 5.24 (m, 2H, NH_2), 3.23

(m, 2H, N_3CH_2), 2.66 (m, 2H, $NH_2\underline{CH_2}$), 1.59 (m, 2H, $N_3CH_2\underline{CH_2}$), 1.45 (m, 2H, $NH_2CH_2\underline{CH_2}$). ^{13}C (125.7 MHz, $CDCl_3$, ppm): δ 50.63, 41.25, 30.05, 25.63. ATR-FTIR: (cm^{-1}): 3370, 3310, 2930, 2860, 2090, 1250, 728. MS (ESI+): $[M+H]^+$ = expected 115.16, found 115.085. The ^1H and ^{13}C chemical shifts of the product were in agreement with those reported in the literature for this compound.[245,247]

(3) 1-(bromomethyl)pyrene

To a flame-dried, 10 mL RBF, 300 mg (1.29 mmol, 1 eq.) of 1-pyrenemethanol was dissolved in 1 mL of THF (anhyd.) under inert argon atmosphere. To this, 874 mg (3.22 mmol, 0.30 mL, 2.5 eq.) of PBr_3 was added very slowly on ice. The solution was left to react for 4 h at RT with constant stirring. The product was isolated through vacuum filtration and washed with Et_2O to give 191.8 mg (0.650 mmol, 50 %) of a colourless solid (**3**). ^1H NMR (500 MHz, $CDCl_3$, ppm): δ 8.35-8.02 (m, 9H, aromatics), 5.24 (s, 2H, CH_2Br). ^{13}C (125.7 MHz, $CDCl_3$, ppm): δ 131.93-122.80, 32.18. ATR-FTIR (cm^{-1}): 3040, 2990, 1590, 1200, 843, 756, 682, 636. The ^1H and ^{13}C chemical shifts of the product were in agreement with those reported in the literature for this compound.[248] Product was used for subsequent step even with minor impurities seen on ^1H NMR.

(4) 1-(azidomethyl)pyrene

To a flame-dried, 10 mL RBF, 191.8 mg (0.650 mmol, 1 eq.) of 1-(bromomethyl)pyrene (**3**) was added under inert argon atmosphere. This was dissolved in 1.5 mL of DMF (anhyd.). To this, 211.2 mg (3.25 mmol, 5.0 eq.) of NaN_3 was slowly added. The solution was heated to 80 °C over 18 h with constant stirring. Once complete, the reaction mixture was transferred to a separatory funnel and 20 mL of H_2O was added, leading to the formation of a colourless

precipitate. The product was extracted with EtOAc (3 × 10 mL) then washed with H_2O (2 × 5 mL). The organic fractions were dried over Na_2SO_4 (anhyd.) then concentrated in vacuo. The product was purified using FCC (20 cm silica, 1.5 cm column diameter) with 5 % EtOAc/Hexanes as the eluent. Fractions containing the desired product appeared as fluorescent spots on TLC under short-wave UV light. Fractions containing the product were dried down to give compound (**4**) as a light-yellow solid. ^{1}H NMR (500 MHz, $CDCl_3$, ppm): δ 8.03 (m, 9H, aromatics), 5.03 (s, 2H, CH_2N_3). ^{13}C (125.7 MHz, $CDCl_3$, ppm): δ 131.82-122.6, 53.09. ATR-FTIR (cm^{-1}): 3040, 2920, 2100, 2080, 1590, 1230, 894, 834, 752, 700. MS (ESI+): [*m/z*] = 257.30, found $[M-H]^-$ = 256.268. The ^{1}H and ^{13}C chemical shifts of the product were in agreement with those reported in the literature for this compound.[248]

8.20 Click Reactions of poly(A) RNA

Reactions with 4-Azidobutylamine

To a 15 mL, sterilized, Falcon™ tube containing 6 mL of 0.2 M NaCl(aq), 1.0 OD of the desired poly(A) sequence was added. The tube was then heated to 95 °C, then slowly cooled to RT over 30 min to ensure no large aggregates of RNA were present. To this Falcon™ tube, 50 eq. of 0.5 M sodium ascorbate (aq), and 50 eq. PMDETA ligand were added. The solution was then degassed for 2 min on a speed-vac to remove any dissolved oxygen which could lead to aerobic degradation of the nucleic acids.[133,249] Then, 2 eq. of 4-azidobutylamine was added for every propargyl group contained within the modified ssRNA sequence. Lastly, 5 eq. of 0.1 M Cu(II) acetate hydrate (aq) was added and the solution was quickly degassed again for another 2 min. The solution was inverted to ensure thorough distribution of the reagents and was left to react for 3 h

on the benchtop. After 3 h, the reaction was stopped through desalting as per Chapter 8.7 with the following modifications: Samples were diluted to 10 mL with 0.1 M sodium acetate followed by the addition of the solution to the C18 column. Sample flowthrough was passed through the column 3 times to ensure complete retention of the derivatized oligonucleotide product. This was followed by washing of the sample with 6 × 8 mL of H_2O (HPLC) to ensure complete removal of the copper salts. Samples were dried down overnight on the speed-vac and then purified through denaturing analytical PAGE (**Figures A.5-A.7**).

Reactions with 1-(azidomethyl)pyrene

Reactions with 1-(azidomethyl)pyrene followed the same general procedure as with 4-azidobutylamine with the following modifications. Due to the inherent insolubility of pyrene compounds in water, 0.05 M solutions of 1-(azidomethyl)pyrene in DMSO were prepared. Prior to degassing, 2 eq. of this pyrene solution were then added to the 15 mL Falcon™ tube for every C2'-*O*-propargyl modification within the poly(A) oligonucleotide set to be coupled. Following the reaction, it was important to dilute the reaction mixtures before desalting to ensure that the organic composition was below 5 % (v/v), otherwise the oligonucleotides may not adhere to the C-18 column.

References

(1) Miescher, J. F. Ueber Die Chemische Zusammensetzung Der Eiterzellen. *Med. Untersuchungen* **1871**, *4*, 441–460.

(2) Hall, K.; Sankaran, N. DNA Translated: Friedrich Miescher's Discovery of Nuclein in Its Original Context. *Br. J. Hist. Sci.* **2021**, 1–9.

(3) Altmann, R. Über Nucleinsäuren (On Nucleic Acids). *Arch. Anat. Physiol.* **1889**, *1*, 524–536.

(4) Klein, W.; Thannhauser, S. J. Experimentelle Studien Uber Den Nucleinstoffwechsel. XXXV. Die Pyrimidinnucleotide Aus Thymusnucleinsaure. *Z. Physiol Chem.* **1935**, *231*, 96.

(5) Howard, G. A.; Lythgoe, B.; Todd, A. R. A Synthesis of Cytidine. *J. Chem. Soc.* **1947**, 1052–1054.

(6) Clark, V. M.; Kirby, G. W.; Todd, A. The Use of Phosphoramidic Esters in Acylations. A New Preparation of Adenosine-5'-Pyrophosphate and Adenosine-5'- Triphosphate. *J. Chem. Soc.* **1957**, 1497–1501.

(7) Chargaff, E.; Vischer, E.; Doniger, R.; Green, C.; Misani, F. The Composition of the Desoxypentose Nucleic Acids of Thymus and Spleen. *J. Biol. Chem.* **1949**, *177* (1), 405–416.

(8) Crick, F.; Watson, J. Molecular Structure of Nucleic Acids. *Nature* **1953**, *171*, 737–738.

(9) Pauling, L.; Corey, R. Structure of the Nucleic Acids. *Nature* **1953**, *171*, 346.

(10) Hargittai, I. The Tetranucleotide Hypothesis: A Centennial. *Struct. Chem.* **2009**, *20*, 753–756.

(11) Furberg, S. On the Structure of Nucleic Acids. *Acta Chem. Scand.* **1952**, *6*, 634–640.

(12) Astbury, W. T. X-Ray Studies of Nucleic Acids. *Symp. Soc. Exp. Biol.* **1947**, *1*, 66–76.

(13) Wilkins, M. H.; Randall, J. T. Crystallinity in Sperm Heads: Molecular Structure of Nucleoprotein in Vivo. *Biochim. biophys. acta* **1953**, *10*, 192–193.

(14) Wilkins, M. H. F.; Stokes, A. R.; Wilson, H. R. Molecular Structure of Deoxypentose Nucleic Acids. *Nature* **1953**, *171*, 738–740.

(15) Franklin, R. E.; Gosling, R. . Molecular Configuration in Sodium Thymonucleate. *Nature* **1953**, *171*, 740–741.

(16) Maddox, B. *Rosalind Franklin: The Dark Lady of DNA*; HarperCollins: New York, 2002.

(17) Crick, F.; Watson, J. D. The Complementary Structure of Deoxyribonucleic Acid. *Proc. R. Soc. A.* **1954**, *223*, 80–96.

(18) Blackburn, M. G.; Gait, M. J.; Loakes, D.; Williams, D. M. DNA and RNA Structure. In *Nucleic Acids in Chemistry and Biology*; RSC Publishing: Cambridge, 2006; pp 13–76.

(19) Ussery, D. W. DNA Structure: A-, B- and Z-DNA Helix Families. In *Encyclopedia of Life Sciences*; John Wiley & Sons, Ltd: Chichester, UK, 2002.

(20) Hud, N. V.; Polak, M. DNA-Cation Interactions: The Major and Minor Grooves Are Flexible Ionophores. *Curr. Opin. Struct. Biol.* **2001**, *11* (3), 293–301.

(21) Privalov, P. L.; Dragan, A. I.; Crane-Robinson, C.; Breslauer, K. J.; Remeta, D. P.; Minetti, C. A. S. A. What Drives Proteins into the Major or Minor Grooves of DNA? *J. Mol. Biol.* **2007**, *365* (1), 1–9.

(22) Wang, A. H. J.; Quigley, G. J.; Kolpak, F. J.; Crawford, J. L.; van Boom, J. H.; van der Marel, G.; Rich, A. Molecular Structure of a Left-Handed Double Helical DNA Fragment at Atomic Resolution. *Nature* **1979**, *282*, 680–686.

(23) Rich, A.; Nordheim, A.; Wang, A. H. J. The Chemistry and Biology of Left-Handed Z-DNA. *Annu. Rev. Biochem.* **1984**, *53*, 791–846.

(24) Peck, L. J.; Nordheim, A.; Rich, A.; Wang, J. C. Flipping of Cloned d(PCpG)n d(PCpG)n DNA Sequences from Right- to Left-Handed Helical Structure by Salt , Co (III), or Negative Supercoiling. *Biochemistry* **1982**, *79*, 4560–4564.

(25) Leontis, N. B.; Westhof, E. Geometric Nomenclature and Classification of RNA Base Pairs. *RNA* **2001**, *7* (4), 499–512.

(26) Felsenfeld, G.; Rich, A. Studies on the Formation of Two- and Three-Stranded Polyribonucleotides. *Biochim Biophys Acta* **1957**, *26* (3), 457–468.

(27) Hoogsteen, K. The Structure of Crystals Containing a Hydrogen-Bonded Complex of 1-Methylthymine and 9-Methyladenine. *Acta Crystallogr.* **1959**, *12* (10), 822–823.

(28) Phan, A. T.; Guéron, M.; Leroy, J. L. The Solution Structure and Internal Motions of a Fragment of the Cytidine-Rich Strand of the Human Telomere. *J. Mol. Biol.* **2000**, *299* (1), 123–144.

(29) Dong, Y.; Yang, Z.; Liu, D. DNA Nanotechnology Based on I-Motif Structures. *Accounts Chem. Res.* **2014**, *47* (6), 1853–1860.

(30) Gehring, K.; Leroy, J. L.; Guéron, M. A Tetrameric DNA Structure with Protonated Cytosine.Cytosine Base Pairs. *Nature* **1993**, *363* (6429), 561–565.

(31) Zeraati, M.; Langley, D. B.; Schofield, P.; Moye, A. L.; Rouet, R.; Hughes, W. E.; Bryan, T. M.; Dinger, M. E.; Christ, D. I-Motif DNA Structures Are Formed in the Nuclei of Human Cells. *Nat. Chem.* **2018**, *10* (6), 631–637.

(32) Benabou, S.; Avino, A.; Eritja, R.; Gonzalez, C.; Gargallo, R. Fundamental Aspects of the Nucleic Acid I-Motif Structures. *RSC Adv.* **2014**, *4*, 26956–26980.

(33) Jin, K. S.; Shin, S. R.; Ahn, B.; Rho, Y.; Kim, S. J.; Ree, M. PH-Dependent Structures of an i-Motif DNA in Solution. *J. Phys. Chem. B* **2009**, *113* (7), 1852–1856.

(34) Cui, J.; Waltman, P.; Le, V. H.; Lewis, E. A. The Effect of Molecular Crowding on the Stability of Human C-MYC Promoter Sequence I-Motif at Neutral PH. *Molecules* **2013**, *18*, 12751–12767.

(35) Sun, D.; Hurley, L. H. The Importance of Negative Superhelicity in Inducing the Formation of G-Quadruplex and i-Motif Structures in the c-Myc Promoter: Implications for Drug Targeting and Control of Gene Expression. *J. Med Chem.* **2009**, *52*, 2863–2874.

(36) Sun, Y.; Yang, B.; Hua, Y.; Dong, Y.; Ye, J.; Wang, J.; Xu, L.; Liu, D. Construction and Characterization of a Mirror-Image L-DNA i-Motif. *ChemBioChem* **2020**, *21* (1–2), 94–97.

(37) Saha, P.; Panda, D.; Paul, R.; Dash, J. A DNA Nanosensor for Monitoring Ligand-Induced i-Motif Formation. *Org. Biomol. Chem.* **2021**, *19*, 1965–1969.

(38) Rhodes, D.; Lipps, H. J. Survey and Summary: G-Quadruplexes and Their Regulatory Roles in Biology. *Nucleic Acids Res.* **2015**, *43* (18), 8627–8637.

(39) Parkinson, G. N.; Lee, M. P. H.; Neidle, S. Crystal Structure of Parallel Quadruplexes from Human Telomeric DNA. *Nature* **2002**, *417* (6891), 876–880.

(40) Lane, A. N.; Chaires, J. B.; Gray, R. D.; Trent, J. O. Stability and Kinetics of G-Quadruplex Structures. *Nucleic Acids Res.* **2008**, *36*, 5482–5515.

(41) Maizels, N.; Gray, L. T. L. T. The G4 Genome. *PLoS Genet.* **2013**, *9* (4), e1003468.

(42) Cayrou, C.; Gregoire, D.; Coulombe, P.; Danis, E.; Mechali, M. Genome-Scale Identification of Active DNA Replication Origins. *Methods* **2012**, *57*, 158–164.

(43) Carvalho, J.; Mergny, J. L.; Salgado, G. F.; Queiroz, J. A.; Cruz, C. G-Quadruplex, Friend or Foe: The Role of the G-Quartet in Anticancer Strategies. *Trends Mol. Med.* **2020**, *26* (9), 848–861.

(44) Moye, A. L.; Porter, K. C.; Cohen, S. B.; Phan, T.; Zyner, K. G.; Sasaki, N.; Lovrecz, G. O.; Beck, J. L.; Bryan, T. M. Telomeric G-Quadruplexes Are a Substrate and Site Localization for Human Telomerase. *Nat. Commun.* **2015**, *6*, 7643.

(45) Wang, Q.; Liu, J.; Chen, Z.; Zheng, K.; Chen, C.; Hao, Y.; Tan, Z. G-Quadruplex Formation at the 3' End of Telomere DNA Inhibits Its Extension by Telomerase, Polymerase and Unwinding by Helicase. *Nucleic Acids Res.* **2011**, *39* (14), 6229–6237.

(46) Prorok, P.; Artufel, M.; Aze, A.; Coulombe, P.; Peiffer, I.; Lacroix, L.; Guedin, A.; Mergny, J. L.; Damaschke, J.; Schepers, A.; Cayrou, C.; Teulade-Fichou, M.-P.; Ballester, B.; Mechali, M. Involvement of G-Quadruplex Regions in Mammalian Replication Origin Activity. *Nat. Commun.* **2019**, *10*, 3274.

(47) Bay, D. H.; Busch, A.; Lisdat, F.; Lida, K.; Ikebukuro, K.; Nagasawa, K.; Karube, I.; Yoshida, W. Identification of G-Quadruplex Structures That Possess Transcriptional Regulating Functions in the Dele and Cdc6 CpG Islands. *BMC Mol. Biol.* **2017**, *18 (1)*, 17.

(48) Wu, G.; Xing, Z.; Tran, E. J.; Yang, D. DDX5 Helicase Resolves G-Quadruplex and Is Involved in MYC Gene Transcriptional Activation. *Proc. Natl. Acad. Sci. U. S. A.* **2019**, *116* (41), 20453–20461.

(49) Jodoin, R.; Carrier, J. C.; Rivard, N.; Bisaillon, M.; Perreault, J.-P. G-Quadruplex Located in the 5'UTR of the BAG-1 MRNA Affects Both Its Cap-Dependent and Cap-Independent

Translation through Global Secondary Structure Maintenance. *Nucleic Acids Res.* **2019**, *47* (19), 10247–10266.

(50) Devi, G.; Zhou, Y.; Zhong, Z.; Toh, D. F. K.; Chen, G. RNA Triplexes: From Structural Principles to Biological and Biotech Applications. *Wiley Interdiscip. Rev. RNA* **2015**, *6* (1), 111–128.

(51) Adams, P. L.; Stahley, M. R.; Kosek, A. B.; Wang, J.; Strobel, S. A. Crystal Structure of a Self-Splicing Group I Intron with Both Exons. *Nature* **2004**, *430*, 45–50.

(52) Toor, N.; Keating, K. S.; Taylor, S. D.; Pyle, A. M. Crystal Structure of a Self-Spliced Group II Intron. *Science.* **2008**, *320*, 77–82.

(53) Klein, D. J.; Schmeing, T. M.; Moore, P. B.; Steitz, T. A. The Kink-Turn: A New RNA Secondary Structure Motif. *EMBO J.* **2001**, *20*, 4214–4221.

(54) Ulyanov, N. B.; Shefer, K.; James, T. L.; Tzfati, Y. Pseudo- Knot Structures with Conserved Base Triples in Telom- Erase RNAs of Ciliates. *Nucleic Acids Res.* **2007**, *35*, 6150–6160.

(55) Shefer, K.; Brown, Y.; Gorkovoy, V.; Nussbaum, T.; Ulyanov, N. B.; Tzfati, Y. A Triple Helix within a Pseudo- Knot Is a Conserved and Essential Element of Telomerase RNA. *Mol. Cell Biol.* **2007**, *27*, 2130–2143.

(56) Olsthoorn, R. C. Reumerman, R.; Hilbers, C. W.; Pleij, C. W.; Heus, H. A. Functional Analysis of the SRV-1 RNA Frameshifting Pseudoknot. *Nucleic Acids Res.* **2010**, *38*, 7665–7672.

(57) Su, L.; Chen, L.; M., E.; Berger, J. M.; Rich, A. Minor Groove RNA Triplex in the Crystal Structure of a Ribosomal Frameshifting Viral Pseudoknot. *Nat. Struct. Biol.* **1999**, *6*, 285–292.

(58) Wilusz, J. E.; JnBaptiste, C. K.; Lu, L. Y.; Kuhn, C. D.; Joshua-Tor, L.; Sharp, P. A. A Triple Helix Stabilizes the 3′ Ends of Long Noncoding RNAs That Lack Poly(A) Tails. *Genes Dev* **2012**, *26*, 2392–2407.

(59) Blackburn, M. G.; Gait, M. J.; Loakes, D.; Williams, D. M. RNA Structure and Function. In *Nucleic Acids in Chemistry and Biology*; RSC Publishing: Cambridge, 2006; pp 253–293.

(60) Olivas, W. M.; Maher, L. J. Overcoming Potassium-Mediated Triplex Inhibition. *Nucleic Acids Res.* **1995**, *23* (11), 1936–1941.

(61) Hu, Y.; Cecconello, A.; Idili, A.; Ricci, F.; Willner, I. Triplex DNA Nanostructures: From Basic Properties to Applications. *Angew. Chemie - Int. Ed.* **2017**, *56* (48), 15210–15233.

(62) Naskar, S.; Guha, R.; Müller, J. Metal-Modified Nucleic Acids: Metal-Mediated Base Pairs, Triples, and Tetrads. *Angew. Chemie - Int. Ed.* **2020**, *59* (4), 1397–1406.

(63) Megger, N.; Welte, L.; Zamora, F.; Muller, J. Metal-Mediated Aggregation of DNA Comprising 2,2'-Bipyridine Nucleoside, an Asymmetrically Substituted Chiral Bidentate Ligand. *Dalt. Trans.* **2011**, *40* (8), 1802–1807.

(64) Su, Y.; Li, D.; Liu, B.; Xiao, M.; Wang, F.; Li, L.; Zhang, X.; Pei, H. Rational Design of Framework Nucleic Acids for Bioanalytical Applications. *Chempluschem* **2019**, *84* (5), 512–523.

(65) Seeman, N. C. Nanomaterials Based on DNA. *Annu. Rev. Biochem.* **2010**, *79*, 65–87.

(66) Hill, A. C.; Hall, J. High-Order Structures from Nucleic Acids for Biomedical Applications. *Mater. Chem. Front.* **2020**, *4* (4), 1074–1088.

(67) Wang, F.; Lv, H.; Li, Q.; Li, J.; Zhang, X.; Shi, J.; Wang, L.; Fan, C. Implementing Digital Computing with DNA-Based Switching Circuits. *Nat. Commun.* **2020**, *11*, 121.

(68) Corbett, K. S.; Edwards, D. K.; Leist, S. R.; Abiona, O. M.; Boyoglu-Barnum, S.; Gillespie, R. A.; Himansu, S.; Schäfer, A.; Ziwawo, C. T.; DiPiazza, A. T.; Dinnon, K. H.; Elbashir, S. M.; Shaw, C. A.; Woods, A.; Fritch, E. J.; Martinez, D. R.; Bock, K. W.; Minai, M.; Nagata, B. M.; Hutchinson, G. B.; Wu, K.; Henry, C.; Bahl, K.; Garcia-Dominguez, D.; Ma, L. Z.; Renzi, I.; Kong, W. P.; Schmidt, S. D.; Wang, L.; Zhang, Y.; Phung, E.; Chang, L. A.; Loomis, R. J.; Altaras, N. E.; Narayanan, E.; Metkar, M.; Presnyak, V.; Liu, C.; Louder, M. K.; Shi, W.; Leung, K.; Yang, E. S.; West, A.; Gully, K. L.; Stevens, L. J.; Wang, N.; Wrapp, D.; Doria-Rose, N. A.; Stewart-Jones, G.; Bennett, H.; Alvarado, G. S.; Nason, M. C.; Ruckwardt, T. J.; McLellan, J. S.; Denison, M. R.; Chappell, J. D.; Moore, I. N.; Morabito, K. M.; Mascola, J. R.; Baric, R. S.; Carfi, A.; Graham, B. S. SARS-CoV-2 MRNA Vaccine Design Enabled by Prototype Pathogen Preparedness. *Nature* **2020**, *586* (7830), 567–571.

(69) Mulligan, M. J.; Lyke, K. E.; Kitchin, N.; Absalon, J.; Gurtman, A.; Lockhart, S.; Neuzil, K.; Raabe, V.; Bailey, R.; Swanson, K. A.; Li, P.; Koury, K.; Kalina, W.; Cooper, D.; Fontes-Garfias, C.; Shi, P. Y.; Türeci, Ö.; Tompkins, K. R.; Walsh, E. E.; Frenck, R.; Falsey, A. R.; Dormitzer, P. R.; Gruber, W. C.; Şahin, U.; Jansen, K. U. Phase I/II Study of COVID-19 RNA Vaccine BNT162b1 in Adults. *Nature* **2020**, *586* (7830), 589–593.

(70) Noor, R. Developmental Status of the Potential Vaccines for the Mitigation of the COVID-19 Pandemic and a Focus on the Effectiveness of the Pfizer-BioNTech and Moderna MRNA Vaccines. *Curr. Clin. Microbiol. Reports* **2021**, *8*, 178-185.

(71) Plasterk, R. H. A. RNA Silencing: The Genome's Immune System. *Science* **2002**, *296* (5571), 1263–1265.

(72) Monia, B. P.; Lesnik, E. A.; Gonzalez, C.; Lima, W. F.; McGee, D.; Guinosso, C. J.; Kawasaki, A. M.; Cook, P. D.; Freier, S. M. Evaluation of 2'-Modified Oligonucleotides Containing 2'-Deoxy Gaps as Antisense Inhibitors of Gene Expression. *J. Biol. Chem.* **1993**, *268* (19), 14514–14522.

(73) Liang, X. H.; Sun, H.; Nichols, J. G.; Crooke, S. T. RNase H1-Dependent Antisense Oligonucleotides Are Robustly Active in Directing RNA Cleavage in Both the Cytoplasm and the Nucleus. *Mol. Ther.* **2017**, *25* (9), 2075–2092.

(74) Lima, J. F.; Cerqueira, L.; Figueiredo, C.; Oliveira, C.; Azevedo, N. F. Anti-MiRNA Oligonucleotides: A Comprehensive Guide for Design. *RNA Biol.* **2018**, *15* (3), 338–352.

(75) Glazier, D. A.; Glazier, D. A.; Liao, J.; Roberts, B. L.; Li, X.; Yang, K.; Stevens, C. M.;

Tang, W.; Tang, W. Chemical Synthesis and Biological Application of Modified Oligonucleotides. *Bioconjug. Chem.* **2020**, *31* (5), 1213–1233.

(76) Singh, A.; Trivedi, P.; Jain, N. K. Advances in SiRNA Delivery in Cancer Therapy. *Artif. Cells Nanomed. Biotechnol.* **2018**, *46* (2), 274–283.

(77) Kole, R.; Krainer, A. R.; Altman, S. RNA Therapeutics: Beyond RNA Interference and Antisense Oligonucleotides. *Nat. Rev. Drug Discov.* **2012**, *11* (2), 125–140.

(78) Nidhi, S.; Anand, U.; Oleksak, P.; Tripathi, P.; Lal, J. A.; Thomas, G.; Kuca, K.; Tripathi, V. Novel CRISPR–Cas Systems: An Updated Review of the Current Achievements, Applications, and Future Research Perspectives. *Int. J. Mol. Sci.* **2021**, *22* (7), 3327.

(79) Jore, M. M.; Brouns, S. J. J.; Van der Oost, J. RNA in Defense: CRISPRs Protect Prokaryotes against Mobile Genetic Elements. *Cold Spring Harb. Perspect. Biol.* **2012**, *4*, a003657.

(80) Barrangou, R.; Fremaux, C.; Deveau, H.; Richards, M.; Boyaval, P.; Moineau, S.; Romero, D. .; Horvath, P. CRISPR Provides Acquired Resistance Against Viruses in Prokaryotes. *Science* **2007**, *315* (5819), 1709–1712.

(81) Sapranauskas, R.; Gasiunas, G.; Fremaux, C.; Barrangou, R.; Horvath, P.; Siksnys, V. The Streptococcus Thermophilus CRISPR/Cas System Provides Immunity in Escherichia Coli. *Nucleic Acids Res.* **2011**, *39* (21), 9275–9282.

(82) Bevacqua, R. J.; Dai, X.; Lam, J. Y.; Gu, X.; Friedlander, M. S. H.; Tellez, K.; Miguel-Escalada, I.; Bonas-Guarch, S.; Atla, G.; Zhao, W.; Kim, S. H.; Dominguez, A. A.; Qi, L. S.; Ferrer, J.; MacDonald, P. E.; Kim, S. K. CRISPR-Based Genome Editing in Primary Human Pancreatic Islet Cells. *Nat. Commun.* **2021**, *12*, 2397.

(83) Langner, T.; Kamoun, S.; Belhaj, K. CRISPR Crops: Plant Genome Editing Towards Disease Resistance. *Annu. Rev. Phytopathol.* **2018**, *56*, 479–512.

(84) Deltcheva, E.; Chylinski, K.; Sharma, C. M.; Gonzales, K.; Chao, Y.; Pirzada, Z. A.; Eckert, M. R.; Vogel, V.; Charpentier, E. CRISPR RNA Maturation by Trans-Encoded Small RNA and Host Factor RNase III. *Nature* **2011**, *471*, 602–607.

(85) Jinek, M.; Chylinski, K.; Fonfara, I.; Hauer, M.; Doudna, J. A.; Charpentier, E. A Programmable Dual-RNA-Guided DNA Endonuclease in Adaptive Bacterial Immunity. *Science* **2012**, *337* (6096), 816–821.

(86) Shu, D.; Shu, Y.; Haque, F.; Abdelmawla, S.; Guo, P. Thermodynamically Stable RNA Three-Way Junction for Constructing Multifunctional Nanoparticles for Delivery of Therapeutics. *Nat. Nanotechnol.* **2011**, *6*, 658–667.

(87) Chen, J. H.; Seeman, N. C. The Synthesis from DNA of a Molecule with the Connectivity of a Cube. *Nature* **1991**, *350*, 631–633.

(88) Chen, J. H.; Kallenbach, N. R.; Seeman, N. C. A Specific Quadrilateral Synthesized from DNA Branched Junctions. *J. Am. Chem. Soc.* **1989**, *111*, 6402–6407.

(89) Zhang, Y.; Seeman, N. C. The Construction of a DNA Truncated Octahedron. *J. Am.*

Chem. Soc. **1994**, *116*, 1661–1669.

(90) Rothemund, P. M. K. Folding DNA to Create Nanoscale Shapes and Patterns. *Nature* **2006**, *440*, 297–302.

(91) Li, H.; Zhang, K.; Pi, F.; Guo, S.; Shlyakhtenko, L.; Chiu, W.; Shu, D.; Guo, P. Controllable Self-Assembly of RNA Tetrahedrons with Precise Shape and Size for Cancer Targeting. *Adv. Mater.* **2016**, *28* (34), 7501–7507.

(92) Mela, I.; Vallejo-Ramirez, P. P.; Makarchuk, S.; Christie, G.; Bailey, D.; Henderson, R. M.; Sugiyama, H.; Endo, M.; Kaminski, C. F. DNA Nanostructures for Targeted Antimicrobial Delivery. *Angew. Chemie* **2020**, *132* (31), 12798–12802.

(93) Ijäs, H.; Hakaste, I.; Shen, B.; Kostiainen, M. A.; Linko, V. Reconfigurable DNA Origami Nanocapsule for PH-Controlled Encapsulation and Display of Cargo. *ACS Nano* **2019**, *13* (5), 5959–5967.

(94) Xu, C.; Li, H.; Zhang, K.; Binzel, D. W.; Yin, H.; Chiu, W.; Guo, P.; Chemistry, P.; Heart, D. M. D.; Comprehensive, J.; State, T. O.; Park, M. Photo-Controlled Release of Paclitaxel and Model Drugs from RNA Pyramids. *Nano Res.* **2019**, *12* (1), 41–48.

(95) Tan, X.; Lu, X.; Jia, F.; Liu, X.; Sun, Y.; Logan, J. K.; Zhang, K. Blurring the Role of Oligonucleotides: Spherical Nucleic Acids as a Drug Delivery Vehicle. *J. Am. Chem. Soc.* **2016**, *138* (34), 10834–10837.

(96) Choi, C. H. J.; Hao, L.; Narayan, S. P.; Auyeung, E.; Mirkin, C. A. Mechanism for the Endocytosis of Spherical Nucleic Acid Nanoparticle Conjugates. *Proc. Natl. Acad. Sci. U. S. A.* **2013**, *110* (19), 7625–7630.

(97) Cutler, J. I.; Auyeung, E.; Mirkin, C. A. Spherical Nucleic Acids. *J. Am. Chem. Soc.* **2012**, *134* (3), 1376–1391.

(98) Shi, B.; Zheng, M.; Tao, W.; Chung, R.; Jin, D.; Ghaffari, D.; Farokhzad, O. C. Challenges in DNA Delivery and Recent Advances in Multifunctional Polymeric DNA Delivery Systems. *Biomacromolecules* **2017**, *18* (8), 2231–2246.

(99) Ho, W.; Gao, M.; Li, F.; Li, Z.; Zhang, X.-Q.; Xu, X. Next-Generation Vaccines: Nanoparticle-Mediated DNA and MRNA Delivery. *Adv. Healthc. Mater.* **2021**, *10* (8), 2001812.

(100) Fong, F. Y.; Oh, S. S.; Hawker, C. J.; Soh, H. T. In Vitro Selection of PH-Activated DNA Nanostructures. *Angew. Chemie - Int. Ed.* **2016**, *55* (49), 15258–15262.

(101) Knutson, S. D.; Sanford, A. A.; Swenson, C. S.; Korn, M. M.; Manuel, B. A.; Heemstra, J. M. Thermoreversible Control of Nucleic Acid Structure and Function with Glyoxal Caging. *J. Am. Chem. Soc.* **2020**, *142* (41), 17766–17781.

(102) Huang, F.; Liao, W.-C.; Sohn, Y. S.; Nechushtai, R.; Lu, C.-H.; Willner, I. Light-Responsive and PH-Responsive DNA Microcapsules for Controlled Release of Loads. *J. Am. Chem. Soc.* **2016**, *138* (28), 8936–8945.

(103) Jeong, M.-J.; Shim, C.-K.; Lee, J.-O.; Kwon, H.-B.; Kim, Y.-H.; Lee, S.-K.; Byun, M.-O.;

Park, S.-C. Plant Gene Responses to Frequency-Specific Sound Signals. *Mol. Breed.* **2008**, *21*, 217–226.

(104) Wang, Y.; Li, J.; Wang, H.; Jin, J.; Liu, J.; Wang, K.; Tan, W.; Yang, R. Silver Ions-Mediated Conformational Switch: Facile Design of Structure-Controllable Nucleic Acid Probes. *Anal. Chem.* **2010**, *82* (15), 6607–6612.

(105) Riemann, A.; Schneider, B.; Ihling, A.; Nowak, M.; Sauvant, C.; Thews, O.; Gekle, M. Acidic Environment Leads to ROS-Induced MAPK Signaling in Cancer Cells. *PLoS One* **2011**, *6* (7), e22445.

(106) Vaupel, P.; Kallinowski, F.; Okunieff, P. Blood Flow, Oxygen and Nutrient Supply, and Metabolic Microenvironment of Human Tumors: A Review. *Cancer Res.* **1989**, *49* (23), 6449–6465.

(107) Cheng, E.; Xing, Y.; Chen, P.; Yang; Sun, Y.; Zhou, D.; Xu, T.; Fan, Q.; Liu, D. A PH-Triggered, Fast-Responding DNA Hydrogel. *Angew. Chemie - Int. Ed.* **2009**, *48* (41), 7660–7663.

(108) Chen, W. H.; Yu, X.; Cecconello, A.; Sohn, Y. S.; Nechushtai, R.; Willner, I. Stimuli-Responsive Nucleic Acid-Functionalized Metal-Organic Framework Nanoparticles Using PH- and Metal-Ion-Dependent DNAzymes as Locks. *Chem. Sci.* **2017**, *8* (8), 5769–5780.

(109) Ochoa, S.; Milam, V. T. Modified Nucleic Acids: Expanding the Capabilities of Functional Oligonucleotides. *Molecules* **2020**, *25* (20), 4659.

(110) Prakash, T. P. An Overview of Sugar-Modified Oligonucleotides for Antisense Therapeutics. *Chem. Biodivers.* **2011**, *8* (9), 1616–1641.

(111) Fresco, J. R.; Doty, P. Polynucleotides. I. Molecular Properties and Configurations of Polyriboadenylic Acid in Solution. *J. Am. Chem. Soc.* **1957**, *79* (14), 3928–3929.

(112) Fresco, J. R.; Klemperer, E. Polyriboadenylic Acid, A Molecular Analogue of Ribonucleic Acid and Desoxyribonucleic Acid. *Ann. N. Y. Acad. Sci.* **1959**, *81*, 730–741.

(113) Rich, A.; Davies, D. R.; Crick, F.; Watson, J. D. The Molecular Structure of Polyadenylic Acid. *J. Mol. Biol.* **1961**, *3* (1), 71–86.

(114) Safaee, N.; Noronha, A. M.; Rodionov, D.; Kozlov, G.; Wilds, C. J.; Sheldrick, G. M.; Gehring, K. Structure of the Parallel Duplex of Poly(A) RNA: Evaluation of a 50 Year-Old Prediction. *Angew. Chemie - Int. Ed.* **2013**, *52* (39), 10370–10373.

(115) Copp, W.; Denisov, A. Y.; Xie, J.; Noronha, A. M.; Liczner, C.; Safaee, N.; Wilds, C. J.; Gehring, K. Influence of Nucleotide Modifications at the C2′ Position on the Hoogsteen Base-Paired Parallel-Stranded Duplex of Poly(A) RNA. *Nucleic Acids Res.* **2017**, *45* (17), 10321–10331.

(116) Gleghorn, M. L.; Zhao, J.; Turner, D. H.; Maquat, L. E. Crystal Structure of a Poly(RA) Staggered Zipper at Acidic PH: Evidence That Adenine N1 Protonation Mediates Parallel Double Helix Formation. *Nucleic Acids Res.* **2016**, *44* (17), 8417–8424.

(117) Zarudnaya, M. I.; Hovorun, D. M. Hypothetical Double-Helical Poly (A) Formation in a

Cell and Its Possible Biological Significance. *IUBMB Life* **1999**, *48*, 581–584.

(118) Pickard, M. A. G.; Brylow, K. B.; Cisco, L. A.; Anecelle, M. R.; Pershun, M. L.; Chandrasekaran, A. R.; Halvorsen, K.; Gleghorn, M. L. Parallel Poly(A) Homo- And Hetero-Duplex Formation Detection with an Adapted DNA Nanoswitch Technique. *RNA* **2020**, *26* (9), 1118–1130.

(119) Chakraborty, S.; Sharma, S.; Maiti, P. K.; Krishnan, Y. The Poly DA Helix: A New Structural Motif for High Performance DNA-Based Molecular Switches. *Nucleic Acids Res.* **2009**, *37* (9), 2810–2817.

(120) Huang, Z.; Liu, B.; Liu, J. Parallel Polyadenine Duplex Formation at Low PH Facilitates DNA Conjugation onto Gold Nanoparticles. *Langmuir* **2016**, *32* (45), 11986–11992.

(121) Kolb, H. C.; Finn, M. G.; Sharpless, K. B. Click Chemistry: Diverse Chemical Function from a Few Good Reactions. *Angew. Chemie - Int. Ed.* **2001**, *40* (11), 2004–2021.

(122) Rostovtsev, V. V.; Green, L. G.; Fokin, V. V.; Sharpless, B. K. A Stepwise Huisgen Cycloaddition Process: Copper(I)-Catalyzed Regioselective "Ligation" of Azides and Terminal Alkynes. *Angew. Chemie - Int. Ed.* **2002**, *41* (14), 2596–2599.

(123) Tornøe, C. W.; Christensen, C.; Meldal, M. Peptidotriazoles on Solid Phase: [1,2,3]-Triazoles by Regiospecific Copper(I)-Catalyzed 1,3-Dipolar Cycloadditions of Terminal Alkynes to Azides. *J. Org. Chem.* **2002**, *67* (9), 3057–3064.

(124) Agard, N. J.; Baskin, J. M.; Prescher, J. A.; Lo, A.; Bertozzi, C. R. A Comparative Study of Bioorthogonal Reactions with Azides. *ACS Chem. Biol.* **2006**, *1* (10), 644–648.

(125) Johansson, J. R.; Beke-Somfai, T.; Said Stålsmeden, A.; Kann, N. Ruthenium-Catalyzed Azide Alkyne Cycloaddition Reaction: Scope, Mechanism, and Applications. *Chem. Rev.* **2016**, *116* (23), 14726–14768.

(126) El-Sagheer, A. H.; Brown, T. A Triazole Linkage That Mimics the DNA Phosphodiester Group in Living Systems. *Q. Rev. Biophys.* **2015**, *48* (4), 429–436.

(127) Baker, Y. R.; Traoré, D.; Wanat, P.; Tyburn, A.; El-Sagheer, A. H.; Brown, T. Searching for the Ideal Triazole: Investigating the 1,5-Triazole as a Charge Neutral DNA Backbone Mimic. *Tetrahedron* **2020**, *76* (7), 130914.

(128) George, J. T.; Srivatsan, S. G. Posttranscriptional Chemical Labeling of RNA by Using Bioorthogonal Chemistry. *Methods* **2017**, *120*, 28–38.

(129) Ren, X.; El-Sagheer, A. H.; Brown, T. Efficient Enzymatic Synthesis and Dual-Colour Fluorescent Labelling of DNA Probes Using Long Chain Azido-DUTP and BCN Dyes. *Nucleic Acids Res.* **2016**, *44* (8), e79.

(130) Pujari, S. S.; Seela, F. Cross-Linked DNA: Propargylated Ribonucleosides as "Click" Ligation Sites for Bifunctional Azides. *J. Org. Chem.* **2012**, *77* (9), 4460–4465.

(131) Pujari, S. S.; Seela, F. Parallel Stranded DNA Stabilized with Internal Sugar Cross-Links: Synthesis and Click Ligation of Oligonucleotides Containing 2′-Propargylated Isoguanosine. *J. Org. Chem.* **2013**, *78* (17), 8545–8561.

(132) El-Sagheer, A. H.; Brown, T. Click Nucleic Acid Ligation: Applications in Biology and Nanotechnology. *Acc. Chem. Res.* **2012**, *45* (8), 1258–1267.

(133) Paredes, E.; Das, S. R. Click Chemistry for Rapid Labeling and Ligation of RNA. *ChemBioChem* **2011**, *12* (1), 125–131.

(134) Mack, S.; Fouz, M. F.; Dey, S. K.; Das, S. R. Pseudo-Ligandless Click Chemistry for Oligonucleotide Conjugation. *Curr. Protoc. Chem. Biol.* **2016**, *8* (2), 83–95.

(135) Liu, L.; Fang, Z.; Zheng, X.; Xi, D. Nanopore-Based Strategy for Sensing of Copper(II) Ion and Real-Time Monitoring of a Click Reaction. *ACS Sensors* **2019**, *4* (5), 1323–1328.

(136) Winz, M. L.; Samanta, A.; Benzinger, D.; Jäschke, A. Site-Specific Terminal and Internal Labeling of RNA by Poly(A) Polymerase Tailing and Copper-Catalyzed or Copper-Free Strain-Promoted Click Chemistry. *Nucleic Acids Res.* **2012**, *40* (10), e78.

(137) Balintová, J.; Špaček, J.; Pohl, R.; Brázdová, M.; Havran, L.; Fojta, M.; Hocek, M. Azidophenyl as a Click-Transformable Redox Label of DNA Suitable for Electrochemical Detection of DNA-Protein Interactions. *Chem. Sci.* **2015**, *6* (1), 575–587.

(138) Chen, J.; Baker, Y. R.; Brown, A.; El-Sagheer, A. H.; Brown, T. Enzyme-Free Synthesis of Cyclic Single-Stranded DNA Constructs Containing a Single Triazole, Amide or Phosphoramidate Backbone Linkage and Their Use as Templates for Rolling Circle Amplification and Nanoflower Formation. *Chem. Sci.* **2018**, *9* (42), 8110–8120.

(139) Pujari, S. S.; Leonard, P.; Seela, F. Oligonucleotides with "Clickable" Sugar Residues: Synthesis, Duplex Stability, and Terminal versus Central Interstrand Cross-Linking of 2′-O-Propargylated 2-Aminoadenosine with a Bifunctional Azide. *J. Org. Chem.* **2014**, *79* (10), 4423–4437.

(140) Ibarra-Soza, J. M.; Morris, A. A.; Jayalath, P.; Peacock, H.; Conrad, W. E.; Donald, M. B.; Kurth, M. J.; Beal, P. A. 7-Substituted 8-Aza-7-Deazaadenosines for Modification of the SiRNA Major Groove. *Org. Biomol. Chem.* **2012**, *10*, 6491–6497.

(141) Phelps, K. J.; Ibarra-Soza, J. M.; Tran, K.; Fisher, A. J.; Beal, P. A. Click Modification of RNA at Adenosine: Structure and Reactivity of 7-Ethynyl- and 7-Triazolyl-8-Aza-7-Deazaadenosine in RNA. *ACS Chem. Biol.* **2014**, *9* (8), 1780–1787.

(142) Kopcial, M.; Wojtczak, B. A.; Kasprzyk, R.; Kowalska, J.; Jemielity, J. N1-Propargylguanosine Modified MRNA Cap Analogs: Synthesis, Reactivity, and Applications to the Study of Cap-Binding Proteins. *Molecules* **2019**, *24* (10), 1899.

(143) Domingo, O.; Hellmuth, I.; Jäschke, A.; Kreutz, C.; Helm, M. Intermolecular "Cross-Torque": The N4-Cytosine Propargyl Residue Is Rotated to the 'CH'-Edge as a Result of Watson-Crick Interaction. *Nucleic Acids Res.* **2015**, *43* (11), 5275–5283.

(144) Grøtli, M.; Douglas, M.; Eritja, R.; Sproat, B. S. 2'-O-Propargyl Oligoribonucleotides: Synthesis and Hybridisation. *Tetrahedron* **1998**, *54* (22), 5899–5914.

(145) Egli, M.; Minasov, G.; Tereshko, V.; Pallan, P. S.; Teplova, M.; Inamati, G. B.; Lesnik, E. A.; Owens, S. R.; Ross, B. S.; Prakash, T. P.; Manoharan, M. Probing the Influence of Stereoelectronic Effects on the Biophysical Properties of Oligonucleotides:

Comprehensive Analysis of the RNA Affinity, Nuclease Resistance, and Crystal Structure of Ten 2′-O-Ribonucleic Acid Modifications. *Biochemistry* **2005**, *44* (25), 9045–9057.

(146) Jana, S. K.; Leonard, P.; Ingale, S. A.; Seela, F. 2′-: O -Methyl- and 2′- O -Propargyl-5-Methylisocytidine: Synthesis, Properties and Impact on the IsoCd-DG and the IsoCd-IsoGd Base Pairing in Nucleic Acids with Parallel and Antiparallel Strand Orientation. *Org. Biomol. Chem.* **2016**, *14* (21), 4927–4942.

(147) Puglisi, J. D.; Tinoco, I. Absorbance Melting Curves of RNA. *Methods Enzymol.* **1989**, *180*, 304–325.

(148) Mergny, J. L.; Lacroix, L. Analysis of Thermal Melting Curves. *Oligonucleotides* **2003**, *13* (6), 515–537.

(149) Harp, J. M.; Coates, L.; Sullivan, B.; Egli, M. Water Structure around a Left-Handed Z-DNA Fragment Analyzed by Cryo Neutron Crystallography. *Nucleic Acids Res.* **2021**, gkab264.

(150) Woody, R. W. Circular Dichroism. *Methods Enzymol.* **1995**, *246*, 34–71.

(151) Noe, C. R.; Winkler, J.; Urban, E.; Gilbert, M.; Haberhauer, G.; Brunar, H. Zwitterionic Oligonucleotides: A Study on Binding Properties of 2′-O-Aminohexyl Modifications. *Nucleosides, Nucleotides and Nucleic Acids* **2005**, *24* (8), 1167–1185.

(152) Hashimoto, H.; Nelson, M. G.; Switzer, C. Formation of Chimeric Duplexes between Zwitterionic and Natural DNA. *J. Org. Chem.* **1993**, *58* (16), 4194–4195.

(153) Hashimoto, H.; Nelson, M. G.; Switzer, C. Zwitterionic DNA. *J. Am. Chem. Soc.* **1993**, *115* (16), 7128–7134.

(154) Noe, C. R.; Brunar, H. Preparation of Modified Oligonucleotides as Active Substances, 1995.

(155) Brunar, H.; Haberhauer, G.; Werner, D.; Noe, C. R. 2'-O-Modified Oligonucleotides: Synthesis and Biophysical Analysis. *Eur. J. Pharm. Sci.* **1994**, *2* (1–2), 150.

(156) Biscans, A.; Rouanet, S.; Bertrand, J. R.; Vasseur, J. J.; Dupouy, C.; Debart, F. Synthesis, Binding, Nuclease Resistance and Cellular Uptake Properties of 2′-O-Acetalester-Modified Oligonucleotides Containing Cationic Groups. *Bioorganic Med. Chem.* **2015**, *23* (17), 5360–5368.

(157) Griffey, R. H.; Monia, B. P.; Cummins, L. L.; Freier, S.; Greig, M. J.; Guinosso, C. J.; Lesnik, E.; Manalili, S. M.; Mohan, V.; Owens, S.; Ross, B. R.; Sasmor, H.; Wancewicz, E.; Weiler, K.; Wheeler, P. D.; Cook, P. D. 2′-O-Aminopropyl Ribonucleotides: A Zwitterionic Modification That Enhances the Exonuclease Resistance and Biological Activity of Antisense Oligonucleotides. *J. Med. Chem.* **1996**, *39* (26), 5100–5109.

(158) Milton, S.; Honcharenko, D.; Rocha, C. S. J.; Moreno, P. M. D.; Edvard Smith, C. I.; Strömberg, R. Nuclease Resistant Oligonucleotides with Cell Penetrating Properties. *Chem. Commun.* **2015**, *51* (19), 4044–4047.

(159) Seio, K.; Tokugawa, M.; Kanamori, T.; Tsunoda, H.; Ohkubo, A.; Sekine, M. Synthesis

and Properties of Cationic 2′-O-[N-(4-Aminobutyl)Carbamoyl] Modified Oligonucleotides. *Bioorganic Med. Chem. Lett.* **2012**, *22* (7), 2470–2473.

(160) Teplova, M.; Wallace, S. T.; Tereshko, V.; Minasov, G.; Symons, A. M.; Cook, P. D.; Manoharan, M.; Egli, M. Structural Origins of the Exonuclease Resistance of a Zwitterionic RNA. *Proc. Natl. Acad. Sci. U. S. A.* **1999**, *96* (25), 14240–14245.

(161) Nawale, G. N.; Bahadorikhalili, S.; Sengupta, P.; Kadekar, S.; Chatterjee, S.; Varghese, O. P. 4′-Guanidinium-Modified SiRNA: A Molecular Tool to Control RNAi Activity through RISC Priming and Selective Antisense Strand Loading. *Chem. Commun.* **2019**, *55* (62), 9112–9115.

(162) Cullis, P. R.; Hope, M. J. Lipid Nanoparticle Systems for Enabling Gene Therapies. *Mol. Ther.* **2017**, *25* (7), 1467–1475.

(163) Piotrowski-Daspit, A. S.; Kauffman, A. C.; Bracaglia, L. G.; Saltzman, M. W. Polymeric Vehicles for Nucleic Acid Delivery. *Adv. Drug Deliv. Rev.* **2020**, *156*, 119–132.

(164) Hall, H. K. Correlation of the Base Strengths of Amines. *J. Am. Chem. Soc.* **1957**, *79*, 5441–5444.

(165) Woodson, S. A.; Koculi, E. Analysis of RNA Folding by Native Polyacrylamide Gel Electrophoresis. *Methods Enzymol.* **2009**, *469*, 189–208.

(166) Steely Jr., T. H.; Gray, D. M.; Ratliff, R. L. CD of Homopolymer DNA/RNA Hybrid Duplexes and Triplexes Containing A/T and A/U Base Pairs. *Nucleic Acids Res.* **1986**, *14*, 10071–10090.

(167) Prakash, T. P.; Püschl, A.; Lesnik, E.; Mohan, V.; Tereshko, V.; Egli, M.; Manoharan, M. 2′-O-[2-(Guanidinium)Ethyl]-Modified Oligonucleotides: Stabilizing Effect on Duplex and Triplex Structures. *Org. Lett.* **2004**, *6* (12), 1971–1974.

(168) Dirks, R. W.; Tanke, Hans, J. Advances in Fluorescent Tracking of Nucleic Acids in Living Cell. *Biotechniques* **2018**, *40* (4), 489–495.

(169) Jett, J. H.; A., K. R.; Martin, J. C.; Marrone, B. L.; Moyzis, R. K.; Ratliff, R. L.; Seitzinger, N. K.; Shera, E. B.; Stewart, C. C. High-Speed DNA Sequencing: An Approach Based upon Fluorescence Detection of Single Molecules. *J. Biomol. Struct. Dyn.* **1989**, *7* (2), 301–309.

(170) Rieder, M. J.; Taylor, S. L.; Tobe, V. O.; Nickerson, D. A. Automating the Identification of DNA Variations Using Quality-Based Fluorescence Re-Sequencing: Analysis of the Human Mitochondrial Genome. *Nucleic Acids Res.* **1998**, *26* (4), 967–973.

(171) Tang, X.; Wang, Y.; Li, H. O.; Sakatsume, O.; Sarai, A.; Yokoyama, K. DNA Fingerprinting Involving Fluorescence-Labeled Termini of Any Enzymatically Generated Fragments of DNA. *Jpn. J. Hum. Genet.* **1994**, *39* (4), 379–391.

(172) Prasad, A.; Mohammad Abid Hasan, S.; Grouchy, S.; Gartia, M. R. DNA Microarray Analysis Using a Smartphone to Detect the BRCA-1 Gene. *Analyst* **2018**, *144* (1), 197–205.

(173) Østergaard, M. E.; Hrdlicka, P. J. Pyrene-Functionalized Oligonucleotides and Locked Nucleic Acids (LNAs): Tools for Fundamental Research, Diagnostics, and Nanotechnology. *Chem. Soc. Rev.* **2011**, *40* (12), 5771–5788.

(174) Yamana, K.; Iwase, R.; Furutani, S.; Tsuchida, H.; Zako, H.; Yamaoka, T.; Murakami, A. 2'-Pyrene Modified Oligonucleotide Provides a Highly Sensitive Fluorescent Probe of RNA. *Nucleic Acids Res.* **1999**, *27* (11), 2387–2392.

(175) Christensen, U. B.; Pedersen, E. B. Intercalating Nucleic Acids Containing Insertions of 1-O-(1-Pyrenylmethyl)Glycerol: Stabilisation of DsDNA and Discrimination of DNA over RNA. *Nucleic Acids Res.* **2002**, *30* (22), 4918–4925.

(176) Korshun, V. A.; Stetsenko, D. A.; Gait, M. J. Novel Uridin-2′-Yl Carbamates: Synthesis, Incorporation into Oligodeoxyribonucleotides, and Remarkable Fluorescence Properties of 2′-Pyren-1-Ylmethylcarbamate. *J. Chem. Soc. Perkin 1* **2002**, *2* (8), 1092–1104.

(177) Nakamura, M.; Fukunaga, Y.; Sasa, K.; Ohtoshi, Y.; Kanaori, K.; Hayashi, H.; Nakano, H.; Yamana, K. Pyrene Is Highly Emissive When Attached to the RNA Duplex but Not to the DNA Duplex: The Structural Basis of This Difference. *Nucleic Acids Res.* **2005**, *33* (18), 5887–5895.

(178) Kalyanasundaram, K.; Thomas, J. K. Environmental Effects on Vibronic Band Intensities in Pyrene Monomer Fluorescence and Their Application in Studies of Micellar Systems. *J. Am. Chem. Soc.* **1977**, *99*, 2039–2044.

(179) Dougherty, G.; Pilbrow, J. R. Physico-Chemical Probes of Intercalation. *Int. J. Biochem.* **1984**, *16* (12), 1179–1192.

(180) Hrdlicka, P. J.; Karmakar, S. 25 Years and Still Going Strong: 2′-O-(Pyren-1-Yl)Methylribonucleotides-Versatile Building Blocks for Applications in Molecular Biology, Diagnostics and Materials Science. *Org. Biomol. Chem.* **2017**, *15* (46), 9760–9774.

(181) Förster, U.; Lommel, K.; Sauter, D.; Grünewald, C.; Engels, J. W.; Wachtveitl, J. 2-(1-Ethynylpyrene)-Adenosine as a Folding Probe for RNA - Pyrene in or Out. *ChemBioChem* **2010**, *11* (5), 664–672.

(182) Kumar, P.; Shaikh, K. I.; Jørgensen, A. S.; Kumar, S.; Nielsen, P. Three Pyrene-Modified Nucleotides: Synthesis and Effects in Secondary Nucleic Acid Structures. *J. Org. Chem.* **2012**, *77* (21), 9562–9573.

(183) Ueda, T.; Kobori, A.; Yamayoshi, A.; Yoshia, H.; Yamaguchi, M.; Murakami, A. RNA-Based Diagnosis in a Multicellular Specimen by Whole Mount in Situ Hybridization Using an RNA-Specific Probe. *Bioorganic Med. Chem.* **2012**, *20* (20), 6034–6039.

(184) Liao, X.; Pan, J.; Zhang, X.; Tang, Q. Sensitive Detection of Argonaute 2 by Triple-Helix Molecular Switch Reaction and Pyrene Excimer Switching. *Aust. J. Chem.* **2020**, *73* (11), 1074–1079.

(185) Kovacic, M.; Podbevsek, P.; Tateishi-Karimata, H.; Takahashi, S.; Sugimoto, N.; Plavec, J. Thrombin Binding Aptamer G-Quadruplex Stabilized by Pyrene-Modified Nucleotides. *Nucleic Acids Res.* **2020**, *48* (7), 3975–3986.

(186) Semikolenova, O. A.; Golyshev, V. M.; Kim, B. H.; Venyaminova, A. G.; Novopashina, D. S. New Two-Component Pyrene Probes Based on Oligo(2'-O-Methylribonucleotides) for MicroRNA Detection. *Russ. J. Bioorganic Chem.* **2021**, *47*, 432–440.

(187) Masuko, M.; Ohtani, H.; Ebata, K.; Shimadzu, A. Optimization of Excimer-Forming Two-Probe Nucleic Acid Hybridization Method with Pyrene as a Fluorophore. *Nucleic Acids Res.* **1998**, *26* (23), 5409–5416.

(188) Copp, W. Influence of Modifications of the Ribose Sugar on the Parallel Stranded Adenosine Duplex. MSc Thesis, Concordia University, QC. 2016.

(189) Cho, N.; Asher, S. A. UV Resonance Raman Studies of DNA-Pyrene Interactions: Optical Decoupling Raman Spectroscopy Selectively Examines External Site Bound Pyrene. *J. Am. Chem. Soc.* **1993**, *115* (14), 6349–6356.

(190) Young, J. S.; Rhee, H.; Joo, T.; Byeang, H. K. Self-Duplex Formation of an A(Py)-Substituted Oligodeoxyadenylate and Its Unique Fluorescence. *J. Am. Chem. Soc.* **2007**, *129* (16), 5244–5247.

(191) Bains, G.; Patel, A. B.; Narayanaswami, V. Pyrene: A Probe to Study Protein Conformation and Conformational Changes. *Molecules* **2011**, *16* (9), 7909–7935.

(192) Yao, C.; Kraatz, H.-B.; Steer, R. P. Photophysics of Pyrene-Labelled Compounds of Biophysical Interest. *Photochem. Photobiol. Sci.* **2005**, *4*, 191–199.

(193) Nakajima, A. Solvent Effect on the Vibrational Structures of the Fluorescence and Absorption Spectra of Pyrene. *Bull. Chem. Soc. Jpn.* **1971**, *44*, 3272–3277.

(194) Winnik, F. M. Photophysics of Preassociated Pyrenes in Aqueous Polymer Solutions and in Other Organized Media. *Chem. Rev.* **1993**, *93* (2), 587–614.

(195) Dioubankova, N. N.; Malakhov, A. D.; Stetsenko, D. A.; Gait, M. J.; Volynsky, P. E.; Efremov, R. G.; Korshun, V. A. Pyrenemethyl Ara-Uridine-2′-Carbamate: A Strong Interstrand Excimer in the Major Groove of a DNA Duplex. *ChemBioChem* **2003**, *4* (9), 841–847.

(196) Croonen, Y.; Geladé, E.; Van Der Zegel, M.; Van Der Auweraer, M.; Vandendriessche, H.; De Schryver, F. C.; Almgren, M. Influence of Salt, Detergent Concentration, and Temperature on the Fluorescence Quenching of 1-Methylpyrene in Sodium Dodecyl Sulfate with m-Dicyanobenzene. *J. Phys. Chem.* **1983**, *87* (8), 1426–1431.

(197) Neidle, S. *Nucleic Acid Structure and Recognition*; Oxford University Press: Oxford, 2002.

(198) Rao, S. N.; Kollman, P. A. Molecular Mechanical Simulations on Double Intercalation of 9-Amino Acridine into d(CGCGCGC) X d(GCGCGCG): Analysis of the Physical Basis for the Neighbor-Exclusion Principle. *Proc. Natl. Acad. Sci. U. S. A.* **1987**, *84* (16), 5735–5739.

(199) Gray, D. M.; Ratliff, R. L. Circular Dichroism Spectra of Poly[d(AC):D(GT)], Poly[r(AC):R(GU)], and Hybrids Poly[d(AC):R(GU)] and Poly[r(AC):D(GT)] in the Presence of Ethanol. *Biopolymers* **1975**, *14* (3), 487–498.

(200) Struther Arnott, R.; Chandrasekaran, R. P.; Millane, H.-S. P. DNA-RNA Hybrid Secondary Structures. *J. Mol. Biol.* **1986**, *188* (4), 631–640.

(201) Zimmerman, S. B.; Pheiffer, B. H. A RNA.DNA Hybrid That Can Adopt Two Conformations: An x-Ray Diffraction Study of Poly(RA).Poly(DT) in Concentrated Solution or in Fibers. *Proc. Natl. Acad. Sci. U. S. A.* **1981**, *78* (1), 78–82.

(202) Kypr, J.; Kejnovska, I.; Renciuk, D.; Vorlickova, M. Circular Dichroism and Conformational Polymorphism of DNA. *Nucleic Acids Res.* **2009**, *37* (6), 1713–1725.

(203) Obika, S.; Sekine, M. *Synthesis of Therapeutic Oligonucleotides*; Springer Nature Singapore: Singapore, 2018.

(204) Liczner, C.; Duke, K.; Juneau, G.; Egli, M.; Wilds, C. J. Beyond Ribose and Phosphate: Selected Nucleic Acid Modifications for Structure-Function Investigations and Therapeutic Applications. *Beilstein J. Org. Chem.* **2021**, *17*, 908–931.

(205) Eckstein, F. Nucleoside Phosphorothioates. *J. Am. Chem. Soc.* **1966**, *88* (18), 4292–4294.

(206) Clavé, G.; Reverte, M.; Vasseur, J.-J.; Smietana, M. Modified Internucleoside Linkages for Nuclease-Resistant Oligonucleotides. *RSC Chem. Biol.* **2021**, No. 1.

(207) Pallan, P. S.; Lybrand, T. P.; Schlegel, M. K.; Harp, J. M.; Jahns, H.; Manoharan, M.; Egli, M. Incorporating a Thiophosphate Modification into a Common RNA Tetraloop Motif Causes an Unanticipated Stability Boost. *Biochemistry* **2020**, *59* (49), 4627–4637.

(208) Mori, K.; Boiziau, C.; Cazenave, C.; Matsukura, M.; Subasinghe, C.; Cohen, J. S.; Broder, S.; Toulme, J. J.; Stein, C. A. Phosphoroselenoate Oligodeoxynucleotides: Synthesis, Physico-Chemical Characterization, Anti-Sense Inhibitory Properties and Anti-HIV Activity. *Nucleic Acids Res.* **1989**, *17* (20), 8207–8219.

(209) Wilds, C. J.; Pattanayek, R.; Pan, C.; Wawrzak, Z.; Egli, M. Selenium-Assisted Nucleic Acid Crystallography: Use of Phosphoroselenoates for MAD Phasing of a DNA Structure. *J. Am. Chem. Soc.* **2002**, *124* (50), 14910–14916.

(210) Hara, R. I.; Saito, T.; Kogure, T.; Hamamura, Y.; Uchiyama, N.; Nukaga, Y.; Iwamoto, N.; Wada, T. Stereocontrolled Synthesis of Boranophosphate DNA by an Oxazaphospholidine Approach and Evaluation of Its Properties. *J. Org. Chem.* **2019**, *84* (12), 7971–7983.

(211) Eckstein, F. A Dinucleoside Phosphorothioate. *Tetrahedron Lett.* **1967**, *8* (13), 1157–1160.

(212) Tang, J. Y.; Temsamani, J.; Agrawal, S. Self-Stabilized Antisense Oligonucleotide Phosphorothioates: Properties and Anti-HIV Activity. *Nucleic Acids Res.* **1993**, *21* (11), 2729–2735.

(213) Koziolkiewicz, M.; Krakowiak, A.; Kwinkowski, M.; Boczkowska, M.; Stec, W. J. Stereodifferentiation--the Effect of P Chirality of Oligo(Nucleoside Phosphorothioates) on the Activity of Bacterial RNase H. *Nucleic Acids Res.* **1995**, *23* (24), 5000–5005.

(214) Koziolkiewicz, M.; Wojcik, M.; Kobylanska, A.; Karwowski, B.; Rebowska, B.; Guga, P.;

Stec, W. J. Stability of Stereoregular Oligo(Nucleoside Phosphorothioate)s in Human Plasma: Diastereoselectivity of Plasma 3'-Exonuclease. *Antisense Nucleic Acid Drug Dev.* **2009**, *7* (1), 43–48.

(215) Roberts, T. C.; Langer, R.; Wood, M. J. A. Advances in Oligonucleotide Drug Delivery. *Nat. Rev. Drug Discov.* **2020**, *19* (10), 673–694.

(216) Crooke, S. T.; Witztum, J. L.; Bennett, C. F.; Baker, B. F. RNA-Targeted Therapeutics. *Cell Metab.* **2018**, *27* (4), 714–739.

(217) Shen, X.; Corey, D. R. Chemistry, Mechanism and Clinical Status of Antisense Oligonucleotides and Duplex RNAs. *Nucleic Acids Res.* **2018**, *46* (4), 1584–1600.

(218) Ali, M. M.; Li, F.; Zhang, Z.; Zhang, K.; Kang, D.-K.; Ankrum, J. A.; Le, C. X.; Zhao, W. Rolling Circle Amplification: A Versatile Tool for Chemical Biology, Materials Science and Medicine. *Chem. Soc. Rev.* **2014**, *43*, 3324–3341.

(219) An, R.; Li, Q.; Fan, Y.; Li, J.; Pan, X.; Komiyama, M.; Liang, X. Highly Efficient Preparation of Single-Stranded DNA Rings by T4 Ligase at Abnormally Low Mg(II) Concentration. *Nucleic Acids Res.* **2017**, *45*, e139.

(220) Cui, Y.; Han, X.; An, R.; Zhou, G.; Komiyama, M.; Liang, X. Cyclization of Secondarily Structured Oligonucleotides to Single-Stranded Rings by Using Taq DNA Ligase at High Temperatures. *RSC Adv.* **2018**, *8* (34), 18972–18979.

(221) Kalinowski, M.; Haug, R.; Said, H.; Piasecka, S.; Kramer, M.; Richert, C. Phosphoramidate Ligation of Oligonucleotides in Nanoscale Structures. *ChemBioChem* **2016**, *17* (12), 1150–1155.

(222) El-Sagheer, A. H.; Brown, T. Single Tube Gene Synthesis by Phosphoramidate Chemical Ligation. *Chem. Commun.* **2017**, *53* (77), 10700–10702.

(223) Gryaznov, S. M.; Letsinger, R. L. Synthesis and Properties of Oligonucleotides Containing Aminodeoxythymidine Units. *Nucleic Acids Res.* **1992**, *20* (13), 3403–3409.

(224) De Mesmaeker, A.; Waldner, A.; Lebreton, J.; Hoffmann, P.; Fritsch, V.; Wolf, R. M.; Freier, S. M. Amides as a New Type of Backbone Modification in Oligonucleotides. *Angew Chem Int Ed Engl.* **1994**, *33* (2), 226–229.

(225) Kuwahara, M.; Takeshima, H.; Nagashima, J.; Minezaki, S.; Ozaki, H.; Sawai, H. Transcription and Reverse Transcription of Artificial Nucleic Acids Involving Backbone Modification by Template-Directed DNA Polymerase Reactions. *Bioorganic Med. Chem.* **2009**, *17* (11), 3782–3788.

(226) Obika, S.; Nanbu, D.; Hari, Y.; Morio, K. I.; In, Y.; Ishida, T.; Imanishi, T. Synthesis of 2'-O,4'-C-Methyleneuridine and -Cytidine. Novel Bicyclic Nucleosides Having a Fixed C3-Endo Sugar Puckering. *Tetrahedron Lett.* **1997**, *38* (50), 8735–8738.

(227) Singh, S. K.; Nielsen, P.; Koshkin, A. A.; Wengel, J. LNA (Locked Nucleic Acids): Synthesis and High-Affinity Nucleic Acid Recognition. *Chem. Commun.* **1998**, No. 4, 455–456.

(228) Koshkin, A.; Singh, S. K.; Nielsen, P.; Meldgaard, M.; Rajwanshi, V. K.; Kumar, R.; Skouv, J.; Nielsen, C. B.; Jacobsen, J. P.; Jacobsen, N.; Olsen, C. E.; Wengel, J. LNA (Locked Nucleic Acids): Synthesis of the Adenine, Cytosine, Guanine, 5-Methylcytosine, Thymine, and Uracil Bicyclonucleoside Monomers, Oligomerisation, and Unprecedented Nucleic Acid Recognition. *Tetrahedron* **1998**, *54*, 3607–3630.

(229) Bondensgaard, K.; Petersen, M.; Singh, S. K.; Rajwanshi, V. K.; Kumar, R.; Wengel, J.; Jacobsen, J. P. Structural Studies of LNA:RNA Duplexes by NMR: Conformations and Implications for RNase H Activity. *Chem. - A Eur. J.* **2000**, *6* (15), 2687–2695.

(230) Petersen, M.; Bondensgaard, K.; Wengel, J.; Jacobsen, J. P. Locked Nucleic Acid (LNA) Recognition of RNA: NMR Solution Structures of LNA:RNA Hybrids. *J. Am. Chem. Soc.* **2002**, *124* (21), 5974–5982.

(231) Platts, J. A.; Howard, S. T.; Bracke, B. R. F. Directionality of Hydrogen Bonds to Sulfur and Oxygen. *J. Am. Chem. Soc.* **1996**, *118* (11), 2726–2733.

(232) Oka, N.; Kondo, T.; Fujiwara, S.; Maizuru, Y.; Wada, T. Stereocontrolled Synthesis of Oligoribonucleoside Phosphorothioates by an Oxazaphospholidine Approach. *Org. Lett.* **2009**, *11* (4), 967–970.

(233) Østergaard, M. E.; De Hoyos, C. L.; Wan, W. B.; Shen, W.; Low, A.; Berdeja, A.; Vasquez, G.; Murray, S.; Migawa, M. T.; Liang, X. H.; Swayze, E. E.; Crooke, S. T.; Seth, P. P. Understanding the Effect of Controlling Phosphorothioate Chirality in the DNA Gap on the Potency and Safety of Gapmer Antisense Oligonucleotides. *Nucleic Acids Res.* **2020**, *48* (4), 1691–1700.

(234) Astakhova, I. K.; Wengel, J. Scaffolding along Nucleic Acid Duplexes Using 2'-Amino-Locked Nucleic Acids. *Acc. Chem. Res.* **2014**, *47* (6), 1768–1777.

(235) Egli, M.; Pallan, P. S. Insights from Crystallographic Studies into the Structural and Pairing Properties of Nucleic Acid Analogs and Chemically Modified DNA and RNA Oligonucleotides. *Annu. Rev. Biophys. Biomol. Struct.* **2007**, *36*, 281–305.

(236) Conlon, P. F.; Eguaogie, O.; Wilson, J. J.; Sweet, J. S. T.; Steinhoegl, J.; Englert, K.; Hancox, O. G. A.; Law, C. J.; Allman, S. A.; Tucker, J. H. R.; Hall, J. P.; Vyle, J. S. Solid-Phase Synthesis and Structural Characterisation of Phosphoroselenolate-Modified DNA: A Backbone Analogue Which Does Not Impose Conformational Bias and Facilitates SAD X-Ray Crystallography. *Chem. Sci.* **2019**, *10* (47), 10948–10957.

(237) Sood, A.; Shaw, B. R.; Spielvogel, B. F. Boron-Containing Nucleic Acids: Synthesis of Oligodeoxynucleoside Boranophosphates. *J. Am. Chem. Soc.* **1990**, *112*, 9000–9001.

(238) Hall, A. H. S.; Wan, J.; Shaughnessy, E. E.; Shaw, B. R.; Alexander, K. A. RNA Interference Using Boranophosphate SiRNAs: Structure-Activity Relationships. *Nucleic Acids Res.* **2004**, *32* (20), 5991–6000.

(239) Bartosik, K.; Debiec, K.; Czarnecka, A.; Sochacka, E.; Leszczynska, G. Synthesis of Nucleobase-Modified RNA Oligonucleotides by Post-Synthetic Approach. *Molecules* **2020**, *25* (15).

(240) Eckhardt, M.; Fu, G. C. The First Applications of Carbene Ligands in Cross-Couplings of

Alkyl Electrophiles: Sonogashira Reactions of Unactivated Alkyl Bromides and Iodides. *J. Am. Chem. Soc.* **2003**, *125* (45), 13642–13643.

(241) Kwon, T.; Piton, N.; Grünewald, C.; Engels, J. W. Synthesis of Pyrene Labeled RNA for Fluorescence Measurements. *Nucleosides, Nucleotides and Nucleic Acids* **2007**, *26* (10–12), 1381–1386.

(242) Grünewald, C.; Kwon, T.; Piton, N.; Förster, U.; Wachtveitl, J.; Engels, J. W. RNA as Scaffold for Pyrene Excited Complexes. *Bioorganic Med. Chem.* **2008**, *16* (1), 19–26.

(243) Kauffman, G. B.; Teter, L. A.; Rhoda, R. N. Recovery of Platinum from Laboratory Residues. In *Inorganic Syntheses*; Kleinberg, J., Ed.; McGraw-Hill, 1963; Vol. 7, pp 232–236.

(244) Tataurov, A. V.; You, Y.; Owczarzy, R. Predicting Ultraviolet Spectrum of Single Stranded and Double Stranded Deoxyribonucleic Acids. *Biophys. Chem.* **2008**, *133* (1–3), 66–70.

(245) Ma, Q.; Yang, H.; Hao, J.; Tan, Y. Synthesis and Aggregation Behavior of Copolymer of Acrylamide with Pseudorotaxane Monomer by Threading Cucurbit[6]Uril onto N′-(4-Vinylbenzyl)-1,4-Diaminobutane Dihydrochloride. *J. Dispers. Sci. Technol.* **2012**, *33* (5), 639–646.

(246) Ju, Y.; Kumar, D.; Varma, R. S. Revisiting Nucleophilic Substitution Reactions: Microwave-Assisted Synthesis of Azides , Thiocyanates , and Sulfones in an Aqueous Medium. *J. Org. Chem.* **2006**, *71*, 6697–6700.

(247) Zhang, Y.; Duan, D.; Zhong, Y.; Guo, X.; Guo, J.; Gou, J. Fe (III) -Catalyzed Aerobic Intramolecular N − N Coupling of Aliphatic Azides with Amines. *Org. Lett.* **2019**, *21* (13), 4960–4965.

(248) Bartels, J. L.; Lu, P.; Walker, A.; Maurer, K.; Moeller, K. D. Building Addressable Libraries: A Site-Selective Click-Reaction Strategy for Rapidly Assembling Mass Spectrometry Cleavable Linkers. *Chem. Commun.* **2009**, 37, 5573–5575.

(249) Burrows, C. J.; Muller, J. G. Oxidative Nucleobase Modifications Leading to Strand Scission. *Chem. Rev.* **1998**, *98* (3), 1109–1151.

Appendix

MS Characterization of Oligonucleotides

Note: MS analyses were performed on different instruments (Q-TOF and Orbitrap) due to a malfunction with the Q-TOF partway through this work.

Oligonucleotide	Expected Mass (Da)	Experimental Mass (Da)
rA_{11}	3559	3559
XrA_{10}	3597	3597
rA_5XrA_5	3597	3597
rA_4XXrA_5	3633.6533	3633.6681
rA_4XXXrA_4	3671.6689	3671.6834
$rA_{10}X$	3597	3597
XrA_9X	3633.6533	3633.6675
rA_{16}	5205	5205
XrA_{15}	5243	5243
$rA_{10}XrA_5$	5243	5243
rA_9XXrA_5	5278.9159	5278.9424
rA_8XXXrA_5	5316.9315	5316.9522
$rA_{15}X$	5243	5243

Table A.1: MS Analysis of Controls and C2'-*O*-Propargyl Functionalized Oligonucleotides.

Oligonucleotide	Expected Mass (Da)	Experimental Mass (Da)
XrA_{10}	3709.7300	3709.7455
rA_5XrA_5	3709.7300	3709.7485
rA_4XXrA_5	3861.8300	3861.8377
rA_4XXXrA_4	4013.9400	4013.9458
$rA_{10}X$	3709.7300	3709.7395
XrA_9X	3861.8300	3861.8260
XrA_{15}	5354.9900	5355.0193
$rA_{10}XrA_5$	5354.9900	5355.0083
rA_9XXrA_5	5507.1000	5507.1000
rA_8XXXrA_5	5659.2000	5659.2061
$rA_{15}X$	5354.9900	5355.0089

Table A.2: MS Analysis of Butylamine-Modified Oligonucleotides.

Oligonucleotide	Expected Mass (Da)	Experimental Mass (Da)
XrA_{10}	3854	3855
rA_5XrA_5	3852.7329	3852.7450
rA_4XXrA_5	4147.8439	4147.8527
rA_4XXXrA_4	4442.9548	4442.9606
$rA_{10}X$	3852.7329	3852.7385
XrA_9X	4147.8439	4147.8541
XrA_{15}	5497.9955	5497.9930
$rA_{10}XrA_5$	5497.9955	5498.0039
rA_9XXrA_5	5796.0100	5793.1180
rA_8XXXrA_5	6088.2174	6088.2283
$rA_{15}X$	5497.9955	5498.0007

Table A.3: MS Analysis of Pyrene-Modified Oligonucleotides.

Oligonucleotide	Expected Mass (Da)	Experimental Mass (Da)
rA_5-L-rA_5	3569.6200	3569.6403
rA_{10}-L	3569.6200	3569.6315
rA_{10}-L-rA_5	5214.8800	5214.8982
rA_{15}-L	5214.8800	5214.9004
$rA_{PS}rA_{10}$	3573.6000	3573.6148

Table A.4: MS Analysis of Backbone-Modified Oligonucleotides.

Analytical Gels of Synthesized Oligonucleotides

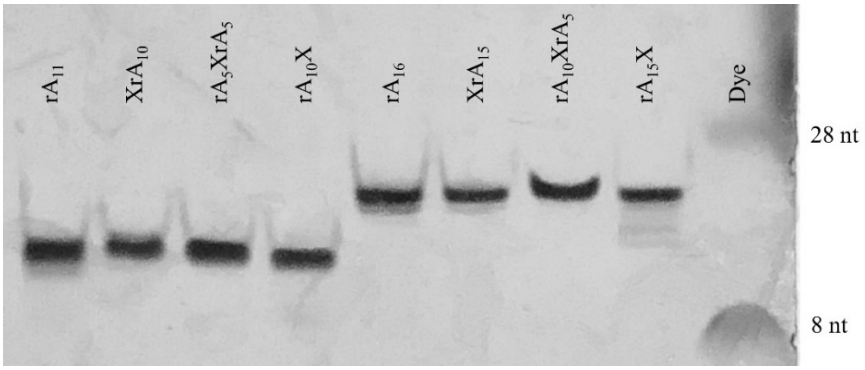

Figure A.1: Purified C2'-*O*-Propargylated poly(A) RNA. 20 % Denaturing acrylamide/bisacrylamide (19:1) gel, run at 200 V for 1 h 9 min and visualized by short-wave UV shadowing. 0.15 OD oligo loaded in 10 µL formamide.

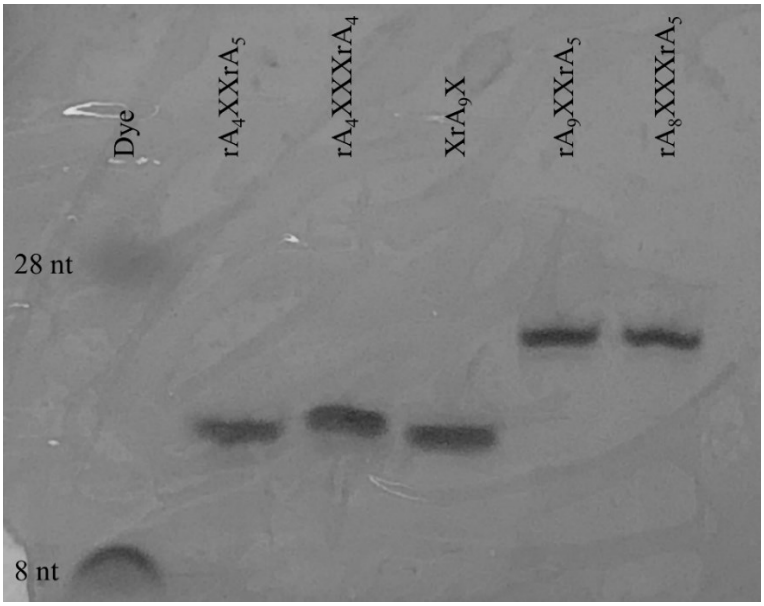

Figure A.2: Purified C2'-*O*-Propargylated poly(A) RNA. 20 % Denaturing acrylamide/bisacrylamide (19:1) gel, run at 200 V for 1 h 48 min and visualized by short-wave UV shadowing. 0.15 OD oligo loaded in 10 µL formamide.

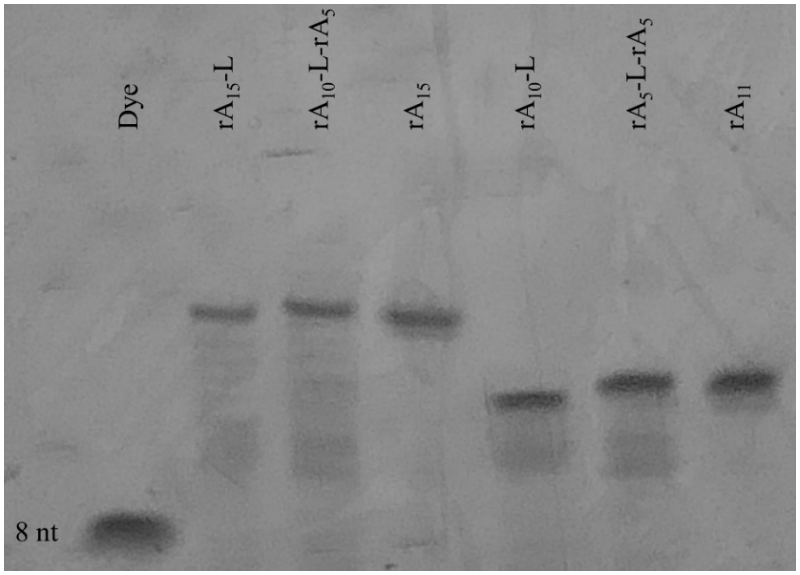

Figure A.3: Crude LNA-Modified poly(A) RNA. 20 % Denaturing acrylamide/bisacrylamide (19:1) gel, run at 200 V for 1 h 30 min and visualized by short-wave UV shadowing. 0.15 OD oligo loaded in 10 µL formamide.

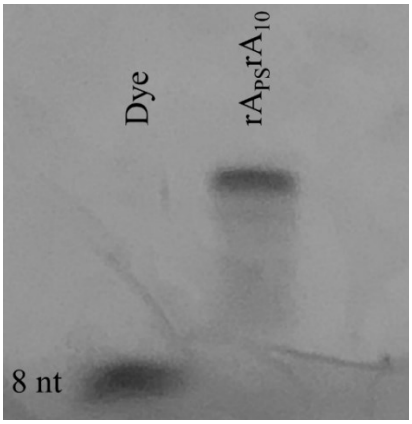

Figure A.4: Crude Phosphorothioate-Modified poly(A) RNA. 20 % Denaturing acrylamide/bisacrylamide (19:1) gel, run at 200 V for 1 h 30 min and visualized by short-wave UV shadowing. 0.15 OD oligo loaded in 10 µL formamide.

Click Reactions with 4-Azidobutylamine

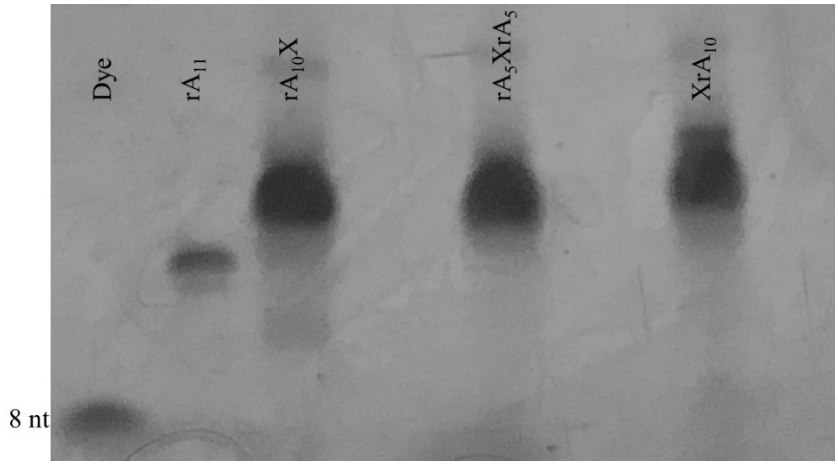

Figure A.5: Crude Butylamine-Modified poly(A) RNA. 20 % Denaturing acrylamide/bisacrylamide (19:1) gel, run at 200 V for 1 h 30 min and visualized by short-wave UV shadowing. 1.0 OD Click reactions loaded in 20 µL formamide.

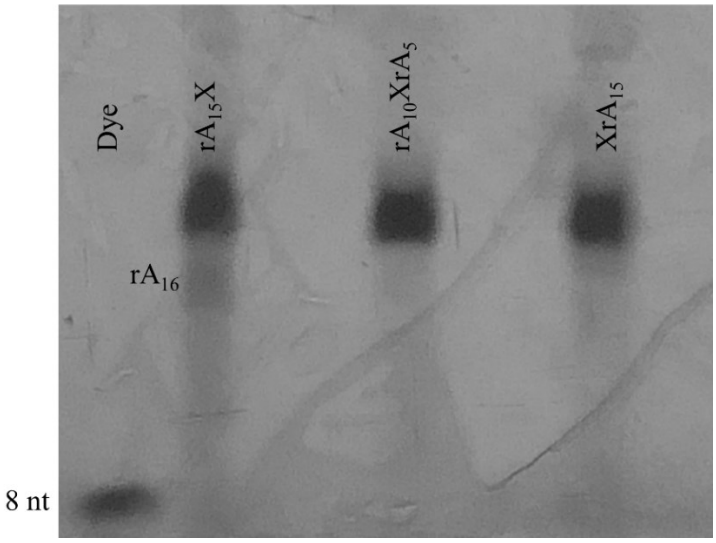

Figure A.6: Crude Butylamine-Modified poly(A) RNA. 20 % Denaturing acrylamide/bisacrylamide (19:1) gel, run at 200 V for 1 h 30 min and visualized by short-wave UV shadowing. 1.0 OD Click reactions loaded in 20 µL formamide.

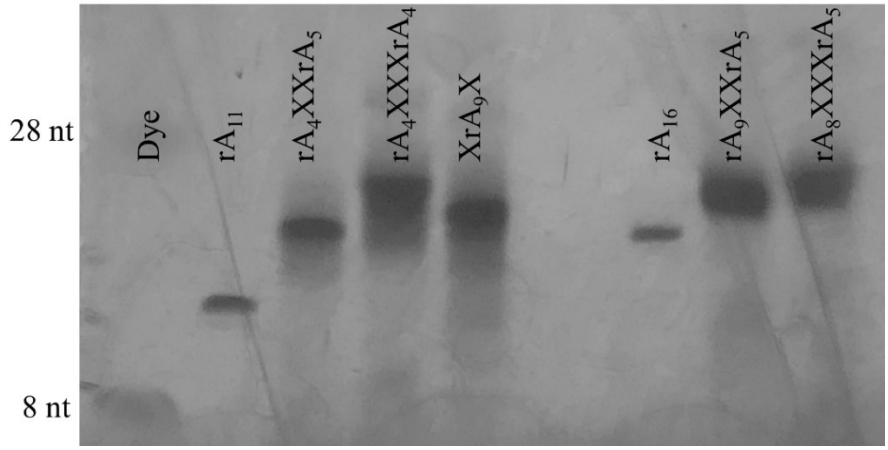

Figure A.7: Crude Butylamine-Modified poly(A) RNA. 20 % Denaturing acrylamide/bisacrylamide (19:1) gel, run at 200 V for 1 h 30 min and visualized by short-wave UV shadowing. 0.5 OD Click reactions loaded in 20 µL formamide.

Click Reactions with 1-(azidomethyl)pyrene

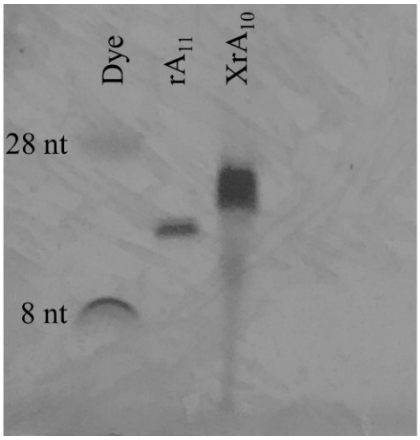

Figure A.8: Crude Pyrene-Modified poly(A) RNA. 20 % Denaturing acrylamide/bisacrylamide (19:1) gel, run at 200 V for 1 h 52 min and visualized by short-wave UV shadowing. 0.8 OD Click reactions loaded in 20 µL formamide.

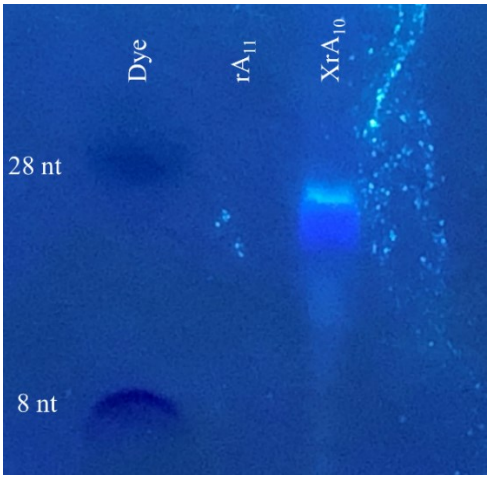

Figure A.9: Crude Pyrene-Modified poly(A) RNA. 20 % Denaturing acrylamide/bisacrylamide (19:1) gel, run at 200 V for 1 h 52 min and visualized by long-wave UV shadowing. 0.8 OD Click reactions loaded in 20 µL formamide.

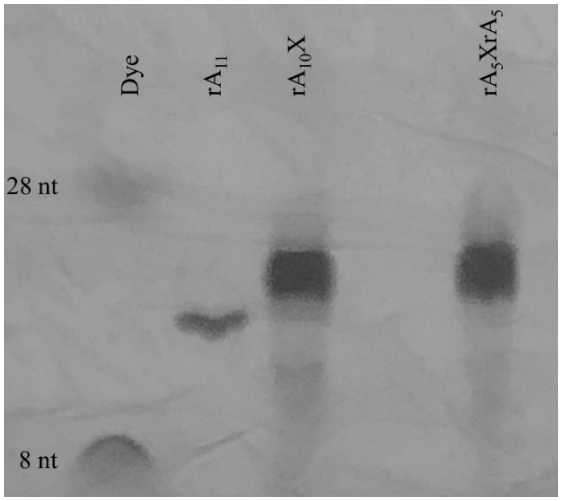

Figure A.10: Crude Pyrene-Modified poly(A) RNA. 20 % Denaturing acrylamide/bisacrylamide (19:1) gel, run at 200 V for 1 h 41 min and visualized by short-wave UV shadowing. 0.8 OD Click reactions loaded in 20 µL formamide.

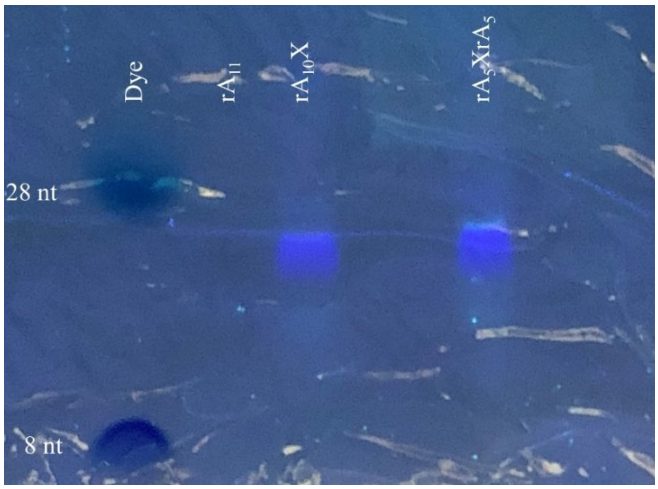

Figure A.11: Crude Pyrene-Modified poly(A) RNA. 20 % Denaturing acrylamide/bisacrylamide (19:1) gel, run at 200 V for 1 h 41 min and visualized by long-wave UV shadowing. 0.8 OD Click reactions loaded in 20 µL formamide.

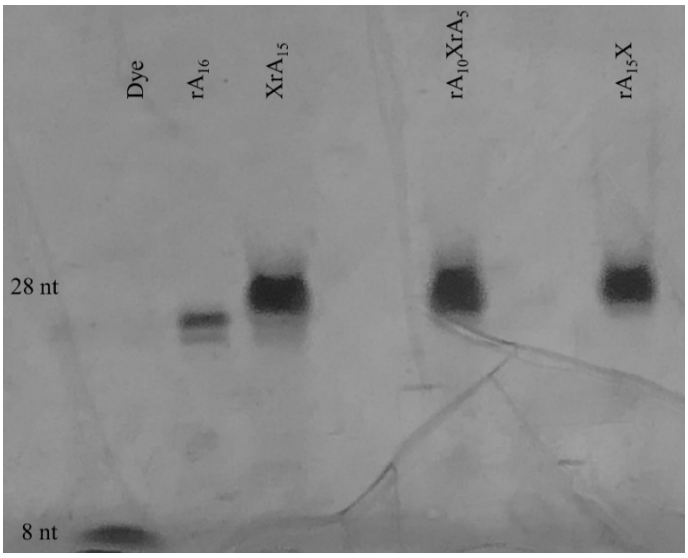

Figure A.12: Crude Pyrene-Modified poly(A) RNA. 20 % Denaturing acrylamide/bisacrylamide (19:1) gel, run at 200 V for 1 h 20 min and visualized by short-wave UV shadowing. 1.0 OD Click reactions loaded in 20 µL formamide.

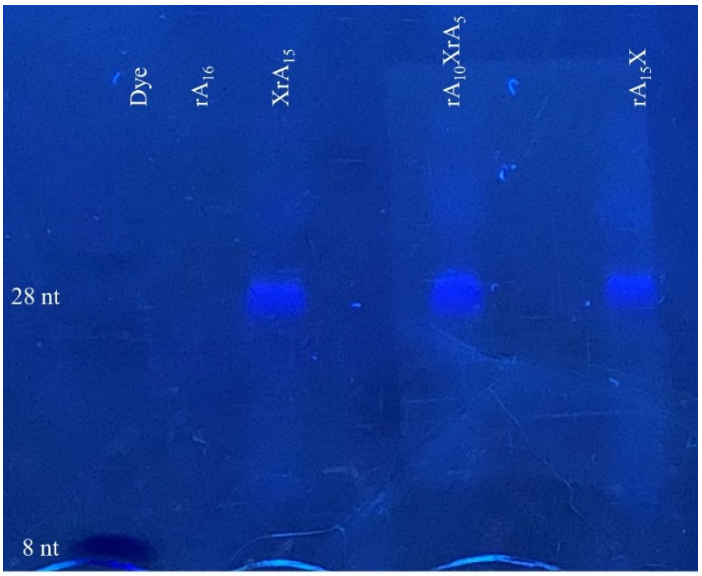

Figure A.13: Crude Pyrene-Modified poly(A) RNA. 20 % Denaturing acrylamide/bisacrylamide (19:1) gel, run at 200 V for 1 h 20 min and visualized by long-wave UV shadowing. 1.0 OD Click reactions loaded in 20 µL formamide.

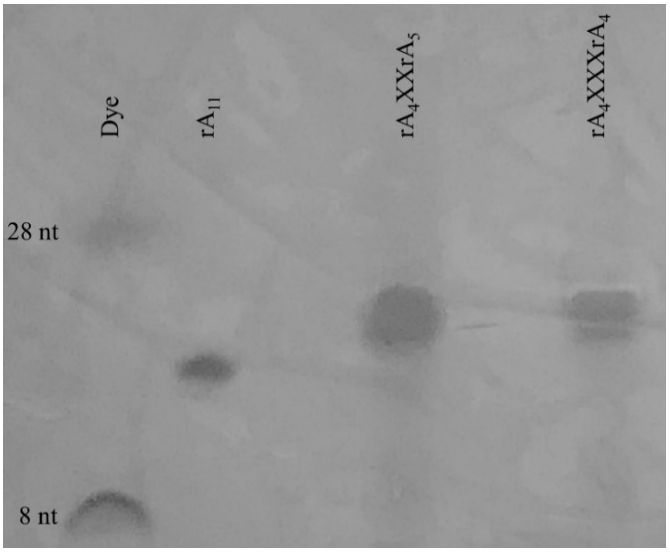

Figure A.14: Crude Pyrene-Modified poly(A) RNA. 20 % Denaturing acrylamide/bisacrylamide (19:1) gel, run at 200 V for 1 h 48 min and visualized by short-wave UV shadowing. 1.0 OD Click reactions loaded in 20 µL formamide.

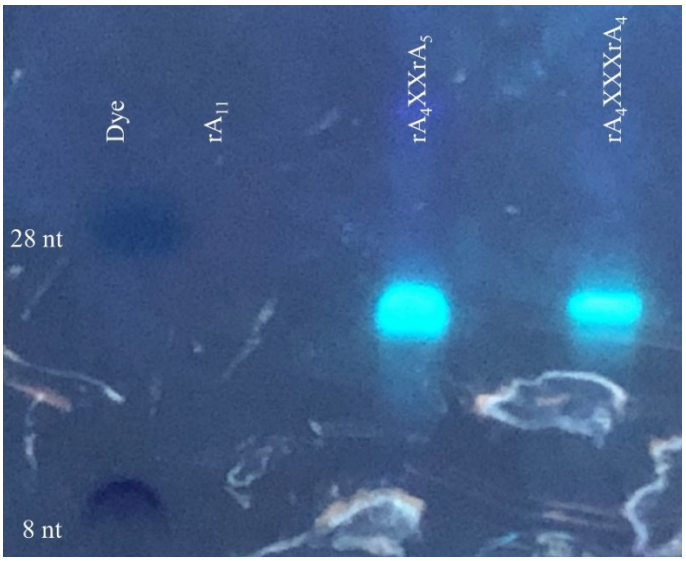

Figure A.15: Crude Pyrene-Modified poly(A) RNA. 20 % Denaturing acrylamide/bisacrylamide (19:1) gel, run at 200 V for 1 h 48 min and visualized by long-wave UV shadowing. 1.0 OD Click reactions loaded in 20 µL formamide.

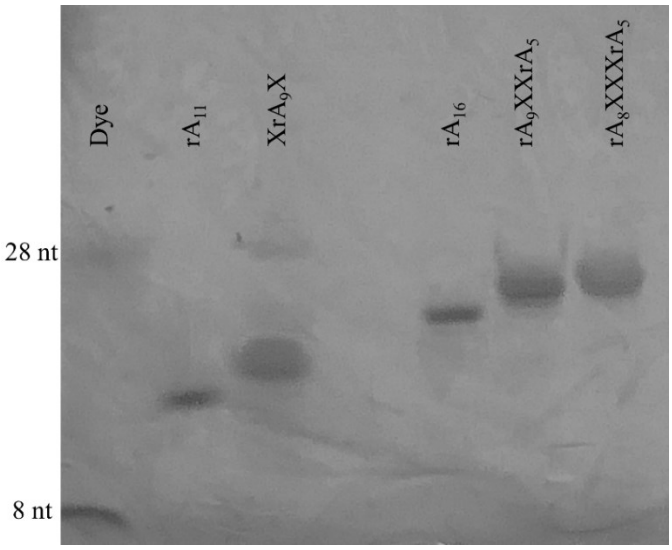

Figure A.16: Crude Pyrene-Modified poly(A) RNA. 20 % Denaturing acrylamide/bisacrylamide (19:1) gel, run at 200 V for 1 h 53 min and visualized by short-wave UV shadowing. 0.8 OD Click reactions loaded in 20 µL formamide.

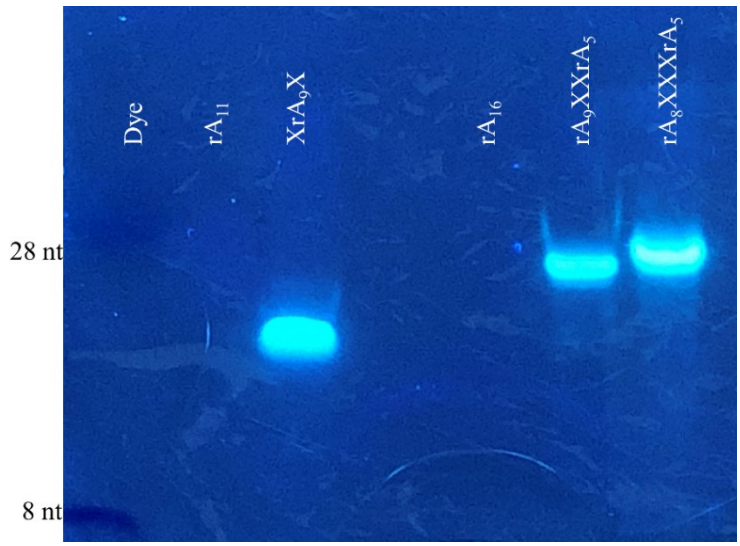

Figure A.17: Crude Pyrene-Modified poly(A) RNA. 20 % Denaturing acrylamide/bisacrylamide (19:1) gel, run at 200 V for 1 h 53 min and visualized by long-wave UV shadowing. 0.8 OD Click reactions loaded in 20 µL formamide.

Diastereomer Separation of Phosphorothioate-Modified poly(A)

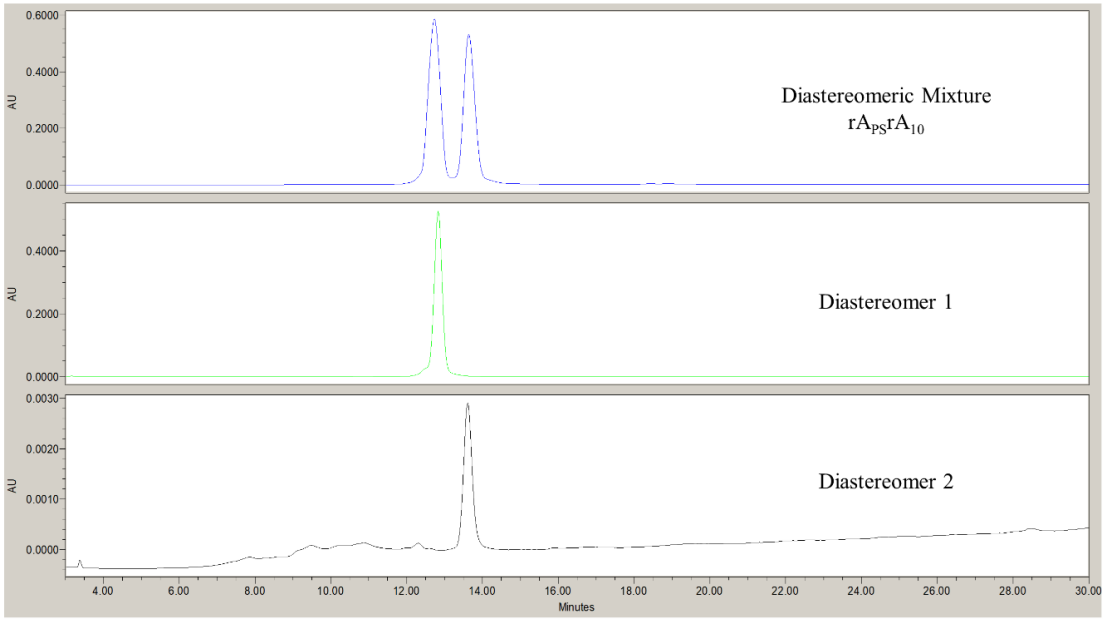

Figure A.18: RP-HPLC Purification of Phosphorothioate-Modified poly(A) RNA.

Crystal Structure Internucleotide-Distance Analysis

Nucleotides	Distance (Å)
rA_1-rA_2	6.31
rA_2-rA_3	6.65
rA_3-rA_4	6.37
rA_4-rA_5	6.67
rA_5-rA_6	6.59
rA_6-rA_7	6.70
rA_7-rA_8	6.53
rA_8-rA_9	6.54
rA_9-rA_{10}	6.42
rA_{10}-rA_{11}	7.25
rA_1(A)-rA_1(B)	12.37
rA_{11}(A)-rA_{11}(B)	12.32

Table A.5: Internucleotide-Distance Analysis of O2' Atoms for an 11-mer poly(A) Duplex Crystallized at pH 7, 4.4 M NH_4Cl, 1 Å Resolution (PDB: 4JRD).[114]

NMR Analysis of Amine and Pyrene Small Molecules

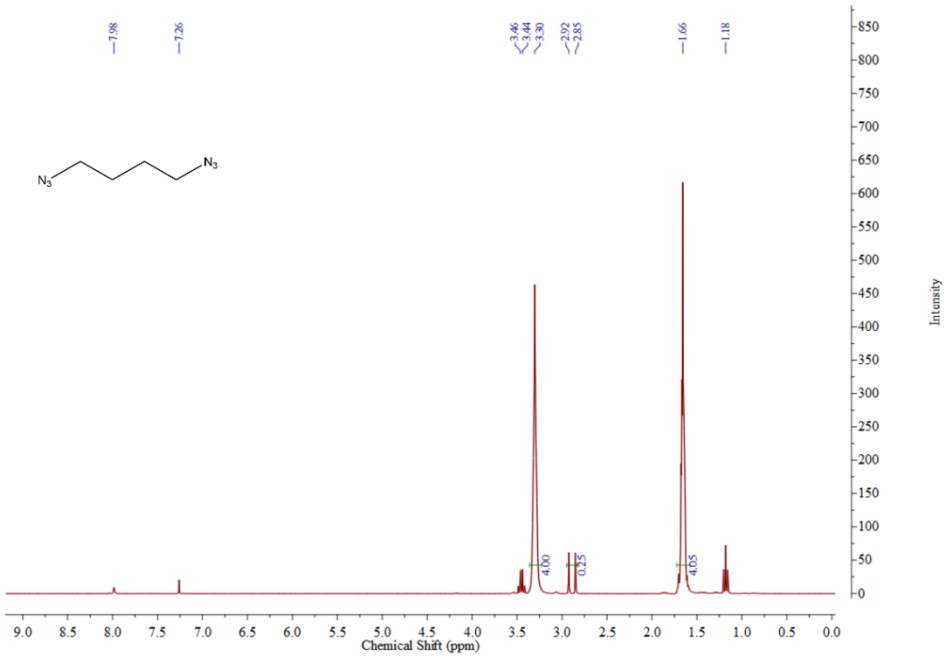

Figure A.19: 500 MHz ^{1}H NMR Spectrum of 1,4-diazidobutane.

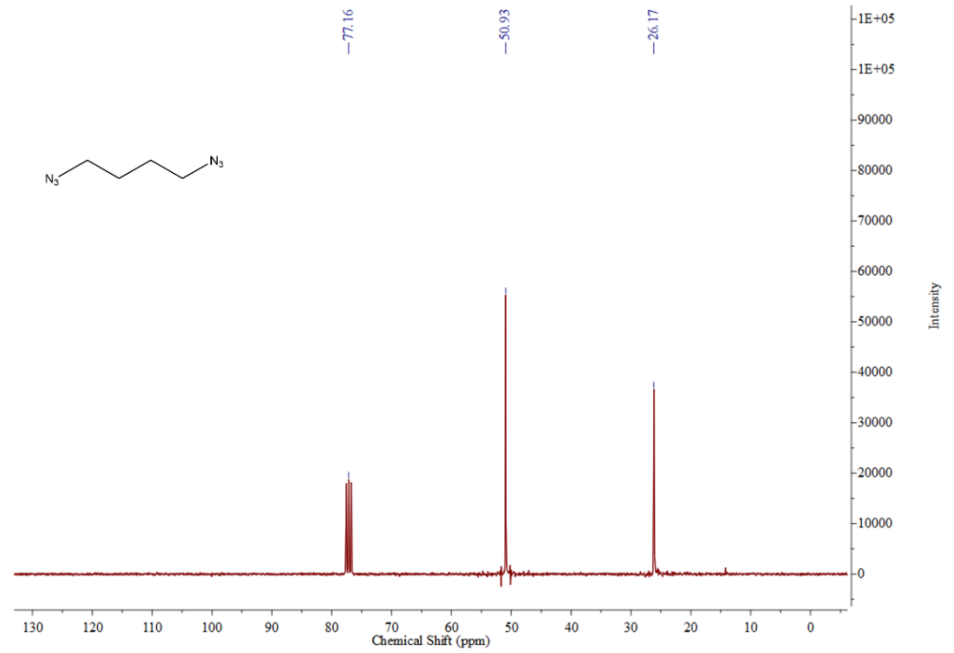

Figure A.20: 125.7 MHz ^{13}C NMR Spectrum of 1,4-diazidobutane.

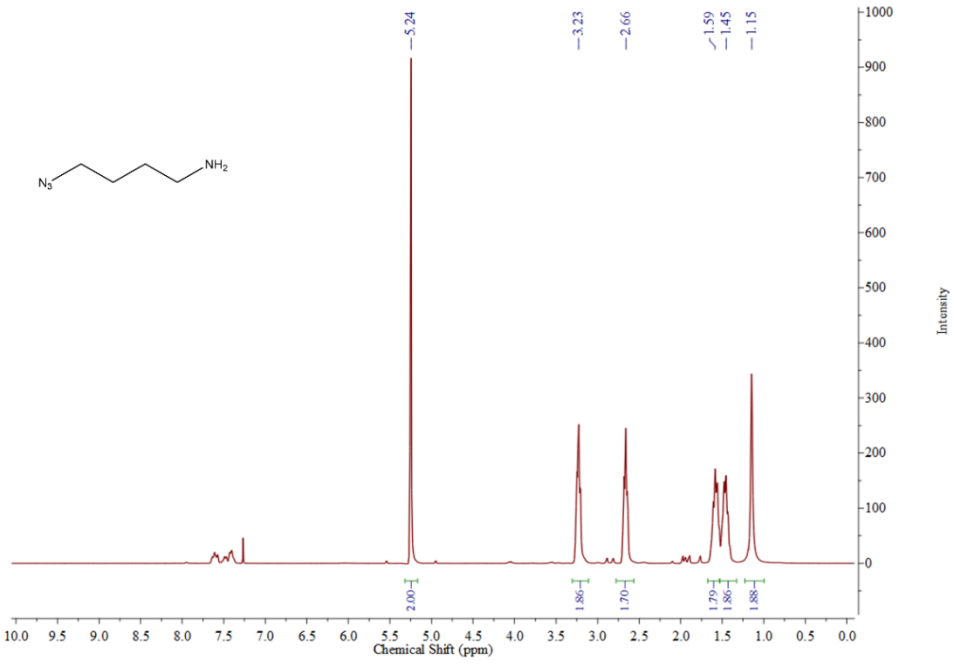

Figure A.21: 500 MHz ^{1}H NMR Spectrum of 4-azidobutylamine.

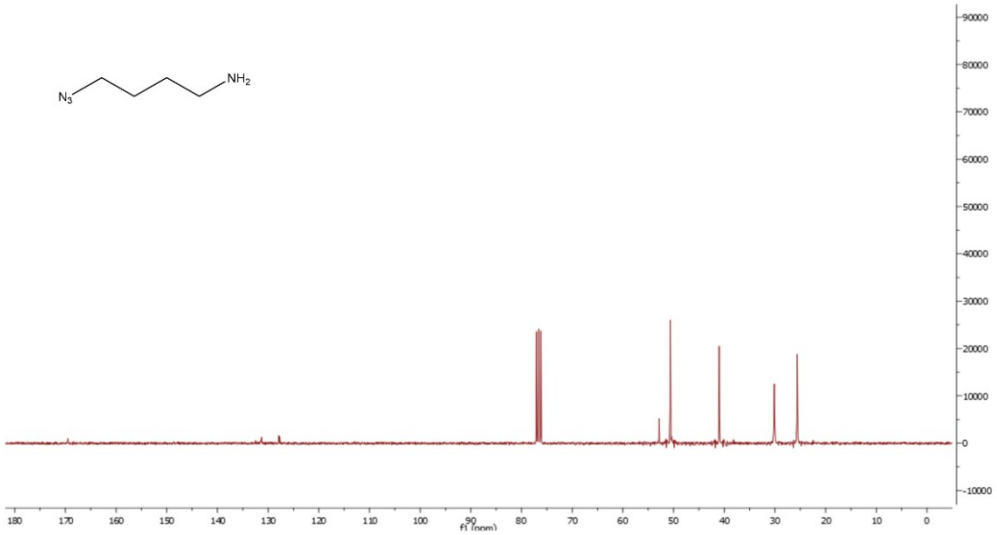

Figure A.22: 125.7 MHz ^{13}C NMR Spectrum of 4-azidobutylamine.

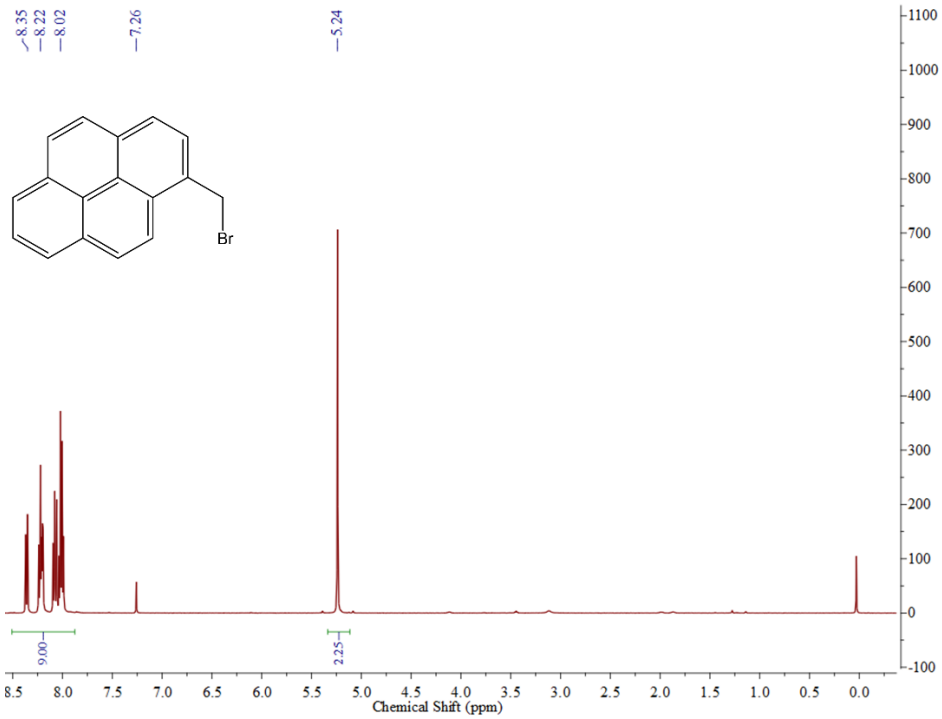

Figure A.23: 500 MHz ^{1}H NMR Spectrum of 1-(bromomethyl)pyrene.

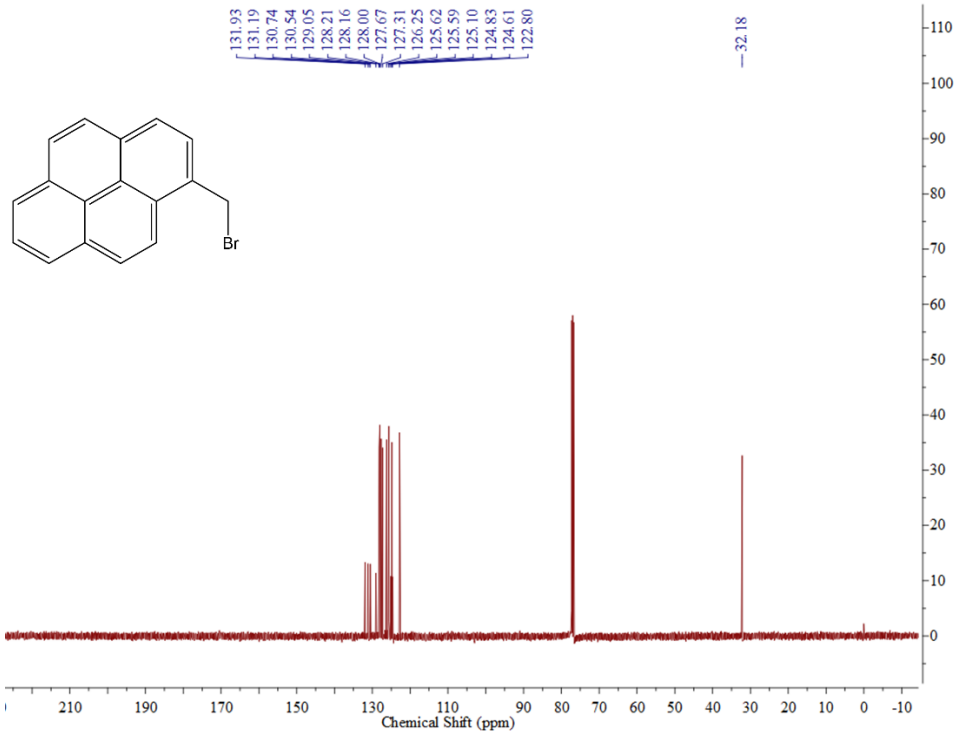

Figure A.24: 125.7 MHz ^{13}C NMR Spectrum of 1-(bromomethyl)pyrene.

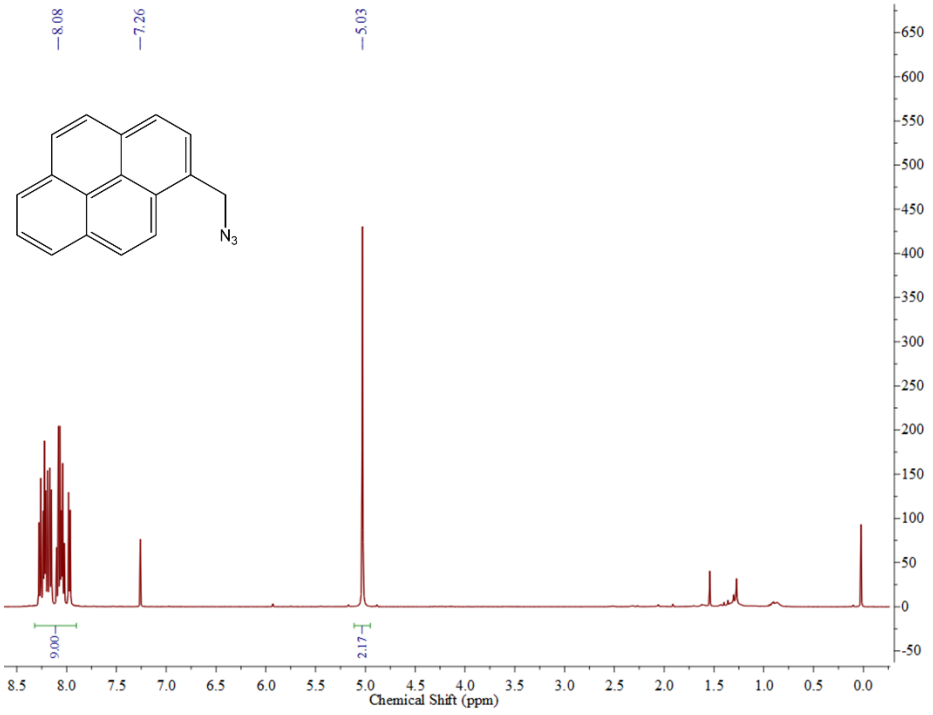

Figure A.25: 500 MHz ^{1}H NMR Spectrum of 1-(azidomethyl)pyrene.

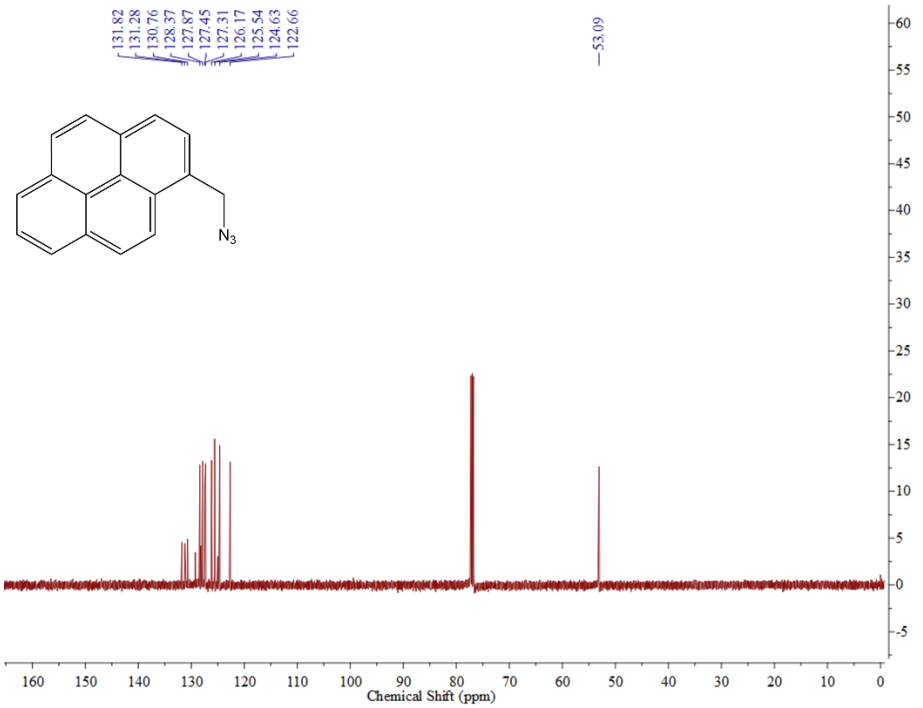

Figure A.26: 125.7 MHz ^{13}C NMR Spectrum of 1-(azidomethyl)pyrene.

FT-IR Analysis of Small Molecules

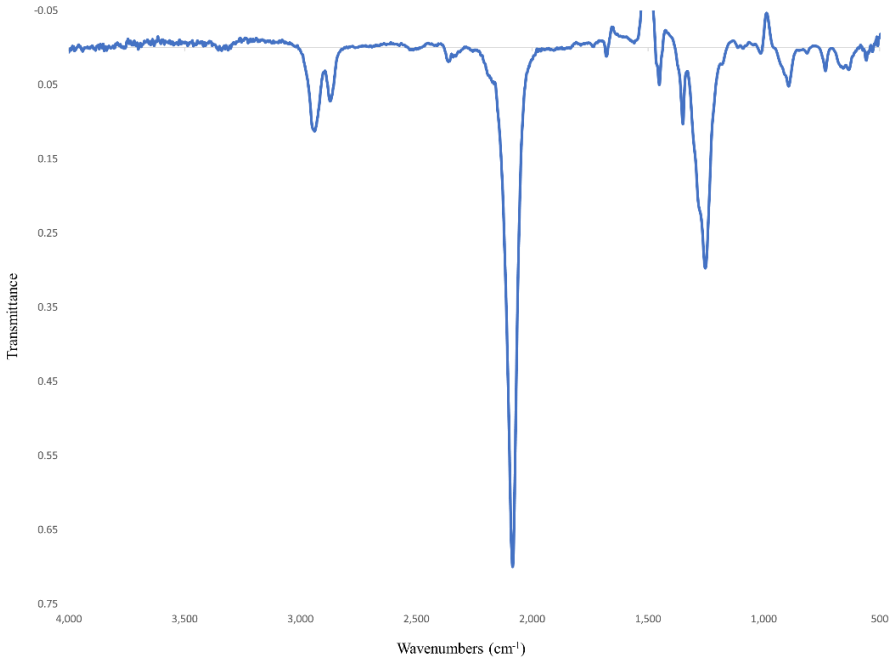

Figure A.27: FT-IR Spectrum of 1,4-diazidobutane.

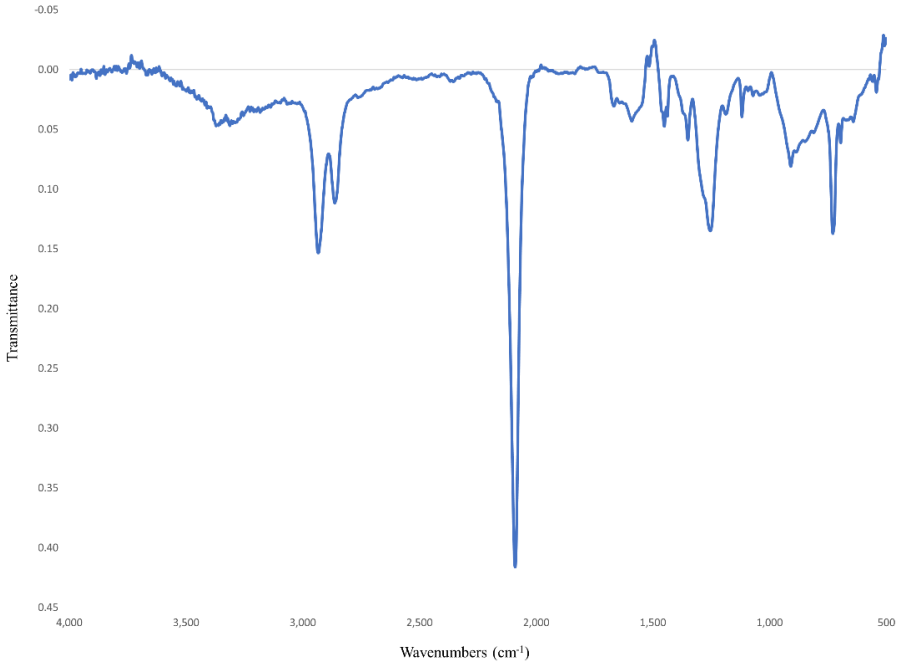

Figure A.28: FT-IR Spectrum of 4-azidobutylamine.

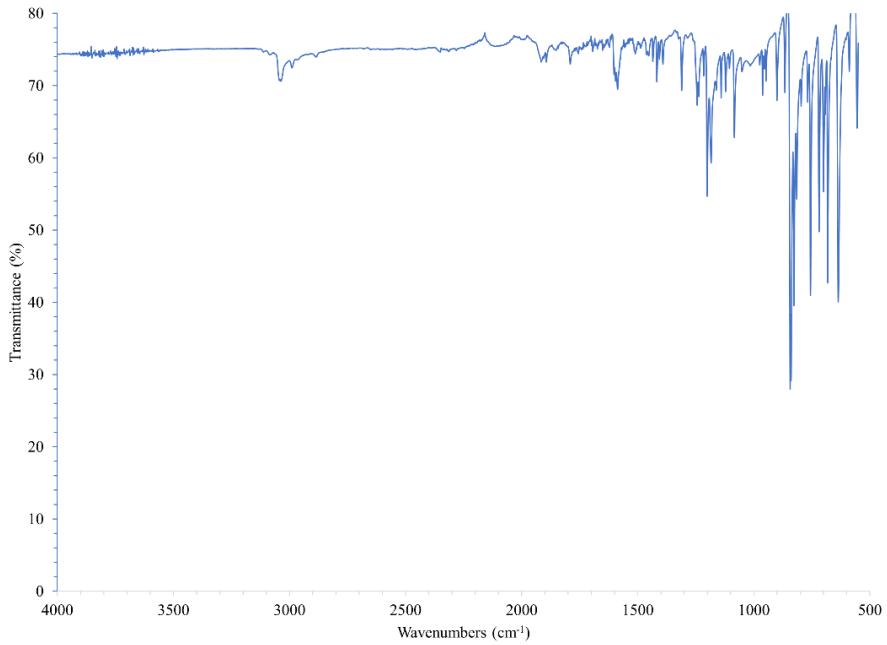

Figure A.29: FT-IR Spectrum of 1-(bromomethyl)pyrene.

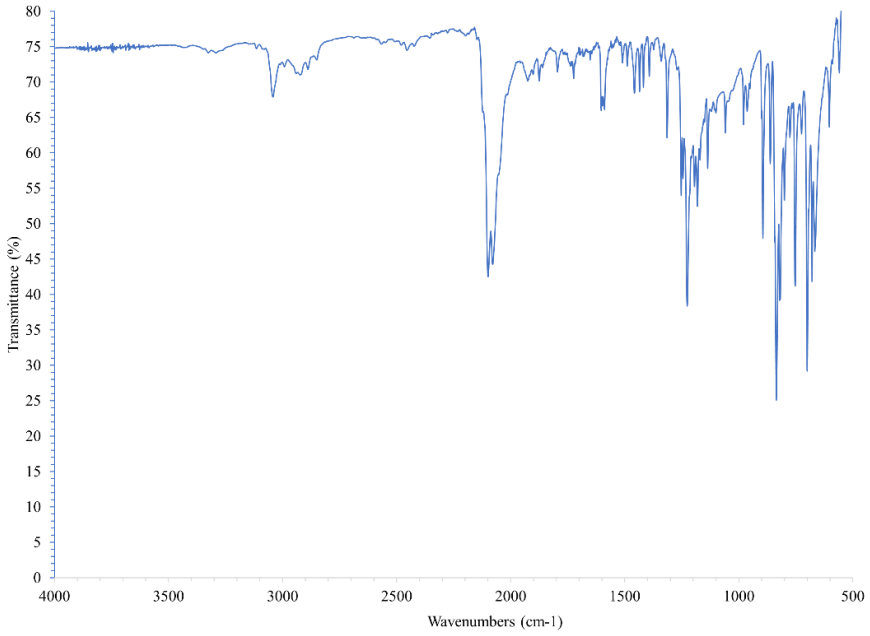

Figure A.30: FT-IR Spectrum of 1-(azidomethyl)pyrene.

ESI(+) Analysis of Small Molecules

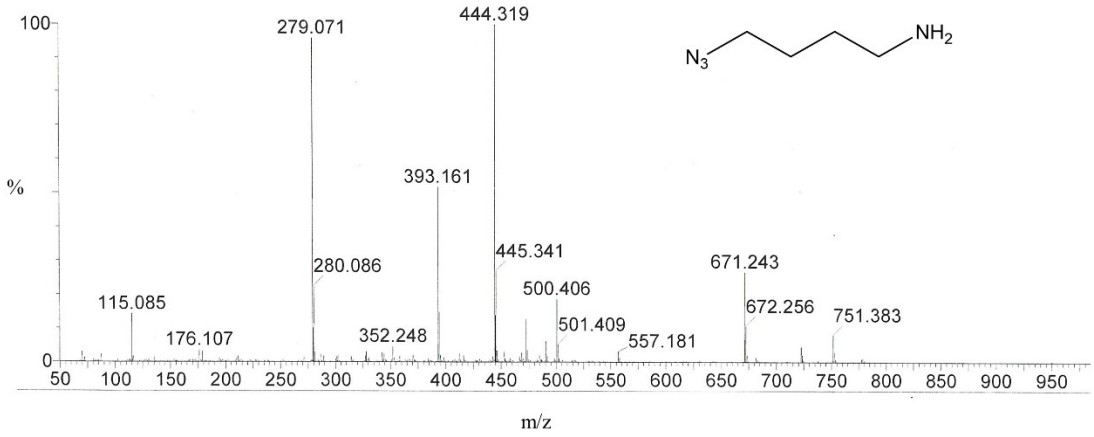

Figure A.31: ESI-MS Spectrum of 4-azidobutylamine.

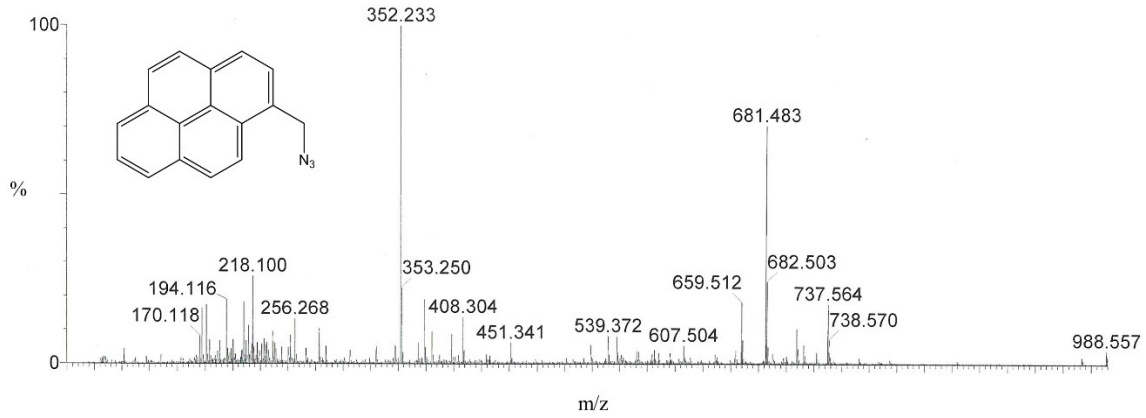

Figure A.32: ESI-MS Spectrum of 1-(azidomethyl)pyrene.

Thermal Reversibility of poly(A) Duplex Unfolding at pH 4 and pH 7

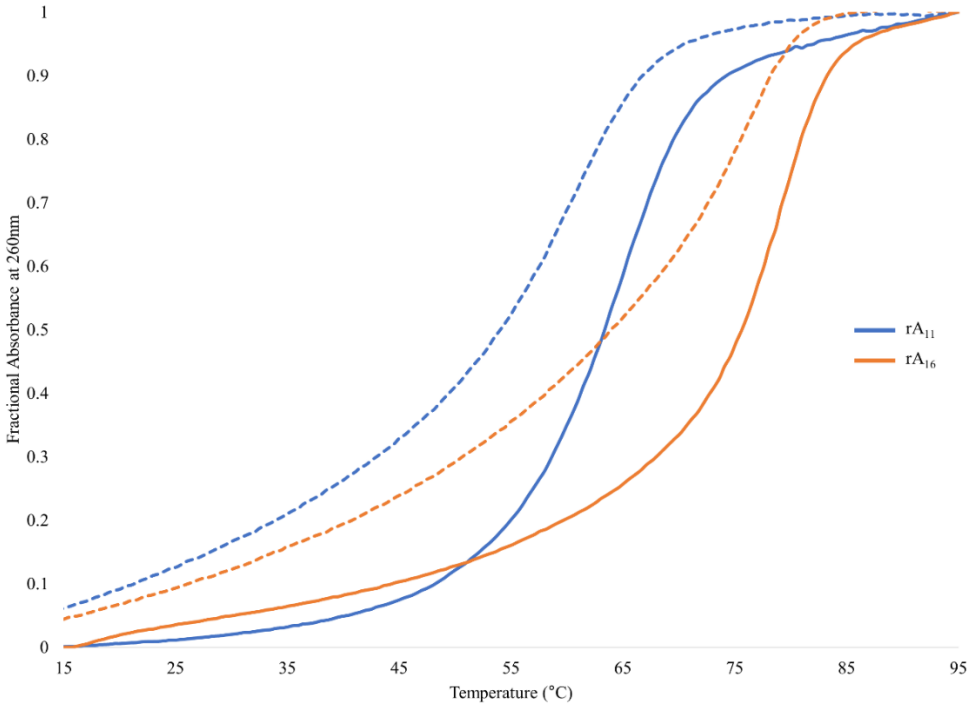

Figure A.33: Thermal Reversibility Profiles at 260 nm of poly(A) Duplexes at pH 4. (Buffer: 40 mM Na_2HPO_4, 30 mM citric acid, pH 4). Single strand concentrations were 3.7 μM for 11-mers and 2.6 μM for 16-mers. (Solid: Heating, Dashed: Cooling).

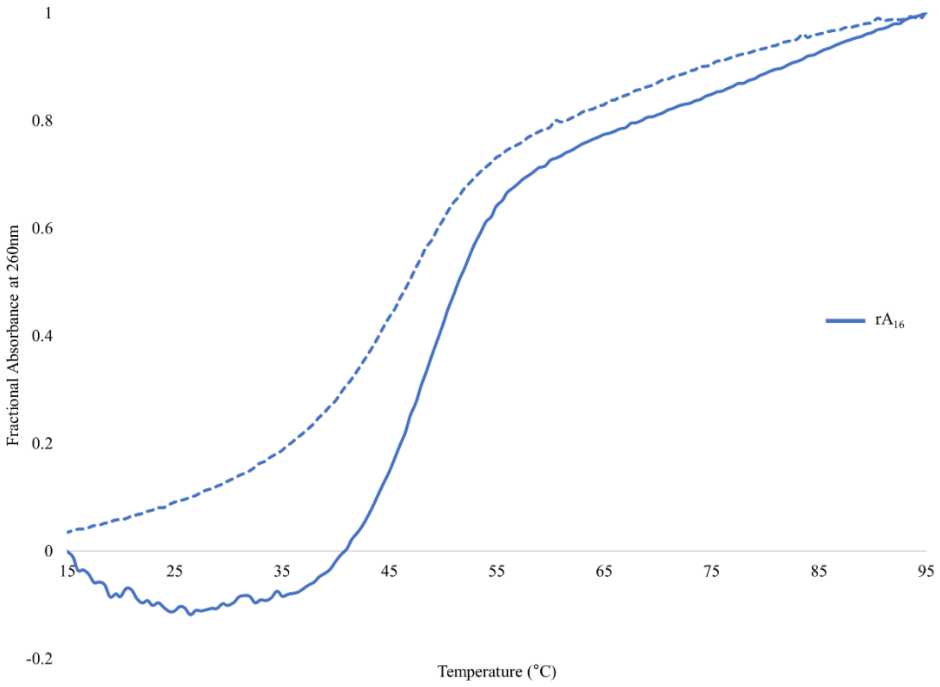

Figure A.34: Thermal Reversibility Profile at 260 nm of a poly(A) Duplex at pH 7. (Buffer: 40 mM Na_2HPO_4, 30 mM citric acid, 4.4 M NH_4Cl, pH 7). 2.6 µM single strand concentrations. (Solid: Heating, Dashed: Cooling).

Photobleaching Analysis of Pyrene-Modified poly(A) Duplex

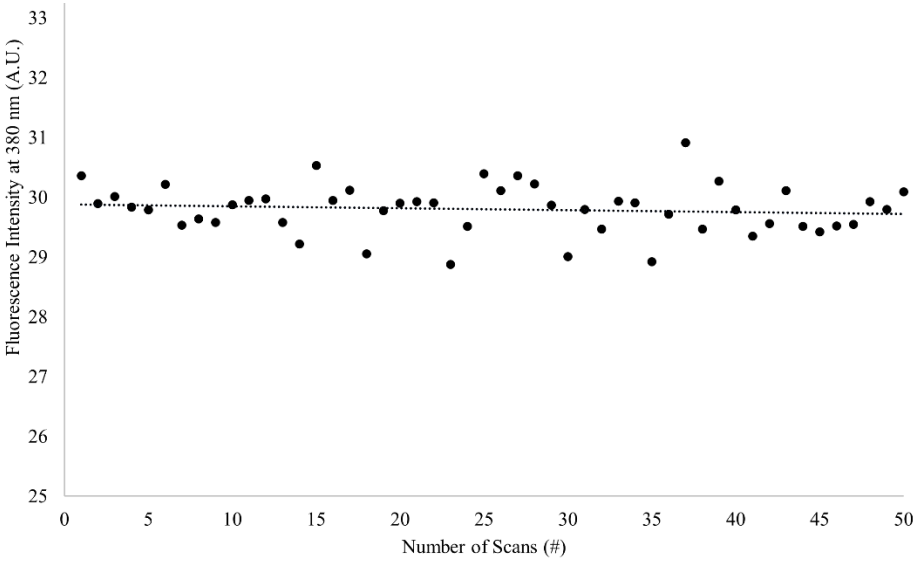

Figure A.35: Photobleaching Analysis of a Pyrene-Modified poly(A) Duplex Formed from rA_5XrA_5 at pH 4. (Buffer: 40 mM Na_2HPO_4, 30 mM citric acid, pH 4). 3.7 µM single strand concentrations.

Melting Analysis of Pyrene-Modified poly(A) at 350 nm

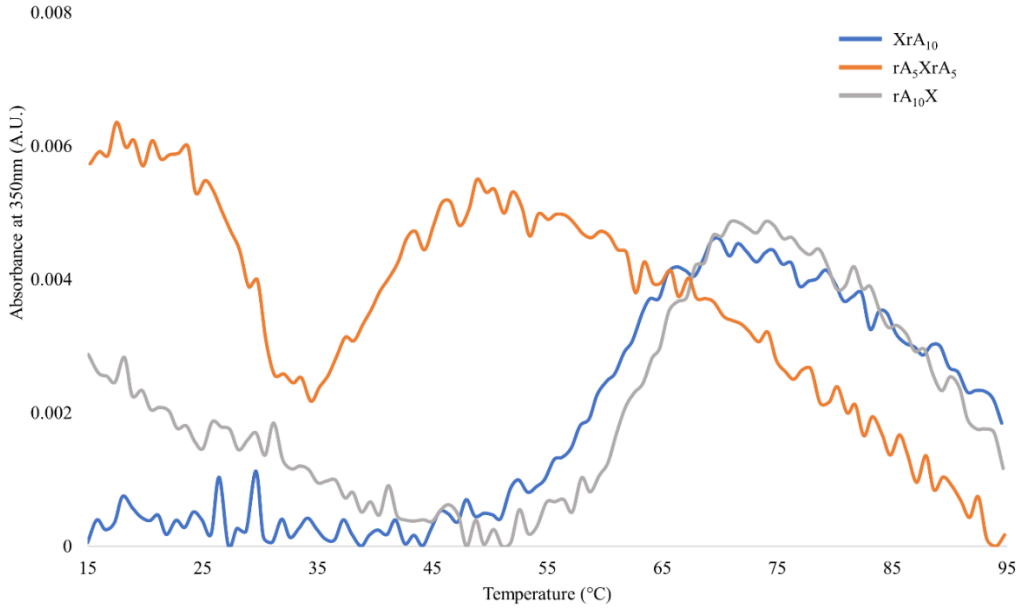

Figure A.36: 350 nm Melting Analysis of Duplexes Formed by Pyrene-Modified poly(A) 11-mers at pH 4. (Buffer: 40 mM Na_2HPO_4, 30 mM citric acid, pH 4). 3.7 µM single strand concentrations.

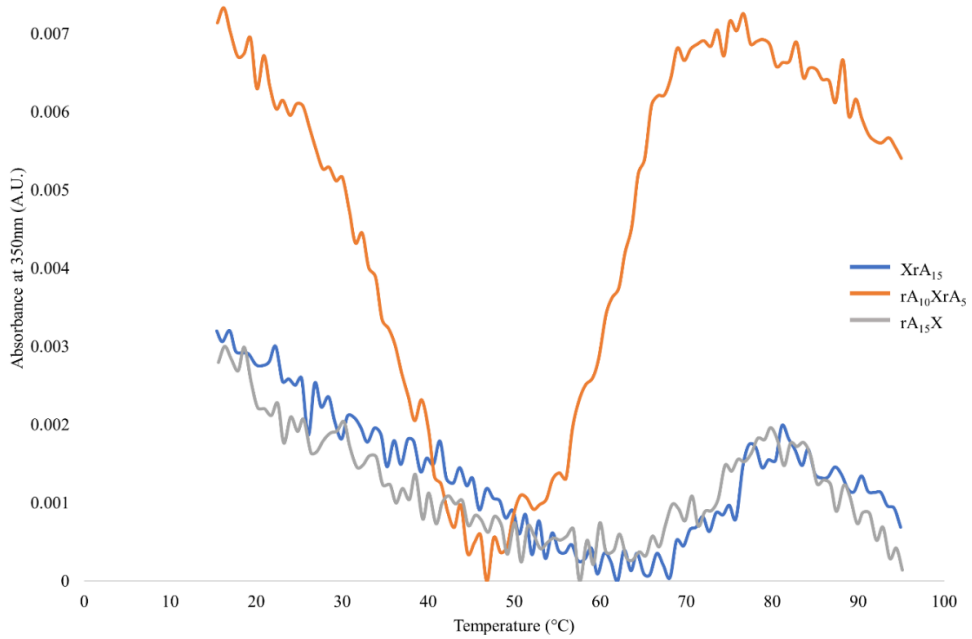

Figure A.37: 350 nm Melting Analysis of Duplexes Formed by Pyrene-Modified poly(A) 16-mers at pH 4. (Buffer: 40 mM Na_2HPO_4, 30 mM citric acid, pH 4). 2.6 µM single strand concentrations.